

Environmentally Benign Mixing of Nanoparticles

by

Ganesh P. Sanganwar

A dissertation submitted to the Graduate Faculty of
Auburn University
in partial fulfillment of the
requirements for the Degree of
Doctor of Philosophy

Auburn, Alabama
May 14, 2010

Keywords: Nanomixing, Nanoparticles, Supercritical Antisolvent, High Pressure Carbon
Dioxide, Dissolution Enhancement, Powder Flow, Homogeneity

Copyright 2010 by Ganesh P. Sanganwar

Approved by

Ram B. Gupta, Chair, Professor of Chemical Engineering
Christopher B. Roberts, Professor of Chemical Engineering
William R. Ravis, Professor of Pharmacal Sciences
Rajesh N. Dave, Professor of Chemical Engineering (NJIT)

Abstract

Due to the increased use of nanocomposites, nanocatalysts, and nanopharmaceuticals, mixing at nanoscale has become important. Conventional mixing techniques can be classified into: (a) dry mixing (mechanical mixing), (b) wet mixing, and (c) simultaneous production of mixed nanoparticles. Dry mixing is in general, not effective in achieving desired mixing at nanoscale, whereas wet mixing suffers from different disadvantages like nanomaterial of interest should be insoluble, has to wet the liquid, and involves additional steps of filtration and drying. This dissertation examines the use of environmentally friendly material, pressurized carbon dioxide, having high density and low viscosity to replace the liquids (e.g., n-hexane, toluene). Various techniques involving high pressure carbon dioxide have been developed for mixing of nanoparticles at the nanoscale.

In the first method (Chapter 2), ultrasound is applied to the suspension of nanopowders in gaseous and supercritical carbon dioxide where high impact collisions during sonication help mixing and the final mixture is obtained by simple depressurization. Results show that mixing in carbon dioxide at higher ultrasound amplitudes is as good as in liquid n-hexane, and the final mixed product does not contain any residual media in contrast to the case of liquid n-hexane.

In the second method (Chapter 3), which was specially applied to drug and excipient nanoparticles, a macroscopic mixture of drug nanoparticles and silica

nanoparticles is first pressurized with supercritical carbon dioxide and then is rapidly depressurized through a nozzle. This method is termed as rapid depressurization of supercritical suspension (RDSS). Effective deagglomeration and nanoscale mixing is achieved using RDSS method leading to increase in the shelf life.

In the third method (Chapter 4), applicability of sonication in liquid CO₂ for mixing of drug (dipyridamole) and excipient nanoparticles is demonstrated for several binary mixtures of the drug and excipients. To intimately mix at nanoscale, macro mixtures of dipyridamole and excipient particles are sonicated in liquid carbon dioxide. Results of drug dissolution and blend homogeneity show effectiveness of the proposed mixing method for fine size particles.

In fourth method (Chapter 5), microparticles of a poorly-water-soluble model drug, nevirapine (NEV) were prepared by supercritical antisolvent (SAS) method and simultaneously deposited on the surface of excipients in a single step to reduce drug-drug particle aggregation. In the method, termed supercritical antisolvent-drug excipient mixing (SAS-DEM), drug particles were precipitated in supercritical CO₂ vessel containing excipient particles in suspended state. A highly ordered NEV-excipient mixture was produced. The produced drug/excipient mixture has a significantly faster dissolution rate as compared to SAS drug microparticles alone or when physically mixed with the excipients.

Future work involves the testing the applicability SAS-DEM method and stirred mixing in liquid CO₂ for mixing and deagglomeration of more variety of drug nanoparticles with various excipients.

Acknowledgements

I would like to express my special thanks to my advisor Dr. Ram B. Gupta, for his continuous guidance, availability for discussion, motivation, and support during my dissertation work. It would have been impossible for me to complete this work without his support. I really appreciate his help in quick arrangement of final defense.

I would like express sincere thanks to my committee members, Dr. Christopher Roberts, Dr. Virginia Davis, Dr. William Ravis, and Dr. Rajesh Dave for their valuable comments and suggestions. Special thanks to Dr. Rajesh Dave for being on the committee and giving me the opportunity to work on Nanoscale Interdisciplinary Research Teams (NIRT) project. His suggestions, delightful talks, and discussions kept me motivated while working on the project. I sincerely thank Dr. Jayachandra Babu for being outside reader within short notice.

Chemical engineering staff, Karen Cochran, Sue Allen, Georgetta Dennis, and Jennifer Harris deserves special thanks for helping me with logistic, academic and financial matters. Department technician, Brian Schwieker, needs of special mention for his great help in experimental setup work. I would also like express my thanks to Dr. Michael Miller (Director, AURIF) for his help in electron microscopy and Dr. Bart Prorok for his advice in energy dispersive spectroscopy.

I would like to thank Department of Chemical Engineering, Samuel Ginn College of Engineering, and Office of International Education for giving me opportunity to do my

doctoral study.

I like to thank Alexandre Ermoline, James Scicolone, Dr.Rajesh Dave, Sateesh Kumar, and Dr. Jayachandra Babu for their valuable research support and being co-authors in published research article.

My group colleagues, Kayoko Ono, Adam Byrd, Melinda Hemmigway, Sandeep Kumar, Lingzhao Kong, Hema Ramsurn, and Courtney Ober need special appreciation for their assistance and creating a joyful environment in the laboratory.

My friends at Auburn, Shirish, Chandan, Sameep, Darshan, Bhushan, Nitin, and Amit, deserve special mention for making my stay more enjoyable. Also my friends from USA, Europe, and India, Sandeep, Sudheer, Nitin, Neeraj, Ashwin, Parag, Jothir, Santosh, Vikrant, Suhas, Anand, Samyak, Sanjeev, Eva, Tareq, and Herman, deserve special thanks for their continuous support and motivation during studies.

My dear parents, though initially reluctant for me going to United States for higher studies, deserve credit for all my achievements. My brother (Shrinivas), sister (Sarika), brother-in-law (Ravindra), nephew (Krishna), and niece (Vaishnavi) needs special mention for their wonderful talk and much needed support and motivation during the studies.

Table of Contents

Abstract.....	ii
Acknowledgements.....	iv
List of Tables.....	xiii
List of Figures.....	xv
1 Introduction.....	1
1.1 Importance of Nanomixing	1
1.2 Research Methods	6
1.2.1 Materials	6
1.2.2 Mixing Methods.....	7
1.3 References	8
2 Nanomixing by Sonication in High-Pressure CO ₂	21
2.1 Abstract	21
2.2 Introduction	22
2.3 Experimental	24
2.3.1 Materials	24
2.3.2 Mixing in gaseous and supercritical CO ₂	25
2.3.3 Mixing in liquid n-hexane.....	26
2.3.4 Mixture Analysis.....	26
2.4 Results and Discussions	29
2.4.1 SiO ₂ /TiO ₂ and SiO ₂ /Al ₂ O ₃ Systems.....	30

2.4.2	SiO ₂ /MWNT and TiO ₂ /MWNT Systems	35
2.5	Conclusions	38
2.6	Acknowledgement.....	39
2.7	References	40
3	Nanoscale Mixing of Itraconazole with Silica.....	64
3.1	Abstract	64
3.2	Introduction	65
3.3	Materials and methods	67
3.3.1	Materials	67
3.3.2	Production of Itraconazole Nanoflakes.....	68
3.3.3	Drug Deagglomeration and Mixing with Silica.....	69
3.3.4	Angle of Repose.....	70
3.3.5	Compressibility index	70
3.3.6	Hausner ratio.....	70
3.3.7	Scanning Electron Microscopy	70
3.3.8	Physical stability	71
3.3.9	Solubility Measurement.....	71
3.3.10	Drug dissolution.....	71
3.4	Results and Discussion.....	72
3.4.1	Deagglomeration and Mixing of Drug Particles with Silica.....	72
3.4.2	Powder flow characterization of drug/silica mixture.....	74
3.4.3	Solubility.....	76
3.4.4	Physical stability upon storage.....	76

3.5	Conclusions	78
3.6	Acknowledgments	78
3.7	References	79
4	Nano-Mixing by Sonication in Liquid CO ₂	95
4.1	Abstract	95
4.2	Introduction	96
4.2.1	Background	99
4.3	Materials and methods	102
4.3.1	Materials	102
4.3.2	Production of dipyridamole nanoflakes	102
4.3.3	Production of polyvinylpyrrolidone nanopowder	103
4.3.4	Deagglomeration and mixing in liquid CO ₂	103
4.3.5	Drug Homogeneity	105
4.3.6	Drug Dissolution	105
4.3.7	Compressibility index	106
4.3.8	Hausner ratio	107
4.3.9	Scanning electron microscopy	107
4.4	Result and Discussion	107
4.4.1	Production of drug and PVP nanopowders	107
4.4.2	Mixing of drug nanoflakes with microfine lactose	109
4.4.3	Deagglomeration and mixing of dipyridamole with PVP	113
4.4.4	Deagglomeration and mixing of lactose/silica and dipyridamole/silica ...	114
4.5	Conclusions	117

4.6	Acknowledgments	118
4.7	References	118
5	Simultaneous Particle Formation and Mixing	145
5.1	Abstract	145
5.2	Introduction	146
5.3	Theoretical Background	148
5.3.1	Particle suspension	148
5.3.2	Mixture definitions	149
5.4	Materials and methods	150
5.4.1	Materials	150
5.4.2	Production and Co-mixing of Microparticles of Drug with Excipients....	150
5.4.3	Preparation of Physical mixture	151
5.4.4	Drug Content Homogeneity	151
5.4.5	Particle Size analysis	152
5.4.6	Dissolution Studies	153
5.4.7	Scanning Electron Microscopy	153
5.4.8	Powder X-ray diffractometry	154
5.4.9	Differential scanning calorimetry	154
5.4.10	Fourier Transform Infrared Spectroscopy (FT-IR spectroscopy)	154
5.5	Result and Discussion	155
5.5.1	Simultaneous particle formation and mixing	155
5.6	Conclusions	163
5.7	Acknowledgment	163

5.8	References	163
6	Dissolution-rate Enhancement by Adsorption onto Silica	185
6.1	Abstract	185
6.2	Introduction	186
6.3	Materials and Method.....	188
6.3.1	Materials	188
6.3.2	Adsorption of drug onto silica	188
6.3.3	Fourier Transform Infrared Spectroscopy (FT-IR spectroscopy)	189
6.3.4	Powder X-ray diffraction	189
6.3.5	Differential scanning calorimetry (DSC).....	189
6.3.6	Scanning electron microscopy (SEM)	190
6.3.7	Saturation Solubility	190
6.3.8	Drug dissolution.....	190
6.3.9	Physical Stability	191
6.4	Result and Discussion	191
6.4.1	Loading of drug onto silica.....	191
6.4.2	Infrared spectroscopy.....	192
6.4.3	Crystallinity.....	192
6.4.4	DSC study.....	193
6.4.5	Morphology.....	193
6.4.6	Saturation solubility	194
6.4.7	Dissolution	194
6.4.8	Physical stability	195

6.5	Conclusions	196
6.6	Acknowledgments	197
6.7	References	198
7	Conclusions and Future Work	209
	Appendix A: Agglomerates and Aggregates	213
A.1	Introduction and Definitions	213
A.2	References	214
	Appendix B: Forces among Nanoparticles	216
B.1	Van der Waals Forces	216
B.1	References	217
	Appendix C: Powder Mixing	219
C.1	Introduction	219
C.2	Definitions	219
C.3	Mixing mechanisms	220
C.4	Characterization of mixture	220
C.5	Mixers ^[9]	223
C.1	References	224
	Appendix D: Excipients	229
D.1	Introduction	229
D.1	References	229
	Appendix E: Drug Nanoparticles Synthesis	233
E.1	Introduction ^[1-4]	233
E.1.1	Wet Milling	233

E.1.2	High-pressure homogenization	234
E.1.3	Emulsification Technology	235
E.1.4	Spray Freezing into Liquid	235
E.1.5	Evaporative precipitation into aqueous solution.....	235
E.1.6	Supercritical Fluid Technology ^[5-9]	236
E.1.7	RESS/RESS-SC/RESOLV/RESAS	236
E.1.8	PGSS	237
E.1.9	GAS/SAS/ASES/SAS-EM/SEDS	238
E.1	References	239
Appendix F:	Ultrasound.....	248
F.1	Introduction	248
F.2	Ultrasound processor and design of probe	248
F.1	References	250
Appendix G:	Publications and Presentations.....	257
G.1	Patent Application	257
G.2	Journal Publications	257
G.3	Conferences.....	258

List of Tables

Table 1.1 Various fluids and their critical temperature and pressure [3].....	19
Table 1.2 Properties of supercritical fluids as compared to liquids and gas [48].	20
Table 2.1 Physical properties of powders.	42
Table 2.2 Experimental conditions for silica/alumina mixing.....	43
Table 2.3 Experimental conditions for silica/titania mixing.....	45
Table 2.4 Experimental conditions for silica/MWNT mixing.....	47
Table 2.5 Experimental conditions for titania/MWNT mixing.	48
Table 3.1 Physical properties of itraconazole.....	92
Table 3.2 Angle of repose, compressibility index, and Hausner ratio for mixtures and individual components.....	93
Table 3.3 Scale of flowability ^a	94
Table 4.1 Physical properties of dipyridamole [25].....	139
Table 4.2 Various properties of CO ₂ at pressure of 78 bar and 5 °C for calculation of acoustic and Blake threshold pressures [41].....	140
Table 4.3 Hamaker constants for solids, fluids and calculated solid-fluid interactions [22, 46-48].....	141
Table 4.4 Details of experiments for sonication in the liquid CO ₂ at 78 bar.....	142
Table 4.5 Handling properties for compounds and mixtures.....	144

Table 4.6 Scale of flowability [64]	144
Table 5.1 Minimum stirrer speed (Njs) required to keep particles just suspended for various compounds.	182
Table 5.2 Particle size (on volume basis) range for compound/mixture.	183
Table 5.3 Relative standard deviation at various drug loadings with excipient(s)	184
Table 6.1 Melting point depression, heat of fusion, and degree of crystallinity for fenofibrate and fenofibrate-silica formulations.	203
Table 6.2. Dissolution-rate constants from three dissolution models.	204
Table 7.1 Hamaker constants for solids, fluids and solid-fluid interactions.....	212
Table C.1 Various types of blenders and their properties [4].	228
Table D.1 Type of excipients used in tablets, capsules and powders [1].	230
Table E.1 Various methods of drug nanoparticles synthesis and their commercial applications [4,5].....	245
Table E.2 Various methods for nanoparticle synthesis and their % usage [6].	246
Table F.1 Application of variable ultrasound amplitude for different processes [3].....	255
Table F.2 Values of various parameters used in calculations of ultrasound horn (probe) length.....	255

List of Figures

Figure 1.1 Typical process flow diagram for tablet manufacture [12].	14
Figure 1.2 Biopharmaceutics Classification System [13].....	14
Figure 1.3 Mechanism of absorption of drug after release from tablet or capsule [14]. ..	15
Figure 1.4 Literature data showing [23] (a) agglomerate and particle size of furosemide drug, (b) effect of agglomeration on dissolution rate, and (c) dissolution rate after dispersion of particles.	16
Figure 1.5 Phase diagram showing supercritical fluid region [49].....	17
Figure 1.6 Summary of various methods developed for mixing of nano/micro particles using carbon dioxide as mixing media.....	18
Figure 2.1 Schematic diagram of the experimental setup for mixing nanopowders in carbon dioxide.....	49
Figure 2.2 Effect of ultrasound amplitude on intensity of segregation for powder mixtures sonicated in CO ₂ at 90×10^5 N/m ² , 45 °C. EDS analysis was performed at accelerating voltage 15 keV.	50
Figure 2.3 Effect of amplitude on intensity of segregation for (a) silica/alumina and (b) silica/titania mixtures sonicated at various pressures in CO ₂ and n-hexane. (Lines are drawn only for visual guidance).	51

Figure 2.4 Intensity of segregation versus average power consumption per unit volume (of carbon dioxide or n-hexane) for (a) silica/alumina, and (b) silica/titania mixtures. (Lines are drawn only for visual guidance). 52

Figure 2.5 SEM image of typical silica agglomerate before sonication. 53

Figure 2.6 TEM images of a silica agglomerate (a), and mixture of silica/titania agglomerates (b) after sonication in CO₂ (pressure 90×10^5 N/m², amplitude 50%). 54

Figure 2.7. SEM images of MWNT and MWNT-silica mixtures produced by sonication in CO₂ at 90×10^5 N/m²: (a) Original MWNT bundles; (b) Overview of MWNT – silica agglomerates produced by sonication at 10% amplitude. Two types of particles were observed: silica agglomerates: silica agglomerates and MWNT – silica bundles; (c) Closeup view of the surface of silica agglomerate shown in (b); (d) Closeup view of MWNT-silica agglomerate represented in (b); (e) Overview of a typical MWNT-silica bundle produced by sonication at 30% amplitude; (f). Closeup view of a surface of a MWNT-silica bundle produced by mixing at 30% amplitude. MWNT-silica mixing product of 50% amplitude has similar appearance. 55

Figure 2.8 SEM images of MWNT-titania mixtures produced by sonication in CO₂ at 90×10^5 N/m²: a) Overview of MWNT - titania agglomerates produced by sonication at 10% amplitude. (b) Overview of MWNT - titania agglomerates produced by sonication at 10% amplitude. (c) MWNT – titania agglomerates produced by sonication at 30% amplitude. (d) MWNT – titania agglomerates produced by sonication at 50% amplitude. (e) Overview of a typical MWNT - titania bundle produced by sonication at 30% amplitude; (f). Example of a compact titania agglomerate found in MWNT - titania

mixtures after sonication with 30% amplitude. These kinds of agglomerates were found in mixtures produced with all other amplitudes considered.	57
Figure 2.9 Photographs of particles obtained by mixing of MWNT with silica in n-hexane at amplitudes: (a). 10%; (b). 50%. Product of MWNT - titania mixing has similar appearance.....	59
Figure 2.10 Closeup of flake surfaces obtained by sonicating MWNT with the powders in n-hexane at various amplitudes: (a)MWNT-silica, 10% amplitude; (b) MWNT-silica, 50% amplitude; (c) MWNT-titania, 10% amplitude; (d). MWNT-titania, 50% amplitude.	60
Figure 2.11 Example of MWNT-silica particle binding after sonication of MWNT and silica particles in n-hexane at 30% amplitude.....	61
Figure 2.12 Reflectance spectra of carbon nanotube-silica mixture produced in CO ₂ at 90×10 ⁵ N/m ² and 45 °C (a) and n-hexane (b) at various amplitudes.....	62
Figure 2.13 Reflectance spectra of carbon nanotube-titania mixture produced in CO ₂ at 90×10 ⁵ N/m ² and 45 °C (a) and n-hexane (b) at various amplitudes.....	63
Figure 3.1 Mechanism for deagglomeration and mixing of particles during the process known as rapid depressurization of supercritical suspension (RDSS) [18].	85
Figure 3.2 Itraconazole nano-flakes (produced using SAS-EM method) cling to the spatula, because of a poor flowability of the drug powder.	85
Figure 3.3 Schematic of supercritical antisolvent with enhanced mass transfer (SAS-EM) apparatus used to produce drug nanoparticles.	86
Figure 3.4 Schematic of rapid depressurization of supercritical suspension (RDSS) apparatus used for mixing of nanoparticles.	86

Figure 3.5 Thermogravimetric analysis (TGA) of itraconazole, showing onset of decomposition at 292.42 °C.	87
Figure 3.6 SEM images of itraconazole obtained from supplier: (a) low magnification, and (b) high magnification.	87
Figure 3.7 SEM images of itraconazole nano-flakes obtained using SAS-EM method: (a) low magnification, showing loose agglomerates, and (b) high magnification, showing individual particles.	88
Figure 3.8 Particle size distribution of randomly selected drug particles (n= 60) produced via the SAS-EM method.	88
Figure 3.9 SEM images of silica agglomerates at (a) low magnification, and (b) high magnification.	89
Figure 3.10 SEM images of RDSS mixture of itraconazole with silica at (a) low magnification and (b) high magnification showing, re-agglomeration in mixed state.	89
Figure 3.11 SEM images of physical (spatula-mixed) mixture of itraconazole nanoflakes with silica showing (a) a separate presence of silica and drug agglomerates and (b) a drug agglomerate at a high magnification.	90
Figure 3.12 SEM images of itraconazole nanoflakes after storage at 90 °C for 25 days, showing (a) low magnification, low magnification; and (b) high magnification, showing fusion of individual nanoflakes.	90
Figure 3.13 RDSS mixture of silica/itraconazole nanoflakes after storage at 90°C for 25 days: (a) optical image and (b) SEM image.	91
Figure 3.14 Dissolution profiles of itraconazole and itraconazole/silica mixture.	91

Figure 4.1 Mechanism of cavitation in the liquid for deagglomeration of particles with subsequent mixing.	126
Figure 4.2 Schematics of supercritical antisolvent with enhanced mass transfer (SAS-EM) apparatus to produce drug nanoparticles.	126
Figure 4.3 Apparatus for sonication in liquid CO ₂ for deagglomeration and mixing.....	127
Figure 4.4 SEM images of dipyrnidamole particles obtained at various conditions: (a) from supplier, (b) SAS, 13 mg drug/ ml methanol, 1 ml/min, (c) SAS-EM, 5 mg drug/ml methanol, 1ml/min, 25% amplitude, (d) SAS-EM, 5mg drug/ml methanol, 1 ml/min , 40% amplitude, (e) SAS-EM, 5mg/ml dichloromethane, 1 ml/min, 40% amplitude, and (f) higher magnification of (e). All the experiments were carried out at 100 bar and 37 °C with CO ₂ (antisolvent) flow rate of 10 g/min.	128
Figure 4.5 Particle size distributions of randomly selected drug particles (n=100) from supplier and SAS-EM method (5 mg drug/ml dichloromethane, 1 ml/min, 40% ultrasound amplitude, 100 bar, 37°C, and 10 g CO ₂ /min).	129
Figure 4.6 SEM images of PVP (a) from supplier, (b) from SAS [20 mg PVP/ml dicholormethane/acentone (25/75 v/v), 0.5 ml /min, 10 g CO ₂ /min, 78 bar, and 35 °C], (c) higher magnification of (b), and (d) from SAS-EM [18 mg PVP/ml dicholormethane/acentone (25/75 v/v), 0.5 ml /min, 10 g CO ₂ /min, 78 bar, 35 °C, and 21 % ultrasound amplitude].	130
Figure 4.7 SEM images of lactose/drug mixture obtained by sonication in CO ₂ at 5 °C, 78 bar, 35 % ultrasound amplitude, and 7.5 MJ/m ³ , and by physical mixing: (a) typical agglomerate of cohesive lactose from the supplier, (b) presence of very fine lactose particles (submicron range) on the surface of larger lactose particle, (c) random and	

interactive ordered mixing of drug particles and lactose particles for 5.31 wt. % of drug in the mixture (arrow shows presence of drug nanoparticles), (d) typical presence of drug particles in drug-lactose mixture for 0.96 wt. % of drug in the mixture, (e) higher magnification of (d) coating of lactose fines on the surface of drug flakes, and (f) physical mixing (5 wt. % drug) showing separate domains of drug and lactose particles.

..... 131

Figure 4.8 Drug dissolution curves (n=3) for nanomixed- drug nanoflakes/lactose-5 wt. % drug (\times), physical mixture -drug nanoflakes/lactose- 5 wt. % drug (\blacktriangle), drug nanoflakes (\blacksquare), and supplier drug (\blacklozenge)..... 132

Figure 4.9 SEM images of deagglomeration and mixing of dipyridamole with PVP at various weight ratios and ultrasonic energy inputs for experimental condition of 35% ultrasound amplitude, 5 °C, and 78 bar: (a) drug/ PVP weight ratio of 1/1, energy input of 2 MJ/m³, (b) drug/ PVP weight ratio of 1/1, energy input of 2 MJ/m³, typical presence of drug particles trapped in PVP agglomerates, (c) drug/ PVP weight ratio of 1/3, energy input of 2 MJ/m³, and (d) drug/ PVP weight ratio of 1/3, energy input of 2 MJ/m³, presence of fused PVP nanoparticles..... 133

Figure 4.10 Effect of ultrasonic energy and temperature on deagglomeration and mixing of dipyridamole and PVP particles at 35% ultrasound amplitude, 78 bar CO₂ pressure, ultrasound energy input 68 MJ/m³, drug/PVP weight ratio 1/1, and 10 °C: (a) presence of typical agglomerate of drug particles held together due to fusion (melting) of PVP, and (b) higher magnification of (a) showing presence of individual drug particles held together by fused (melted) PVP..... 134

Figure 4.11 Effect of ultrasonic energy on deagglomeration and coating of silica particles on microfine lactose at 35% ultrasound amplitude, 5°C, 1/10 (w/w), and 78 bar (a) typical silica (R972) agglomerate, (b) presence of R972 silica agglomerates at ultrasound energy of 3.5 MJ/m³, (c) deagglomeration and coating of R972 silica agglomerates at ultrasound energy of 3.5 MJ/m³, (d) presence of R972 silica agglomerates in the size of 400-600 nm on the surface of microfine lactose, (e) presence of very thin coating of R972 silica on the surface of microfine lactose at ultrasound energy of 7.5 MJ/m³, (f) higher magnification of thin coating of R972 silica on the surface of microfine lactose, and (g) presence of M5 silica agglomerates even at 7.5 MJ/m³ ultrasound energy. 136

Figure 4.12 Effect of ultrasonic energy on deagglomeration and coating of silica particles on drug nanoparticles at 35% ultrasound amplitude, 7.5 MJ/m³, 5 °C, 1/4 (w/w), and 78 bar: (a) highly deagglomerated drug nanoparticles after mixing with R972 silica, (b) close-up of coating of R972 silica onto drug particle surface, (c) fusion of some drug particles during mixing, and (d) presence of M5 silica agglomerates. 137

Figure 4.13 Effect of higher ultrasonic energy on deagglomeration and coating of M5 silica particles on drug nanoparticles at 65% ultrasound amplitude, 15°C, 1/4 (w/w), 143.78 MJ/m³ and 68 bar: (a) presence of drug/silica agglomerates, and (b) presence of aggregate of drug particles. 138

Figure 5.1 Different type of mixing with their homogeneity factor dependent on influence of gravitational and surface forces [24]. 169

Figure 5.2 Schematic of apparatus for simultaneous particle formation and mixing using supercritical antisolvent (SAS-DEM). 170

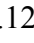
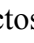
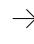
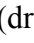
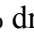
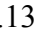



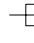
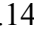
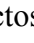
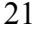



Figure 5.3 SEM images of (a) supplier drug, (b) drug produced by SAS, (b1) higher magnification of (b) showing individual particle, and (b2) close-up of (b1) showing particle made up of aggregates of several micron size particles..... 171

Figure 5.4 Particle size distribution on volume basis of (---) supplier drug, (—) drug produced by SAS, (-----) SAS-DEM mixture (drug/lactose) – 10 wt. % drug, (- · -) SAS-DEM mixture (drug/lactose) – 22 wt. % drug, and (- · -) SAS-DEM mixture (drug/lactose) – 54 wt. % drug..... 172

Figure 5.5 SEM images of drug and lactose mixture prepared by SAS-DEM method: (a) lactose particles (b) formation of interactive (ordered) mixture in which drug particles coated onto larger lactose particles for drug loading of 8 wt. % in the mixture, (c) higher magnification of (b) showing individual lactose particle and drug particles on the surface on lactose, (d) formation of ordered random mixture for drug loading of 22, 31, and 54 wt. %, and (e) presence of drug agglomerates at drug loading of 31 and 54 wt. % 173

Figure 5.6 SEM images of drug and MCC mixture prepared by SAS-DEM method: (a) MCC particles (b) formation of interactive (ordered) mixture in which drug particles coated onto larger MCC particles for drug loading of 8 wt. % in the mixture, (c) higher magnification of (b) showing individual MCC particle and drug particles on the surface on MCC, (d) formation of ordered random mixture for drug loading of 21, 37, and 51 wt. %, (e) presence of drug agglomerates at drug loading of 37 and 51 wt. %, and (f) random mixture (spatula mixing) of drug (by SAS) and MCC at 10 wt. % drug loading 175

Figure 5.7 SEM images of (a) lactose surface and (b) lactose surface in drug and lactose mixture by SAS-DEM..... 175

Figure 5.8 XRD of drug from supplier (continuous line) and drug obtained by SAS method (dotted line).....	176
Figure 5.9 XRD of physical mixture (obtained by spatula mixing) of lactose and SAS drug (continuous line) and mixture of lactose and drug obtained by SAS-DEM method (dotted line).....	176
Figure 5.10 FT-IR spectra of (a) supplier drug, (b) SAS drug, (c) physical mixture (spatula mixing) of SAS-DEM drug/lactose, (d) SAS-DEM mixture of drug/lactose, (e) physical mixture of SAS drug/MCC, and (f) SAS-DEM mixture of drug/MCC.	177
Figure 5.11 DSC thermographs of (a) supplier drug, (b) SAS drug, and (c) SAS-DEM mixture of drug/MCC- 21 wt. % drug loading.	178
Figure 5.12 Dissolution profiles (from top to bottom) of (a)  SAS-DEM mixture (drug/lactose) – 10 wt. % drug, (b)  SAS-DEM mixture (drug/lactose) – 21 wt. % drug, (c)  SAS-DEM mixture (drug/lactose) – 31 wt. % drug, (d)  SAS-DEM mixture (drug/lactose) – 54 wt. % drug, (e)  physical mixture of SAS drug/lactose – 20 wt. % drug, (f)  supplier drug, and (g)  SAS drug.	179
Figure 5.13 Dissolution profiles (from top to bottom) of (a)  SAS-DEM mixture (drug/MCC) – 13 wt. % drug, (b)  SAS-DEM mixture (drug/MCC) – 21 wt. % drug, (c)  SAS-DEM mixture (drug/MCC) – 37 wt. % drug, (d)  SAS-DEM mixture (drug/ MCC) – 51 wt. % drug, (e)  physical mixture of SAS drug/ MCC – 20 wt. % drug, (f)  supplier drug, and (g)  SAS drug.....	180
Figure 5.14 Dissolution profiles (from top to bottom) of (a)  SAS-DEM mixture (drug/lactose & MCC) – 13 wt. % drug, (b)  SAS-DEM mixture (drug/ lactose & MCC) – 21 wt. % drug, (c) SAS-DEM mixture (drug/ lactose & MCC) – 37 wt. %	

drug, (d) \blacksquare SAS-DEM mixture (drug/ lactose & MCC) – 51 wt. % drug, (e) \blacktriangle physical mixture of SAS drug/ lactose & MCC – 20 wt. % drug, (f) \square supplier drug, and (g) \blacktriangleleft SAS drug.	181
Figure 6.1 Schematic of supercritical CO ₂ apparatus for drug adsorption onto silica....	205
Figure 6.2 FTIR spectra of (a) silica, (b) physical mixture of fenofibrate and silica, and (c) fenofibrate adsorbed onto silica formulation.....	205
Figure 6.3 XRD of (I) crystalline fenofibrate, and (II) (a) silica, (b) formulation A, (c) formulation B, (d) formulation A after 1 month storage, and (e) formulation B after 1 month storage.....	206
Figure 6.4 SEM micrographs of (a) microcrystalline fenofibrate, and (b) fenofibrate adsorbed onto silica.....	207
Figure 6.5 Dissolution profiles of fenofibrate and fenofibrate-silica formulations.	208
Figure A.1 Cartoon showing agglomerate, sub agglomerates, and primary agglomerates [2].....	215
Figure A.2 Images of silica (a) sub agglomerates and (b) chain of nanoparticles.....	215
Figure B.1 Cartoon representing (a) host particle of diameter “d” separated by distance “h” and (b) host particles separated by guest particle.....	218
Figure B.2 Effect of guest particle on ratio of attractive force with spacer and without spacer for various host particle size.....	218
Figure C.1 Different type of mixing with their homogeneity factor dependent on influence of gravitational and surface forces [1].	226
Figure C.2 Scale of Segregation [8].....	227
Figure E.1 Schematic of high-pressure homogenization technique [1].....	241

Figure E.2 Schematic of rapid expansion of supercritical suspension (RESS).	241
Figure E.3 Schematic of rapid expansion of supercritical solution with solid co-solvent.	241
Figure E.4 Schematics of rapid expansion of supercritical solution in liquid solvent....	242
Figure E.5 Schematic for particles from gas saturated solution (PGSS).	242
Figure E.6 Schematics of supercritical antisolvent (SAS)/ gas antisolvent (GAS)/aerosol solvent extraction (ASES).....	243
Figure E.7 Schematics of solution enhanced dispersion by supercritical fluids (SEDS).	244
Figure E.8 Schematics of supercritical antisolvent with enhanced mass transfer (SAS- EM).	244
Figure F.1 Cartoon representing the cavitation cycle [www.sonics.biz]	252
Figure F.2 Cartoon representing the various components of ultrasonic processor and their functions [www.sonics.biz].	252
Figure F.3 Arrangement of ultrasound horn (probe) inside the pressure vessel [www.sonics.biz]	253
Figure F.4 Cartoon showing design parameters of horn (probe).	254

1 INTRODUCTION

1.1 Importance of Nanomixing

Nanoparticles offer unique properties due to their small size and high surface area [1, 2]. For example, the percent of surface molecules increases from 0.30 for a particle size of 1,000 nm to 27.1 for a particle size of 10 nm [3]. Nanoparticles have potential applications in the field of biomedical (e.g. quantum dots for disease detection, nanosilver coating on wound dressing), pharmaceuticals (e.g. nanoparticles of poorly water soluble drugs for bioavailability enhancement), personal care (e.g. sunscreen lotion containing inorganic nanoparticles of titanium and zinc oxide), surfaces (e.g. higher surface area of drug nanoparticles for high dissolution rates, activity of catalyst, coating for self cleaning surfaces like on glass windows of automobiles), environmental (e.g. for effective water filtration systems), energy (e.g. high energy density and fast charging batteries like lithium titanate nanomaterial, high performance solar cells like use of titania and carbon nanotube films, hydrogen storage, catalyst for various reactions), magnetic (e.g. application of nanomagnetic particles for better contrast MRI images), optical (e.g. antireflection coatings), mechanical (e.g. nanocomposites which are lighter and stronger), and electronic (e.g. high conductivity materials). Unfortunately, the high surface area of particles causes them to agglomerate (more discussion has been presented in Appendix A on term agglomeration) due to high interparticle van der Waals attractions

especially for particle sizes less than 50 μm [4], making them lose some of their unique properties. For example, highly dispersed or deagglomerated carbon nanotubes (CNTs) in epoxy composites have better rheological, mechanical, electrical, and thermal properties as compared to agglomerated CNTs [5]. Mixture consisting of nanocrystalline copper and cobalt in deagglomerated state shows better magnetic properties than mixtures having agglomerated particles [6]. A deagglomerated and mixed thermite mixture of aluminium and iron oxide as well as titanium and carbon shows a better burning rate than a mixture containing agglomerated component particles [7, 8]. The agglomeration can be avoided by adding spacer material [9] (brief discussion has been presented in Appendix B on attractive forces in nanoparticles and effect of spacer particle on these forces), but it is important to have a spacer particle around each nanoparticle to preserve its properties. Hence, it is most important to mix nanoparticles of different materials effectively. Mixing of solid particles is widely practiced in various industries including pharmaceutical, food, cosmetics, fertilizers, pigment, detergent, animal feed, etc. Recent increase in the popularity of nanocomposites, nanocatalyst and nano-pharmaceuticals demands effective mixing of nanoparticles, which often poses challenges due to the small size. Often processes of mixing involve the breaking of micro-agglomerates and then subsequent mixing with other (inert) nano materials to prevent preferential agglomeration of same material particles. Nanomixing can also be achieved by simultaneous production of different nanoparticles in the same reaction chamber (e.g. titania/silica by flame aerosol synthesis or flame synthesis of metal and oxide nanoparticles) for nanocomposite applications. However, there are many situations when simultaneous production is not possible, and the separately produced particles must be mixed.

Powder mixing (more discussion has been presented in Appendix C) is a very important unit operation in the pharmaceutical industry as it directly affects the drug content uniformity in the final drug (API, active pharmaceutical ingredient) and excipient (filler) mixture [10, 11]. Appendix D gives examples of excipients used in the manufacturing of tablets, capsules, and powders [12]. More than 80% of the pharmaceuticals manufactured are in solid dosage forms mainly in tablets and capsules (Figure 1.1 shows a typical manufacturing process for tablets) where content homogeneity or uniformity is important issue to the dose uniformity of the final product. More than 40% of the drugs or 2 out of 3 drugs in discovery pipeline are poorly water soluble, having solubility less than 100 µg/ml. When the ratio of drug dose to lowest drug saturation solubility (in the pH range of 1-8) is greater than 250, the drug is called as poorly water soluble. For example, if drug has dosage of 250 mg and saturation solubility less than 1 mg/ml, then drug is called poorly water soluble. Bioavailability (% drug absorbed in the body into the circulation) of poorly-water-soluble hydrophobic drugs (Figure 1.2, Class II in Biopharmaceutics Classification System) is limited by their solubility and dissolution rate [13]. Figure 1.3 shows mechanism of absorption of drug in gastrointestinal tract after release from tablet or capsule [14]. Dissolution rate of drug is given by the Noyes-Whitney equation [15]

$$\text{Dissolution rate} = \frac{A.D}{h} \left(C_s - \frac{X_d}{V} \right) \quad (1)$$

where, A is surface area, D is diffusion coefficient, h is boundary layer thickness, C_s is saturation solubility, X_d is the amount dissolved, V is volume of fluid. Therefore, the dissolution rate can be improved by decreasing the particle size (by increasing surface area) and/or crystallinity (e.g. solid dispersion, amorphous drug formulation) [16-18].

Other ways of increasing the drug dissolution rate are complexing with cyclodextrin and salt formation which both techniques found to increase saturation solubility of the drug. Also Freundlich-Ostwald suggested that saturation solubility of a nanosized particle increases as compared to a larger particle size. The Freundlich-Ostwald equation for increase in saturation solubility of nanosized drug particle is given as follows [19]

$$C_s = C_\infty \exp\left[\frac{2\gamma M}{r\rho RT}\right] \quad (2)$$

where, C_s is the saturation solubility of nanosized API (active pharmaceutical ingredient), C_∞ is the saturation solubility of an infinitely large API crystal, γ is the crystal-medium interfacial tension, r is the particle radius, ρ is the density of particle, M is the molecular weight of compound, R is the gas constant, T is the temperature. Typical value of γ is 15-20 mN m⁻¹. However, the fine drug particles have a high tendency to agglomerate due to van der Waals attraction or hydrophobicity, decreasing surface area over the time [20-22], this in turn causes decrease in the dissolution rate or bioavailability [22, 23]. De Villier [23] has studied effect of furosemide drug particles agglomeration on dissolution rate. He has observed a substantial decrease in dissolution rate of finer drug particles due to agglomeration. After dispersion of drug agglomerates, finer particles showed highest dissolution rate (Figure 1.4). Agglomeration of particles can affect granulation, fluidization, mixing, and blending operations [24]. The presence of cohesive-particle agglomerates decreases the efficiency of mixers and affects the powder flow due to bridging and spatial heterogeneity [25]. For a better uniformity of drug formulation or obtaining homogeneous mixture (especially for cohesive powder mixtures having a low drug dosage), it is very important to deagglomerate fine cohesive drug particles and intimately mix them with excipients to prevent further agglomeration during subsequent

unit operations.

Recently, drug delivery by inhalation has increased, creating the demand for the efficient deagglomeration and mixing of cohesive drug particles with excipients like lactose. Currently, available mixers are not effective in deagglomeration of highly-cohesive drug particles smaller than 10 μm in size; or they require very high shear or impaction, which indeed act as a particle size reduction device rather than a conventional mixer [26]. For example, rotary and vibratory ball mills can be used for mixing of fine powders [27, 28]; however the use of high energy may affect the crystal lattice of the particles which can influence the physico-chemical stability. The tumbler, most common mixing equipment in pharmaceutical industry, is not effective if de-agglomerates is required [29]. Formation of random and interactive ordered mixture by deagglomeration and mixing of drug with excipient improves dissolution rate (and bioavailability) of poorly water soluble drugs [30-33]. Preblending which involves deagglomeration and mixing of cohesive drug particles with excipients found to be useful and has been suggested during various drug mixing studies in the literature [10, 34].

Preblending of drug particles with excipients such as silica, lactose, etc. have advantages including: (a) improved flowability of drug powder or reduced segregation which leads to effective mixing with other excipient using conventional mixers [35], (b) decreased electrostatic charge of fine drug particles (charging of drug nanoparticles can lead to several problems in mixing or other operations due to clinging of particles to vessel wall surface or agitator surface [36]), (c) increased effective wetting (due to hydrophilicity of excipient particles) and increases prevention of re-agglomeration of drug particle during dissolution (Hydrophobic drugs suffer from wetting and re-

agglomeration in dissolution media [37-40]), and (d) better drug homogeneity of drug in the dose.

Various recent studies involving dispersion of nanoparticle agglomerates (especially silica) in liquid media have been carried out in the systems involving high shear stresses such as high shear impeller mixers, high pressure dispersion system, rotor-stator system, etc. [41-44]. Linsenbuhler and Wirth [45] have carried out deagglomeration and coating of silica nanoparticles on the lactose particles using rotor-stator system (Ultra-Turrax-Disperser) involving liquid nitrogen as a media; although they did not study deagglomeration and mixing with cohesive drug nanoparticles.

Various methods of nanoparticles mixing for such cases are introduced and compared by Wei et al. [46] and Yang et al. [47]. It was shown that the rapid expansions of particle suspensions and wet mixing in n-hexane using ultrasound show better performance than other methods (e.g., magnetically assisted impact mixing and stirred mixing in high pressure CO₂). Mixing of nanoparticles with sonication in liquid medium involves cavitation and intense agitation of liquid due to ultrasound propagation. Sonication in liquids (e.g., n-hexane, water) has several disadvantages, such as material has to wet the liquid and involves additional steps of filtration and drying as well as the mixture contains residual solvent.

1.2 Research Methods

1.2.1 Materials

Due to application of nanomixing in various fields, nanomaterials are selected to represent their application in different fields. Therefore in the broader sense,

nanomaterials are differentiated in two classes as inorganic and organic. For inorganic class, nanomaterials like silica (SiO_2), alumina (Al_2O_3), titania (TiO_2) and multiwalled carbon nanotubes (MWNT) are selected for studies. Silica has been used as a glidant in pharmaceutical industry as well as it has application in ceramic nanocomposites. Titania has been known for its photo catalytic activity as well as finding titania/carbon nanotube composites finding application in next generation solar cells. All nanomaterials from inorganic class were obtained from a commercial supplier like Degussa Inc. For organic class, ideal candidates for studies were pharmaceutical poorly water soluble drugs. The organic drug nanomaterials (itraconazole, dipyridamole, and nevirapine) were prepared into the laboratory using the supercritical antisolvent (SAS) / supercritical antisolvent solvent-enhanced mass transfer (SAS-EM) method due to unavailability of drug in nanoscale from commercial suppliers. Drug nanoparticles can be synthesized using various methods whose brief descriptions can be found in Appendix E.

1.2.2 *Mixing Methods*

In this work, we replace liquid media (e.g., n-hexane) for mixing of nanomaterials by carbon dioxide. Carbon dioxide is an environmentally benign, inert, non toxic, non flammable, inexpensive, low viscosity fluid along with comparatively higher molar density. Supercritical carbon dioxide was utilized as the antisolvent in SAS-EM method for drug nanoparticles synthesis and was used also as the media in the mixing methods, due to its mild critical point (73.7 bar and 31.1°C) and suitability for processing of pharmaceutical compounds (Table 1.1) [3]. Table 1.2 shows comparison of properties of Supercritical fluid with liquid and gases [48]. Supercritical fluids (CO_2) have unique

properties like diffusivity which is 100 times greater than liquids and density which can be easily changed with pressure. Figure 1.4 shows phase diagram for carbon dioxide [49]. Upon depressurization, CO₂ leaves the solid matrix without any residues. Use of CO₂ for mixing can also decrease the presence of residual solvents in drug nanoparticles which are produced by other methods (e.g., wet milling). The following methods (Figure 1.6) were developed by applying various types of forces in CO₂ media and demonstrated for deagglomeration and mixing of nanopowders: (1) rapid depressurization of supercritical suspension (RDSS), (2) sonication in high pressure CO₂, (3) sonication in liquid CO₂, (4) simultaneous particle formation and mixing, and (5) stirred mixing in liquid CO₂ (future work).

1.3 References

- [1] M. G. Lines. Nanomaterials for practical functional uses. *J Alloys Compd.* 449 (2008) 242-5.
- [2] M. C. Roco. Nanoparticles and nanotechnology research. *J Nanopart Res.* 1 (1999) 1-6.
- [3] R. B. Gupta, U. B. Kompella, eds. *Nanoparticle technology for drug delivery.* New York: Taylor & Francis 2006.
- [4] J. A. Kurkela, D. P. Brown, J. Raula, E. I. Kauppinen. New apparatus for studying powder deagglomeration. *Powder Technol.* 180 (2008) 164-71.
- [5] Y. S. Song, J. R. Youn. Influence of dispersion states of carbon nanotubes on physical properties of epoxy nanocomposites. *Carbon.* 43 (2005) 1378-85.
- [6] Y. Champion, H. Meyer, J.-L. Bonnentien, E. Chassaing. Fabrication of Cu-Co

nanogranular bulk materials by mixing of nanocrystalline powders. *J Magn Magn Mater.* 241 (2002) 357-63.

[7] E. Marioth, H. Kroeber, S. Loebbecke, I. Fuhr, H. Krause. Desagglomeration and mixing of nanoparticles using rapid expansion of supercritical dispersions. *PARTEC*. Nuremberg, Germany 2007.

[8] C.-C. Chen, C.-K. Yu. Two-dimensional image characterization of powder mixing and its effects on the solid-state reactions. *Mater Chem Phys.* (2004) 227-37.

[9] J. H. Werth, Linsenbuhler, S. M. Dammer, Z. Frakas, H. Hinrichsen, K.-E. Wirth. Agglomeration of charged nanopowders in suspensions. *Powder Technol.* 133 (2003) 106-12.

[10] T. P. Garcia, A. Carella, V. Pansa. Identification of factors decreasing the homogeneity of blend and tablet uniformity. *Pharm Technol.* (2004(March)).

[11] M. M. DeVilliers, J. G. VanderWatt. The measurement of mixture homogeneity and dissolution to predict the degree of drug agglomerate breakdown achieved through powder mixing. *Pharm Res.* 11 (1994) 1557-61.

[12] K. Y. Fung, K. M. Ng. Product-centered processing: pharmaceutical tablets and capsules. *AIChE J.* 49 (2003) 1193-215.

[13] G. L. Amidon, H. Lennernas, V. P. Shah, J. R. Crison. A theoretical basis for a biopharmaceutical drug classification: the correlation of in vitro drug product dissolution and in vivo bioavailability. *Pharm Res.* 12 (1995) 413-20.

[14] J. B. Dressman, C. Reppas. In vitro-in vivo correlations for lipophilic, poorly water-soluble drugs. *Eur J Pharm Sci.* 11 (2000) S73-S80.

[15] A. Noyes, W. Whitney. The rate of solution of solids substances in their own

solutions. *J Am Chem Soc.* 19 (1897) 930-4.

[16] A. Jounela, P. Pentikainen, A. Sothmann. Effect of particle size on the bioavailability of digoxin. *Eur J Clin Pharmacol.* 8 (1975) 365-70.

[17] G. G. Liversidge, K. C. Cundy. Particle size reduction for improvement of oral bioavailability of hydrophobic drugs: absolute oral bioavailability of nanocrystalline danazol in beagle dogs. *Int J Pharm.* 125 (1995) 91-7.

[18] N. Rasenack, B. W. Muller. Dissolution rate enhancement by in situ micronization of poorly water-soluble drugs. *Pharm Res.* 19 (2002) 1894-900.

[19] F. Kesisoglou, S. Panmai, Y. Wu. Nanosizing - Oral formulation development and biopharmaceutical evaluation. *Adv Drug Delivery Rev.* 59 (2007) 631-44.

[20] A. J. Aguiar, A. W. Zelmer, A. W. Kinkel. Deaggregation behavior of a relatively insoluble substituted benzoic acid and its sodium salt. *J Pharm Sci.* 56 (1967) 1243-52.

[21] P. Finholt, S. Slovang. Dissolution kinetics of drugs in human gastric juice the role of surface tension. *J Pharm Sci.* 57 (1968) 1322-6.

[22] E. Swanepoel, W. Liebenberg, M. M. D. Villiers. Dissolution properties of proxicam powders and capsules as a function of particle size and the agglomeration of powders. *Drug Dev Ind Pharm.* 26 (2000) 1067-76.

[23] M. M. D. Villiers. Influence of agglomeration of cohesive particles on the dissolution behaviour of furosemide powder. *Int J Pharm (Kidlington).* 136 (1996) 175-9.

[24] J. K. Prescott, R. A. Barnum. On the powder flowability. *Pharm Technol.* 10 (2000) 60-84.

[25] K. Thalberg, D. Lindholm, A. Axelsson. A comparison of different flowability tests for powders for inhalation. *Powder Technol.* 146 (2004) 206-13.

- [26] N. Harnby, M. F. Edwards, A. W. Nienow. *Mixing in process industries*. London: Butterworth 1990.
- [27] I. Krycer, J. A. Hersey. A comparative study of comminution in rotary and vibratory ball mill. *Powder Technol.* 27 (1980) 137-41.
- [28] I. Krycer, J. A. Hersey. Fine powder mixing in vibratory ball mill. *Int J Pharm.* 6 (1980) 119-29.
- [29] N. Harnby. An engineering view of pharmaceutical powder mixing. *Pharm Sci Technol Today.* 3 (2000) 303-9.
- [30] C. Nystrom, M. Westerberg. The use of ordered mixtures for improving the dissolution rate of low solubility compounds. *J Pharm Pharmacol.* 38 (1986) 161-5.
- [31] C.-L. Teng, C. Hsiao, J. Gatts, inventors; Impax Laboratories, Inc., assignee. Drug delivery system for enhanced bioavailability of hydrophobic active ingredients. United States patent US 6531158 B1. 2003.
- [32] J. W. McGinity, C.-T. Ku, R. Bodmeier, M. R. Harris. Dissolution and uniformity of ordered mixes of micronized griseofulvin and a perfectly compressible excipient. *Drug Dev Ind Pharm.* 11 (1985) 891-900.
- [33] N. H. Shah, W. Phuapradit, M. Bachynsky, M. H. Infled, K. Iqbal, A. W. Malick. High energy ordered mixture for improving the dissolution rate of sparingly soluble compounds. *Drug Dev Ind Pharm.* 20 (1994) 873-88.
- [34] O. S. Sudah, P. E. Arratia, D. Coffin-Beach, F. J. Muzzio. Mixing of cohesive pharmaceutical formulations in tote (bin) blenders. *Drug Dev Ind Pharm.* 28 (2002) 905-18.
- [35] I. Zimmermann, K. Meyer. Effects of glidant in binary powder mixtures. *Powder*

Technol. 139 (2004) 40-54.

[36] H. Watanabe, M. Ghadiri, T. Matsuyama, L. Y. Ding, K. G. Pitt, H. Maruyama, et al. Triboelectrification of pharmaceutical powders by particle impact. *Int J Pharm.* 334 (2007) 149-55.

[37] B. Always, R. Sangchantra, P. J. Stewart. Modeling the dissolution of diazepam in lactose interactive mixtures. *Int J Pharm.* 130 (1996) 213-24.

[38] J. Liu, J. Stewart. Deaggregation during dissolution of benzodiazepines in interactive mixtures. *J Pharm Sci.* 87 (1998) 1632-8.

[39] P. J. Stewart, F.-Y. Zhao. Understanding agglomeration of indomethacin during the dissolution of micronised indomethacin mixtures through dissolution and de-agglomeration modeling approaches. *Eur J Pharm Biopharm.* 59 (2005) 315-23.

[40] M. Westerberg, C. Nystrom. Physicochemical aspects of drug release. Part 18. Use of a surfactant and disintegrant for improving drug dissolution rate from ordered mixtures. *STPPharm Sci.* 3 (1993) 142-7.

[41] J. Baldyga, W. Orciuch, L. Makowski, K. Malik, G. Oezcan-Taskin, W. Eagles, et al. Dispersion of nanoparticle clusters in rotor-stator mixer. *Ind Eng Chem Res.* (2008).

[42] P. Ding, A. W. Pacek. De-agglomeration of silica nanoparticles in the presence of surfactants. *J Dispersion Sci Technol.* 29 (2008) 593-9.

[43] R. Wengler, H. Nirschl. Turbulent hydrodynamic stress induced dispersion and fragmentation of nanoscale agglomerates. *J Colloid Interface Sci.* 306 (2007) 262-73.

[44] L. Xie, C. D. Rielly, G. Ozcan-Taskin. Break-up of nanoparticle agglomerates by hydrodynamically limited processes. *J Dispersion Sci Technol.* 29 (2008) 573-9.

[45] M. Linsenbuhler, K.-E. Wirth. An innovative dry powder coating process in non-

polar liquids producing tailor-made micro-particles. Powder Technol. 158 (2005) 3-20.

[46] D. Wei, R. Dave, R. Pfeffer. Mixing and characterization of nanosized powders: an assesment of different techniques. J Nanopart Res. 4 (2002) 21-41.

[47] J. Yang, Y. Wang, R. N. Dave, R. Pfeffer. Mixing of nano-particles by rapid expansion of high-pressure suspensions. Adv Powder Technol. 14 (2003) 71-93.

[48] T. Yasuji, H. Takeuchi, Y. Kawashima. Particle design of poorly water-soluble drug substances using supercritical fluid technologies. Adv Drug Delivery Rev. 60 (2008) 388-98.

[49] R. B. Gupta, J. J. Shim. Solubility in supercritical carbon dioxide. New York: Taylor and Francis Group 2007.

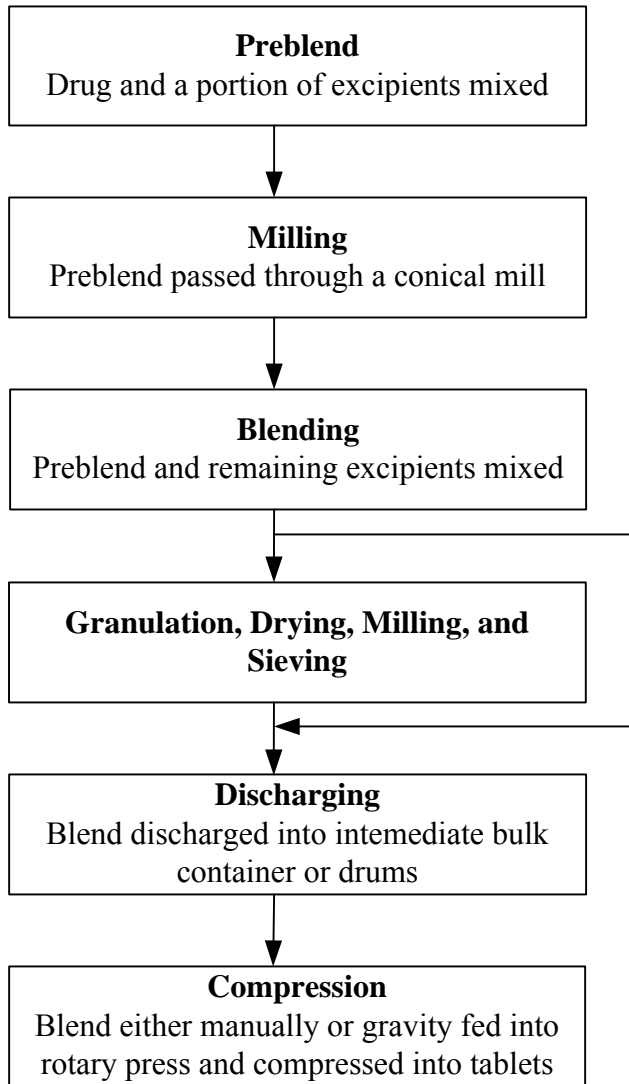


Figure 1.1 Typical process flow diagram for tablet manufacture [12].

<p>Class I High Solubility, High permeability compounds</p>	<p>Class II Low-Solubility, High permeability compounds</p>
<p>Class III High Solubility, Low-permeability compounds</p>	<p>Class IV Low-Solubility, Low permeability compounds</p>

Figure 1.2 Biopharmaceutics Classification System [13].

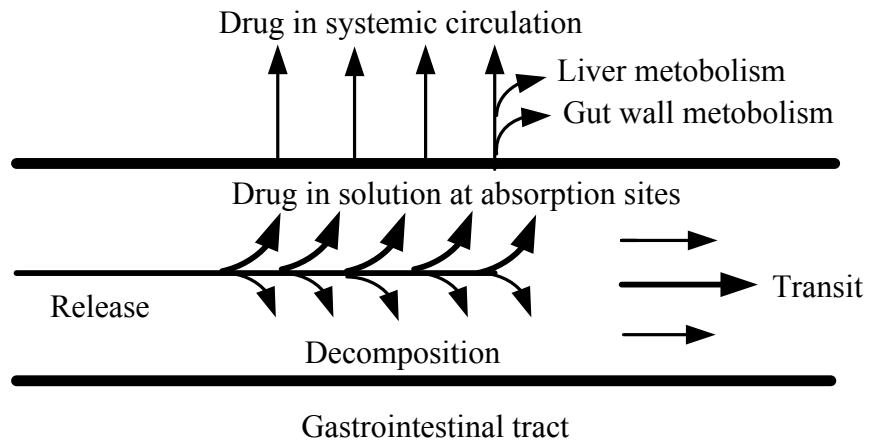


Figure 1.3 Mechanism of absorption of drug after release from tablet or capsule [14].

Table 1
Mean volume particles size, before and after dispersion, of different sized microfine furoseamide powders

Powder	Agglomerates		Dispersed particles	
	Size (μm)	Method	Size (μm)	Method
A	108	Helos	3	Rodos
B	38	Helos	10	Rodos
C	27	Helos	19	Rodos

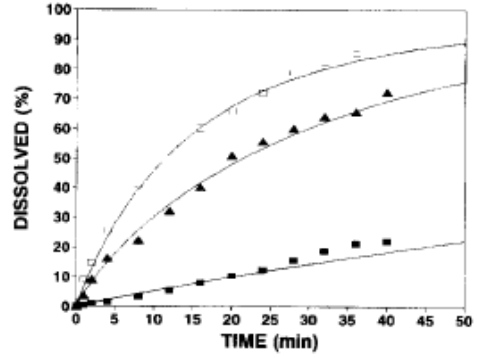


Fig. 2. Dissolution of different sized furoseamide particles before dispersion: (■) powder A; (Δ) powder B and (\square) powder C. Markers represent the mean measured values and lines the best fit according to Eq. (1).

(a)

(b)

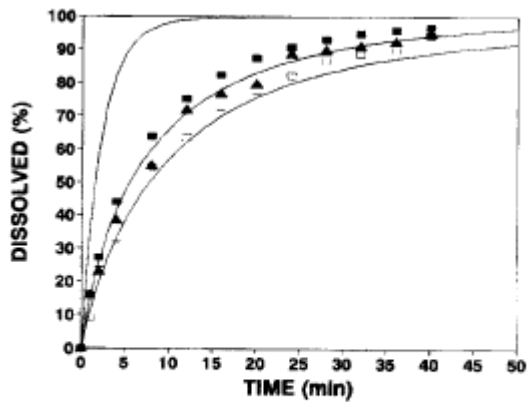


Fig. 3. Dissolution of different sized furoseamide particles after dispersion: (■) powder A; (Δ) powder B and (\square) powder C. Markers represent the mean measured values and lines the best fit according to Eq. (1).

(c)

Figure 1.4 Literature data showing [23] (a) agglomerate and particle size of furoseamide drug, (b) effect of agglomeration on dissolution rate, and (c) dissolution rate after dispersion of particles.

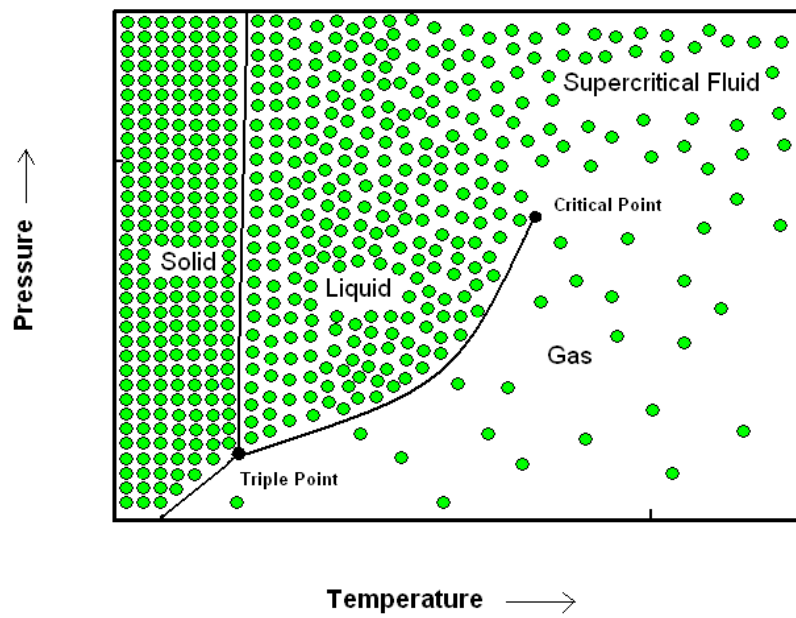


Figure 1.5 Phase diagram showing supercritical fluid region [49].

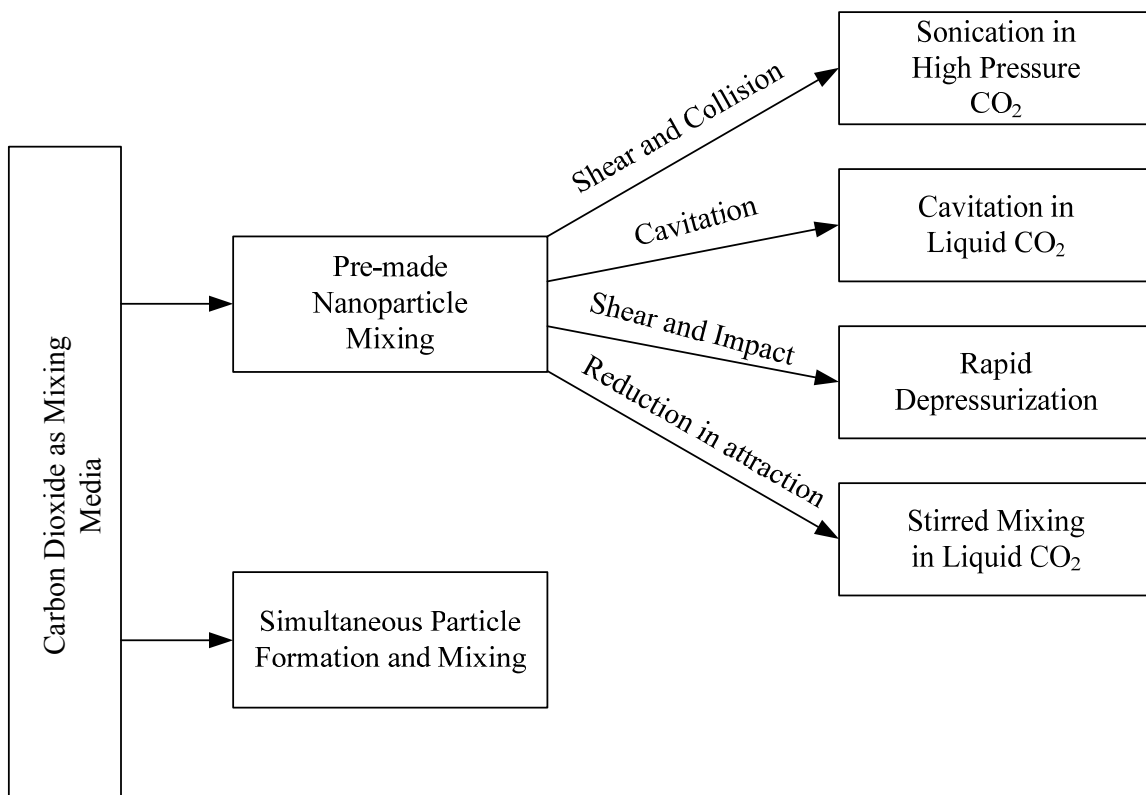


Figure 1.6 Summary of various methods developed for mixing of nano/micro particles using carbon dioxide as mixing media.

Table 1.1 Various fluids and their critical temperature and pressure [3].

Supercritical fluid	T_c (°C)	P_c (bar)
Ethylene	9.3	50.3
Trifluoromethane (fluoroform)	25.9	47.5
Chlorotrifluoromethane	28.9	39.2
Ethane	32.3	48.8
Carbon dioxide	31.1	73.7
Dinitrogen monoxide (laughing gas)	36.5	72.6
Sulfur hexafluoride	45.5	37.6
Chlorodifluoromethane	96.4	49.1
Propane	96.8	43.0
Ammonia	132.4	112.7
Dimethyl ether	126.8	52.4
Trichlorofluoromethane	198.0	44.1

Isopropanol	235.2	47.6
Cyclohexane	280.3	40.7
Toulene	318.6	41.1
Water	374.0	220.5
Ethanol	240.8	61.4

Table 1.2 Properties of supercritical fluids as compared to liquids and gas [48].

Property	Liquid	SCF	Gas
Density (kg/m ³)	1000	200-900	0.6-1
Viscosity (μPa.s)	10 ⁻³	10 ⁻⁵ -10 ⁻⁴	10 ⁻⁵
Diffusion Coefficient (m ² /s)	<10 ⁻⁹	10 ⁻⁷ -10 ⁻⁸	10 ⁻⁵
Heat Conductivity (W/mK)	<10 ⁻¹	10 ⁻³ -10 ⁻¹	10 ⁻³

2 NANOMIXING BY SONICATION IN HIGH-PRESSURE CO₂

2.1 Abstract

Due to the increased use of nanocomposites, mixing at nanoscale has become important. Current mixing techniques can be classified into: (a) dry mixing (mechanical mixing), (b) wet mixing, and (c) simultaneous production of mixed nanoparticles (when possible). Dry mixing is in general not effective in achieving desired mixing at nanoscale, whereas wet mixing suffers from different disadvantages like nanomaterial of interest should be insoluble, has to wet the liquid, and involves additional steps of filtration and drying. This paper examines the use of pressurized carbon dioxide having high density and low viscosity to replace the liquids (e.g., n-hexane, toluene). Ultrasound is applied to the suspension of nanopowders in gaseous and supercritical carbon dioxide where high impact collisions during sonication help mixing and the final mixture is obtained by simple depressurization. The method is tested for binary mixture of alumina/silica, silica/titania, MWNT (multiwalled carbon nanotubes)/silica, and MWNT/titania. The effects of sonication intensity and pressure on the degree of mixing are studied. Comparative study is also done with liquid n-hexane as a mixing media. Quantitative characterization (e.g., mean composition standard deviation, intensity of segregation) of mixing of alumina/silica and silica/titania is done with energy dispersive x-ray spectroscopy, and that of MWNT/silica and MWNT/titania is done using field emission

scanning electron microscopy and day-light illumination spectrophotometry. Results show that mixing in carbon dioxide at higher ultrasound amplitudes is as good as in liquid n-hexane, and the final mixed product does not contain any residual media as in the case of liquid n-hexane.

2.2 Introduction

Nanoparticles offer unique properties due to their small size and high surface area [1,2]. Unfortunately, the high surface area of particles causes them to agglomerate due to high interparticle van der Waals attractions [3], making them lose some of their unique properties. The agglomeration can be avoided by adding spacer material [4], but it is important to have spacer particle around each nanoparticle to preserve its properties. Hence, it is most important to mix nanoparticles of different materials effectively. Mixing of solid particles is widely practiced in various industries including pharmaceutical, food, cosmetics, fertilizers, pigment, detergent, animal feed, etc. Recent increase in the popularity of nanocomposites, nanocatalyst and nano-pharmaceuticals demands effective mixing of nanoparticles, which often poses challenges due to the small size. Often processes of mixing involve the breaking of micro-agglomerates and then subsequent mixing with other (inert) nano material to prevent preferential agglomeration of same material particles. Nanomixing can also be achieved by simultaneous production of different nanoparticles in same reaction chamber (e.g. titania/silica by flame aerosol synthesis or, flame synthesis of metal and oxide nanoparticles) for nanocomposite applications. However, there are many situations when simultaneous production is not possible, and the separately produced particles must be mixed. Various methods of

nanoparticles mixing for such cases are introduced and compared by Wei et al. [5] and Yang et al. [6]. It was shown that the rapid expansions of suspension of particles and wet mixing in n-hexane with ultrasound show better performance than other methods (e.g., magnetically assisted impact mixing, and stirred mixing). Mixing of nanoparticles with sonication in liquid medium involves cavitation and intense agitation of liquid due to ultrasound propagation. Organic liquids, such as n-hexane, are suitable for insoluble inorganic material also those which wet the n-hexane for better result. Therefore for organic material, n-hexane is not a good choice of solvent. In addition, the wet mixing using a solvent involves additional steps of filtration and drying.

In this work, we propose to replace n-hexane by carbon dioxide. Carbon dioxide is an environmentally benign, inert, non toxic, non flammable, inexpensive, low viscosity fluid along with comparatively higher molar density. These unique properties of high pressure carbon dioxide help in propagation of ultrasound. Pressure amplitudes created during propagation of ultrasound cause particles suspended in high pressure CO₂ media to be put into oscillatory motion. This involves motion of particles from a region of high pressure (compression) to low pressure (rarefaction), which induces collisions of particles with each other resulting into breakage of loose agglomerates and mixing of dissimilar particles. The final mixture is easily separated from CO₂ by depressurization. Also material does not have to wet the media; hence this method can be applied to a wide range of material mixtures. Here, the method is tested for binary mixtures of alumina (Al₂O₃), silica (SiO₂), and titania (TiO₂) along with multiwalled carbon nanotubes (MWNT).

Silica and alumina have weak cohesive attraction among its particles, hence its

micro-agglomerates are easier to break, whereas titania has strong cohesive attraction among its particles, and hence its agglomerates are relatively difficult to break. The weak agglomeration of alumina and silica powders is evident from their free flowing nature in contrast to titania powders. Silica has been used extensively in food and pharmaceutical industries because it helps in free flowing of powder which is due to silica nanoparticles surrounding host particles.

Mixing of silica/alumina and silica/titania were studied quantitatively by energy dispersive x-ray spectroscopy (EDS). Intensity of segregation of mixture was taken as criteria for degree of mixing. The qualitative analysis of mixing of MWNT with silica or titania was carried out using field emission secondary electron microscopy (FESEM), because of the distinct difference in size and shape of component particles. Day-light spectrophotometry was also used to characterize MWNT mixtures due to difference in color of mixture (in visible light spectrum) with increase in homogeneity.

2.3 Experimental

2.3.1 Materials

Bone dry CO₂ (Airgas) and HPLC grade n-hexane (Fisher Scientific Inc.) were used without any pretreatment. Also alumina (Al₂O₃, Aeroxide Alu C), silica (SiO₂, Aerosil R972), titania (TiO₂, Aeroxide P25) nanopowders (Degussa Inc.) and multiwalled carbon nanotubes (Cheap Tubes Inc.) were used as received. Some physical properties of these powders according to manufacturer's specification are given in Table 2.1.

2.3.2 *Mixing in gaseous and supercritical CO₂*

Figure 2.1 shows the schematic diagram of experimental setup used for mixing powders in carbon dioxide. It consists of compressed carbon dioxide gas cylinder, chiller, piston pump (Thar Technology) for pumping CO₂, preheater, ultrasonic processor (Sonics and Materials Inc.) producing ultrasonic waves at a frequency of 20 kHz with maximum power capability of 600 W, and a 120 ml stainless steel mixing vessel heated by heating tape. The ultrasonic processor consists of three major components: an ultrasonic power supply, a transducer, and a horn with 0.75 inch tip diameter. Temperature and pressure inside the mixing vessel were measured with a thermocouple and a pressure gauge, and tape heating was controlled by temperature controller. To prevent the loss of powders during the vessel depressurization, a filter (Fisher Scientific) at the top exit of the vessel was installed.

The ultrasonic processor is designed to deliver constant amplitude (61 μm at 100% amplitude settings for a horn used in these experiments), i.e. it automatically adjusts power to maintain constant amplitude during the operation. Therefore, power delivered from the processor depends on the resistance to the movement of horn which is affected by setup and process parameters, such as volume of a mixing vessel, horn size, mixture viscosity, pressurized environment etc. All experiments were conducted at constant amplitude, and power was monitored.

Nanopowders in weight ratio of 1:1 (100 mg: 100 mg) were loaded into a stainless steel vessel and then carbon dioxide was introduced. The horn was immersed into the vessel, so that only 100 ml of its volume was available for mixing. Vessel pressure was maintained within $\pm 3.5 \times 10^5 \text{ N/m}^2$ and $\pm 0.1 \text{ }^\circ\text{C}$ at the start of each experiment. The

vessel was heated with the heating tape to 45 °C in all experiments. After reaching desired pressure and temperature in the vessel, ultrasound was applied for 10 min at particular amplitude to cause mixing. After mixing, the vessel was slowly depressurized to prevent carry over of particles with CO₂. Further loss of particle was prevented using filter at the top exit of the vessel. After complete depressurization, vessel was opened, and powder was collected for analysis.

2.3.3 *Mixing in liquid n-hexane*

The same ultrasonic processor, described above, was used in experiments with mixing in n-hexane. Ultrasound was applied to suspension of powder mixture (100 mg: 100 mg) in 100 ml n-hexane contained in beaker. To prevent loss of n-hexane, as temperature increases during sonication, the beaker was kept in an ice bath so that temperature during experiments stayed in the range from 5 to 10 °C. After the application of ultrasound for 10 minutes, suspension was filtered and the powders were collected and dried in an oven at 80 °C for 12 hours.

2.3.4 *Mixture Analysis*

In case of silica/alumina and silica/titania mixtures, quantitative analysis of degree of mixing was performed using energy-dispersive X-ray spectroscopy (EDS) of a field-emission scanning electron microscope (JEOL 7000F and Leo 1530 VP) equipped with x-ray detector from Princeton Gamma Tech and Oxford Instruments. For analysis, mixed powder samples were compressed into wafers of about 1 mm thickness and 13 mm diameter using a die (International Crystal Laboratory) in mechanical press (Fred S.

Carver) with the loads of 5-8 tons applied for 4 minutes. Two representative areas of size $21.94 \times 16.46 \mu\text{m}$ were selected on the pellet surface, and in each area atomic composition at 20 randomly selected points (each spot size is of $\sim 1 \mu\text{m}$; i.e., 3×3 pixels, each pixel of $0.35 \mu\text{m}$) was obtained with EDS.

Taking into account that the only sources of Al, Si and Ti elements in the samples are their oxides, and assuming the complete stoichiometry of these oxides as Al_2O_3 , SiO_2 , TiO_2 , concentrations of Al, Si and Ti atoms measured at each spot were converted to the weight concentrations of respective oxides, normalized so that

$$a + b = 1 \quad (1)$$

where a and b are the weight concentrations of Al_2O_3 and SiO_2 in alumina/silica, and TiO_2 and SiO_2 in titania/silica mixtures, respectively. As a result of N such measurements, average concentrations \bar{a} and \bar{b} and variance σ^2 was found:

$$\sigma^2 = \frac{\sum_{i=1}^N (a_i - \bar{a})^2}{N-1} = \frac{\sum_{i=1}^N (b_i - \bar{b})^2}{N-1} \quad (2)$$

As a measure of degree of mixing, the intensity of segregation, parameter, introduced by Danckwerts [7], was used:

$$I = \frac{\sigma^2}{\bar{a}\bar{b}} \quad (3)$$

Intensity of segregation is a variance of concentrations in a mixture normalized by the variance in completely segregated, unmixed powders. Thus, in case of complete segregation of two components, the index of segregation is 1. On the other hand, since the volume spotted by EDS (an order of microns) technique is much higher than primary particle size (tens of nanometers), i.e. the size of the smallest units of mixture, the index

of segregation for a perfect random mixture would be close, and at the current level of scrutiny for all practical purposes can be taken as equal, to 0. Therefore, the index of segregation shows how good the mixture is, and can vary in the range from 0 (complete uniform mixture) to 1 (completely unmixed components).

All samples were analyzed at 10 mm working distance. Voltage range of 1.5-3 (accelerating voltage/critical excitation energy) was found to be optimum for EDS analysis [8]. Considering excitation energy for titanium (K-edge excitation energy, 4.931 keV), electron beam voltage of 10 keV has been used in all analysis unless it is mentioned otherwise.

In the case of MWNT mixture with titania and silica, qualitative visual evaluation of mixture quality was done using field emission secondary electron microscope (FESEM, JEOL 6700/7000F and Leo 1530 VP). In addition, the reflectance curves of the mixtures were obtained from day-light illumination spectrophotometer (Minolta spectrophotometer CM-508D) that provided supplementary information regarding the mixture quality. For reflectance measurements, the samples were placed into a plastic sample holder with 13 mm in diameter and 5 mm in depth, and the surface of the powder was smoothed carefully with a spatula trying to avoid compaction of the powder. Daylight standard illuminant D65, a $d/2^\circ$ optical geometry (the sample is illuminated diffusively, the reflection is detected at 2° relative to the normal to the sample surface) and specular excluded reflection were used in all the measurements.

2.4 Results and Discussions

Table 2.2-5 show the details of experiments for mixing of various nanopowders. Though all the experiments started at fixed temperatures and pressures, they were increasing during sonication, and this increase is more significant, the higher the amplitude is (and, therefore, the power delivered from the horn to the process). Due to the ultrasonic energy input, kinetic energy (i.e. temperature) of molecules of fluid media rises, which for closed volume of fluid results in increase of the fluid pressure. In spite of the use of a temperature controller, cooling of the vessel through the walls was not efficient enough to keep steady temperature. The amount of power consumed fluctuates during sonication; therefore, power fluctuation range is mentioned in the above tables.

A better deagglomeration and mixing at the higher pressures can be explained as follows: Particles in the ultrasound field experience different forces, including radiation force which is transfer of momentum from molecules of fluid to particles suspended in it, fluid drag which acts in an opposite direction of fluid flow, and buoyancy force which acts in direction opposite of gravitational forces [9,10]. These forces promote particle interactions. For example, radiation force moves the particles from the region of high pressure to region of low pressure during ultrasound propagation. Higher is the amplitude of the ultrasonic wave; greater is the force with which particles collide with each other. During the propagation of ultrasound, pressure gradient is created in the fluid elements which give rise to net flow of fluid; this phenomenon is termed acoustic streaming. Depending on ultrasonic intensities and size of vessel in which medium is confined by rigid walls; streams can be laminar or turbulent. The acoustic streaming provides mechanical grinding of particles due to impaction against wall or horn surface, which is

more significant for hard and large particles than for soft particles. Seipenbusch et al. [11] and Froeschke et al.[12] have shown that with enough impaction velocity (impact energy), fragmentation of agglomerates can take place (with average primary particle size between 8-95 nm). Acoustic wake effect is another reason for the interaction of particles which is caused due to asymmetric flow field created around moving particle at moderate Reynolds number. When particles oscillate, surrounding flow field is disturbed, creating wake behind it. The next particle near the wake moves with a high speed towards first particle in the low pressure wake region. This effect causes attraction of particles, leading to collisions and re-agglomeration of different materials and thus promoting mixing.

2.4.1 *SiO₂/TiO₂ and SiO₂/Al₂O₃ Systems*

Before carrying out experiments at various pressures, a preliminary study was performed on the effect of amplitude on intensity of segregation for mixing powders in carbon dioxide at a specific pressure of 90×10^5 N/m². Figure 2.2 represents the results of this study, which show that for sufficiently high amplitudes (higher than 50%) intensity of segregation does not change significantly, in particular for alumina/silica mixtures (Here the EDS analysis was carried out at 15 keV of an electron beam accelerating voltage). Since statistical analysis of a mixture with EDS is a rather time-consuming and laborious procedure, our further study was limited to 50% amplitude.

Figures 2.3 and 2.4 shows the results of EDS analysis for alumina/silica and titania/silica mixtures produced at various amplitudes both in supercritical (at 90×10^5 N/m²) and gaseous (at 21×10^5 N/m² and 55×10^5 N/m²) CO₂, as well as in liquid n-hexane. Figure 2.3 shows the results as a function of amplitude which is a controllable

variable, while Figure 2.4 shows the same results but plotted as a function of power which cannot be directly controlled. For all the mixtures considered, the intensity of segregation generally decreases with amplitude, and at high enough amplitudes, as was already noted, the difference in intensity of segregation between different mixtures becomes almost indistinguishable. The effect of CO₂ pressure on intensity of segregation has both similarities and some differences for two powder systems considered. In both cases, at low pressure 21×10^5 N/m², the increase of amplitude doesn't have any considerable effect on mixing quality at low amplitudes, with significant drop of intensity of segregation at 50% amplitude. At higher pressures, no significant difference of intensity of segregation was observed for silica/alumina system (Figure 2.3a). In fact, at 10% amplitude, pressure does not have a pronounced effect on intensity of segregation at all pressures considered here. Therefore, the main influence of pressure for this system is that at high pressures, the highest degree of mixing is observed already at 30% amplitude, while for the low pressure higher amplitude, 50%, is required to obtain the same mixing quality. In case of silica/titania (Figure 2.3b) system, the best mixing was achieved at 55×10^5 N/m² at any amplitude, (though, again, at 50% amplitude the difference between mixtures produced at any pressure becomes insignificant), and in contrast to the mixing at low pressure, at 55×10^5 N/m² and 90×10^5 N/m² increase of amplitude from 10% to 30% leads to the gradual increase of mixing, achieving its maximum, at 50%. Mixing in n-hexane shows better results at lower amplitudes than in CO₂. A high degree of mixing has been obtained for alumina/silica sonicated in n-hexane even at low amplitude of 10%. At higher amplitudes mixing in CO₂ becomes as good as in n-hexane, at least in the limits of our EDS resolution (lateral resolution of a micro-meter).

It is worthwhile comparing the two powder systems to see which one is easier to mix. Alumina/silica mixture sonicated at $55 \times 10^5 \text{ N/m}^2$ and $90 \times 10^5 \text{ N/m}^2$ achieves its maximum homogeneity at lower amplitude (30%) than titania/silica mixture (50%). This would be in accord with the common understanding that cohesive forces between titania particles are stronger than between alumina particles, thus requiring higher energy for deagglomeration of titania agglomerates. Unfortunately, the direct comparison of the results obtained by EDS analysis for different systems may lead to erroneous conclusions. X-ray generation and propagation inside any medium depends on the properties of the medium, thus changing the parameters at which the EDS analysis is performed. One of such most obvious and important parameters relevant to our case is the sampling volume, i.e. the volume where the detected X-rays were generated, which the value of intensity of segregation. For random mixtures, the larger the sampling volume, lower the intensity of segregation. Some impression regarding the sampling volume can be obtained from the depth of X-ray range production in material, which can be estimated by Anderson–Hasler expression [8].

$$R = \frac{0.0064(E_o^{1.68} - E_c^{1.68})}{\rho} \quad (4)$$

where R is the depth of x-ray generation (μm), E_o is the electron beam energy (keV), and ρ is the sample density (g/cm^3). E_c is the critical ionization energy (keV), which can be taken as an absorption edge of a corresponding electron shell (or a subshell), K - edge in the current case. Assuming that pressed powder wafer has zero porosity and neglecting non-uniformity of the components distribution, the effective density of the wafer can be used, which is about 3.1 g/cm^3 for both powder systems. K-edge energy for Ti is 4.965 keV, and 1.560 keV for Al [8]. Then the X-ray generation depth calculated from Eq.1 is

0.68 μm and 0.94 μm for Ti and Al X-rays correspondingly. Therefore, we can expect that the sampling volume of silica/titania is smaller than that of silica/alumina mixture, and the possibility that this is the reason that intensity of segregation silica/titania is higher at 30% amplitude, cannot be ruled out completely.

It is interesting to look at the mixing process from the point of view of power needed to effectively mix the powder, which is a very important issue for large scale industrial mixing. Power consumed in the process generally increases with pressure and amplitude. Figure 2.4 shows the dependence of intensity of segregation on power consumption for sonication at various conditions. It is noted that continuous measurements of power vs. time could not be made; only the maximum and minimum power values during sonication were recorded. Hence the power on abscissa is not the time averaged power, but the mean between the maximum and minimum power values. Nevertheless, these results show that the similar mixing quality, as in n-hexane, can be obtained by mixing in pressurized CO_2 with less energy consumption, i.e. mixing in CO_2 is not only as efficient as mixing in liquid hexane, but also more beneficial energetically. As was already seen above, a very high pressure (and supercritical conditions, particularly) is not necessary to obtain a high mixing quality; moreover, using lower pressure with high enough amplitude can be more energetically efficient. For example, it follows from Figures 2.4 and 2.5 that energetically the most energy efficient process conditions of all considered are: mixing in CO_2 at $21 \times 10^5 \text{ N/m}^2$ and 50% amplitude for silica/alumina and either $21 \times 10^5 \text{ N/m}^2$ or $55 \times 10^5 \text{ N/m}^2$ and 50% amplitude for silica/titania system. Sonication was also carried out at atmospheric pressure in gaseous CO_2 , and mixing of a very poor quality was obtained even with amplitudes higher than

50%, which confirms the requirement of pressurized medium for the effective mixing, at least, in the range of amplitudes and power provided by the sonicator.

The mixing results indicate that high degree of deagglomeration takes place during sonication of powders in CO₂ as can be illustrated in Figures 2.5 and 2.6. Original silica agglomerates (Figure 2.5) are rather large, up to tens (or even hundreds) of microns, and have a fractal hierarchical structure built by a large number of sub-agglomerates which in turn consist of primary agglomerates [13]. After sonication the original agglomerates break down to the primary agglomerates of a micron-order size that have net-like structure formed by sintered particle chains (Figure 2.6a). Some impression about mixing quality can be obtained from Figure 2.6b that shows silica and titania agglomerates intimately mixed at submicron scale, noting the entire image area is less than 1 μm^2 .

Capabilities of our mixture characterization method are limited in the sense that the volume of sample analyzed as well as lateral resolution with EDS is large (the order of microns) compared to primary particle sizes (tens of nanometers). Therefore, for powders mixed at nanoscale, intensity of segregation that reflects the compositional non-homogeneity, first, would not differ much for different mixtures, and, second, can even sometimes be so small that it becomes comparable with the uncertainties of determination of composition at each point by EDS. This fact was also pointed out in Wei et al. [5] and Yang et al. [6] indicating that another method of higher “resolution” is needed to resolve the question if we could achieve even higher mixing beyond 50% amplitude. Next, another interesting system is analyzed because the two constituents of the mixtures can be easily identified at nano-scale using FESEM imaging.

2.4.2 *SiO₂/MWNT and TiO₂/MWNT Systems*

Qualitative analysis of mixing of MWNT/silica and MWNT/titania was done with field emission scanning electron microscopy (FESEM) and day light illumination spectrophotometry. Mixing of powders was carried in supercritical CO₂ (90×10^5 N/m², 45 °C) and n-hexane at different amplitudes.

Figure 2.7 represents an original bundle of MWNT (Figure 8a) used in the experiments and products of sonication of MWNT with silica (Figure 2.7b-e) at 90 bar and 45 °C and different sonication amplitudes. Figure 2.7(b) shows two typical types of agglomerates found in the mixture after sonication. One is an agglomerate of SiO₂, as seen from the close-up view of its surface in Figure 2.7(c), and the other represents a bundle of carbon nanotubes with silica agglomerates of both submicron and micron sizes distributed on the surface and inside the MWNT bundle (Figure 2.7(d)). Apparently, some deagglomeration of nanoparticles and partial mixing with carbon nanotubes occurred at this amplitude, but large amounts of silica still form separate agglomerates with the size in the range of tens of microns. Figure 2.7(e) shows a typical MWNT bundle observed at 30% amplitude mixing. No essential difference in size compared with the original, unprocessed MWNT bundles was observed, which means that sonication did not lead to any significant deagglomeration of MWNT. At the same time no individual silica agglomerates were found in this mixture. The high magnification image of the surface of MWNT-silica bundle in Figure 2.7(e) is somewhat similar to the one observed at 10%, except higher degree of particle deagglomeration and their more uniform distribution among nanotubes were observed in this case. No differences between mixing with 30 and

50% amplitudes could be resolved by the SEM image analysis. Figure 2.8 shows MWNT/titania mixtures produced in supercritical CO₂ at various sonication amplitudes. At low 10% amplitude (Figure 2.8a) large aggregates of nanotubes and TiO₂ agglomerates are formed with large well segregated areas of MWNT and titania nanoparticles as is illustrated in Figure 2.8b. At higher amplitudes (Figure 2.8c,d) well-separated individual MWNT-titania bundles in the range from 1 to 10 μm can be seen whose surface contains smaller agglomerates distributed more evenly among the nanotubes (Figure 2.8e). Therefore, it can be inferred from SEM images that deagglomeration of TiO₂ particles and, probably, carbon nanotubes, as well as their mixing are not as efficient as in case of higher amplitudes. At the same time, at all amplitudes, large compact agglomerates consisting essentially of TiO₂ particles having an approximately spherical shape were found in mixtures, which is the evidence of failure to break particle agglomerates even at higher amplitudes or of the parallel process of agglomeration/compaction (Figure 2.8f).

Product of mixed nanopowders in n-hexane has a distinctively different morphology compared with those obtained in CO₂. Figure 2.9 is a photograph of MWNT - silica mixed in n-hexane that reveals the chunky nature and flaky shape of the particles in the very broad size range from microns up to centimeter. In case of MWNT-titania mixtures, clear distinct white color silica nanoparticle agglomerates can be detected visually in the mixture produced at 10% amplitude, while at 30% amplitude and higher, only dark colored mixture can be seen. Though it is not seen from Figure 2.9, since the photograph contrast was changed to better reveal white spots on the flake surface, apart from the large white silica agglomerates found on the surface of flakes at 10% amplitude,

the flakes themselves were noticeably different in color, darker in case of higher amplitudes. High magnification SEM images of the flakes (Figure 2.10a-d) produced at low and high amplitudes show the distinct differences in the surfaces of the flakes, which are similar for both systems studied. At 10% amplitude, large amount of nanoparticles are distributed on the surface forming some kind of matrix into which the MWNT are embedded, while in case of 50% amplitude the surface consists mostly of MWNT among which small agglomerates are dispersed. Note also that at low amplitude mixture the MWNTs have some preferred orientation, which, probably, can be explained by alignment of nanotubes in ultrasonic field in the direction of the wave propagation. In case of 50% amplitude MWNT are distributed more chaotically without any preferential orientation. The distinct difference of the MWNT-nanopowders mixed in n-hexane with those mixed in CO₂ is also observed in the nature binding between MWNT and nanoparticles in case of n-hexane mixing. Figure 2.11 that shows the attachment of nanoparticles to the nanotube walls is very typical for MWNT-nanopowders processed in n-hexane. This was not observed in case of CO₂ mixing.

Although SEM image analysis can reveal qualitative information regarding the mixture structure and difference in degree of mixing at lower 10% amplitude as compared to higher amplitudes, it fails to show significant difference between higher amplitude mixing. Additional information of mixing quality was obtained from color of powder mixtures obtained by diffuse reflectance spectroscopy in the visible spectrum. Diffuse reflectance spectroscopy has been already used for powder mixing and dispersion quality assessment by color [14] and a great deal of theoretical as well as experimental work has been devoted to this problem [15-17]. The reflectance spectrum of a powder

mixture can depend on many factors, such as separation between particles, particle or agglomerate size, porosity, organization of powder mixtures [18] etc., thus such factors should be properly taken into account when applying this method for mixture characterization. However, in the current study, the observed changes in color are utilized only as supplemental information to the one obtained from SEM images. The reasoning for the change of a reflectance spectrum of a mixture is as follows: better mixing involves better deagglomeration of particles which leads to decrease of reflection due to transmission of light through the particle to the opaque surface of nanotubes. Another factor is deeper penetration of particles inside nanotube bundles for better quality mixtures. Therefore, it can be expected that the spectrum shifts in the direction of the spectrum of nanotubes for well mixed powders.

Reflectance curves of mixtures obtained after sonication at various amplitudes, as well as of pure MWNT and hand mixed powder samples shown for comparison are presented in Figures 2.12 and 2.13. With increasing amplitude, the spectra tend to the spectrum of pure MWNT. The reflectance curve of the mixture produced at 10% amplitude differs essentially from the spectra of both pure MWNT and mixtures at higher amplitudes. Small differences in the spectra exists even between 30 and 50 % amplitude mixtures, which indicates the process of improving mixing with amplitude even at high values of amplitudes.

2.5 Conclusions

The use of supercritical fluids as a replacement of liquid solvent in wet sonication mixing process is examined for the purpose of nano powder mixing. In the wet

mixing process, nanomaterial of interest should be insoluble, has to wet the liquid, and the final nanomixed product needs to be filtrated and dried. In addition, flammability and the residual solvent are major concerns when organic liquids (e.g., n-hexane, toluene) are used. Replacement of the organic solvent by supercritical CO₂ removes many of such drawbacks. From results it appears that ultrasonic mixing, carried in high pressure carbon dioxide involving high impact collisions between particles/agglomerates and against rigid surface (horn surface and vessel walls), were enough to deagglomerate particles and mix them as well. These high impact collisions seem to achieve similar results as through work done by cavitation (in liquid n-hexane) phenomenon which breaks the micro-agglomerates. The high impact collisions (among particles and against rigid wall and horn) are possible due to high molar density and low viscosity of carbon dioxide. High amplitude (30-50%) gave good results at various selected molar densities (pressure) of carbon dioxide except for MWNT-titania mixture. Degree of mixing/homogeneity for selected nanopowders was fairly constant at different selected pressure ranges for high ultrasound amplitude ($\geq 50\%$). Nanomixing in CO₂ for silica/alumina and silica/titania mixture is as good as in n-hexane. But in the case of CO₂, mixed powder is free of organic solvent and the powder recovery is simpler.

2.6 Acknowledgement

The authors (RND and RBG) gratefully acknowledge financial support from the National Science Foundation through NIRT grant DMI-0506722 as well as a fellowship to JVS from an NSF grant DMI-0441086. Partial support from EEC-0540855 to RND and AE is also acknowledged.

2.7 References

- [1] M. G. Lines. Nanomaterials for practical functional used. *J Alloys Compd.* 449 (2008) 242-5.
- [2] M. C. Roco. Nanoparticles and nanotechnology research. *J Nanopart Res.* 1 (1999) 1-6.
- [3] J. A. Kurkela, D. P. Brown, J. Raula, E. I. Kauppinen. New apparatus for studying powder deagglomeration. *Powder Technol.* 180 (2008) 164-71.
- [4] J. H. Werth, Linsenbuhler, S. M. Dammer, Z. Frakas, H. Hinrichsen, K.-E. Wirth, et al. Agglomeration of charged nanopowders in suspensions. *Powder Technol.* 133 (2003) 106-12.
- [5] D. Wei, R. Dave, R. Pfeffer. Mixing and characterization of nanosized powders: an assesment of different techniques. *J Nanopart Res.* 4 (2002) 21-41.
- [6] J. Yang, Y. Wang, R. N. Dave, R. Pfeffer. Mixing of nano-particles by rapid expansion of high-pressure suspensions. *Adv Powder Technol.* 14 (2003) 71-93.
- [7] P. W. Danckwerts. The definition and measurement of some characteristics of mixtures. *Appl Sci Res.* A3 (1952) 279-96.
- [8] J. Goldstein, D. Newbury, D. Joy, C. Lyman, P. Echlin, E. Lifshin, et al. *Scanning Electron microscopy and X-ray Microanalysis.* 3rd ed. New York: Springer Science and business media Inc. 2003.
- [9] R. J. Townsend, M. Hill, N. R. Harris, N. M. White. Modelling of particle paths passing through an ultrasonic standing wave. *Ultrasonics.* 42 (2004) 319-24.
- [10] V. F. Humphrey. *Ultrasound and matter-Physical interactions.* *Prog Biophys Mol*

Biol. 93 (2007) 195-211.

[11] M. Seipenbusch, P. Toneva, W. Peukert, A. P. Weber. Impact fragmentation of metal nanoparticles agglomerates. Part Part Syst Charact. 24 (2007) 193-2000.

[12] S. Froeschke, K. Stefanie, A. P. Weber, G. Kapser. Impact fragmentation of nanoparticles agglomerates. J Aerosol Sci. 34 (2003) 275-87.

[13] C. H. Nam, R. Pfeffer, R. N. Dave, S. Sundaresan. Aerated vibrofluidization of silica nanoparticles. AIChE J. 50 (2004) 1776-85.

[14] D. G. Pope, J. L. Lach. Some aspects of solid-state stability and diffuse reflectance spectroscopy. Pharma Acta Helv. 50 (1975) 165-77.

[15] E. A. Schatz, ed. Modern aspects of reflectance spectroscopy. New York.: Plenum 1968.

[16] J. H. Nobbs. Kubelka-Munk theory and prediction of reflectance. Rev Prog Color Relat. 15 (1985) 66-75.

[17] H. S. Shah, A. A. Thaker. Theoretical aids for the determination of colorimetric curves of binary powder mixtures. Opt Soci Am. 29 (1990) 1034-9.

[18] J. Barra, A. Ulrich, F. Falson-Reig, E. Doelker. Color as an indicator of the organization and compactibility of binary powder mixes. Pharm Dev Technol. 5 (2000) 87-94.

Table 2.1 Physical properties of powders.

Material	Avg. Particle Size (nm)	Bulk Density (g/cm ³)	True Density (g/cm ³)	Wettability	Specific surface area (m ² /g)	Supplier
Al ₂ O ₃	13	0.05	2.20	Hydrophilic	110	Degussa, Inc.
SiO ₂	25	0.05	2.20	Hydrophobic	114	Degussa, Inc.
TiO ₂	25	0.18	4.26	Hydrophilic	48	Degussa, Inc.
MWNT	OD 20-30 [*]	2.1	----	Amphiphilic	----	Cheap Tubes, Inc.

^{*} Outside diameter is shown; length of MWNT is 10-30 μm and inside diameter is 5-10 nm.

Table 2.2 Experimental conditions for silica/alumina mixing.

Experimental Conditions	Media	CO ₂ Density (kg/m ³)	CO ₂ Viscosity (μPa·s)	Amplitude (%)	Power consumed (W)	Temperature after sonication (°C)	Pressure after sonication (10 ⁻⁵ N/m ²)
21 × 10 ⁵ N/m ² , 45 °C	CO ₂	38.372	16.143	10	3-6	45.5	21
				30	9-10	45.9	21
				50	10-20	50.6	21
55 × 10 ⁵ N/m ² , 45 °C	CO ₂	124.48	17.503	10	7-8	45.3	55
				30	20-25	48.3	80
				50	50-55	49.8	59
90 × 10 ⁵ N/m ² , 45 °C	CO ₂	339.84	25.599	10	10-20	45.7	90
				30	30-35	49.3	97
				50	45-50	54.0	114

$1 \times 10^5 \text{ N/m}^2$,	n-	10	20-25	---	---
5-10 °C	hexane	30	28-30	---	---
		50	30-31	---	---

Table 2.3 Experimental conditions for silica/titania mixing.

Experimental Conditions	Media	Amplitude (%)	Power consumed (W)	Temperature after sonication (°C)	Pressure after sonication (10^{-5} N/m ²)
21×10^5 N/m ² , 45 °C	CO ₂	10	5-10	45.3	21
		30	13-15	46.2	21
		50	25-27	50.2	21
55×10^5 N/m ² , 45 °C	CO ₂	10	8-9	45.7	55-59
		30	15-20	47.3	55-59
		50	20-25	48.3	55-59
90×10^5 N/m ² , 45 °C	CO ₂	10	7-10	46.0	90
		30	25-30	47.3	93
		50	30-35	50.1	100
1×10^5 N/m ² , 5-10 °C	n-hexane	10	25-30	---	---
		30	30-33	---	---

50

30-35

Table 2.4 Experimental conditions for silica/MWNT mixing.

Experimental Conditions	Media	Amplitude (%)	Power consumed (W)	Temperature after sonication (°C)	Pressure after sonication (10^{-5} N/m ²)
90×10^5 N/m ² , 45 °C	CO ₂	10	4-10	45.3	90
		30	30-35	47.4	90-93
		50	40-45	50.6	97
1×10^5 N/m ² , 5 °C	n-	10	19-20	10	---
	hexane	30	20-25	10	---
		50	30-35	10	---

Table 2.5 Experimental conditions for titania/MWNT mixing.

Experimental Conditions	Medium	Amplitude (%)	Power consumed (W)	Temperature after sonication (°C)	Pressure after sonication (10 ⁻⁵ N/m ²)
90 × 10 ⁵ N/m ² , 45 °C	CO ₂	10	10-20	45.9	90
		30	20-25	47.8	90-93
		50	30-40	50.6	90-93
1 × 10 ⁵ N/m ² , 5 °C	n-hexane	10	20-21	10	---
		30	29-30	10	---
		50	29-30	10	---

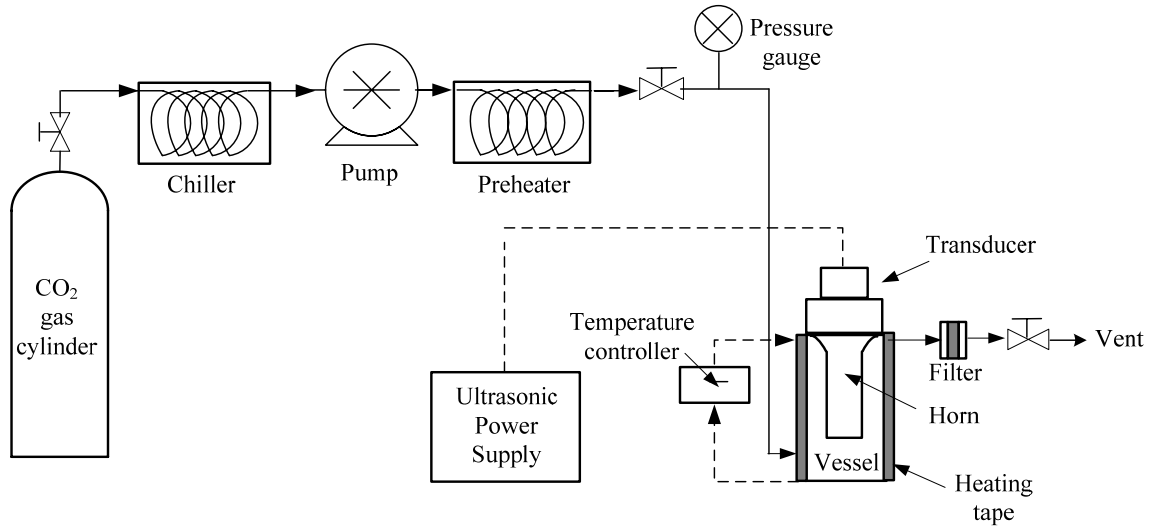


Figure 2.1 Schematic diagram of the experimental setup for mixing nanopowders in carbon dioxide.

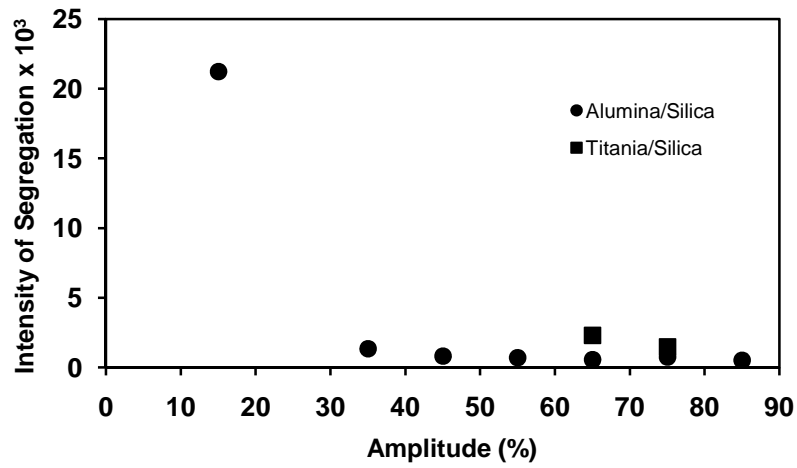
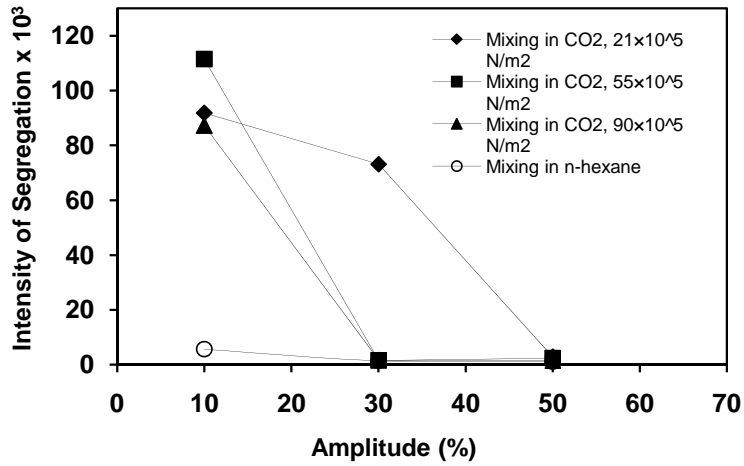
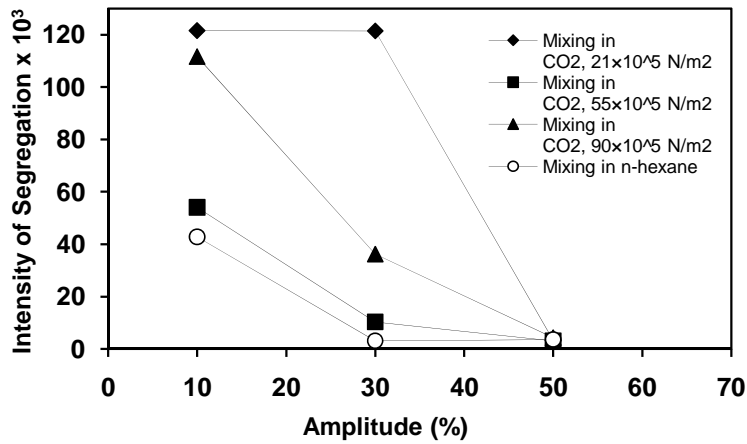


Figure 2.2 Effect of ultrasound amplitude on intensity of segregation for powder mixtures sonicated in CO₂ at 90×10^5 N/m², 45 °C. EDS analysis was performed at accelerating voltage 15 keV.

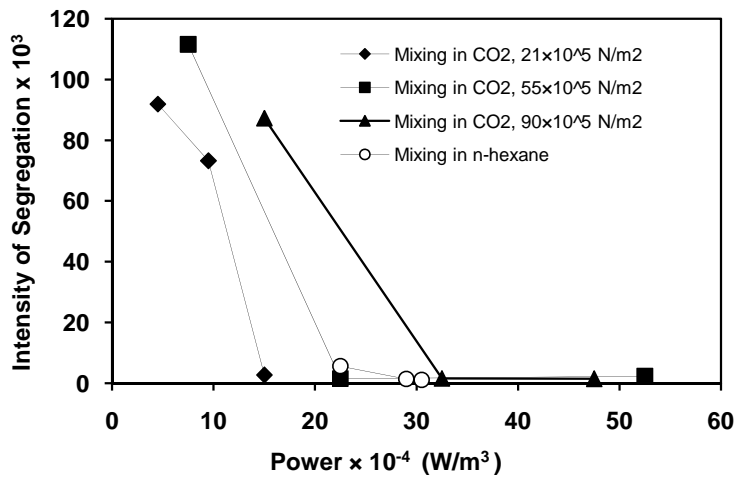


(a).

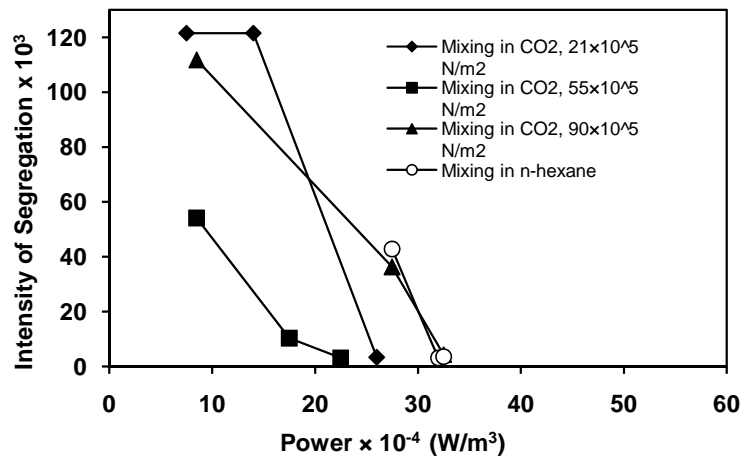


(b).

Figure 2.3 Effect of amplitude on intensity of segregation for (a) silica/alumina and (b) silica/titania mixtures sonicated at various pressures in CO₂ and n-hexane. (Lines are drawn only for visual guidance).



(a).



(b).

Figure 2.4 Intensity of segregation versus average power consumption per unit volume (of carbon dioxide or n-hexane) for (a) silica/alumina, and (b) silica/titania mixtures. (Lines are drawn only for visual guidance).

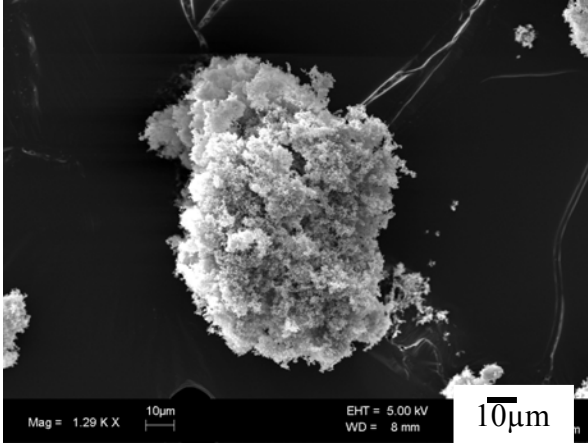
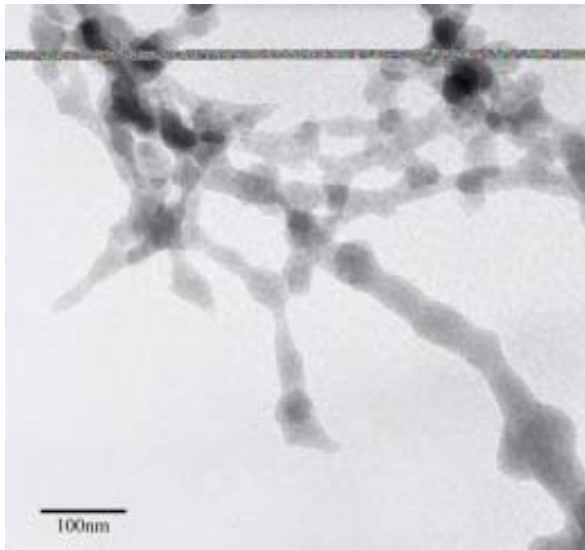
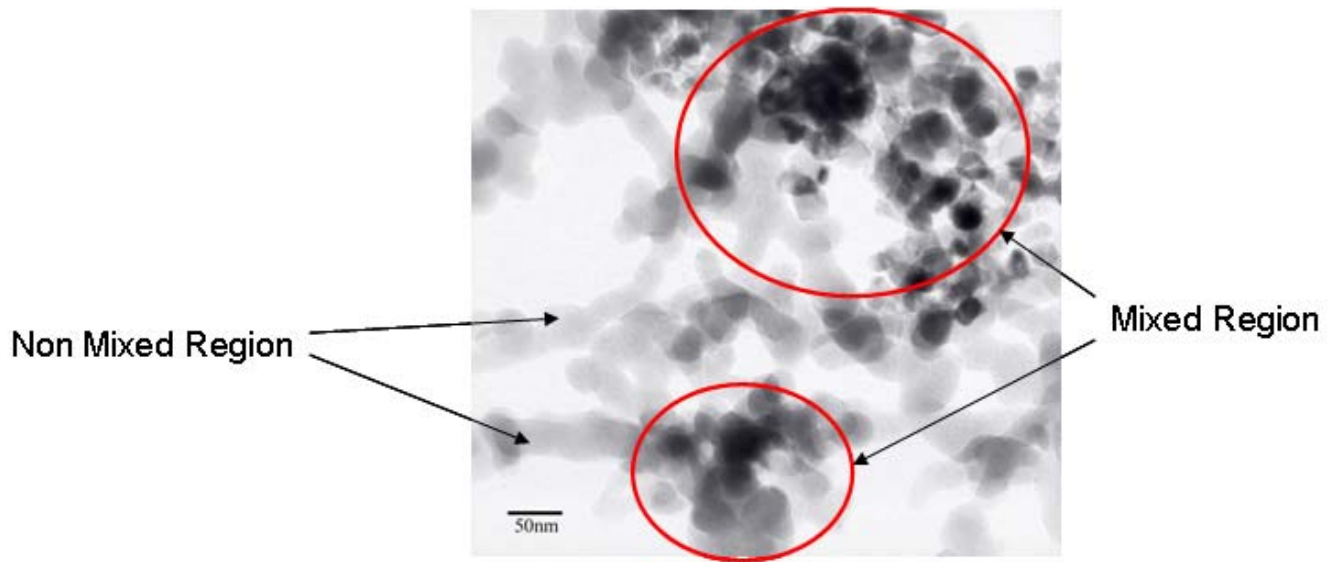


Figure 2.5 SEM image of typical silica agglomerate before sonication.

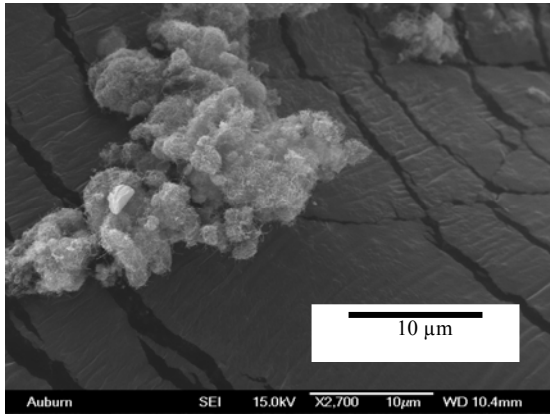


(a).

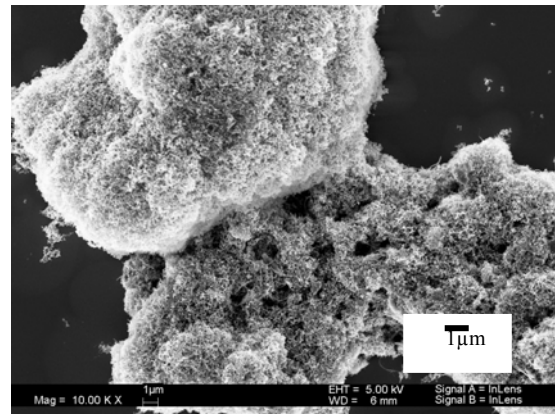


(b).

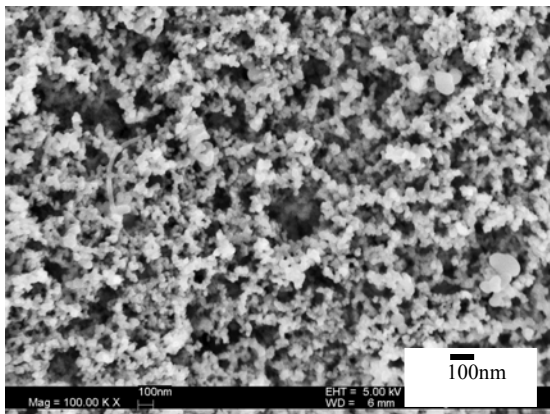
Figure 2.6 TEM images of a silica agglomerate (a), and mixture of silica/titania agglomerates (b) after sonication in CO_2 (pressure $90 \times 10^5 \text{ N/m}^2$, amplitude 50%).



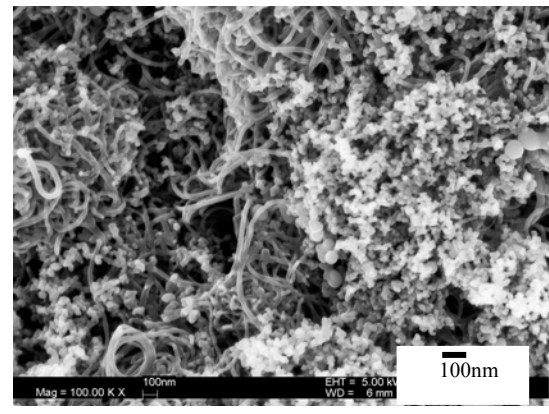
(a)



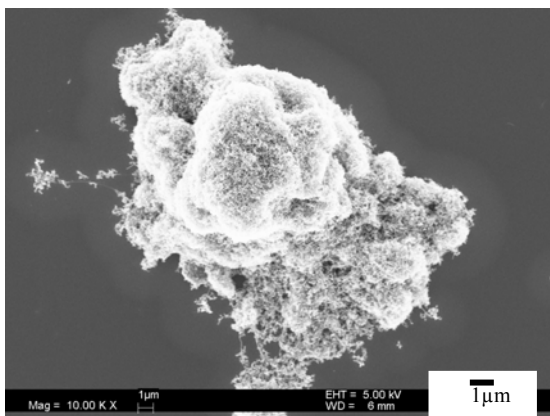
(b)



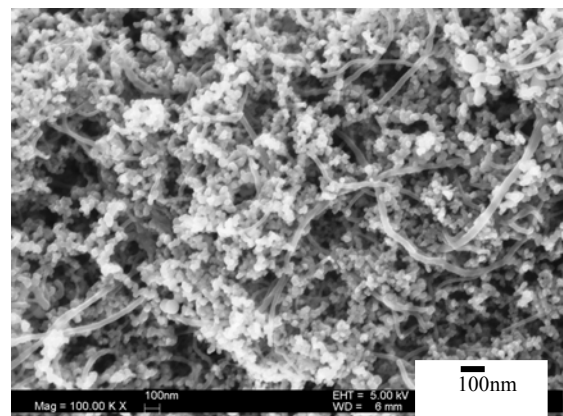
(c)



(d)



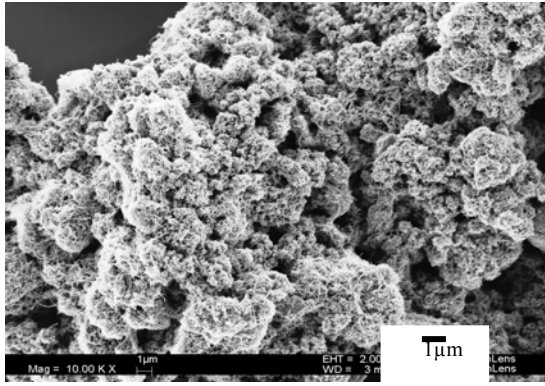
(e)



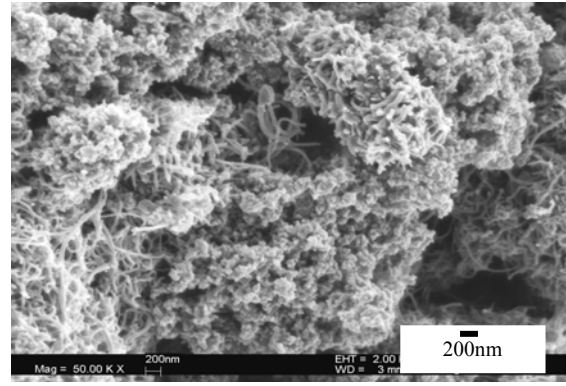
(f)

Figure 2.7. SEM images of MWNT and MWNT-silica mixtures produced by sonication in CO_2 at $90 \times 10^5 \text{ N/m}^2$: (a) Original MWNT bundles; (b) Overview of MWNT – silica agglomerates produced by sonication at 10% amplitude. Two types of particles were observed: silica agglomerates and MWNT – silica bundles; (c)

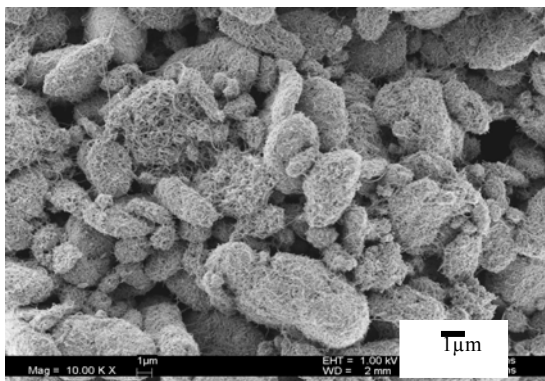
Closeup view of the surface of silica agglomerate shown in (b); (d) Closeup view of MWNT-silica agglomerate represented in (b); (e) Overview of a typical MWNT-silica bundle produced by sonication at 30% amplitude; (f). Closeup view of a surface of a MWNT-silica bundle produced by mixing at 30% amplitude. MWNT-silica mixing product of 50% amplitude has similar appearance.



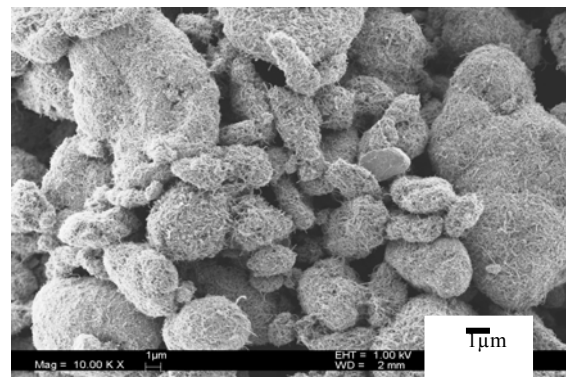
(a)



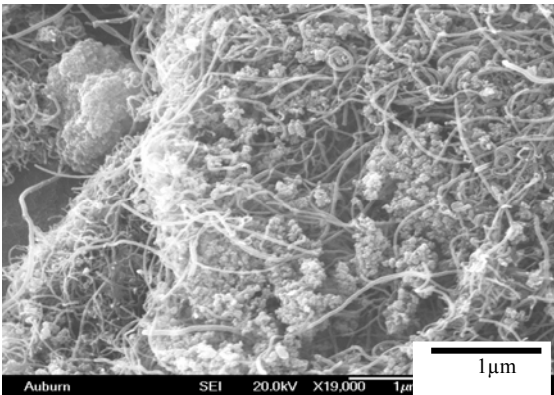
(b)



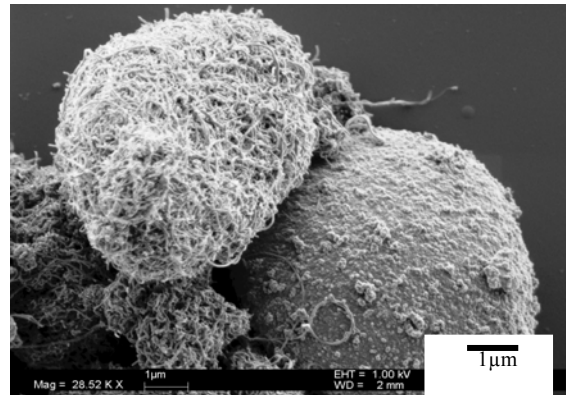
(c)



(d)



(e)



(f)

Figure 2.8 SEM images of MWNT-titania mixtures produced by sonication in CO₂ at 90×10^5 N/m²: a) Overview of MWNT - titania agglomerates produced by sonication at 10% amplitude. (b) Overview of MWNT - titania agglomerates produced by sonication at 10% amplitude. (c) MWNT – titania agglomerates produced by sonication at 30%

amplitude. (d) MWNT – titania agglomerates produced by sonication at 50% amplitude. (e) Overview of a typical MWNT - titania bundle produced by sonication at 30% amplitude; (f). Example of a compact titania agglomerate found in MWNT - titania mixtures after sonication with 30% amplitude. These kinds of agglomerates were found in mixtures produced with all other amplitudes considered.

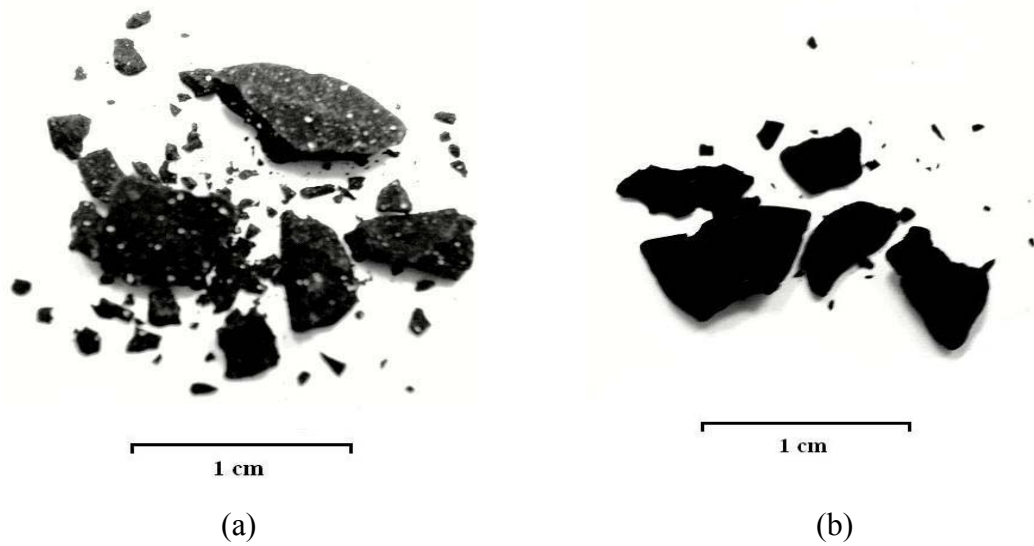
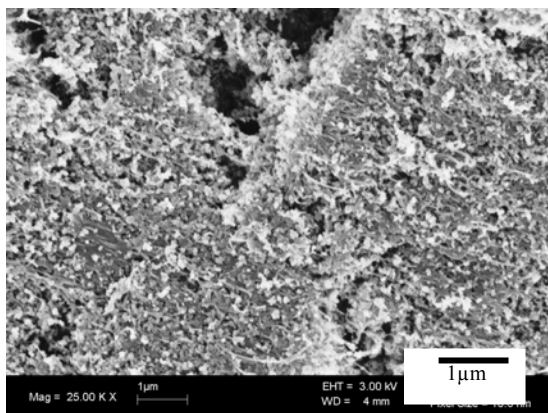
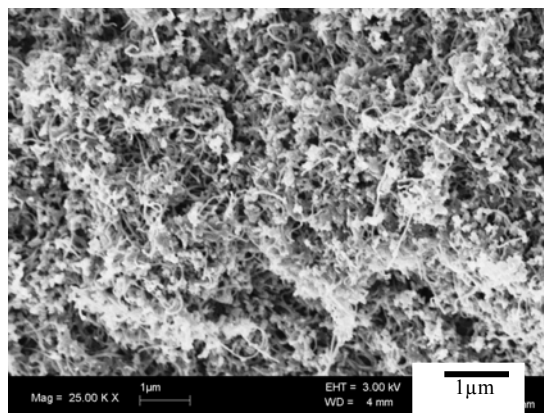


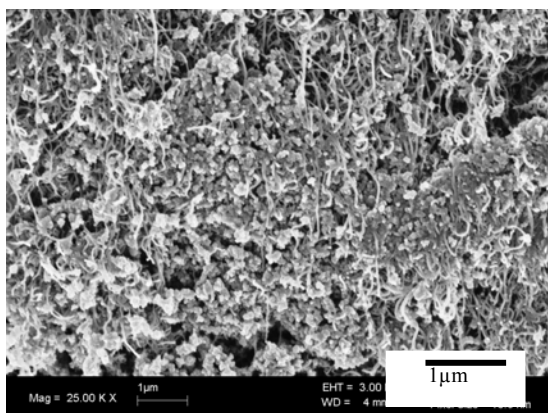
Figure 2.9 Photographs of particles obtained by mixing of MWNT with silica in n-hexane at amplitudes: (a). 10%; (b). 50%. Product of MWNT - titania mixing has similar appearance.



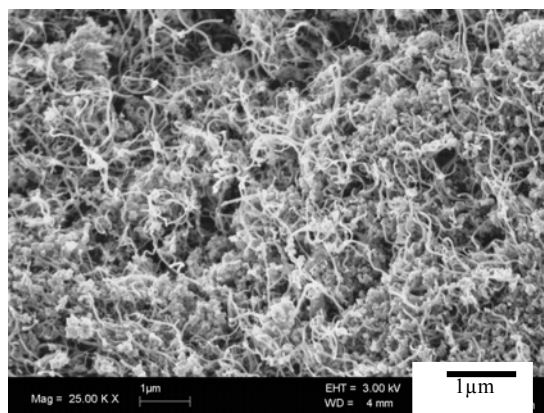
(a)



(b)



(c)



(d)

Figure 2.10 Closeup of flake surfaces obtained by sonicating MWNT with the powders in n-hexane at various amplitudes: (a) MWNT-silica, 10% amplitude; (b) MWNT-silica, 50% amplitude; (c) MWNT-titania, 10% amplitude; (d) MWNT-titania, 50% amplitude.

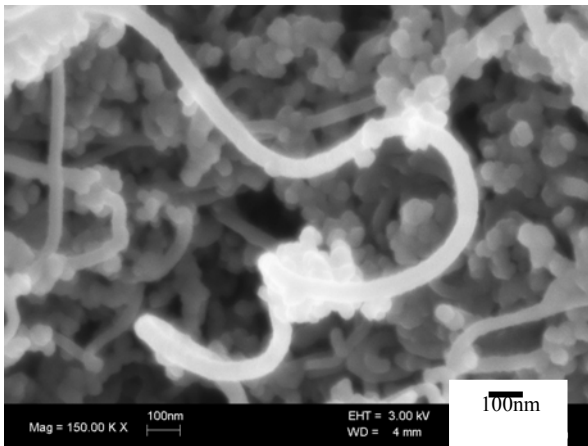
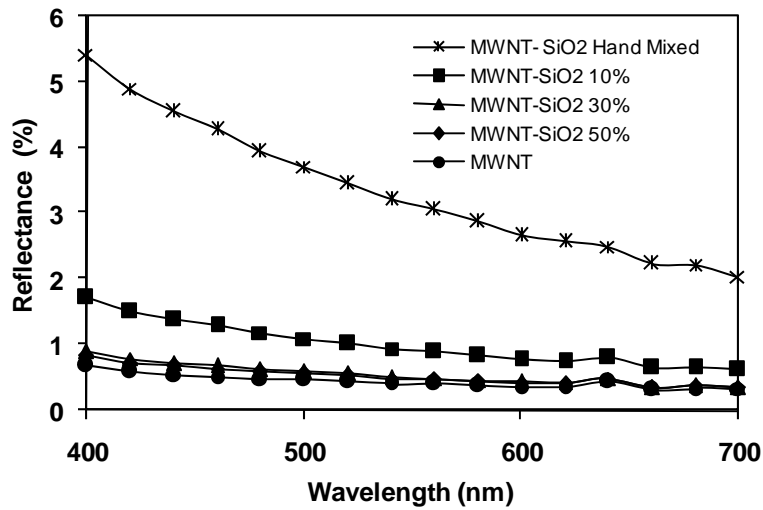
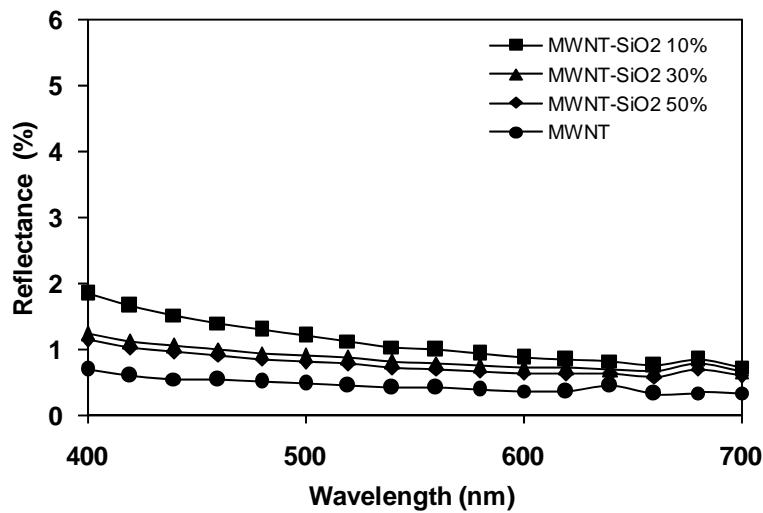


Figure 2.11 Example of MWNT-silica particle binding after sonication of MWNT and silica particles in n-hexane at 30% amplitude.

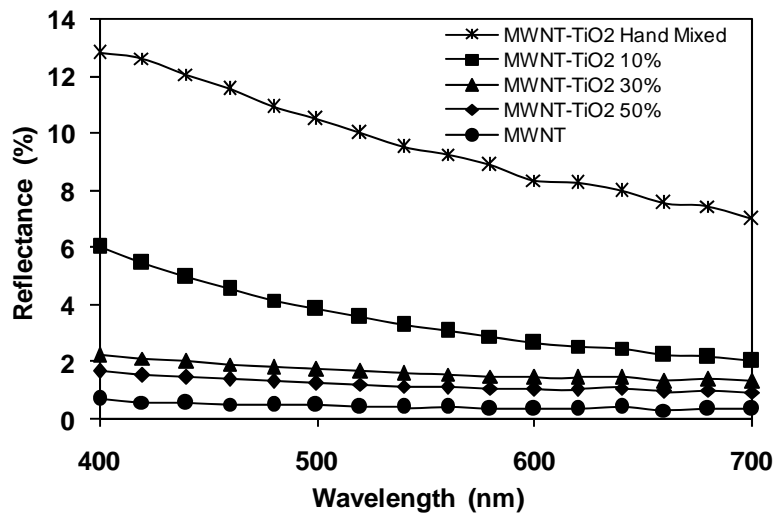


(a).

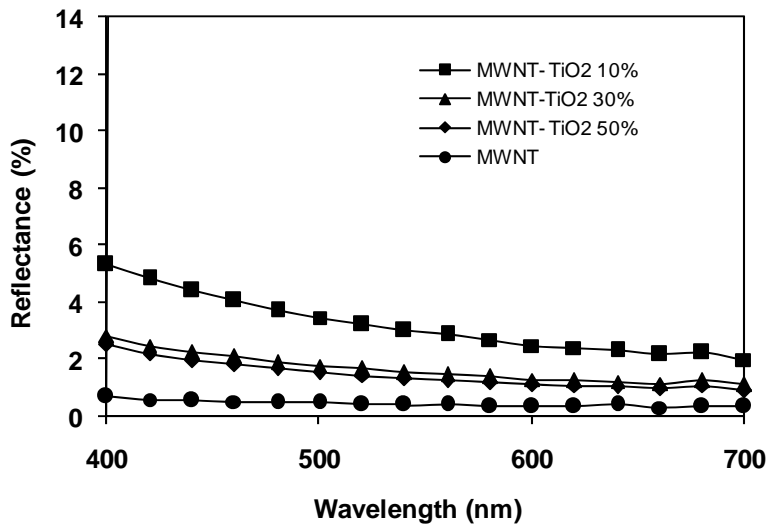


(b).

Figure 2.12 Reflectance spectra of carbon nanotube-silica mixture produced in CO₂ at 90×10^5 N/m² and 45 °C (a) and n-hexane (b) at various amplitudes.



(a).



(b).

Figure 2.13 Reflectance spectra of carbon nanotube-titania mixture produced in CO₂ at $90 \times 10^5 \text{ N/m}^2$ and 45 °C (a) and n-hexane (b) at various amplitudes.

3 NANOSCALE MIXING OF ITRACONAZOLE WITH SILICA

3.1 Abstract

Nanoflakes of itraconazole, which is a poorly water-soluble antifungal drug, are produced using a procedure known as supercritical antisolvent solvent with enhanced mass transfer (SAS-EM) method. The nanoflakes show poor flowability and shelf life, each of which is improved by mixing with silica nanoparticles. To intimately mix at nanoscale level, a macroscopic mixture of itraconazole nanoflakes and silica nanoparticles first is pressurized with supercritical carbon dioxide and then is rapidly depressurized through a nozzle. The rapid depressurization of supercritical suspension (RDSS) causes deagglomeration and mixing, due to a high CO₂ expansion velocity. Upon mixing, because of presence of silica nanoparticles between itraconazole nanoflakes, growth of the drug particles during storage is avoided or reduced and particle flow properties are significantly improved. The handling properties are characterized such as the angle of repose, compressibility index, and Hausner ratio. Physical stability (shelf-life) of drug and drug/silica mixture is tested by storing the samples for 25 days at 90 °C. Agglomeration and growth of pure drug nanoflakes during storage leads to substantial decrease in the dissolution rate. However, when the drug nanoflakes are mixed with silica nanoparticles, the dissolution rate almost remains constant during storage. Thus, effective

deagglomeration and nanoscale mixing lead to increase in the shelf life.

3.2 Introduction

The bioavailability of poorly water-soluble hydrophobic drugs (Class II in Biopharmaceutics Classification System) can be increased by their saturation solubility and dissolution rate in the gastrointestinal tract [1]. The dissolution rate can be improved by decreasing the particle size and/or crystallinity. Several studies have been conducted out to increase the dissolution rate of drugs by decreasing the particle size, by creating nanoparticles and micro-particles [2-4]. However, the fine drug particles have a high tendency to agglomerate, because of van der Waals attraction or hydrophobicity, thus decreasing surface area over the time [5-8], which, in turn, causes decrease in the dissolution rate or bioavailability [7-9].

Powder mixing is a very important unit operation in pharmaceutical industry, because it directly affects the drug content uniformity in the final drug/excipient mixture. Particle agglomeration can affect granulation, fluidization, mixing, and blending operations [10,11]. The presence of cohesive particle agglomerates decreases the efficiency of mixers, and it affects the powder flow, because of bridging and spatial heterogeneity [12]. The deagglomeration and mixing of fine cohesive drug particles are important to prevent their further reagglomeration, as well as for obtaining better homogeneity of formulation (especially for low drug dosage formulation). Currently available mixers are not effective in regard to the deagglomeration of highly-cohesive drug particles $< 10 \mu\text{m}$ in size, or they require very high shear or impaction, which, indeed, act as a particle size-reduction device rather than a conventional mixer [13]. For

example, rotary and vibratory ball mills can be used to mix fine powders [14,15]; however, the use of high energy may affect the crystal lattice of the particles, which can influence the physico-chemical stability. The tumbler, most common mixing equipment in pharmaceutical industry, is not effective if de-agglomerates is required [16].

Several methods for mixing nanoparticles have been presented in the literature [17]. Rapid depressurization of supercritical suspension (RDSS) [18] and sonication in liquids have been observed to perform better than other nanomixing methods. So far, these methods have been tested with inorganic nanopowders. Sonication in liquids (e.g., n-hexane) has several disadvantages (for example, the material must wet the liquid) and involves additional steps of filtration and drying; in addition the mixture contains residual solvent.

In this study, RDSS is tested for the deagglomeration and mixing of itraconazole nanoflakes with silica nanoparticles. Drug nanoflakes are produced using methodology known as supercritical antisolvent with enhanced mass transfer (SAS-EM) [19]. Supercritical carbon dioxide was utilized both as the antisolvent in the SAS-EM method and as the suspension media in RDSS process, because of its mild critical point (73.7 bar and 31.1°C) and suitability for processing of pharmaceutical compounds. Upon depressurization, CO₂ leaves the solid matrix without any residues. RDSS process (Figure 3.1) involves breakage of particle agglomerates upon rapid depressurization or expansion with subsequent mixing.

Mixing of drug particles with silica has advantages, including (a) an improvement in the flowability of drug powder, which leads to effective mixing with other excipient, using conventional mixers; (b) decrease of electrostatic charge of fine drug particles; (c)

effective wetting (due to hydrophilicity of silica particles); and (d) prevention of re-agglomeration of drug particles during dissolution. Typically drug nanoparticles get charged during production; for the sake of illustration, Figure 3.2 shows charged itraconazole nanoflakes, clinging to a metal spatula. The charging of drug nanoparticles can lead to several problems in mixing or other operations, because of clinging of particles to vessel wall or agitator surfaces [20]. In addition, the hydrophobic drugs suffer from the problems of poor wetting and re-agglomeration in the dissolution media [21-24]. Nonporous fumed silica is used in oral formulations as a glidant [25-27]. In this work, pharmaceutical grade fumed silica [28] consists of (200-300 nm in length) aggregates of primary nanoparticles 9-30 nm in size is utilized. These highly structured aggregates also form 30-44 μm macroscopic agglomerates with a very high void volume (>98%). Itraconazole is hydrophobic/lipophilic drug ($\log P = 6.939$, $pK_a = 3.7$) and is practically insoluble in water (see Table 3.1) [29]. Hence, the bioavailability of itraconazole solely depends on dissolution rate in the gastrointestinal tract. Itraconazole is used as an antifungal agent (triazole type) for the treatment of blastomycosis, histoplasmosis, and aspergillosis infections. Traditionally, itraconazole is taken in the form of capsules or oral solutions, which are available in dosage strength of 200-400 mg/day.

3.3 Materials and methods

3.3.1 Materials

Itraconazole (micronized, Hawkins), fumed silica (CAB-O-SIL M-5P, Cabot Corp., Inc. hydrophilic, surface area = $200 \pm 15 \text{ m}^2/\text{g}$, tapped density = 40 g/l), dichloromethane (99.9% pure, Sigma-Aldrich), sodium chloride (ACS grade, Fisher

Scientific), sodium dodecyl sulfate (>99% pure, Sigma-Aldrich), hydrochloric acid (ACS grade, Fisher Scientific), acetonitrile (ACS grade, Fisher Scientific), and CO₂ (bone dry, Air Gas) were used as received.

3.3.2 *Production of Itraconazole Nanoflakes*

Itraconazole drug particles were produced by SAS-EM method that was previously developed in our laboratory. A schematic of the SAS-EM process is shown in Figure 3.3. More details of the process are presented elsewhere [19]. Drug was dissolved in methylene chloride at 5 mg/ml concentration. The flow rate of drug solution was maintained at 1 ml/min, while the antisolvent flow rate (supercritical CO₂) was kept at 10 gm/min. A capillary nozzle (PEEKsil, Upchurch Scientific) with a diameter of 75 µm was used for delivery of the drug solution onto the surface of ultrasound horn inside the pressure vessel (as of shown in Figure 3.3). Process was carried out at a pressure of 100 bar and a temperature of 40 °C. A constant ultrasound amplitude of 25% (total ultrasonic power rating is 750 W at 100% amplitude) was used during the entire process. The ultrasonic processor is designed to deliver constant amplitude (15 µm at 25% amplitude settings for a horn used in these experiments); i.e., the processor automatically adjusts the power to maintain constant amplitude during the operation. Therefore, power delivered from the processor is dependent on the resistance to the movement of horn, which is affected by set-up and process parameters, such as volume of a vessel, horn size, and the mixture viscosity, pressure, and temperature.

In one semi-batch, 800 mg of drug was processed. The procedure is repeated until desired amount of drug powder produced via SAS-EM (about 5 gm) is obtained

(collection efficiency of particles is approximately 60%-70% in each experiment).

3.3.3 *Drug Deagglomeration and Mixing with Silica*

Figure 3.4 shows the schematic of RDSS apparatus used for mixing drug particles with silica nanoparticles. Experimental setup consists of mainly CO₂ supply [CO₂ gas cylinder, chiller, pump, and heater], a tubular pressure vessel (10 ml), a motor, and an expansion vessel (100 ml). Initially, spatula-mixed drug and silica (200 mg: 200 mg) mixture was loaded into the tubular pressure vessel. CO₂ was supplied from the top of the tubular vessel to maintain the desired pressure of 82±3.5 bar. The desired temperature (45±0.1°C) was maintained by the controlled heating of vessel and the entering CO₂. A stainless steel solid rod (1/8 in. in diameter) that was attached to the motor runs into tubular vessel through a Teflon ferrule, which aids in the flow of powder mixture by acting as a stirrer. The motor was operated at a speed of 100 rpm. Supercritical suspension is expanded in an expansion vessel through a capillary nozzle 400 µm in diameter and 10 cm long (PEEK, Upchurch Scientific). The pressure into tubular vessel was maintained by continuous supply of CO₂ (as high as 50 gm/min) through pump for 1 min, to completely expand the loaded powder mixture. A transient back pressure of up to 18 bar was observed in the expansion vessel. A loss of particles from expansion vessel was prevented by a filter (200 nm pore size, PTFE, Fischer Scientific) that was installed at the exit. After complete expansion of the mixture, the expansion vessel was opened and mixture was collected for analysis. Experiments were performed multiple times to obtain sufficient quantity of silica/drug mixture (final mixture is obtained by combining all the samples from a given experiment).

3.3.4 *Angle of Repose*

Angle of repose was measured by flowing 25 mL powder through a firmly fixed funnel (with diameter of 0.8 cm at the tip) from a height of 5 cm onto the flat surface. The pile of powder was photographed using a digital camera that was attached to the tripod stand. Angle of repose was measured from the photographs using Vistamatrix software (<http://www.skillcrest.com/>). All the measurements were done in triplicates and the standard deviation was calculated.

3.3.5 *Compressibility index*

Compressibility index (C.I.) of the powders was calculated using aerated (bulk) and tapped densities. To measure tapped density, powder is filled into graduated cylinder and tapped 200 times mechanically or until no further change in volume occurs.

$$\text{compressibility index (\%)} = \frac{\text{Tapped density} - \text{Aerated (bulk) density}}{\text{Tapped density}} \times 100$$

3.3.6 *Hausner ratio*

Hausner ratio is obtained by dividing tapped density by aerated (bulk) density. The ratio indicates how well the powder is compacted after mechanical tapping.

$$\text{Hausner Ratio} = \frac{\text{Tapped density}}{\text{Aerated (bulk) density}}$$

3.3.7 *Scanning Electron Microscopy*

Surface morphologies of the drug and drug/silica mixture were studied using environmental scanning electron microscopy (SEM) system (Zeiss EVO 50). The Sample

is sprinkled on the surface of two sided adhesive carbon tape using brush that is affixed to an aluminum stub and a thin coating of gold is applied onto the sample using sputter coater before the SEM analysis.

3.3.8 *Physical stability*

To test the physical stability (shelf life), samples were tested both before and after storage. Closed glass vials that contained drug sample (equivalent to 15 mg of drug) were kept in the oven for 25 days at 90 °C. The 90 °C temperature is well below the 292 °C decomposition temperature of itraconazole, as shown in the thermogravimetric analysis (TGA) of the pure drug in Figure 3.5.

3.3.9 *Solubility Measurement*

Saturation solubility of itraconazole was obtained by stirring excess amount of drug in 100 mL of 0.1 N HCl that contained 0.3 % w/v sodium dodecyl sulfate and 0.2% w/v NaCl at 37 °C in a horizontal shaker for 24 h. Exposure to ambient light was avoided by wrapping the flask with aluminum foil. After equilibration, the solution was filtered using 200-nm inline syringe filter (Alltech; PTFE, 17 mm in size) to remove any suspended particles. The dissolved drug concentration was measured using UV spectroscopy at a wavelength (λ) of 260 nm.

3.3.10 *Drug dissolution*

Drug dissolution was performed by placing the sample (equivalent to 15 mg of drug) in 400 ml freshly prepared 0.1 N (pH=1.2 \pm 0.1) HCl solution that contained 0.3 %

w/v sodium dodecyl sulfate and 0.2% w/v NaCl at 37 °C in a horizontal shaker (Environ Shaker, Lab-line Instruments) at 100 rpm. Three-mililiter (3-ml) samples were drawn at time interval of 10, 20, 30, 45, 60, 75, and 90 min. Change in volume of the solution due to sample withdrawal was considered during concentration determinations. Solutions were filtered using 200-nm inline syringe filter (Alltech; PTFE, 17 mm in size), to remove any suspended particles. Drug concentrations were measured using UV spectroscopy (Spectronic Genesys 2) at $\lambda = 260$ nm. Calibration of drug concentration was obtained by dissolving the drug in acetonitrile and then diluting with 0.1 N HCl solution. Drug dissolution was performed in triplicates. The ratio of saturation drug concentration to the actual drug concentration in dissolution media was 7:1, which is more than the 3:1 that is required to maintain the desired sink condition [30].

3.4 Results and Discussion

3.4.1 Deagglomeration and Mixing of Drug Particles with Silica

Itraconazole particles that were obtained from the supplier exhibited a size range of 3-60 μm (see Figure 3.6). In comparison, itraconazole particles produced via the SAS-EM method were observed to be flakes with a thickness of up to 150 nm. Primary particle sizes of itraconazole were found in the range of submicron to 14 μm (see Figure 3.7). The aspect ratios of particles produced via SAS-EM method were in the range of 1-4, compared to the range of 8-10 observed for drug particles that were obtained from the supplier. Particle size distribution of randomly selected particles (n=60) is presented in

Figure 3.8. Because of very high overlapping (agglomeration) and irregular shape of particles, particle sizes were measured from SEM images using an image analysis tool (Image J). Because of high surface area of the drug nanoflakes that were produced, loose agglomeration or overlapping of several primary particles was observed. The sizes of these loose drug agglomerates are observed to be as high as 50 μm (see Figure 3.7). The drug particle sizes obtained via SAS-EM method depends primarily on ultrasound amplitude or power. It has been shown that with increase in ultrasound amplitude (power) size of particle obtained decreases [31,32]. Higher amplitude can also cause reagglomeration/aggregation of particles during processing. Therefore ultrasound amplitude of 25% was used in this study. Others parameters, such as drug solution flow rate, type of solvent, drug concentration in the solvent, pressure, temperature and the antisolvent (CO_2) flow rate also affect particle size. More details on the effect of process parameters on particle size has been published elsewhere [33-36]. Silica agglomerates of sizes up to 80 μm have been also seen (see Figure 3.9), which are composed of several sub-agglomerates, whereas the sub-agglomerates are composed of several primary silica nanoparticles.

Figure 3.10 shows silica nanoparticles/itraconazole nanoflakes mixture produced via RDSS mixing, in which a deagglomeration of drug nanoflakes as well as silica nanoparticles is observed. The presence of loose drug agglomerates decreased substantially, and several individual particle and/or small drug agglomerates with layer (particle coating) of silica was observed (see Figure 3.10a). No silica agglomerates were

observed, which confirms complete deagglomeration of silica particles. Deagglomeration can be attributed to the penetration of supercritical CO₂ into the nanopores of agglomerates, and then upon depressurization CO₂ expands rapidly breaking the agglomerates [17,18,37]. However re-agglomeration of some drug particles was observed which results in compact agglomerates [38] of drug particles with layer of silica particles on it (see Figure 3.10b). The average size of these compact agglomerates was about 15 μm, while some other agglomerates were as large as 30 μm. The final silica/itraconazole mixture contains 40:60 ratio (by weight) of silica to itraconazole (which is measured by dissolving mixture in acetonitrile and filtering the solution through 200-nm syringe filter for concentration measurement using UV-spectroscopy), as compared to 50:50 weight ratio of silica and itraconazole loaded into tubular vessel at the start of each experiment. The decrease in proportion of silica in silica/drug mixture can be attributed to (i) errors while loading the samples, (ii) the attachment of silica fines to the walls of tubular and expansion vessels, and (iii) to losses through the filter.

For comparison, Figure 3.11 shows silica nanoparticles/drug nanoflakes mixture produced using simple spatula mixing. Here, the presence of unmixed agglomerates confirms that simple mixing is not adequate for agglomerates that are composed of nanoparticles.

3.4.2 *Powder flow characterization of drug/silica mixture*

Flowability of a powder is affected by various physical factors, including size and shape of particles, aerated (bulk) and true densities, moisture content, crystal form, surface electrostatic charge, and the types of equipment used for handling, storing, and

processing [11,39]. Powder flow characterization of drug and drug/silica mixture was done using angle of repose, compressibility index, and Hausner ratio, because these are convenient and simple methods for semi-cohesive powders [40-43].

The angle of repose increases as the particle sphericity decreases and/or cohesiveness increases. Various forces that influence the angle of repose include friction, surface tension due to the presence of moisture, mechanical interlocking, electrostatic, and van der Waals attraction in case of fine particles [40]. For itraconazole nano-flakes agglomeration, mechanical (due to the flat rectangular shape), electrostatic (charging of particles during SAS-EM production), and van der Waal's forces will have a key role, whereas surface tension force will be less important, because of hydrophobic nature of the drug. Table 3.2 Angle of repose, compressibility index, and Hausner ratio for mixtures and individual components shows results of tests that involve the angle of repose, compressibility index, and Hausner ratio tests. The scale of flowability, based on these properties, is given in the Table 3.3. Silica is used as a glidant in pharmaceutical industry due to its excellent flow properties, which is evident from its results for angle of repose, compressibility index, and Hausner ratio ("excellent" flow characteristics). Micronized drug from supplier has "passable" flow characteristics, while nanoflake drug produced by SAS-EM method has "poor" flow characteristics due to small particle size and a high van der Waals attraction. For a physical mixture (hand mixed by spatula) of nanoflake drug and silica nanoparticles, the angle of repose value is in between that for individual components. However, when the mixing is performed via RDSS, a significant improvement in flow properties was observed, with "good to fair" characteristic flow. The improvement can be attributed to a layer (particle coating) of silica nanoparticles

onto the drug nanoflakes and deagglomeration of the nanoflakes, resulting in a decrease in attractive forces among drug particles [18,25,26,44].

3.4.3 *Solubility*

Itraconazole is a weak base ($pK_a = 3.7$), and it has very low solubility in acidic and aqueous media. Solubility of itraconazole is in the range of 4-12 $\mu\text{g/ml}$ depending on pH of media: the solubility decreases as the pH increases [45,46]. The presence of surfactant in the dissolution media can enhance the solubility by several fold [47]. We have measured a solubility of 270 $\mu\text{g/ml}$ in 0.1 N HCl that contains 0.3% w/v sodium dodecyl sulphate surfactant and 0.2% w/v NaCl.

3.4.4 *Physical stability upon storage*

To accelerate the study, the storage at different higher temperatures is studied and then an Arrhenius correlation is used to predict shelf-life at ambient conditions [48]. In this study, a high temperature was used during storage in order to accelerate growth of drug nanoflakes, if any. The physical stability of the SAS-EM drug and drug/silica mixture was tested after storing the samples for 25 days at 90 °C. No change in the UV spectrum was observed, which confirms chemical stability of the drug. Figure 3.12 shows increase in agglomerate size of pure drug particles, up to 50-200 μm range. Figure 3.12(b) shows close-up view of the agglomerated drug particles, which shows the fusion of particles or forming of hard agglomerates upon storage. The large big agglomerates may be composed of both soft (easily breakable) and compact structures. For the mixture of silica nanoparticles and itraconazole that was obtained via RDSS mixing, there is no

significant change in agglomerate size at microscopic level, whereas at the bulk level, loose agglomerates are formed (Figure 3.13), which can be attributed to the loss of moisture from silica upon heating at 90 °C and readsorption of moisture under analysis conditions (23 °C, 50% relative humidity).

Dissolution studies were conducted, both before and after storage, to evaluate the physical stabilities of pure drug and the mixture. Figure 3.14 shows dissolution profiles for various cases. A substantially high dissolution rate (95% drug dissolved in 20 minutes) for itraconazole nanoflakes was observed, compared to dissolution rate (40% drug dissolved in 20 minutes) of micronized drug from the supplier, before storage. The significant increase can be attributed to the increase in the surface area upon particle size reduction.

Upon storage, drug nanoflakes undergo agglomeration, forming a combination of hard and soft agglomerates, which leads to a significant decrease in dissolution rate (only 46% drug dissolved in 20 minutes). Hence, the benefit of increase in surface area due to particle size reduction is lost upon storage. Upon RDSS mixing of silica nanoparticles and itraconazole nanoflakes, some loss of very fine particles occurs due to high CO₂ velocities in the expansion chamber, specially the drug particles smaller than the 200 nm filter pores as well as due to attachment of particles on the surface of tubular and expansion vessel walls (which are difficult to remove/collect even by scraping with a brush). As a result, the mixture shows a slower release (68% drug released in 20 minutes) than pure drug particles. However, the dissolution profile for the RDSS mixture does not significantly change upon storage. A minor decrease in the initial dissolution rate is due to the formation of loose agglomerates (Figure 3.13a). However, after 60 min, the amount

of drug dissolved in both cases (drug/silica mixture before and after storage) is almost same (80% of the drug dissolved in 60 min for the mixture before storage, versus 75% the drug dissolved in 60 min for the mixture after storage). Hence, nanoscale mixing of drug nanoflakes with silica nanoparticles, using RDSS method, helps to maintain the physical stability/shelf life.

3.5 Conclusions

The pure itraconazole nanoflakes have poor flowability and show significantly reduced dissolution rate upon storage, due to particle agglomeration and fusion. When the drug nanoflakes are mixed with silica nanoparticles using rapid depressurization of supercritical suspension process, particles deagglomerate and mix at nanoscale. The mixture has a much better flowability than pure drug nanoflakes, and it maintains a constant dissolution rate upon storage. The re-agglomeration of itraconazole is prevented due to presence of silica nanoparticles between the nanoflakes, which improves the physical stability or shelf life.

3.6 Acknowledgments

Financial support from National Science Foundation through NIRT grant DMI-0506722, experimental assistance from Andrew Scott (a NSF REU student for site 0552557), and technical discussion on RDSS with Prof. Rajesh N. Dave (NJIT, Newark) are highly appreciated.

3.7 References

- [1] G. L. Amidon, H. Lennernas, V. P. Shah, J. R. Crison. A theoretical basis for a biopharmaceutical drug classification: the correlation of in vitro drug product dissolution and in vivo bioavailability. *Pharm Res.* 12 (1995) 413-20.
- [2] G. G. Liversidge, K. C. Cundy. Particle size reduction for improvement of oral bioavailability of hydrophobic drugs: absolute oral bioavailability of nanocrystalline danazol in beagle dogs. *Int J Pharm.* 125 (1995) 91-7.
- [3] A. Jounela, P. Pentikainen, A. Sothmann. Effect of particle size on the bioavailability of digoxin. *Eur J Clin Pharmacol.* 8 (1975) 365-70.
- [4] N. Rasenack, B. W. Muller. Dissolution rate enhancement by in situ micronization of poorly water-soluble drugs. *Pharm Res.* 19 (2002) 1894-900.
- [5] P. Finholt, S. Slovang. Dissolution kinetics of drugs in human gastric juice the role of surface tension. *J Pharm Sci.* 57 (1968) 1322-6.
- [6] A. J. Aguiar, A. W. Zelmer, A. W. Kinkel. Deaggregation behavior of a relatively insoluble substituted benzoic acid and its sodium salt. *J Pharm Sci.* 56 (1967) 1243-52.
- [7] E. Swanepoel, W. Liebenberg, M. M. D. Villiers. Dissolution properties of proxicam powders and capsules as a function of particle size and the agglomeration of powders. *Drug Dev Ind Pharm.* 26 (2000) 1067-76.
- [8] M. D. Ticehurst, P. A. Basford, C. I. Dallman, T. M. Lukas, P. V. Marshall, G. Nichols. Characterisation of the influence of micronization on the crystallinity and physical stability of revatropate hydrobromide. *Int J Pharm.* 193 (2000) 247-59.
- [9] M. M. DeVilliers. Influence of agglomeration of cohesive particles on the dissolution behaviour of furosemide powder. *Int J Pharm.* 136 (1996) 175-9.

- [10] M. M. DeVilliers, J. G. VanderWatt. The measurement of mixture homogeneity and dissolution to predict the degree of drug agglomerate breakdown achieved through powder mixing. *Pharm Res.* 11 (1994) 1557-61.
- [11] J. K. Prescott, R. A. Barnum. On the powder flowability. *Pharm. Technol.* 10 (2000) 60-84.
- [12] K. Thalberg, D. Lindholm, A. Axelsson. A comparison of different flowability tests for powders for inhalation. *Powder Technol.* 146 (2004) 206-13.
- [13] N. Harnby, M. F. Edwards, A. W. Nienow. *Mixing in process industries.* London: Butterworth 1990.
- [14] I. Krycer, J. A. Hersey. A comparative study of comminution in rotary and vibratory ball mill. *Powder Technol.* 27 (1980) 137-41.
- [15] I. Krycer, J. A. Hersey. Fine powder mixing in vibratory ball mill. *Int J Pharm.* 6 (1980) 119-29.
- [16] N. Harnby. An engineering view of pharmaceutical powder mixing. *Pharm Sci Technol Today.* 3 (2000) 303-9.
- [17] D. Wei, R. Dave, R. Pfeffer. Mixing and characterization of nanosized powders: an assesment of different techniques. *J. Nanopart Res.* 4 (2002) 21-41.
- [18] J. Yang, Y. Wang, R. N. Dave, R. Pfeffer. Mixing of nano-particles by rapid expansion of high-pressure suspensions. *Adv Powder Technol.* 14 (2003) 71-93.
- [19] R. B. Gupta, P. Chattopadhyay, inventors; Method of forming nanoparticles and microparticles of controllable size using supercritical fluids with enhanced mass transfer. United States Patent 6620351. 2003.
- [20] H. Watanabe, M. Ghadiri, T. Matsuyama, L. Y. Ding, K. G. Pitt, H. Maruyama, et

al. Triboelectrification of pharmaceutical powders by particle impact. *Int J Pharm.* 334 (2007) 149-55.

[21] B. Always, R. Sangchantra, P. J. Stewart. Modeling the dissolution of diazepam in lactose interactive mixtures. *Int J Pharm.* 130 (1996) 213-24.

[22] M. Westerberg, C. Nystrom. Physicochemical aspects of drug release. Part 18. Use of a surfactant and disintegrant for improving drug dissolution rate from ordered mixtures. *STP Pharm Sci.* 3 (1993) 142-7.

[23] J. Liu, J. Stewart. Deaggregation during dissolution of benzodiazepines in interactive mixtures. *J Pharm Sci.* 87 (1998) 1632-8.

[24] P. J. Stewart, F.-Y. Zhao. Understanding agglomeration of indomethacin during the dissolution of micronised indomethacin mixtures through dissolution and deagglomeration modeling approaches. *Eur J Pharm Biopharm.* 59 (2005) 315-23.

[25] I. Zimmermann, K. Meyer. Effects of glidant in binary powder mixtures. *Powder Technol.* 139 (2004) 40-54.

[26] S. Jonat, S. Hasenzahl, M. Drechsler, P. Albers, K. G. Wagner, P. C. Schmidt. Investigation of compacted hydrophilic and hydrophobic colloidal silicon dioxides as glidants for pharmaceutical excipients. *Powder Technol.* 141 (2004) 31-43.

[27] J. Yang, A. Silva, A. Banerjee, R. N. Dave, R. Pfeffer. Dry particle coating for improving the flowability of cohesive powders. *Powder Technol.* 158 (2005) 21-33.

[28] Cabot Corp. Influence of CAB-O-SIL^R M-5P on the angle of repose and flow rates of the pharmaceutical powders. 2004.

[29] D. S. Wishart, C. Konx, A. C. Guo, S. Shrivastava, M. Hassanali, P. Stothard, et al. Drugbank: a comprehensive resource for in silico drug discovery and exploration.

Nucleic Acids Res. 34 (2006) D668-D72.

[30] United States Pharmacopeial Convention. In Vitro and in vivo evaluation of dosage forms. USP28. Presented at United States Pharmacopeial Convention, Rockville, MD, 2005; Paper No. 1088.

[31] P. Chattopadhyay, R. B. Gupta. Protein nanoparticles formation by supercritical antisolvent with enhanced mass transfer. *AIChE J.* 48 (2002) 235-44.

[32] P. Chattopadhyay, R. B. Gupta. Production of griseofulvin nanoparticles using supercritical CO₂ antisolvent with enhanced mass transfer. *Int J Pharm.* 228 (2001) 19-31.

[33] P. Chattopadhyay, R. B. Gupta. Supercritical CO₂-based production of fullerene nanoparticles. *Ind Eng Chem Res.* 39 (2000) 2281-9.

[34] G. A. Sacha, W. J. Schmitt, S. L. Nail. Identification of critical process variables affecting particle size following precipitation using a supercritical fluid. *Pharm Dev Technol.* 11 (2006) 187-94.

[35] M.-S. Kim, S. Lee, J.-S. Park, J.-S. Woo, S.-J. Hwang. Micronization of cilostazol using supercritical antisolvent process: effect of process parameters. *Powder Technol.* 177 (2007) 64-70.

[36] E. Reverchon, I. D. Marco. Supercritical antisolvent precipitation of cephalosporins. *Powder Technol.* 164 (2006) 139-46.

[37] O. Brandt, A. M. Rajahusmi, P. Roth. First observations on break up of particle agglomerates in shock waves. *Exp Fluids.* 5 (1987) 86-94.

[38] G. Nichols, S. Byard, M. J. Bloxham, J. Botterill, N. J. Dawson, A. Dennis, et al. A review of the terms agglomerate and aggregate with a recommendation for nomenclature used in powder and particle characterization. *J Pharm Sci.* 91 (2002) 2103-

9.

[39] S. N. Bhattachar, D. B. Hedden, A. M. Olsofsky, X. Qu, W.-Y. Hsieh, K. G. Canter. Evaluation of the vibratory feeder method for assessment of powder flow properties. *Int J Pharm.* 269 (2004) 385-92.

[40] D. Geldart, I. M. F. Wouters. Characterising semi-cohesive powders using angle of repose. *Part Part Syst Charact.* 13 (1996) 254-9.

[41] A. Schussele, A. Bauer-Brandl. Note on the measurement of flowability according to the european pharmacopiea. *Int J Pharm.* 257 (2003) 301-4.

[42] G. E. Amidon, M. S. Bergren, D. J. W. Grant, K. Marshall, S. Itai. Physical test methods for powder flow characterization of pharmaceutical materials: A review of methods. *Pharmacoepial Forum.* 25 (1999) 8298-308.

[43] N.-O. Lindberg, M. Palsson, A.-C. Pihl, R. Freeman, T. Freeman, H. Zetzener, et al. Flowability measurements of pharmaceutical powder mixtures with poor flow using five different techniques. *Drug Dev Ind Pharm.* 30 (2004) 785-91.

[44] M. Linsenbuhler, K.-E. Wirth. An innovative dry powder coating process in non-polar liquids producing tailor-made micro-particles. *Powder Technol.* 158 (2005) 3-20.

[45] D. A. Miller, J. T. McConville, W. Yang, R. O. W. III, J. W. McGinity. Hot-melt extrusion for enhanced delivery of drug particles. *J Pharm Sci.* 96 (2007) 361-76.

[46] S. G. Kapsi, J. W. Ayres. Processing factors in development of solid solution formulation of itraconazole for enhancement of drug solution and bioavailability. *Int J Pharm.* 229 (2001) 193-203.

[47] S. Jamzad, R. Fassihi. Role of surfactant and pH on dissolution properties of fenofibrate and glipizide-technical note. *AAPS Pharm Sci Tech.* 7 (2006) E1-E6.

[48] K. C. Waterman, A. J. Carella, M. J. Gumkowski, P. Lukulay, B. C. MacDonald, M. C. Roy, et al. Improved Protocol and Data Analysis for Accelerated Shelf-Life Estimation of Solid Dosage Forms. *Pharm Res.* 24 (2007) 780-9.

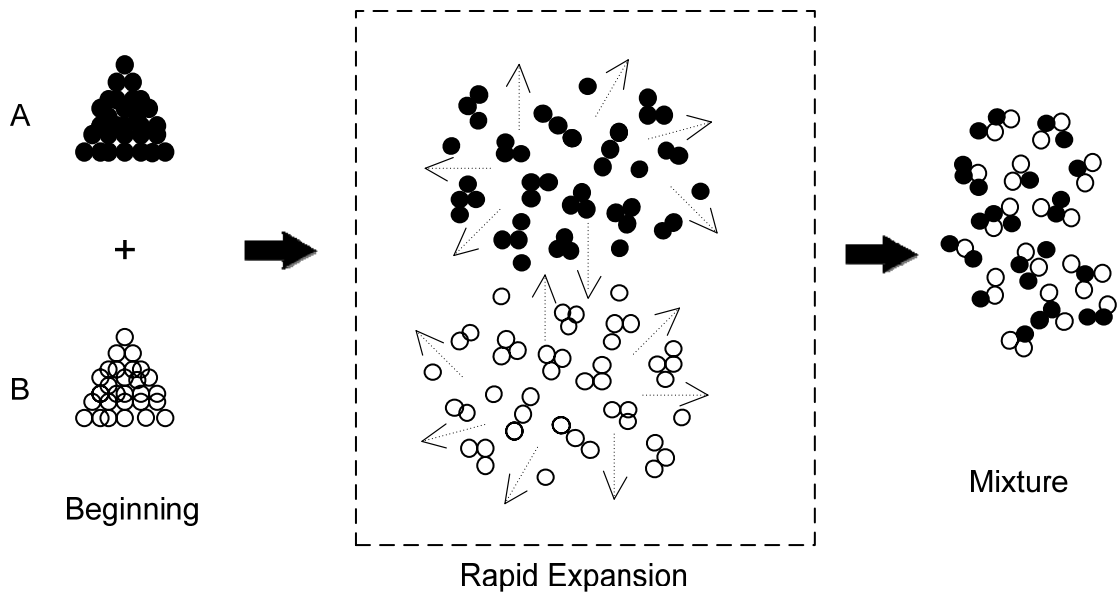


Figure 3.1 Mechanism for deagglomeration and mixing of particles during the process known as rapid depressurization of supercritical suspension (RDSS) [18].



Figure 3.2 Itraconazole nano-flakes (produced using SAS-EM method) cling to the spatula, because of a poor flowability of the drug powder.

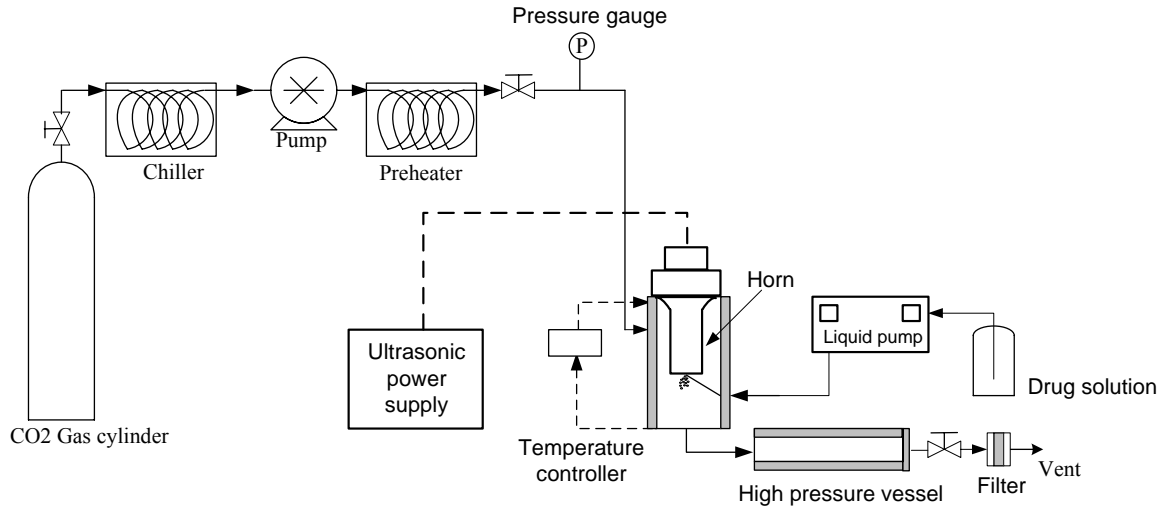


Figure 3.3 Schematic of supercritical antisolvent with enhanced mass transfer (SAS-EM) apparatus used to produce drug nanoparticles.

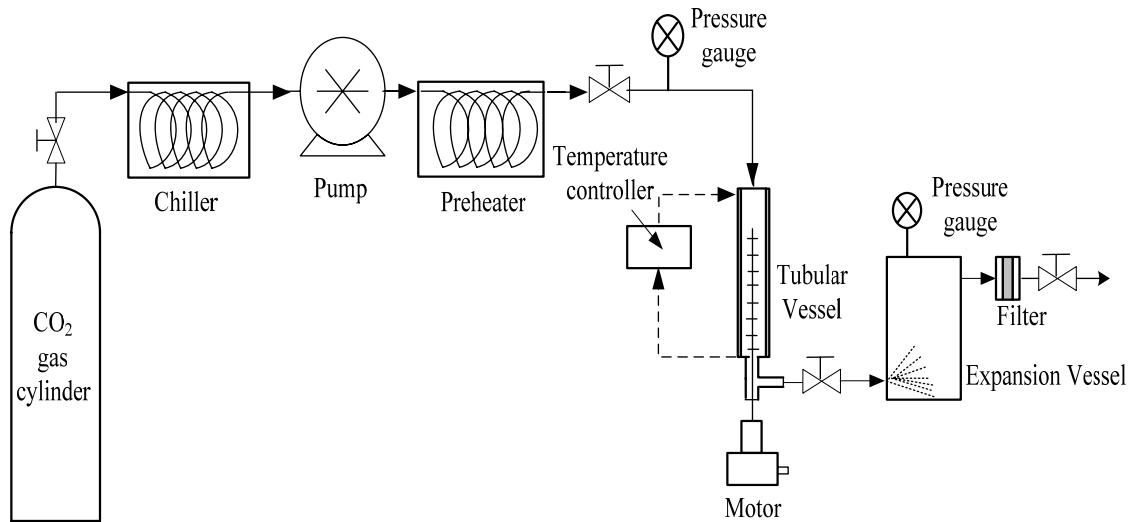
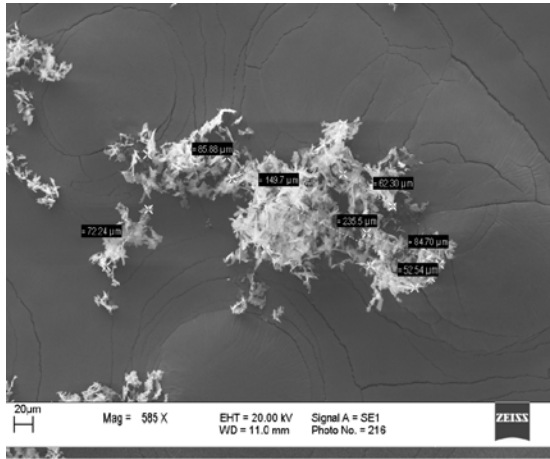
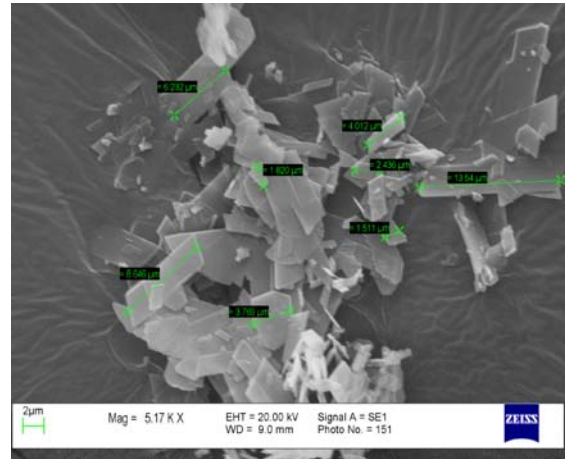


Figure 3.4 Schematic of rapid depressurization of supercritical suspension (RDSS) apparatus used for mixing of nanoparticles.



(a)



(b)

Figure 3.7 SEM images of itraconazole nano-flakes obtained using SAS-EM method: (a) low magnification, showing loose agglomerates, and (b) high magnification, showing individual particles.

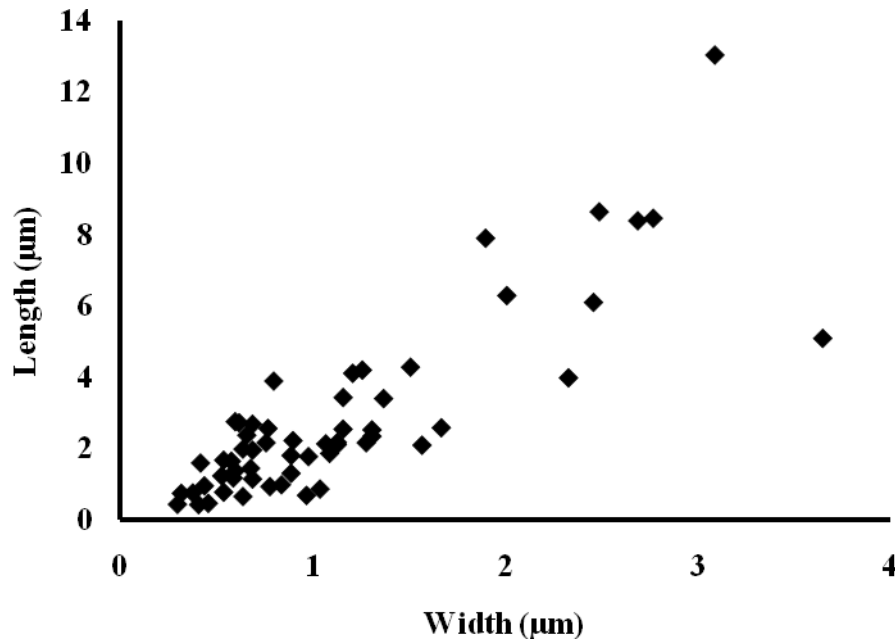


Figure 3.8 Particle size distribution of randomly selected drug particles (n= 60) produced via the SAS-EM method.

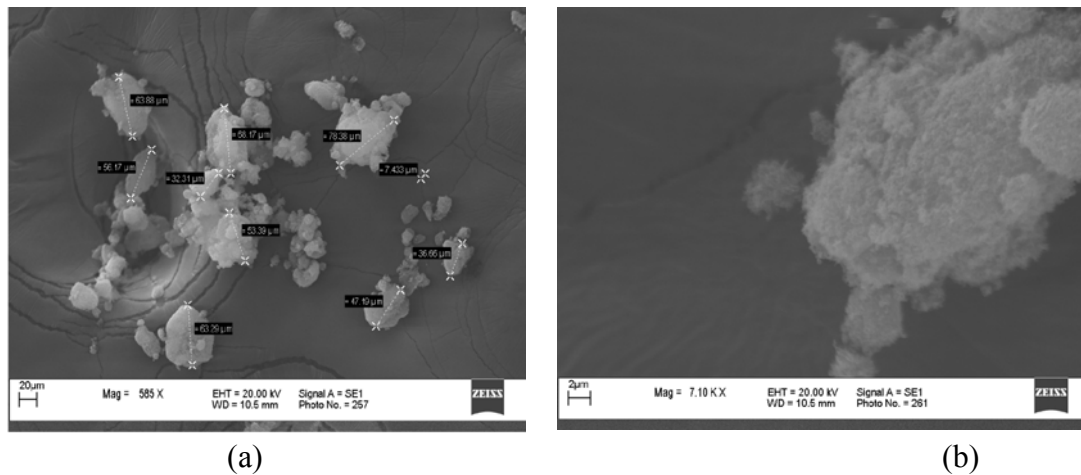


Figure 3.9 SEM images of silica agglomerates at (a) low magnification, and (b) high magnification.

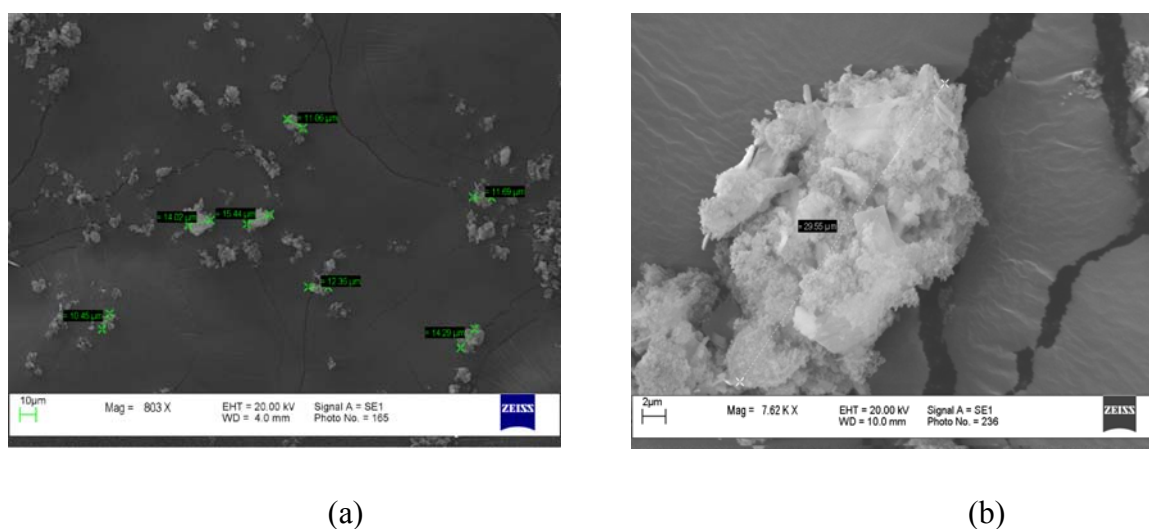
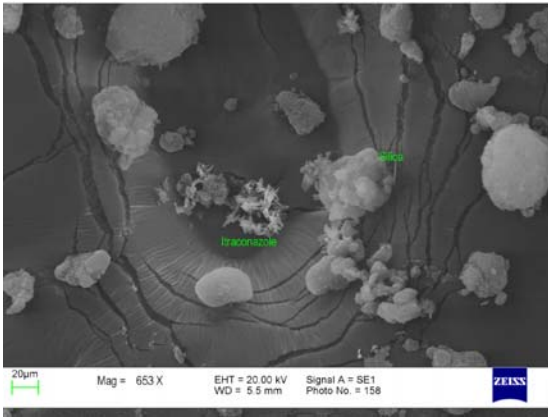
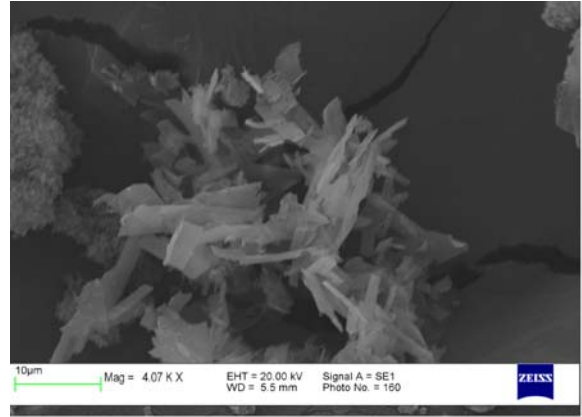


Figure 3.10 SEM images of RDSS mixture of itraconazole with silica at (a) low magnification and (b) high magnification showing, re-agglomeration in mixed state.

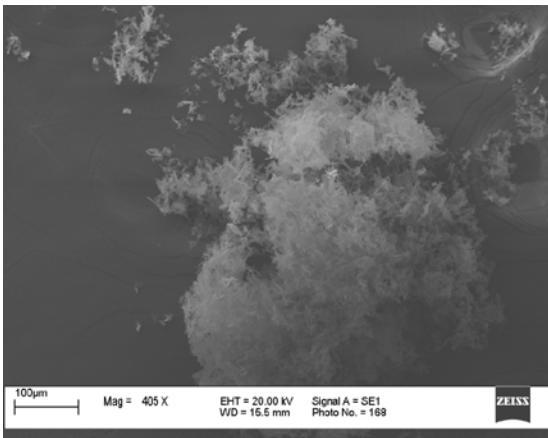


(a)

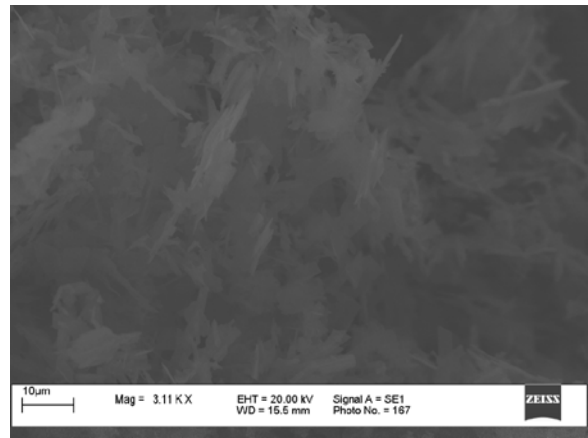


(b)

Figure 3.11 SEM images of physical (spatula-mixed) mixture of itraconazole nanoflakes with silica showing (a) a separate presence of silica and drug agglomerates and (b) a drug agglomerate at a high magnification.

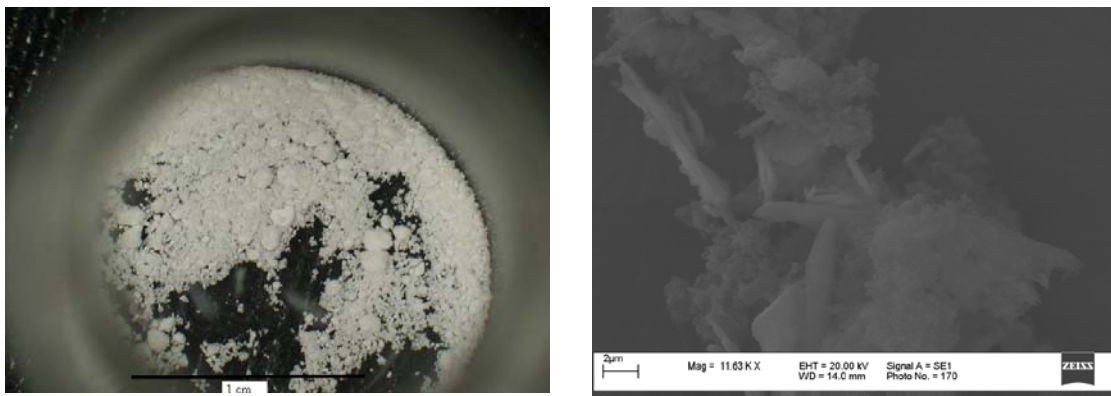


(a)



(b)

Figure 3.12 SEM images of itraconazole nanoflakes after storage at 90 °C for 25 days, showing (a) low magnification, low magnification; and (b) high magnification, showing fusion of individual nanoflakes.



(a)

(b)

Figure 3.13 RDSS mixture of silica/itraconazole nanoflakes after storage at 90°C for 25 days: (a) optical image and (b) SEM image.

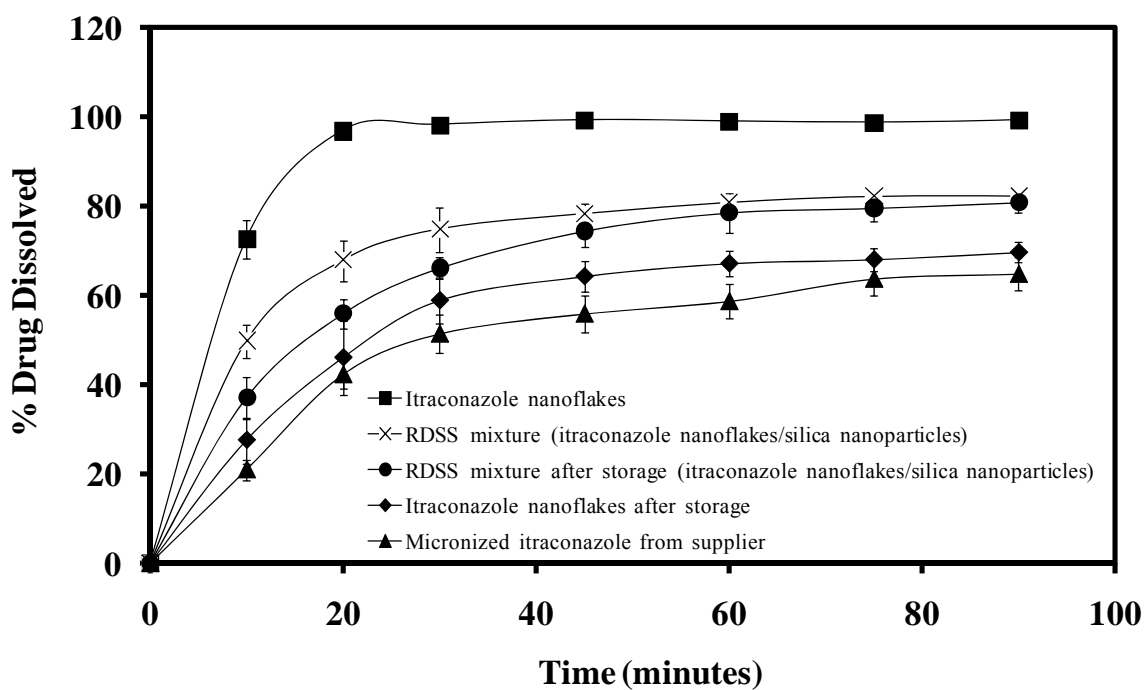


Figure 3.14 Dissolution profiles of itraconazole and itraconazole/silica mixture.

Table 3.1 Physical properties of itraconazole

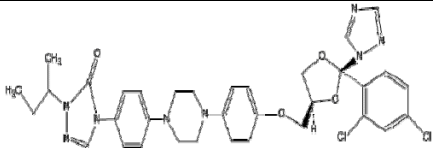
Drug name	Drug structure	Empirical formula	Mol.Wt.	Melting point (°C)
Itraconazole	 <p>The chemical structure of itraconazole consists of a 1,2,4-triazole ring substituted with a 2-hydroxypropyl group and a 2,2-dimethyl-1,3-dioxolane ring. This dioxolane ring is linked via an ester bond to a piperazine ring, which is further connected to a biphenyl system. One of the phenyl rings of the biphenyl system is substituted with a 2,4-dichlorophenyl group.</p>	$C_{35}H_{38}Cl_2N_8O_4$	705.64	166.2

Table 3.2 Angle of repose, compressibility index, and Hausner ratio for mixtures and individual components

Component or Mixture	Angle of Repose (°)	Aerated Density (mg/ml)	Tapped Density (mg/ml)	Compressibility Index, CI (%)	Hausner Ratio
Silica	30 ± 0.9	41.0	44.2	12.4	1.12
Itraconazole (Supplier)	41.6 ± 1.0	256.9	391.4	52.4	1.52
Itraconazole (SAS-EM)	46.3 ± 0.3	36.4	55.7	52.9	1.53
Physical Mixture – Itraconazole(SAS-EM) and silica	41.7 ± 2.6	39.8	49.8	25.0	1.25
RDSS-Itraconazole (SAS-EM) and silica	34.7 ± 1.7	105.4	120.5	14.3	1.14

Table 3.3 Scale of flowability ^a

Flow Character	Angle of Repose (°)	CI (%)	Hausner Ratio
Excellent	25-30	< 10	1.00-1.11
Good	31-35	11-15	1.12-1.18
Fair	36-40	16-20	1.19-1.25
Passable	41-45	21-25	1.26-1.34
Poor	46-55	36-31	1.35-1.45
Very poor	56-65	32-37	1.46-1.59
Very Very poor	>66	>38	>1.60

^a Data taken from ref [42].

4 NANO-MIXING BY SONICATION IN LIQUID CO₂

4.1 Abstract

Nanoparticles (about 200 nm thick and 600-12000 nm long flakes) of dipyridamole, a poorly water-soluble anti-thrombosis drug, are produced by supercritical antisolvent solvent with enhanced mass transfer method. Applicability of sonication in liquid CO₂ for mixing of drug and excipient nanoparticles is demonstrated for several binary mixtures of drug and excipient. The drug particles are mixed with three different excipients: silica nanoparticles, lactose microparticles, and polyvinylpyrrolidone nanoparticles. To intimately mix at nanoscale, macro mixtures of dipyridamole and excipient particles are sonicated in liquid carbon dioxide. The effects of ultrasonic energy, amplitude, and component weight ratio are studied for the binary mixtures. Characterization of mixing is done using several methods. Scanning electron microscopy is used as a primary method for microscopic analysis. Two macroscopic effects, drug dissolution and blend homogeneity (relative standard deviation), are used to characterize mixing quality of drug/lactose mixture. Results of drug dissolution and blend homogeneity show effectiveness of the proposed mixing method for fine size particles. Material handling properties of drug/silica and lactose/silica mixtures were examined. Upon mixing, the handling properties are significantly improved as measured by compressibility index and Hausner ratio. Liquid CO₂ offers an environmentally benign

media for mixing. In addition, the mixture obtained does not contain any residual solvent as compared to the sonication in organic liquids. Upon depressurization, CO₂ is easily removed from the mixture providing a facile recovery of the product.

4.2 Introduction

The bioavailability of poorly water-soluble hydrophobic drugs (Class II in Biopharmaceutics Classification System) is limited by their solubility and dissolution rate [1]. However, the dissolution rate can be improved by decreasing the particle size and/or crystallinity [2-4]. Several studies have been carried out to increase the dissolution rate of drugs by decreasing the particle size by creating nano- and micro-particles. However, the fine drug particles have a high tendency to agglomerate due to van der Waals attraction or hydrophobicity, decreasing surface area over the time [5-7], which in turn causes a decrease in the dissolution rate or bioavailability [7-9].

Powder mixing is a very important unit operation in pharmaceutical industry as it directly affects the drug content uniformity in the final drug/excipient mixture [10, 11]. The increased use of nano/micro size drug particles demands efficient deagglomeration and mixing of cohesive drug particles with excipients like lactose. The agglomeration of particles can affect granulation, fluidization, mixing, and blending operations [12]. The presence of cohesive- particle agglomerates decreases the efficiency of mixers as well as affects the powder flow due to bridging and spatial heterogeneity [13]. For a better uniformity of drug formulation or obtaining homogeneous mixture (especially for cohesive powder mixtures having a low drug content), it is very important to deagglomerate fine cohesive drug particles and intimately mix them with excipients to

prevent further agglomeration during subsequent unit operations. Currently available mixers are not effective in deagglomeration of highly-cohesive drug particles smaller than 10 μm in size; or they require very high shear or impaction, which indeed act as a particle size reduction device rather than a conventional mixer [14]. For example, rotary and vibratory ball mills can be used for mixing of fine powders [15, 16]; however the use of high energy may affect the crystal lattice of the particles which can influence the physico-chemical stability. The tumbler, most common mixing equipment in pharmaceutical industry, is not effective if de-agglomeration is required [17]. Various recent studies involving dispersion of nanoparticle agglomerates (especially silica) in liquid media have been carried out in the systems involving high shear stresses including high shear impeller mixers, high pressure dispersion system, rotor-stator system, etc. [18-21]. Linsenbuhler and Wirth 2005 [22] have carried out deagglomeration and coating of silica nanoparticles on the lactose particles using rotor-stator system (Ultra-Turrax-Disperser) involving liquid nitrogen as a medium although they did not study deagglomeration and mixing with cohesive drug nanoparticles.

Several methods for the mixing of nanoparticles have been presented in the literature [23]. Rapid depressurization of supercritical suspension (RDSS) [9, 24] and sonication in liquids (n-hexane) are found to perform better than other nanomixing methods. So far, these methods have been tested with inorganic nanopowders. Sonication in liquids (e.g., n-hexane, water) has several disadvantages like material has to wet the liquid and involves additional steps of filtration and drying as well as the residual solvent in the final mixture.

In this study, sonication in liquid CO_2 is proposed for deagglomeration and

mixing of dipyridamole nanoparticles with various excipients of different particle sizes. We have chosen polyvinylpyrrolidone (PVP), lactose and silica as excipients for the study. Sonication energy and amplitude will affect these materials differently due to variations in their physical-chemical properties. Experiments were executed at various weight ratios and ultrasonic energies using constant ultrasound amplitude. The characterization of mixtures is mainly done with scanning electron microscopy and supported by drug homogeneity, drug dissolution, and handling properties. Dipyridamole is a hydrophobic/lipophilic ($\log P = 1.5$, $pK_a = 6.4$, $T_g = 40\text{ }^\circ\text{C}$) drug and is practically insoluble in water [25]. Physical properties of dipyridamole are given in Table 4.1. Dipyridamole is used as an antithrombotic agent at lower dosages, and as a vasodilatic agent at higher dosages. Its bioavailability solely depends on the dissolution rate in the gastrointestinal tract. Dipyridamole has yellowish green color which is also helpful in the visual inspection of mixing.

Drug nanoparticles are produced by supercritical antisolvent with enhanced mass transfer (SAS-EM) method [26]. Supercritical carbon dioxide was utilized as an antisolvent in SAS-EM method, and liquid CO_2 as a medium in the sonication, due to its mild critical point (73.7 bar and 31.1°C) and suitability for the processing of pharmaceutical compounds. Upon depressurization, CO_2 leaves the solid matrix without any residues. Sonication in CO_2 (Figure 4.1) involves the breakage of particle agglomerates and subsequent mixing due to cavitation.

The proposed method can be used for preblending of cohesive drug with excipients which involves breaking of drug agglomerates and subsequent mixing with excipient. Formation of random and interactively ordered mixture by deagglomeration of

drug and mixing with excipient improves dissolution rate (bioavailability) of poorly water- soluble drugs [27-30]. Preblending is found to be useful and has been suggested during various drug mixing studies in the literature [10, 31].

The preblending of drug particles with excipients (e.g., silica, lactose, etc.) has advantages including: (a) an improvement in the flowability of drug powder or reduction in segregation which leads to effective mixing with other excipients using conventional mixers [32], (b) a decrease of electrostatic charge of fine drug particles (e.g., charge on drug nanoparticles can lead to several problems in mixing or other operations due to clinging of particles to vessel wall surface or agitator surface [33]), (c) effective wetting (i.e., due to hydrophilicity of excipient particles) and prevention of reagglomeration of drug particle during dissolution (e.g., hydrophobic drugs suffer from wetting and reagglomeration in dissolution media [34-37]), and (d) a better drug homogeneity in a dosage.

4.2.1 *Background*

Sonication in liquids

The nanoparticles can be effectively dispersed by sonication in liquids (e.g., water, n-hexane, etc.). Propagation of ultrasound through fluid media creates high and low pressure cycles. During low pressure cycle in the liquid media, small vapor cavities are created, which grow to attain a resonance size during further cycles. During the next high pressure cycle cavities violently collapse creating shock waves and liquid jet streams. This phenomenon, termed as cavitation, produces transient high local pressures and high temperatures [38]. It has been observed that the micro agglomerates of nanoparticles can

be broken by cavitation [39]. The agglomerate breakage is a function of power input, pressure amplitude, suspension volume, and agglomerate size. The liquid jet streams created during cavitations are effective in overcoming cohesive forces among particles when wetted in the liquid.

Sonication in liquid CO₂ can break agglomerates of nanoparticles by cavitation and cause mixing of different nanoparticles (Figure 4.1). Due to high vapor pressure of carbon dioxide, it is possible to create cavitation phenomenon even at high pressures as opposed to that in liquids like water. The acoustic pressure above Blake threshold pressure has to be applied in order to start the initiation of cavitation bubble. The acoustic pressure (P_A) and Blake threshold pressure (P_B) are calculated [40]

$$P_A = \sqrt{2 \times \rho \times c \times I_{US}} \quad (1)$$

$$P_B = P_0 - P_V + \frac{4}{3} \sigma \times \sqrt{\frac{2}{3} \times \frac{\sigma}{\left(P_0 + 2 \times \frac{\sigma}{R_0} - P_V \right) \times R_0^3}} \quad (2)$$

where ρ is density of fluid, c is speed of sound, I_{US} is intensity of ultrasound, P_0 is external pressure, P_V is vapor pressure, σ is surface tension, and R_0 is equilibrium radius of the bubble (cavity). The properties of CO₂ for the calculation of P_A and P_B are given in Table 4.2 [41]. At our processing condition of 78 bar and 5 °C, acoustic pressure (1.9 bar) is lower than Blake threshold pressure (38.5 bar). During sonication, heating is expected near the probe surface, which will decrease P_B as temperature increases rapidly, therefore lower threshold pressures can be expected in actual practice [40]. The presence of cavitation can be confirmed by doing experiment in pressure vessel with quartz window as well as by hearing cavitation sounds as it made in the ambient liquids. CO₂ pressure of 78 bar (higher than vapor pressure, 38.5 bar) was used during the experiments

to ensure liquid phase. A low temperature of 5 °C was used in order to reduce any aggregation of drug particles or soft excipient particles due to collisions during sonication. In addition to cavitation, ultrasonic field itself causes deagglomeration and mixing of nanoparticles.

Attractive forces in nanoparticles

As particle size decreases, the forces of attraction between particles like van der Waals, electrostatic, and capillary forces becomes dominant as compared to gravitational force. If we neglect electrostatic force due to the absence of charge on particle and the capillary force due to hydrophobicity of particles, van der Waals forces will be mainly responsible for the agglomeration of nanoparticles, given as [42]

$$F_{VdW} = \frac{A_{121}d}{24h^2} \quad (3)$$

where A_{11} is Hamaker constant for the solid, A_{22} is Hamaker constant for the fluid, d is diameter of particle, $A_{121} = A_{11} + A_{22} - 2A_{12}$, $A_{12} = \sqrt{A_{11}A_{22}}$ (using the most common geometric mean), and h is separation distance between particles (usually 4 °A). Therefore, for a given particle size with particular separation distance, the attraction force is proportional to the Hamaker constant A_{121} . A decrease in Hamaker constant A_{121} will be helpful in the deagglomeration and subsequent mixing of fine particles. Hamaker constant for liquid CO₂ (A_{22}) can be calculated as [43]

$$A_{22} = 24\pi\gamma_2(d_0^2)_2 \quad (4)$$

where γ_2 is surface tension (for 78 bar and 5°C, 6.36×10^{-3} N/m, [44]) and d_0 is approximately equal to the molecular diameter of material (~ 0.34 nm [45]). Table 4.3 shows Hamaker constants A_{11} , A_{22} , and A_{121} for various solid, fluid, and fluid-solid

interactions, respectively [22, 46-48]. Usually, water is the most effective in decreasing attractive forces between particles. Liquid CO₂ is comparable to liquid nitrogen or n-hexane for solid- fluid interactions. CO₂ is the preferred choice due to the ease of separation (by simple depressurization), environmental friendliness, and relative moderate temperature and pressure conditions for its liquid phase.

4.3 Materials and methods

4.3.1 Materials

Dipyridamole (Sigma- Aldrich), fumed silica (hydrophilic, surface area 200±15 m²/g, tapped density 40 g/l, CAB- O- SIL^R M- 5P, Cabot Corp.), R972 silica (hydrophobic, surface area 114 m²/g, bulk density 0.05 g/ml, Degussa), lactose monohydrate (received as a gift, D50 ≤ 5 μm and D90 ≤ 10μm, Lactochem Microfine, Friesland Foods Domo, The Netherlands), polyvinylpyrrolidone K30 (Sigma- Aldrich), methanol (HPLC grade, Pharmaco- AAPER), and CO₂ (bone dry, Air Gas) were used as received.

4.3.2 Production of dipyridamole nanoflakes

Dipyridamole drug particles were produced by SAS-EM method (Figure 4.2), which was previously developed in our laboratory. More details of the process are presented elsewhere [49]. Drug solution was prepared by dissolving drug in methylene chloride at 5 mg/ml concentration. Flow rate of drug solution was maintained at 1 ml/min while antisolvent flow rate (supercritical CO₂) was kept at 10 gm/min. The capillary nozzle (PEEKsil, Upchurch Scientific) of 75 μm in diameter was used for the delivery of

drug solution on the surface of ultrasound horn inside the pressure vessel. Ultrasound amplitude of 40% (24 μm , total ultrasonic power rating of 750 W) was applied during the whole process. Process was carried out at 100 bar pressure and temperature of 37 °C. In one semi-batch, 500 mg of drug was processed. Procedure was repeated until the desired amount of SAS-EM produced drug powder was obtained (up to 4-5 g).

4.3.3 *Production of polyvinylpyrrolidone nanopowder*

Polyvinylpyrrolidone (PVP) nanoparticles were produced by SAS (supercritical antisolvent) method. Details of the process are presented elsewhere [50, 51]. PVP was dissolved in dichloromethane/acetone (25/75, v/v) mixture at 20 mg/ml concentration. Flow rate of drug solution was maintained at 0.5 ml/min while antisolvent flow rate (supercritical CO₂) was kept at 10 gm/min. Capillary nozzle (PEEKsil, Upchurch Scientific) of 75 μm in diameter was used for the delivery of PVP solution. Process was carried out at 78 bar and 35 °C. In one semi-batch, 1 g of PVP was processed. Procedure was repeated until the desired amount of SAS produced by PVP powder was obtained (up to 2- 3 g).

4.3.4 *Deagglomeration and mixing in liquid CO₂*

Figure 4.3 shows the schematic diagram of experimental setup used for mixing powders in carbon dioxide. It consists of compressed carbon dioxide gas cylinder, chiller, piston pump for pumping CO₂, an ultrasonic processor (Sonics and Materials) producing ultrasonic waves at a frequency of 20 kHz with maximum power capability of 750 W, and a 120 ml stainless steel mixing vessel cooled by ice bath. The ultrasonic processor consists of three major components: an ultrasonic power supply, a transducer,

and a horn with 0.75 in. tip diameter. The temperature and pressure inside the mixing vessel were measured with a thermocouple and a pressure gauge. To prevent the loss of powders during the vessel depressurization, a filter (Millipore Inc., Fluoropore membrane filter, Polytetrafluoroethylene bonded to high density polyethylene, 0.22 μm) was installed at the top exit of the vessel.

The ultrasonic processor is designed to deliver constant amplitude (61 μm at 100% amplitude settings for a horn used in these experiments), i.e. it automatically adjusts power to maintain constant amplitude during the operation. Therefore, power delivered from the processor depends on the resistance to the movement of horn which is affected by setup and process parameters, such as volume of a mixing vessel, horn size, mixture viscosity, pressure, etc. All experiments were conducted at constant amplitude of 35% ($\sim 21 \mu\text{m}$).

Binary mixtures of nanoparticles, in a given weight ratio, were loaded into a stainless steel vessel and then carbon dioxide was introduced. The horn was immersed into the vessel, so that only 100 ml of vessel volume was available for mixing. Vessel pressure was maintained within ± 3.5 bar at the start of each experiment. The vessel was cooled to 5 ± 1 $^{\circ}\text{C}$ in all experiments unless otherwise mentioned. After reaching the desired pressure and temperature in the vessel, ultrasound was applied in pulse mode of 3 s (3 s on, 3 s off) to supply particular amount of energy at constant amplitude to cause mixing. Time taken by ultrasonic processor to supply particular amount of the energy was also recorded. After mixing, the vessel was slowly depressurized to prevent carryover of particles with CO_2 . Further loss of particle was prevented using filter at the top exit of the vessel. After complete depressurization, vessel was allowed to warm up to room

temperature and then opened, and powder was collected for analysis.

4.3.5 *Drug Homogeneity*

Mixing of drug with lactose at loadings of 0.18, 1, and 4.93 wt. % (300 mg of total weight loaded into pressure vessel) has been carried out at ultrasound energy of 7.5 MJ/m³ and 35% amplitude. For determination of drug concentration in the final mixture after sonication, first the mixture (10 mg) was dissolved into methanol. The concentration of drug is obtained using UV spectroscopy at wavelength of 290 nm after filtering the solution through 200 nm syringe filter (Fisher Scientific) to remove lactose particles. Also any absorbance at 290 nm due to lactose was checked for lactose in methanol solution. Relative standard deviation of drug for 10 samples was calculated using the following equations:

$$RSD = \frac{\sigma}{C} \quad (5)$$

$$\sigma^2 = \frac{\sum_{i=1}^n (\bar{C} - C_i)^2}{n-1} \quad (6)$$

where n is the total number of samples, σ^2 is the variance, σ is the standard deviation, \bar{C} is the mean concentration determined experimentally, and C_i is the sample concentration. Concentration or content variation (σ^2) is the sum of (a) variance due to variation in weight of sample, (b) variance due to analytical errors, and (c) variance due to mixing.

4.3.6 *Drug Dissolution*

Drug dissolution was performed by placing the sample (equivalent to 10 mg of

drug) in 900 ml freshly prepared acetate buffer (pH=5) in a USP II dissolution apparatus at 37 °C and 75 rpm. Three-mililiter (3-ml) samples were drawn at time intervals of 5, 10, 20, 30, 45, 60, 75, and 90 min. Change in the volume of the solution due to sample withdrawal was considered during concentration determinations. Solutions were filtered using 200- nm inline syringe filter (Alltech; PTFE, 17 mm in size), to remove any suspended particles. Drug concentrations were measured using UV spectroscopy (Spectronic Genesys 2) at $\lambda = 284$ nm. Calibration of drug concentration was obtained by dissolving the drug in methanol and then diluting with acetate buffer. Drug dissolution was performed in triplicates. The ratio of saturation drug concentration (~ 73 $\mu\text{g/ml}$ experimentally determined) to the actual drug concentration in dissolution media (~ 11 $\mu\text{g/ml}$) was 6.6:1, which is more than the 3:1 that is required to maintain the desired sink condition. Complete dissolution of drug was observed within 180 min. for the drug samples which were not dissolved in 90 min. Dipyridamole is a weakly basic drug (pKa = 6.4) with aqueous solubility of 0.008 mg/ml [52]. Due to very low aqueous solubility, acetate buffer of pH =5 was chosen to perform dissolution study to have the desired sink condition.

4.3.7 *Compressibility index*

Compressibility index (*CI*) of powders was calculated using aerated (bulk) and tapped densities. For measuring tapped density, powder was filled into graduated cylinder and tapped 500 times mechanically or until no further change in volume occurs (1250 taps) using tap density tester (Pharma Alliance Group) for USP II method .

$$CI(\%) = \frac{\text{Tapped density} - \text{Aerated (bulk) density}}{\text{Tapped density}} \times 100 \quad (7)$$

4.3.8 *Hausner ratio*

Hausner ratio was obtained by dividing tapped density by aerated (bulk) density. The ratio indicates powder compacted after mechanical tapping.

$$\text{Hausner Ratio} = \frac{\text{Tapped density}}{\text{Aerated (bulk) density}} \quad (8)$$

4.3.9 *Scanning electron microscopy*

Surface morphologies of the various mixtures were studied using environmental scanning electron microscope (Zeiss EVO 50). The sample was spread using a brush onto one surface of two sided adhesive carbon tape on aluminum stub, and a thin coating (~15 nm) of gold is applied onto the sample using sputter coater (Electron Microscopy Services, EMS 550X) before microscopy.

4.4 Result and Discussion

In this study, application of sonication in liquid CO₂ is demonstrated by mixing various binary mixtures of different particle size and shape. Details of experiments are given in Table 4.4.

4.4.1 *Production of drug and PVP nanopowders*

Figure 4a shows the rectangular to globular shaped particles of drug obtained from the supplier. Initially dipyrindamole particles were produced by SAS (supercritical antisolvent) method by using methanol as a solvent, which gave fiber like long nanoflakes (Figure 4b) as compared to globular shaped particles from the supplier. Various studies on re- crystallization of drug by SAS method have observed a change in

particle morphology [53, 54]. Figure 4 c- e shows drug particles obtained by SAS- EM method. The drug particle sizes obtained from SAS-EM method primarily depend on ultrasound amplitude. It has been shown that with an increase in ultrasound amplitude (power) size of particle decreases [49, 54]. Increasing the amplitude from 25% to 40% for the same drug concentration (in methanol), there was a decrease in size (length) of particles. Figure 4c-d shows the decrease in length as well as formation of submicron size nanoflakes upon increase in ultrasound amplitude. Figure 4e shows a further decrease in particle size (as compared to Figure 4d) upon changing solvent to dichloromethane. Methanol is a better solvent for (saturation solubility of drug ~35 mg/ml) dipyridamole than dichloromethane (saturation solubility of drug ~ 6 mg/ml). Therefore a high degree of supersaturation can be achieved for drug- dichloromethane solution upon the introduction of antisolvent (supercritical CO₂). A higher supersaturation leads to the formation of large number of nuclei whose growth is limited by drug concentration in the vessel. The particle size distribution of randomly selected drug particles (n= ~100) obtained by SAS- EM method using dichloromethane as solvent at 40% ultrasound amplitude is shown in Figure 5. The drug particles were found to be flakes of up to 200 nm in thickness. Primary particle sizes of dipyridamole produced by SAS-EM method were found in the range of submicron to 35 µm (Figure 5b) as compared to a micron to 40 µm size particles from the supplier (Figure 5a). The other process parameters like solution flow rate, type of solvent, drug concentration, pressure, temperature and antisolvent (CO₂) flow rate do affect primary particle size. More details on the effect of process parameters can be found elsewhere [53, 55]. The presence of some larger drug nanoflakes will help in analyzing mixing of drug with excipients like lactose using SEM

due to distinct size difference with lactose microfines. Because of the high surface area of the produced drug nanoflakes, loose agglomeration or overlapping of several primary particles was observed. The sizes of these loose drug agglomerates can be seen as high as 30 μm (Figure 4d).

Figure 6 shows images of PVP particles obtained from supplier, SAS, and SAS-EM methods. The PVP particles from the supplier are in the range of 20-100 (Figure 6a) as compared to 0.30-0.60 μm size particles by SAS method. PVP nanoparticles obtained by SAS method formed agglomerates of particles in the size range of 30-100 μm . The effect of process parameters (for SAS) such as solvent, molecular weight of PVP, and nozzle diameter on particle sizes was studied in detail by Ghokale et al. 2007 [51]. In the case of PVP, the application of ultrasound (SAS-EM method) was not useful in decreasing particle size. PVP particles became fuse (Figure 6 (d)) when even lower limit amplitude (21%) of ultrasound was applied. This fusion of PVP nanoparticles can be attributed to the impact collisions (against vessel wall and/or among particles) and also softness of the material. In addition, high pressure CO_2 can lower glass transition temperature of polymer significantly [56] promoting more fusion.

4.4.2 *Mixing of drug nanoflakes with microfine lactose*

Drug nanoflakes were mixed in various proportions (0.14, 0.96, and 5.31 wt. % measured experimentally) with lactose microfines. To demonstrate the usefulness of sonication in liquid CO_2 for nanomixing, experiments are carried out at various ultrasonic energy and constant amplitude (35%). The characterization of mixture was done microscopically using SEM. Drug content homogeneity and drug dissolution were used

to characterize mixture at macroscopic level.

4.4.2.1 Mixture characterization by SEM

Figure 4.7 shows SEM images of lactose and lactose-drug mixtures. Lactose obtained from supplier is in the cohesive agglomerate form with size ranging from few microns up to 200 microns (Figure 4.7a). Primary particle size of lactose ranges from submicron (200 nm) to 10 microns with $D_{50} \leq 5 \mu\text{m}$ (Figure 4.7b). Figure 4.7c shows random and interactively ordered type of mixing for drug– lactose mixture with 5 wt. % drug loading. Deagglomeration of lactose agglomerates has been observed in all mixing conditions. Figure 4.7d- e shows interactively ordered type of mixing for drug-lactose mixture (coating of very fine lactose particles on drug particle, also reverse can be true with high drug concentration for fine drug particles) with 1 wt. % drug loading. The fine particles present on the surface of drug flakes are assumed to be that of lactose due to higher wt. % (99%) in the mixture. Only larger drug nanoflakes distinctly were located due to size/shape similarity of smaller nanoflakes with lactose fines. Figure 7f shows physical mixing, (spatula mixing for 2 min) of drug with lactose showing separate regions of drug and lactose particles.

4.4.2.2 Drug content homogeneity

For the drug-lactose mixture, the relative standard deviation (RSD) decreases as the drug content increases. Results yielded RSDs of 3.8, 3.37, and 2.3 % for drug contents of 0.14, 0.96, and 5.31 wt. % for drug/lactose mixture, respectively. This trend is consistent with various mixing studies done for the characterization of drug

homogeneity [57-59]. Variation in ultrasonic energy and amplitude can play a role in drug homogeneity. The mixing studies performed by Malmqvist and Nystrom, 1984 [60] have shown that the contribution of sampling and analytical errors to a RSD can be as high as 2%. Therefore with RSD as low as 3.8 % (n=10) even for drug content of 14 µg in 10 mg (sample size) of mixture with only energy input of 7.5 MJ/m³ shows effectiveness of sonication (cavitation and ultrasonic field) in deagglomeration and mixing of drug with microfine lactose. For the random and interactive mixtures, RSD is reciprocal of square root of sample size [59]. The formation of random and interactive mixture was also confirmed for 5 wt. % drug in drug/lactose mixture. For sample size of 30 mg, RSD of 1.25 was observed experimentally as compared to theoretical value of 1.33. Therefore in an increase in sample size; a further decrease in RSD for drug/lactose mixture can be obtained. Due to the yellowish green color of drug particle, mixing quality can also be observed visually for drug/lactose mixture. Homogeneous color (yellowish white) was observed for mixtures even at drug content of 0.14 wt. %. Previous experience with other nanoparticle mixtures suggests that non homogeneous color regions can be seen easily for bad mixing quality mixtures. Results confirm the potential of mixing by sonication in liquid CO₂ for preblending of drug with excipient like microfine lactose for low drug content dosages of high homogeneity.

4.4.2.3 Drug dissolution

The extent/quality of mixing for lactose/drug mixture can also be determined indirectly by measuring how fast drug dissolves in the dissolution media. Higher dissolution rate informs about presence of deagglomerated drug particles in a mixture as

compared to only agglomerated drug particles. Figure 4.8 shows the dissolution curves for nanomixed drug/lactose (5 wt. % drug), physical mixture of drug/lactose obtained by spatula mixing (5 wt. % drug), drug nanoflakes (obtained by SAS-EM method), and supplier drug. Dissolution curves for drug nanoflakes and supplier drug were identical even though there was a significant difference in their particle size distribution (Figure 4.5). Similarity in the dissolution curve of drug nanoflakes and supplier drug is due to presence of agglomerated drug nanoflakes in dissolution media which was also confirmed during visual observation. Drug nanoflakes were in the agglomerated state in dissolution media were also due to the lack of wetting. Due to the presence of drug nanoflake agglomerates, the benefits of size reduction can not be seen. In the case of nanomixed drug nanoflakes/ lactose mixture, a rapid dispersion or deagglomeration of drug particles has been visually observed in the dissolution media due to the instantaneous dissolution of lactose particles which were surrounding the drug nanoflakes. An efficient dispersion of drug nanoflakes (for nanomixed drug/lactose mixture with 5 wt. % drug) leads to complete drug dissolution in less than 45 min as compared to ~62% (of total drug) in the case of physical mixture and ~54% for drug nanoflakes. Higher dissolution rate of drug nanoflakes in nanomixed drug/lactose mixture was also due to proper wetting of individual drug particles which were surrounded by lactose particles. Therefore efficient deagglomeration or mixing is required in order to see the benefits of nano/micro sizing in the case of poorly water- soluble drugs. The rate of drug dissolution (bulk effect) can be used along with SEM characterization (microscopic observation) and drug homogeneity (macroscopic quantification) as a tool to determine the extent of mixing of nano/micron sized drug particles with excipients.

4.4.3 *Deagglomeration and mixing of dipyridamole with PVP*

PVP has been used in the solid dispersions of poorly water- soluble drugs as well as a binder. It has been found that PVP prevents re-crystallization of amorphous drug during the storage. For example, up to 50 wt. % drug in drug/PVP mixture is found to be stable during storage, but at higher concentrations drug starts to recrystallize losing benefits of making solid dispersion [61]. In this study nanoparticles of PVP are mixed with drug nanoparticles in order to see how mixing is affected due to the soft material. PVP particles can prevent reagglomeration and helps in redispersion of drug particles if they are mixed intimately with drug nanoflakes. Figure 4.9 shows deagglomeration and mixing of dipyridamole with PVP at various conditions. Experiments for drug/PVP mixture were done at lower ultrasonic energy due to the possibility of fusion of PVP particles. Even at ultrasonic energy input of 2 MJ/m^3 , deagglomerated drug and PVP particles, and embedded (trapped) drug particles in PVP agglomerates were found (Figure 4.9a- b). The process serves the purpose of the prevention of reagglomeration of drug particles but forms bigger mixed agglomerate due to high cohesiveness of PVP particles. With the increase in PVP/drug weight ratio from 1/1 to 3/1, more presence of deagglomerated PVP and drug nanoparticles can be seen easily as compared to trapped drug nanoparticles inside PVP agglomerates (Figure 4.9c). A typical example of fusion of PVP nanoparticles upon sonication is shown in Figure 4.9d. Figure 4.10 shows the effect of excessive sonication on the mixing of drug with PVP. With sonication energy input of 68 MJ/m^3 , drug particles are held together by fused PVP particles forming bigger mixed agglomerates (Figure 4.10a). Figure 4.10b shows close-up of PVP fused-drug agglomerate showing sharp edges as well as individual particles which can also confirm

the absence of fusion of drug particles. PVP fused-drug nanoparticle agglomerates can be an alternative to solid dispersions at higher drug loading, as fused PVP will prevent reagglomeration of drug particles in further drug formulation operations.

4.4.4 *Deagglomeration and mixing of lactose/silica and dipyridamole/silica*

Experiments were done for mixing lactose/drug with hydrophilic/hydrophobic silica at various proportions. Effect of ultrasonic energy on mixing quality of samples has been seen. Characterization of mixtures was performed using SEM and handling properties.

4.4.4.1 *Mixture characterization by SEM*

Figure 11a shows the image of silica (hydrophobic R972) agglomerate. Non-porous fumed silica is used in oral formulations as a glidant [24, 32, 62]. In this work, pharmaceutical grade fumed silica (hydrophobic R972, and hydrophilic M5) consisting of 200-300 nm in length with aggregates of primary nanoparticles (9-30 nm) are utilized. These highly structured aggregates also form 30- 44 μm macro agglomerates with a very high void volume (>98%). Hydrophilic silica has a tendency to adsorb moisture up to 9 wt. % at greater than 70% relative humidity which can result into less deagglomeration during sonication because of capillary forces among silica particles.

At sonication energy input of 3.5 MJ/m^3 for R972 silica/lactose mixture (1/10, w/w), the presence of several intact silica agglomerates (Figure 4.11b) as well as deagglomerated silica coated onto lactose particles (Figure 4.11c) was observed. Deagglomerated silica was in the range of 200-400 nm coated onto the surface of some of

lactose particles (Figure 4.11d). With the increase in energy input to 7.5 and 12.5 MJ/m³, almost complete deagglomeration of silica (R972) was observed (one or two silica agglomerates can be seen in the sample analyzed) and the presence of highly deagglomerated silica covering the surface of lactose particles can be seen (Figure 4.11e-f). For the case of hydrophilic silica (M5) mixing with lactose (1/10, w/w) at lower energy input of 7.5 MJ/m³ silica agglomerates can be observed easily. Even with an increase in sonication energy input to 12.5 MJ/m³, deagglomeration of hydrophilic silica was incomplete. Linsenbuhler et al. [22] have shown that in a non-polar dispersant media, stabilization of hydrophilic silica is difficult as compared to hydrophobic silica due to hydrophobic/hydrophilic repulsion. These interactions can be determined from interfacial energy and surface tension between two phases. Linsenbuhler et al. have also observed larger agglomerates of hydrophilic silica after dispersing (using rotor-stator system) in liquid nitrogen (a non-polar liquid). Hence, hydrophilic silica can be easily stabilized in polar media as opposed to non-polar media. Similarly in the case of liquid CO₂ (a relatively non-polar media), reagglomeration of hydrophilic silica may have occurred during sonication which resulted into an inefficient deagglomeration and coating of lactose particles at given sonication energy. Another main reason for the insufficient deagglomeration of hydrophilic silica agglomerate can be due to the presence of hydrogen bonds. Hydrophilic silica has silanol (SiOH) groups which form hydrogen bond with other silica particles. The energy required for the breakage of hydrogen bond ($\sim 5.64 \times 10^{-13}$ J, [22]) is several times greater than van der Waals energy of attraction ($\sim 7.7 \times 10^{-19}$ J). Due to hydrophobicity of R972 silica (stabilization in non-polar liquid CO₂) and the absence of hydrogen bonding, better deagglomeration and coating of

lactose was achieved at lower sonication energy as compared to hydrophilic M5 silica.

The results for dipyridamole/silica (4/1, w/w) mixing are similar to those for lactose/silica mixing. At higher dipyridamole/silica weight ratio, several uncoated drug particles were observed while at lower weight ratio (1/1, w/w), trapped drug particles inside silica agglomerates were observed. Figure 4.12 shows images of the dipyridamole/silica mixture. Highly deagglomerated and coated (with silica R972) drug particles (up to individual particle) can be seen in Figure 4.12a-b at sonication energy of 7.5 MJ/m^3 . Due to the interparticle collision, fusion of some smaller drug particles resulted into larger drug particle (Figure 4.12c). For hydrophilic M5 silica mixing with drug nanoparticles, silica agglomerates, trapped/embedded drug particles inside silica agglomerates, and deagglomerated silica coated onto drug particles can be seen at sonication energy of 7.5 MJ/m^3 (Figure 4.12d). Even at high sonication energy of 143.8 MJ/m^3 , complete deagglomeration of M5 silica particles did not occur (Figure 4.13a). However, due to the high energy input, aggregation of some drug nanoparticles occurred (Figure 4.13b).

4.4.4.2 Handling properties of lactose/silica and dipyridamole/silica mixtures

Flowability of a powder is affected by various physical factors including particle size and shape, aerated (bulk) and true densities, moisture content, crystal form, surface electrostatic charge, and the types of equipment used for handling, storing, and processing [12]. Powder flow characterization of lactose/silica and drug/silica mixture was done using compressibility index and Hausner ratio, as these are two convenient and simple methods for semi-cohesive powders [63, 64]. Table 4.5 shows the results of the

compressibility index and Hausner ratio tests. The scale of flowability based on these properties is given in the Table 4.6 [64] . Silica is used as a glidant in pharmaceutical industry due to its excellent flow properties, which is evident from its results for compressibility index and Hausner ratio (“Good to Fair” flow characteristics). Micronized lactose from supplier and nanoparticle drug produced by SAS-EM method has “Very Poor” flow characteristics due to small particle size and a high van der Waals attraction. When the mixing of drug with hydrophobic silica (R972) was done by sonication in liquid CO₂, significant improvement in flow properties was observed, giving “Excellent” characteristic flow. The improvement can be attributed to layer (particle coating) of silica nanoparticles onto the drug nanoparticles and deagglomeration of the drug particles, resulting in a decrease in attractive forces among drug particles. The improvement in flow properties of M5/lactose mixture is small; with “Passable” flow characteristic, which is due to hydrophilic silica and lower energy of 3.5 MJ/m³ used to obtain silica M5/lactose mixture. It has been found from various studies that hydrophobic silica coated materials show better flowability properties than hydrophilic silica [32, 65]. Visual observations can also confirm the flowability of mixture (bad, fair, good etc) by examining flow while rotating vial containing powder radially.

4.5 Conclusions

Sonication in liquid CO₂ as a novel method for the mixing of drug nanoparticles with excipient nano/micro particles is successfully demonstrated. Based on electron microscopy, drug dissolution, and handling properties, the produced mixtures have a high quality of mixing. In the case of silica, hydrophobic/hydrophilic interactions between the

medium and the excipient play an important role in deagglomeration. For maximum mixing, there appear to be an optimum energy input. Mixing method demonstrated here has a potential in preparations of high content homogeneity formulations especially for low dosage drugs. And, due to effective deagglomeration and mixing of drug nanoparticles with excipients, drug particle agglomeration can be prevented in further processing of the nanomixtures for final dosage formulation.

4.6 Acknowledgments

Financial support from the National Science Foundation through NIRT grant DMI-0506722 is highly appreciated. Authors are thankful to Prof. Rajesh N. Dave of NJIT for technical discussions.

4.7 References

- [1] G. L. Amidon, H. Lennernas, V. P. Shah, J. R. Crison. A theoretical basis for a biopharmaceutical drug classification: the correlation of in vitro drug product dissolution and in vivo bioavailability. *Pharm Res (N Y)*. 12 (1995) 413-20.
- [2] A. Jounela, P. Pentikainen, A. Sothmann. Effect of particle size on the bioavailability of digoxin. *Eur J Clin Pharmacol*. 8 (1975) 365-70.
- [3] G. G. Liversidge, K. C. Cundy. Particle size reduction for improvement of oral bioavailability of hydrophobic drugs: absolute oral bioavailability of nanocrystalline danazol in beagle dogs. *Int J Pharm (Kidlington)*. 125 (1995) 91-7.
- [4] N. Rasenack, B. W. Muller. Dissolution rate enhancement by in situ micronization of poorly water-soluble drugs. *Pharm Res (N Y)*. 19 (2002) 1894-900.

- [5] A. J. Aguiar, A. W. Zelmer, A. W. Kinkel. Deaggregation behavior of a relatively insoluble substituted benzoic acid and its sodium salt. *J Pharm Sci.* 56 (1967) 1243-52.
- [6] P. Finholt, S. Slovang. Dissolution kinetics of drugs in human gastric juice the role of surface tension. *J Pharm Sci.* 57 (1968) 1322-6.
- [7] E. Swanepoel, W. Liebenberg, M. M. D. Villiers. Dissolution properties of proxicam powders and capsules as a function of particle size and the agglomeration of powders. *Drug Dev Ind Pharm.* 26 (2000) 1067-76.
- [8] M. M. D. Villiers. Influence of agglomeration of cohesive particles on the dissolution behaviour of furosemide powder. *Int J Pharm (Kidlington).* 136 (1996) 175-9.
- [9] G. P. Sanganwar, R. B. Gupta. Enhancement of shelf-life and handling properties of drug nanoparticles: mixing of itraconazole with silica at nanoscale. *Ind Eng Chem Res.* 47 (2008) 4717-25.
- [10] T.P. Garcia, A. Carella, and V. Pansa. Identification of factors decreasing the homogeneity of blend and tablet uniformity. *Pharmaceutical Technology.* 28:110, 112, 114, 116, 118, 120-122 (2004).
- [11] M. M. DeVilliers, J. G. VanderWatt. The measurement of mixture homogeneity and dissolution to predict the degree of drug agglomerate breakdown achieved through powder mixing. *Pharm Res (N Y).* 11 (1994) 1557-61.
- [12] J. K. Prescott, R. A. Barnum. On the powder flowability. *Pharmaceutical Technology.* 10 (2000) 60-84.
- [13] K. Thalberg, D. Lindholm, A. Axelsson. A comparison of different flowability tests for powders for inhalation. *Powder Technol.* 146 (2004) 206-13.
- [14] N. Harnby, M. F. Edwards, A. W. Nienow. *Mixing in process industries.* London:

Butterworth 1990.

- [15] I. Krycer, J. A. Hersey. A comparative study of comminution in rotary and vibratory ball mill. *Powder Technol.* 27 (1980) 137-41.
- [16] I. Krycer, J. A. Hersey. Fine powder mixing in vibratory ball mill. *Int J Pharm (Kidlington)*. 6 (1980) 119-29.
- [17] N. Harnby. An engineering view of pharmaceutical powder mixing. *Pharmaceutical Science Technology Today*. 3 (2000) 303-9.
- [18]. J. Baldyga, W. Orciuch, L. Makowski, K. Malik, G. Oezcan-Taskin, W. Eagles, and G. Padron. Dispersion of nanoparticle clusters in rotor-stator mixer. *Ind Eng Chem Res.* 47:3652-3663 (2008).
- [19] P. Ding, A. W. Pacek. De-agglomeration of silica nanoparticles in the presence of surfactants. *J Dispersion Sci Technol.* 29 (2008) 593-9.
- [20] R. Wengler, H. Nirschl. Turbulent hydrodynamic stress induced dispersion and fragmentation of nanoscale agglomerates. *J Colloid Interface Sci.* 306 (2007) 262-73.
- [21] L. Xie, C. D. Rielly, G. Ozcan-Taskin. Break-up of nanoparticle agglomerates by hydrodynamically limited processes. *J Dispersion Sci Technol.* 29 (2008) 573-9.
- [22] M. Linsenbuhler, K.-E. Wirth. An innovative dry powder coating process in non-polar liquids producing tailor-made micro-particles. *Powder Technol.* 158 (2005) 3-20.
- [23] D. Wei, R. Dave, R. Pfeffer. Mixing and characterization of nanosized powders: an assessment of different techniques. *J Nanopart Res.* 4 (2002) 21-41.
- [24] J. Yang, Y. Wang, R. N. Dave, R. Pfeffer. Mixing of nano-particles by rapid expansion of high-pressure suspensions. *Adv Powder Technol.* 14 (2003) 71-93.
- [25] D. S. Wishart, C. Konx, A. C. Guo, S. Shrivastava, M. Hassanali, P. Stothard, et

- al. Drugbank: a comprehensive resource for in silico drug discovery and exploration. *Nucleic Acids Res.* 34 (2006) D668-D72.
- [26] R. B. Gupta, P. Chattopadhyay, inventors; Method of forming nanoparticles and microparticles of controllable size using supercritical fluids with enhanced mass transfer. United States of America patent 6620351. 2003.
- [27] C. Nystrom, M. Westerberg. The use of ordered mixtures for improving the dissolution rate of low solubility compounds. *J Pharm Pharmacol.* 38 (1986) 161-5.
- [28] C.-L. Teng, C. Hsiao, J. Gatts, inventors; Impax Laboratories, Inc., assignee. Drug delivery system for enhanced bioavailability of hydrophobic active ingredients. United States patent US 6531158 B1. 2003.
- [29] J. W. McGinity, C.-T. Ku, R. Bodmeier, M. R. Harris. Dissolution and uniformity of ordered mixes of micronized griseofulvin and a perfectly compressible excipient. *Drug Dev Ind Pharm.* 11 (1985) 891-900.
- [30] N. H. Shah, W. Phuapradit, M. Bachynsky, M. H. Infled, K. Iqbal, A. W. Malick. High energy ordered mixture for improving the dissolution rate of sparingly soluble compounds. *Drug Dev Ind Pharm.* 20 (1994) 873-88.
- [31] O. S. Sudah, P. E. Arratia, D. Coffin-Beach, F. J. Muzzio. Mixing of cohesive pharmaceutical formulations in tote (bin) blenders. *Drug Dev Ind Pharm.* 28 (2002) 905-18.
- [32] I. Zimmermann, K. Meyer. Effects of glidant in binary powder mixtures. *Powder Technol.* 139 (2004) 40-54.
- [33] H. Watanabe, M. Ghadiri, T. Matsuyama, L. Y. Ding, K. G. Pitt, H. Maruyama, et al. Triboelectrification of pharmaceutical powders by particle impact. *Int J Pharm*

(Kidlington). 334 (2007) 149-55.

[34] B. Always, R. Sangchantra, P. J. Stewart. Modeling the dissolution of diazepam in lactose interactive mixtures. *Int J Pharm (Kidlington)*. 130 (1996) 213-24.

[35] J. Liu, J. Stewart. Deaggregation during dissolution of benzodiazepines in interactive mixtures. *J Pharm Sci*. 87 (1998) 1632-8.

[36] P. J. Stewart, F.-Y. Zhao. Understanding agglomeration of indomethacin during the dissolution of micronised indomethacin mixtures through dissolution and de-agglomeration modeling approaches. *Eur J Pharm Biopharm*. 59 (2005) 315-23.

[37] M. Westerberg, C. Nystrom. Physicochemical aspects of drug release. Part 18. Use of a surfactant and disintegrant for improving drug dissolution rate from ordered mixtures. *STPPharm Sci*. 3 (1993) 142-7.

[38] K. S. Suslick. Sonochemistry. *Kirk Othemer Encyclopedia of Chemical Technology*:1-21.

[39] K. K. Kusters, S. E. Pratsinis, S. G. Thoma, D. M. Smith. Ultrasonic fragmentation of agglomerate powders. *Chem Eng Sci*. 48 (1993) 4119-27.

[40] M. W. A. Kuijpers, D. v. Eck, M. F. Kemmere, J. T. F. Keurentjes. Cavitation-induced reactions in high pressure carbon dioxide. *Science*. 298 (2002) 1969-71.

[41] NIST Chemistry WebBook. [cited March 2008]; Available from: <http://webbook.nist.gov/chemistry/>

[42] J. N. Israelachvili. Intermolecular and surface forces. London: Academic Press 1985.

[43] I. I. Frenkel. Kinetic theory of liquids. New York: Dover Publications 1955.

[44] D. P. Singh, M. Lal, B. Singh. Ultrasonic investigations of liquid carbon dioxide.

Acoustics Letters. 15 (1992) 235-41.

[45] H. Omia, T. Uedaa, K. Miyakuboa, T. Eguchia. Dynamics of CO₂ molecules confined in the micropores of solids as studied by ¹³C NMR Appl Surf Sci. 252 (2005) 660-7.

[46] E.R. Beach, G.W. Tormoen, J. Drelich, and R. Han. Pull-off force measurements between rough surfaces by atomic force microscope. J Colloid Interface Sci. 247:84-99 (2002).

[47] M. M. Kohonen, H. K. Christenson. Adsorption from pure and mixed vapours of n-hexane and n-perfluorohexane. European Physical Journal E. 6 (2001) 315-23.

[48] S.-U. Lee, S.-H. Lee, J.-G. Park. Interaction forces between silica particles and wafer surfaces during chemical mechanical planarization of copper. Journal of Electrochemical Society. 150 (2003) G327-G32.

[49] P. Chattopadhyay, R. B. Gupta. Production of griseofulvin nanoparticles using supercritical CO₂ antisolvent with enhanced mass transfer. Int J Pharm (Kidlington). 228 (2001) 19-31.

[50] P. Chattopadhyay, R. B. Gupta. Supercritical CO₂-based production of fullerene nanoparticiles. Ind Eng Chem Res. 39 (2000) 2281-9.

[51] A. Gokhale, B. Khusid, R. N. Dave, R. Pfeffer. Effect of solvent strength and operating pressure on the formation of submicrometer polymer particles in supercritical microjets. J Supercrit Fluids. 43 (2007) 341-56.

[52] E. S. Kostewicz, U. Brauns, R. Becker, J. B. Dressman. Forecasting the oral absorption behavior of poorly soluble weak bases using solubility and dissolution studies in biorelevant media. Pharm Res (N Y). 19 (2002) 345-9.

- [53] M.-S. Kim, S. Lee, J.-S. Park, J.-S. Woo, S.-J. Hwang. Micronization of cilostazol using supercritical antisolvent process: effect of process parameters. *Powder Technol.* 177 (2007) 64-70.
- [54] P. Chattopadhyay, R. B. Gupta. Protein nanoparticles formation by supercritical antisolvent with enhanced mass transfer. *AIChE J.* 48 (2002) 235-44.
- [55] I. D. Marco, E. Reverchon. Supercritical antisolvent micronization of cyclodextrins. *Powder Technol.* 183 (2008) 239-46.
- [56] R. G. Wissinger, M. E. Paulaitis. Swelling and sorption in polymer-CO₂ mixtures at elevated pressures. *J Polym Sci, Part B: Polym Phys.* 25 (1987) 2497-510.
- [57] W. Kornchankul, E. Hamed, N. H. Parikh, A. Sakr. Effect of drug proportion and mixing time on the content uniformity of a low dose drug in a high shear mixer. *Pharmazie.* 57 (2002) 49-53.
- [58] N. A. Orr, E. Shotton. The mixing of cohesive powders. *Chemical Engineer.* 269 (1973) 12-9.
- [59] S. Sundell-Bredenberg, C. Nystrom. The Possibility of achieving an interactive mixture with high dose homogeneity containing an extremely low proportion of micronised drug. *Eur J Pharm Sci.* 12 (2001) 285-95.
- [60] K. Malmqvist, C. Nystrom. Studies on direct compression of tablets IX. The effect of scaling-up on the preparation of ordered mixtures in double cone mixers. *Acta Pharm Suec.* 21 (1984) 21-30.
- [61] E. Karavas, M. Georgarakis, A. Docoslis, D. Bikiaris. Combining SEM, TEM, and micro-Raman techniques to differentiate between the amorphous molecular level dispersions and nanodispersions of a poorly water soluble drug within a polymer matrix.

Int J Pharm (Kidlington). 340 (2007) 76-83.

[62] S. Jonat, S. Hasenzahl, M. Drechsler, P. Albers, K. G. Wagner, P. C. Schmidt. Investigation of compacted hydrophilic and hydrophobic colloidal silicon dioxides as glidants for pharmaceutical excipients. Powder Technol. 141 (2004) 31-43.

[63] A. Schussele, A. Bauer-Brandl. Note on the measurement of flowability according to the european pharmacopeia. Int J Pharm (Kidlington). 257 (2003) 301-4.

[64] G. E. Amidon, M. S. Bergren, D. J. W. Grant, K. Marshall, S. Itai. Physical test methods for powder flow characterization of pharmaceutical materials: A review of methods. Pharmacoepial Forum. 25 (1999) 8298-308.

[65] J. Yang, A. Silva, A. Banerjee, R. N. Dave, R. Pfeffer. Dry particle coating for improving the flowability of cohesive powders. Powder Technol. 158 (2005) 21-33.

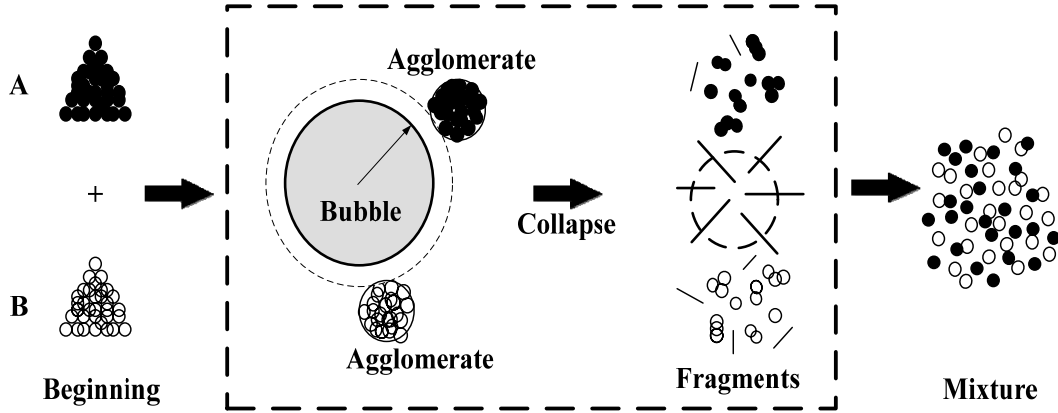


Figure 4.1 Mechanism of cavitation in the liquid for deagglomeration of particles with subsequent mixing.

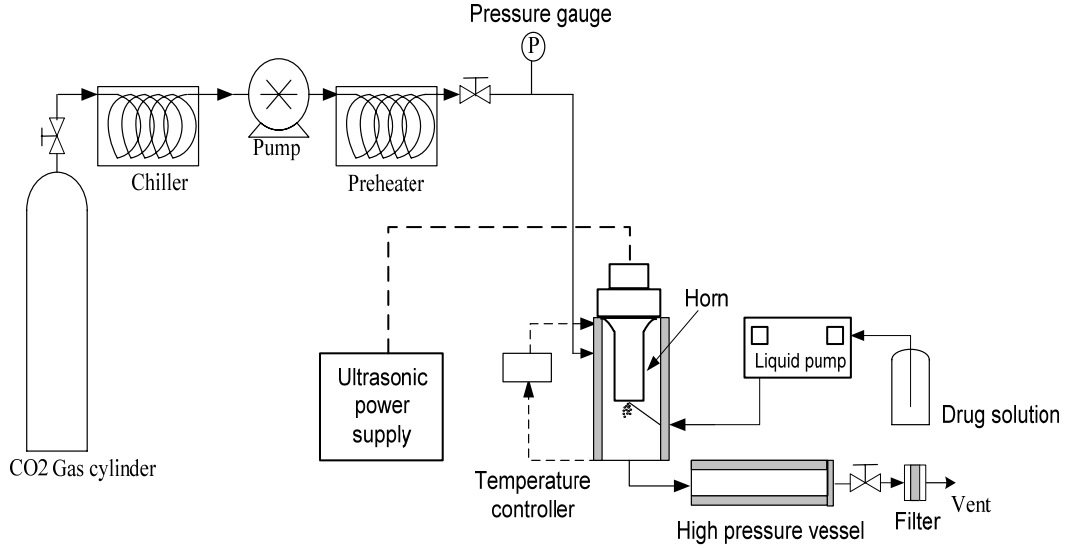


Figure 4.2 Schematics of supercritical antisolvent with enhanced mass transfer (SAS-EM) apparatus to produce drug nanoparticles.

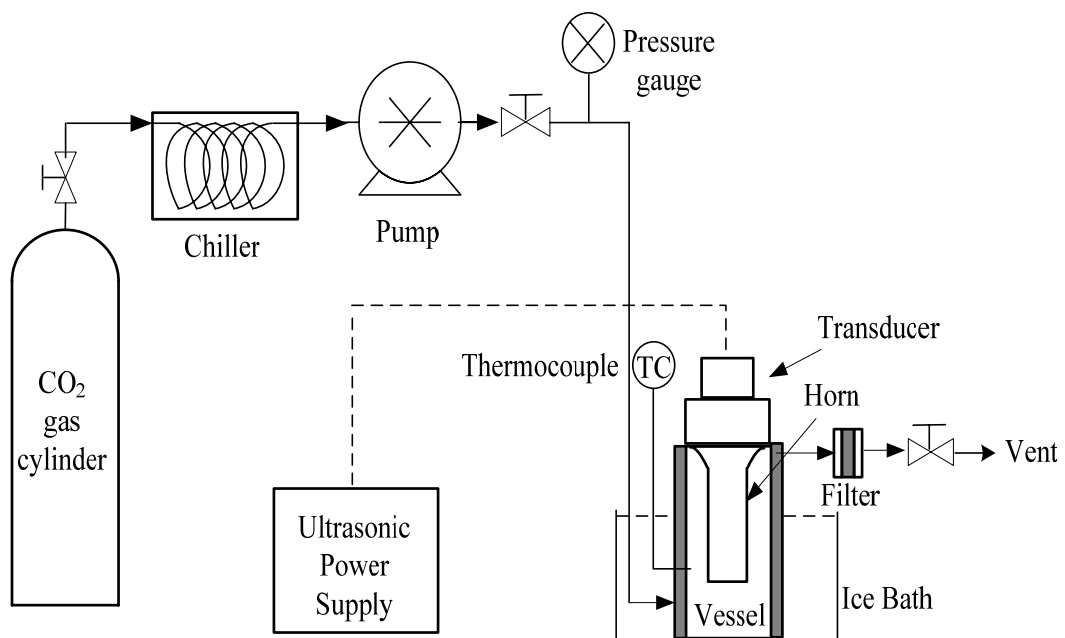


Figure 4.3 Apparatus for sonication in liquid CO₂ for deagglomeration and mixing.

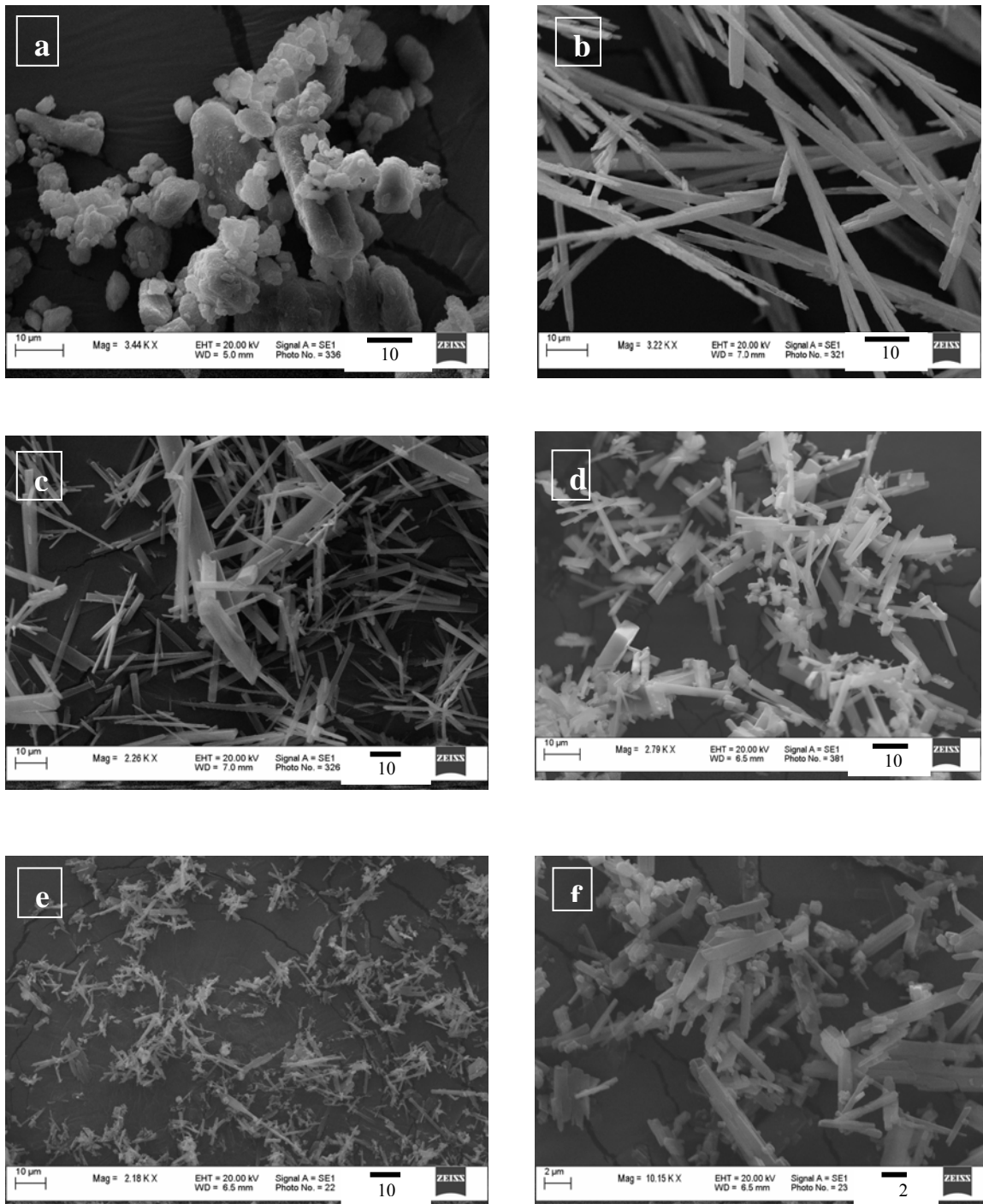


Figure 4.4 SEM images of dipyridamole particles obtained at various conditions: (a) from supplier, (b) SAS, 13 mg drug/ ml methanol, 1 ml/min, (c) SAS-EM, 5 mg drug/ml methanol, 1ml/min, 25% amplitude, (d) SAS-EM, 5mg drug/ml methanol, 1 ml/min, 40% amplitude, (e) SAS-EM, 5mg/ml dichloromethane, 1 ml/min, 40% amplitude, and (f) higher magnification of (e). All the experiments were carried out at 100 bar and 37 °C with CO₂ (antisolvent) flow rate of 10 g/min.

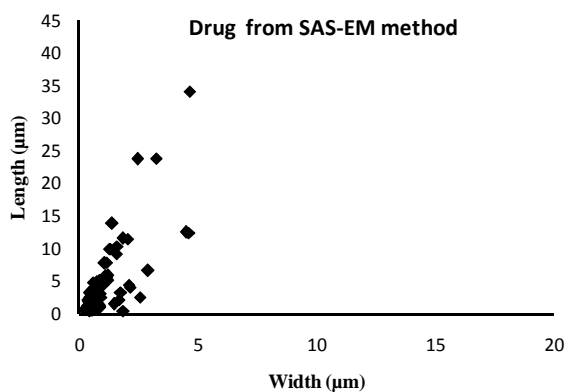
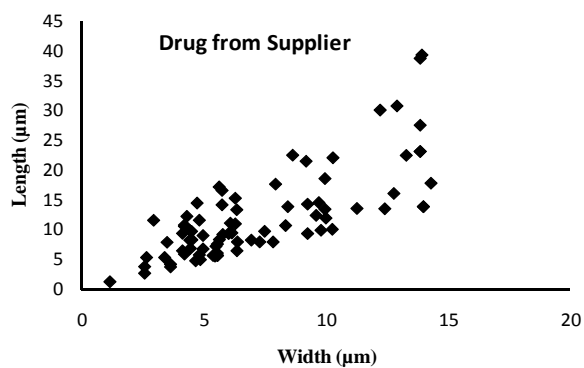


Figure 4.5 Particle size distributions of randomly selected drug particles (n=100) from supplier and SAS-EM method (5 mg drug/ml dichloromethane, 1 ml/min, 40% ultrasound amplitude, 100 bar, 37°C, and 10 g CO₂/min).

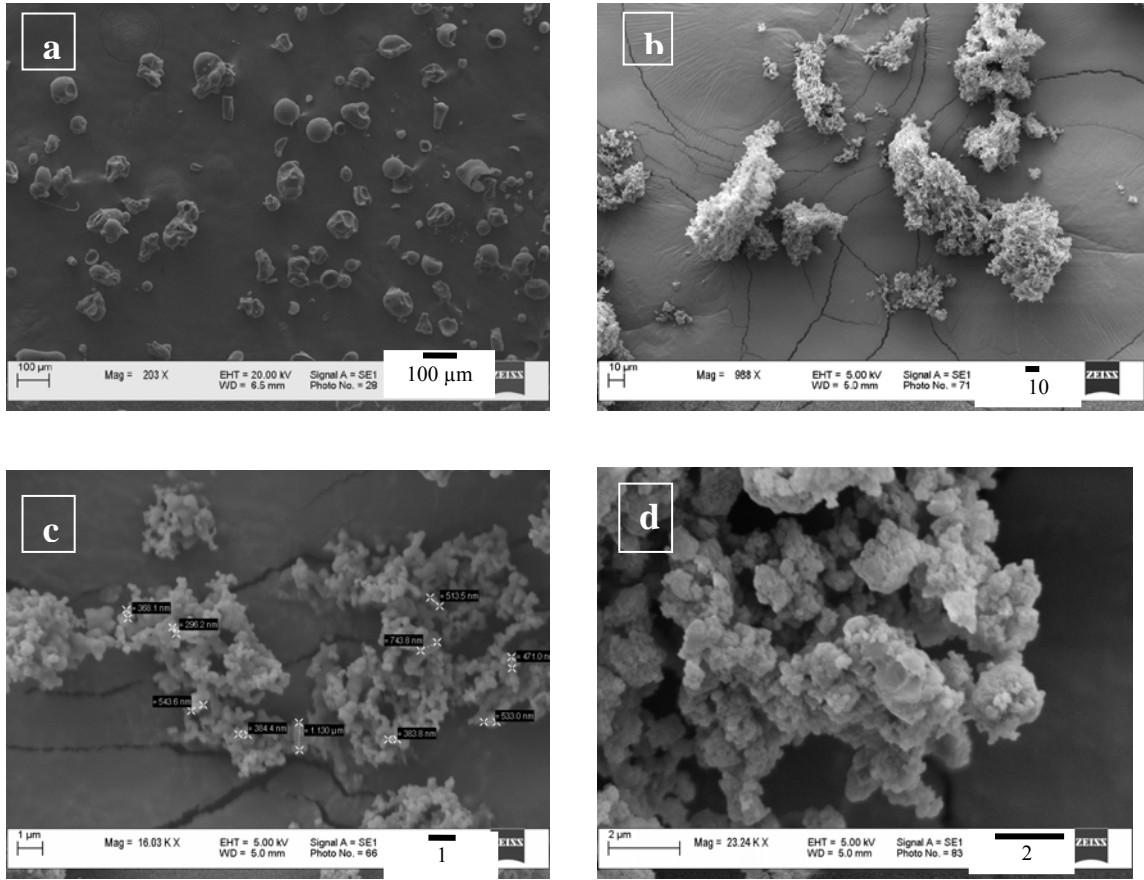


Figure 4.6 SEM images of PVP (a) from supplier, (b) from SAS [20 mg PVP/ml dichloromethane/acetonone (25/75 v/v), 0.5 ml /min, 10 g CO₂/min, 78 bar, and 35 °C], (c) higher magnification of (b), and (d) from SAS-EM [18 mg PVP/ml dichloromethane/acetonone (25/75 v/v), 0.5 ml /min, 10 g CO₂/min, 78 bar, 35 °C, and 21 % ultrasound amplitude].

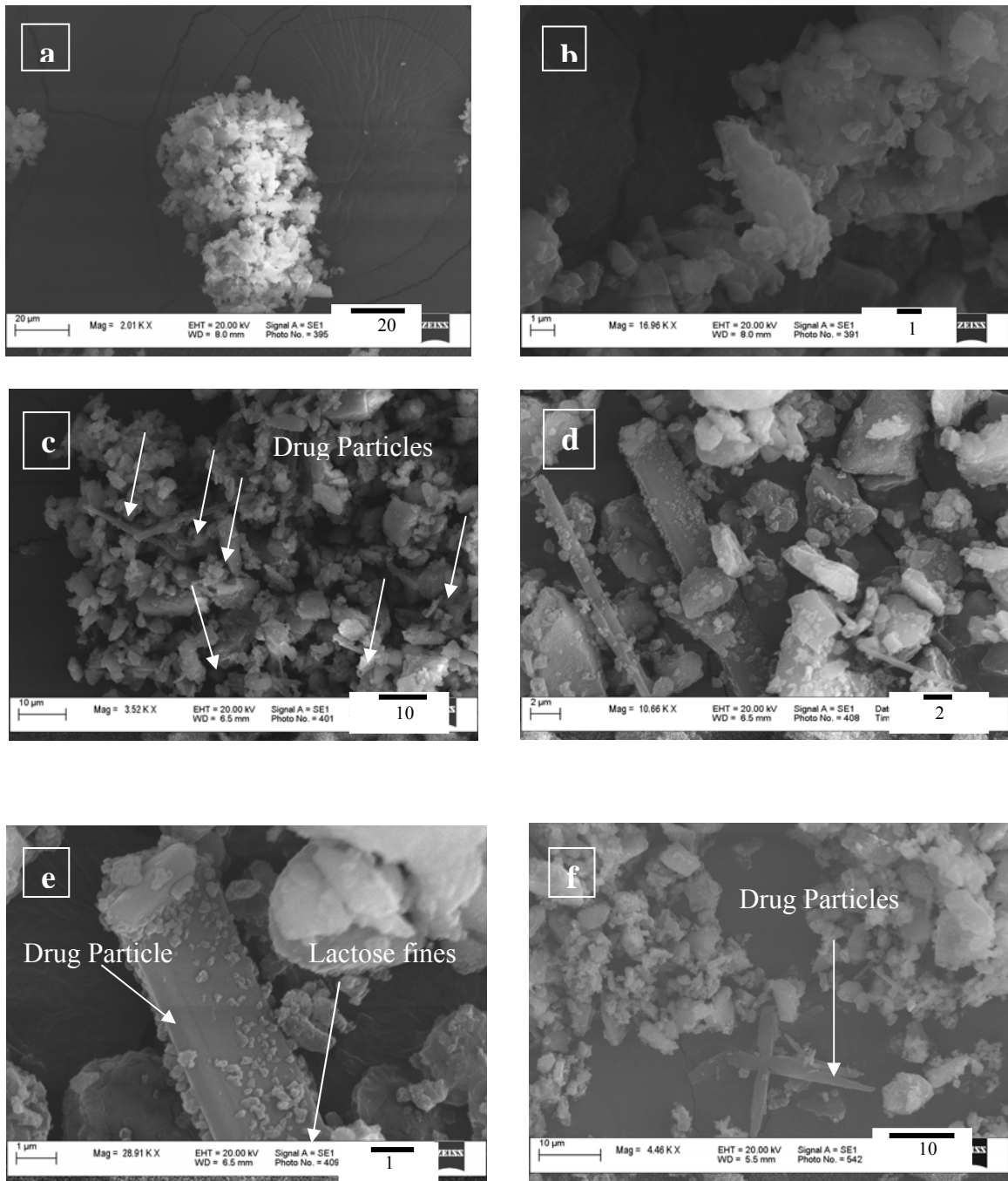


Figure 4.7 SEM images of lactose/drug mixture obtained by sonication in CO₂ at 5 °C, 78 bar, 35 % ultrasound amplitude, and 7.5 MJ/m³, and by physical mixing: (a) typical agglomerate of cohesive lactose from the supplier, (b) presence of very fine lactose particles (submicron range) on the surface of larger lactose particle, (c) random and interactive ordered mixing of drug particles and lactose particles for 5.31 wt. % of drug in the mixture (arrow shows presence of drug nanoparticles), (d) typical presence of drug particles in drug-lactose mixture for 0.96 wt. % of drug in the mixture, (e) higher magnification of (d) showing coating of lactose fines on the surface of drug flakes, and (f) physical mixing (5 wt. % drug) showing separate domains of drug and lactose particles.

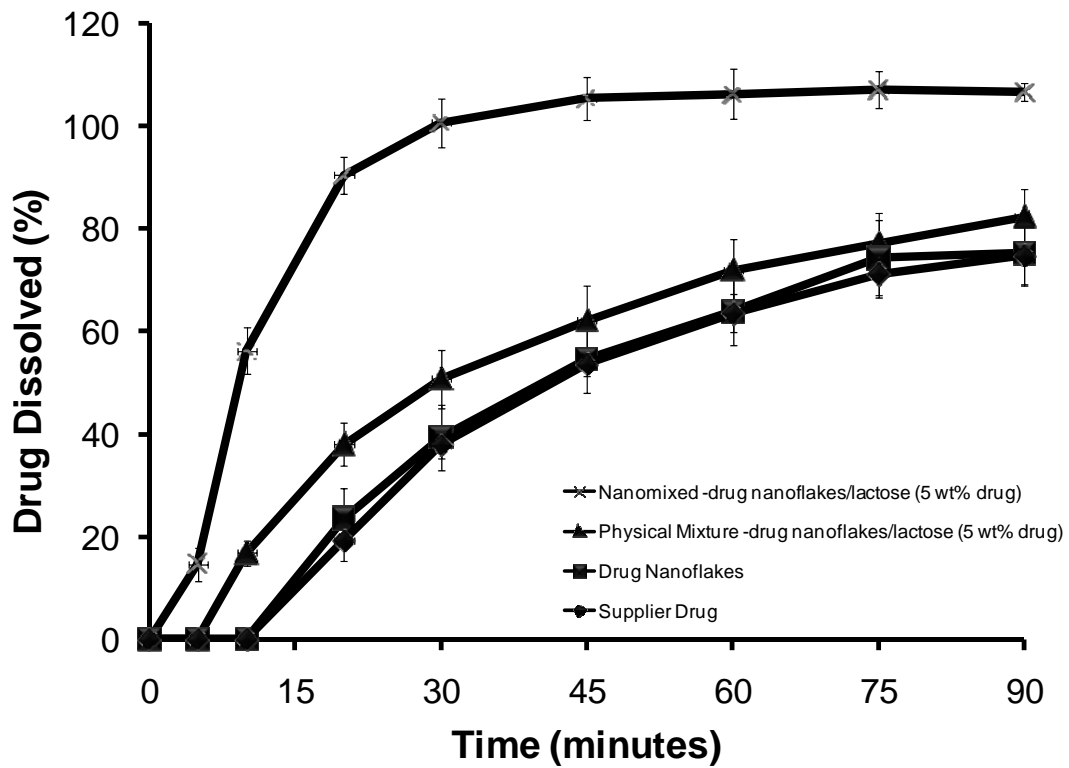


Figure 4.8 Drug dissolution curves (n=3) for nanomixed- drug nanoflakes/lactose-5 wt. % drug (\times), physical mixture -drug nanoflakes/lactose- 5 wt. % drug (\blacktriangle), drug nanoflakes (\blacksquare), and supplier drug (\blacklozenge).

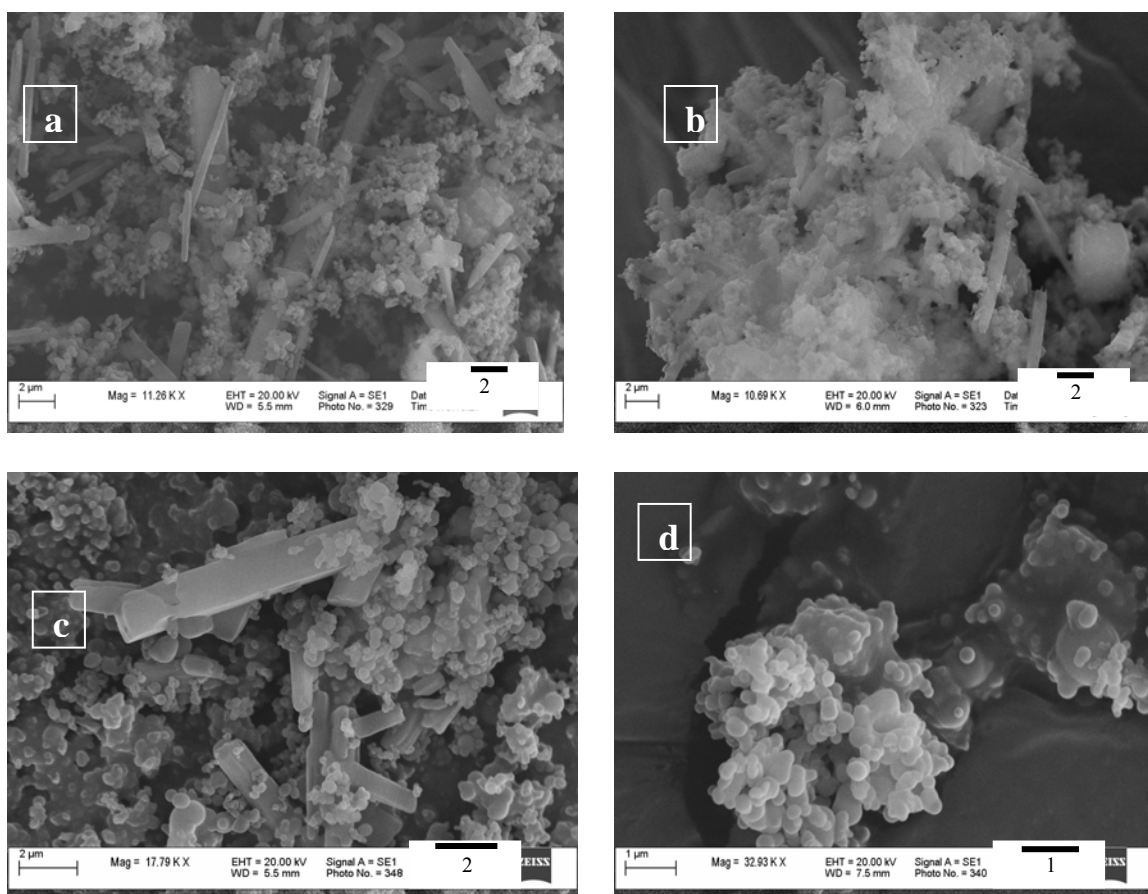


Figure 4.9 SEM images of deagglomeration and mixing of dipyrindamole with PVP at various weight ratios and ultrasonic energy inputs for experimental condition of 35% ultrasound amplitude, 5 °C, and 78 bar: (a) drug/ PVP weight ratio of 1/1, energy input of 2 MJ/m³, (b) drug/ PVP weight ratio of 1/1, energy input of 2 MJ/m³, typical presence of drug particles trapped in PVP agglomerates, (c) drug/ PVP weight ratio of 1/3, energy input of 2 MJ/m³, and (d) drug/ PVP weight ratio of 1/3, energy input of 2 MJ/m³, presence of fused PVP nanoparticles.

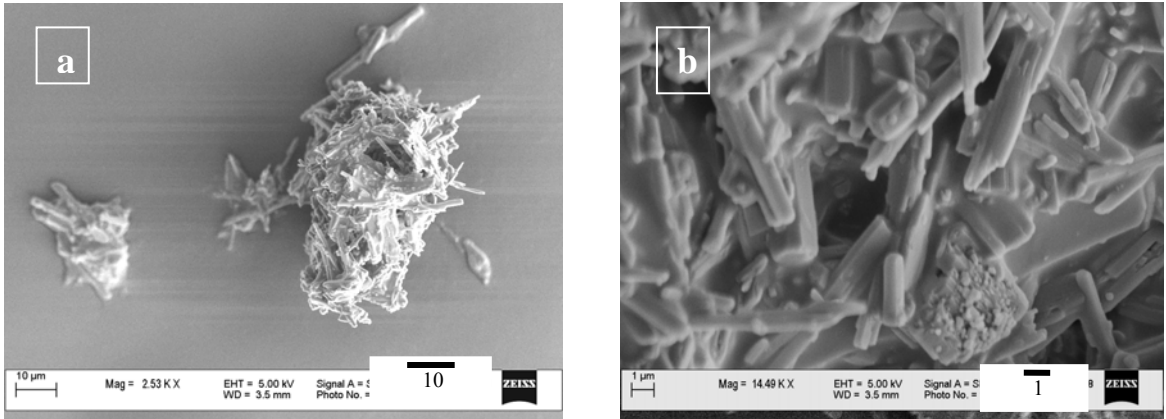
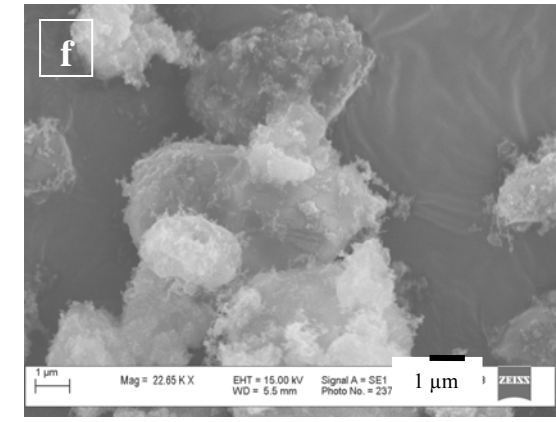
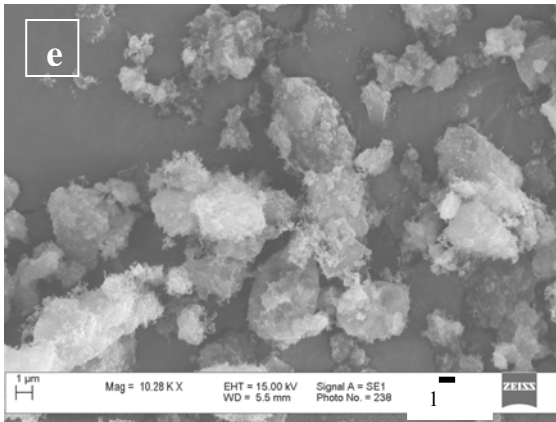
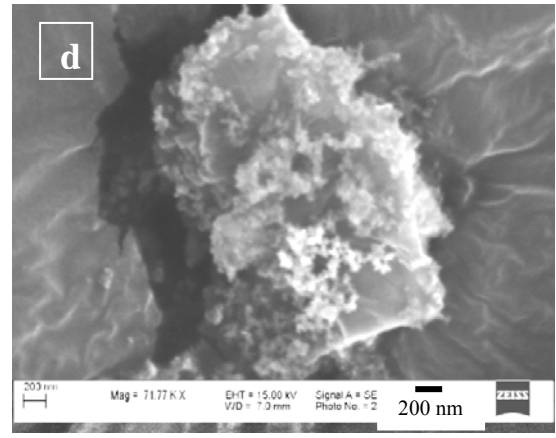
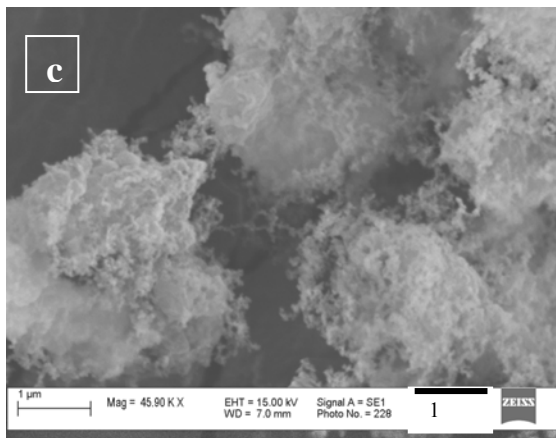
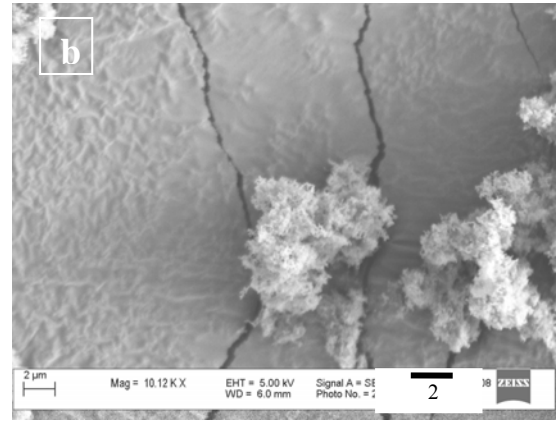
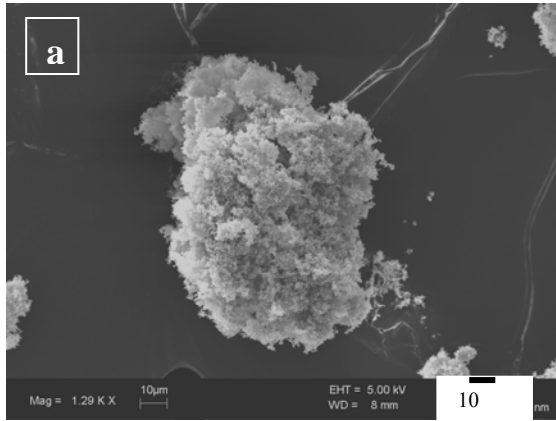


Figure 4.10 Effect of ultrasonic energy and temperature on deagglomeration and mixing of dipyrindamole and PVP particles at 35% ultrasound amplitude, 78 bar CO₂ pressure, ultrasound energy input 68 MJ/m³, drug/PVP weight ratio 1/1, and 10 °C: (a) presence of typical agglomerate of drug particles held together due to fusion (melting) of PVP, and (b) higher magnification of (a) showing presence of individual drug particles held together by fused (melted) PVP.



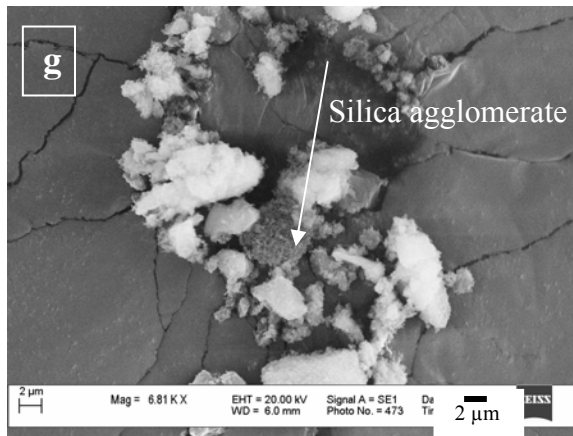


Figure 4.11 Effect of ultrasonic energy on deagglomeration and coating of silica particles on microfine lactose at 35% ultrasound amplitude, 5°C, 1/10 (w/w), and 78 bar (a) typical silica (R972) agglomerate, (b) presence of R972 silica agglomerates at ultrasound energy of 3.5 MJ/m³, (c) deagglomeration and coating of R972 silica agglomerates at ultrasound energy of 3.5 MJ/m³, (d) presence of R972 silica agglomerates in the size of 400-600 nm on the surface of microfine lactose, (e) presence of very thin coating of R772 silica on the surface of microfine lactose at ultrasound energy of 7.5 MJ/m³, (f) higher magnification of thin coating of R972 silica on the surface of microfine lactose, and (g) presence of M5 silica agglomerates even at 7.5 MJ/m³ ultrasound energy.

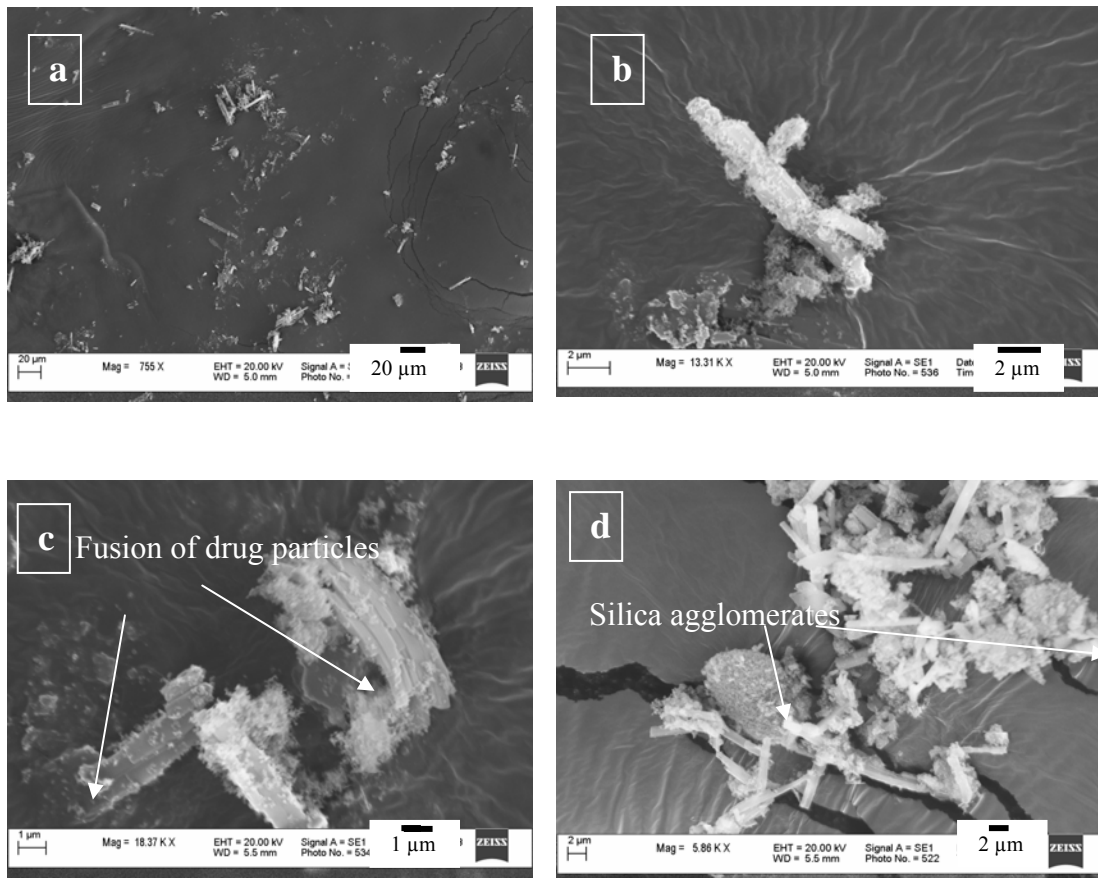


Figure 4.12 Effect of ultrasonic energy on deagglomeration and coating of silica particles on drug nanoparticles at 35% ultrasound amplitude, 7.5 MJ/m^3 , $5 \text{ }^\circ\text{C}$, 1/4 (w/w), and 78 bar: (a) highly deagglomerated drug nanoparticles after mixing with R972 silica, (b) close-up of coating of R972 silica onto drug particle surface, (c) fusion of some drug particles during mixing, and (d) presence of M5 silica agglomerates.

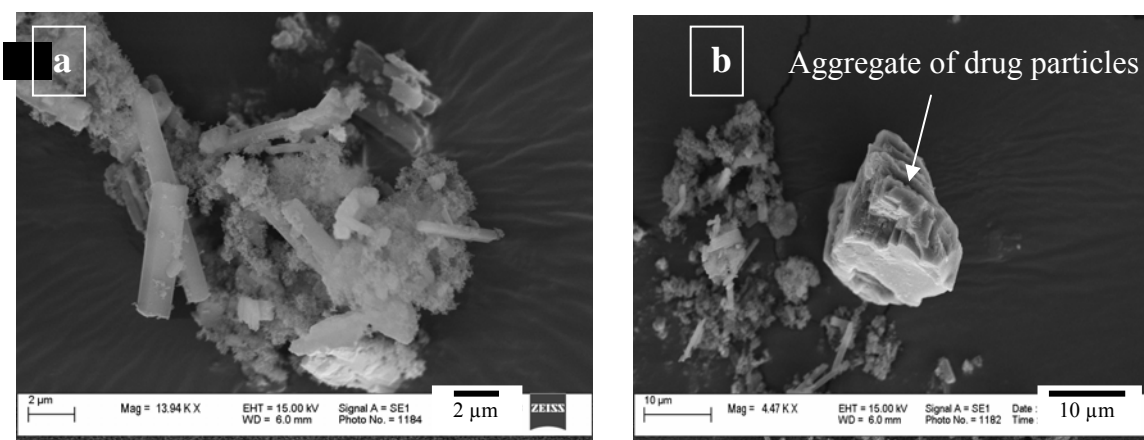


Figure 4.13 Effect of higher ultrasonic energy on deagglomeration and coating of M5 silica particles on drug nanoparticles at 65% ultrasound amplitude, 15°C, 1/4 (w/w), 143.78 MJ/m³ and 68 bar: (a) presence of drug/silica agglomerates, and (b) presence of aggregate of drug particles.

Table 4.1 Physical properties of dipyridamole [25]

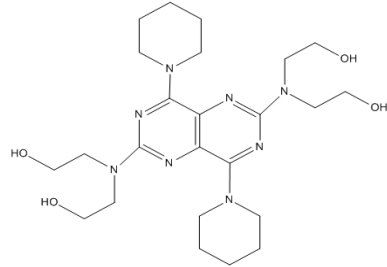
Drug name	Drug structure	Empirical formula	Mol.Wt.	Melting point (°C)
Dipyridamole		$C_{24}H_{40}N_8O_4$	504.63	163

Table 4.2 Various properties of CO₂ at pressure of 78 bar and 5 °C for calculation of acoustic and Blake threshold pressures [41]

Properties	Value
Density of Fluid	936.3 kg/m ³
Speed of sound	570.2 m/s
Average power (for 35%amplitude)	10-15 W
Area of ultrasound horn	2.85 cm ²
Ultrasound Intensity	7 W/cm ²
External Pressure	78 bar
Vapor Pressure	38.5 bar
Surface Tension	0.00636 N/m
Equilibrium bubble (cavity) radius	10 ⁻⁵ m

Table 4.3 Hamaker constants for solids, fluids and calculated solid-fluid interactions [22, 46-48]

Solid	Hamaker Constant (J)	Air	Liquid	Liquid	n-hexane	Water
		(approx. to nitrogen)	Nitrogen (at - 196 °C)	CO ₂ (at 78 bar and 5 °C)		
		$\sim 10^{-25}$	$\sim 10^{-20}$	1.9×10^{-20}	2.4×10^{-20}	$\sim 10^{-19}$
Lactose	7.2×10^{-20}	7.18×10^{-20}	2.8×10^{-20}	1.1×10^{-21}	1.3×10^{-20}	2.3×10^{-21}
Silica	5×10^{-19}	5.0×10^{-19}	3.7×10^{-19}	2.2×10^{-19}	3.4×10^{-19}	1.5×10^{-19}

Table 4.4 Details of experiments for sonication in the liquid CO₂ at 78 bar

Mixture	Weight ratio (mg/mg)	Energy (MJ/m ³)	Amplitude (%)	Temperature ^a (°C)	Mixing Time (seconds)
Dipyridamole/Lactose	3/297	7.5	35	5.1	113
Dipyridamole/Lactose	1.5/298.5	7.5	35	4.3	50
Dipyridamole/Lactose	0.5/299.5	7.5	35	4.5	90
Dipyridamole/Lactose	14.8/285	7.5	35	5.0	92
Dipyridamole/Povidone	20/20	2.0	35	5.2	19
Nanopowder					
Dipyridamole/Povidone	7/21	2.0	35	4.5	38
Nanopowder					
Dipyridamole/Povidone	100/100	68.0	35	9.1	180
Nanopowder					
Silica R972/Lactose	10/100	3.5	35	3.8	26
Silica R972/Lactose	10/100	7.5	35	5.3	80

Silica M5/Lactose	10/100	12.5	35	4.8	69
Silica M5/Lactose	10/100	3.5	35	4.2	96
Silica M5/Lactose	10/100	7.5	35	4.0	64
Silica	2/20	3.5	35	4.3	110
R972/Dipyridamole					
Silica	5/20	7.5	35	4.1	120
R972/Dipyridamole					
Silica	10/20	7.5	35	3.9	71
R972/Dipyridamole					
Silica M5/Dipyridamole	2/20	3.5	35	4.8	19
Silica M5/Dipyridamole	2/20	7.5	35	4.4	112
Silica M5/Dipyridamole	5/20	7.5	35	4.2	202
Silica M5/Dipyridamole	10/20	7.5	35	4.2	135
Silica M5/Dipyridamole	5/20	143.78	65	14.8	100

^a Temperature mentioned here is at the start of experiment though it didn't increase much (less than 1 °C) due to application of ultrasound by pulse mode as well as vessel was in ice bath.

Table 4.5 Handling properties for compounds and mixtures.

Component or Mixture	Aerated Density (mg/ml)	Tapped Density (mg/ml)	CI (%)	Hausner Ratio
Silica M5 (hydrophilic)	37.88	47.36	25.0	1.25
Silica R972 (Hydrophobic)	37.13	45.97	19.2	1.23
Microfine Lactose	285.1	434.1	34.3	1.52
Dipyridamole	87.0	127.5	31.8	1.47
^a Lactose/silica M5 (hydrophilic) sonicated mixture	168.5	215.6	21.8	1.28
^b Dipyridamole/Silica R972 (hydrophobic) sonicated mixture	150.3	167	10.0	1.11

^aMixtures were obtained by sonication in liquid CO₂ at 35% ultrasound amplitude, 5°C, 78 bar, 3.5MJ/m³ : (a) 1/10 (w/w, silica M5/lactose), and (b) 1/4 (w/w, silica R972/dipyridamole)

Table 4.6 Scale of flowability [64]

Flow Character	CI (%)	Hausner Ratio
Excellent	< 10	1.00-1.11
Good	11-15	1.12-1.18
Fair	16-20	1.19-1.25
Passable	21-25	1.26-1.34
Poor	36-31	1.35-1.45
Very poor	32-37	1.46-1.59
Very very poor	>38	>1.60

5 SIMULTANEOUS PARTICLE FORMATION AND MIXING

5.1 Abstract

Microparticles of a poorly-water-soluble model drug, nevirapine (NEV) were prepared by supercritical antisolvent (SAS) method and simultaneously deposited on the surface of excipients such as lactose and microcrystalline cellulose in a single step to reduce drug-drug particle aggregation. In the proposed method, termed supercritical antisolvent-drug excipient mixing (SAS-DEM), drug particles were precipitated in supercritical CO₂ vessel containing excipient particles in suspended state. Drug/excipient mixtures were characterized for surface morphology, crystallinity, drug-excipient physicochemical interactions, and molecular state of drug. In addition, the drug content uniformity and dissolution rate were determined. A highly ordered NEV-excipient mixture was produced. The SAS-DEM treatment was effective in overcoming drug-drug particle aggregation and did not affect the crystallinity or physico-chemical properties of NEV. The produced drug/excipient mixture has a significantly faster dissolution rate as compared to SAS drug microparticles alone or when physically mixed with the excipients.

5.2 Introduction

Particle size plays an important role in the dissolution rate of poorly soluble drugs belonging to biopharmaceutical classification system class II [1]. Particle size reduction to micro- and nano-meter size range has been in practice for improving the solubility and bioavailability of BCS-II drugs [2-4]. Micronization / nano sizing of drug is also desired in the formulation for aerosol and inhalation products, where particles $< 5 \mu\text{m}$ are preferred due to better deposition of drug particles in the lung alveolar sacs for enhancing drug absorption and bioavailability. However, the micronized and nano-sized drug particles have a high tendency to agglomerate due to a) their high surface free energy, b) van der Waals attraction, c) hydrophobic interactions, etc., leading to disadvantages of decrease in the drug solubility, dissolution rate or bioavailability [5-10].

Powder mixing is an important unit operation in pharmaceutical industry as it directly affects the drug content uniformity in the final drug/excipient mixture [11, 12]. The increased use of micronized / nano-sized drug particles demands efficient deagglomeration and deaggregation in the pharmaceutical processing. The agglomeration of particles can affect granulation, fluidization, mixing, and blending operations [13]. The presence of cohesive-particle agglomerates decreases the efficiency of mixers as well as affects the powder flow due to bridging and spatial heterogeneity [14]. For a better drug content uniformity of the formulation and obtaining a homogeneous mixture (especially for cohesive powder mixtures having a low drug content), it is very important to deagglomerate fine cohesive drug particles and intimately mix them with excipients to prevent further drug-drug agglomeration during subsequent unit operations. Currently available mixers are not effective in deagglomeration of highly-cohesive drug particles;

or they require very high shear or impaction, which indeed act as a particle size reduction device rather than a conventional mixer [15]. For example, rotary and vibratory ball mills can be used for mixing of fine powders [16, 17]; however the use of high energy may affect the crystal lattice of the particles which can influence the physico-chemical stability of the drug and excipients. The tumbler mixer, most common mixing equipment in pharmaceutical industry, is not effective if de-agglomeration of micron / nano-sized particles is required [18].

Here we propose supercritical antisolvent-drug excipient mixing (SAS-DEM) method for micro/nano drug particle formation and prevention of drug-drug particle agglomeration by mixing with excipient particles in a single step. In this method, drug particles are formed in presence of suspended excipient particles in supercritical CO₂. The supercritical anti-solvent (SAS) process utilized in this work uses environmentally benign antisolvent (e.g., near or supercritical CO₂) for micron / nanosized particle formation. This method is suitable for most cases where drug and excipient are insoluble or poorly soluble in supercritical CO₂. Drug/excipient mixture is obtained by simple depressurization. Highly homogenous drug/excipient mixture can be obtained by the process which exhibits significantly higher drug dissolution rate (and bioavailability) when compared to drug/excipient mixture obtained by conventional physical mixing.

The unique advantage of this process is that there is no additional requirement of mixing step after micro/nano sizing of drug particles. Method also reduces the toxicity during handling of highly potent nano/micro size drug due to dilution of the drug with excipient and reduction in various handling steps.

In this study, we demonstrate the simultaneous production and co-mixing

(deagglomeration) of microparticles of the drug with the excipients for improving dissolution concept for a poorly water soluble model drug, nevirapine (NEV), and excipients such as spray dried lactose and microcrystalline cellulose (MCC). Nevirapine is a non-nucleoside reverse transcriptase inhibitor used for treatment of HIV-1 infection and AIDS. It is a hydrophobic drug with a log octanol-water partition coefficient (log P) =2.5, $T_m = 244.5^\circ\text{C}$, and $\text{pKa} = 2.8$, [19, 20]) and is practically insoluble in water (0.1 mg/ml). The drug/excipient mixtures were characterized by Fourier transform infrared spectrometry (FT-IR), differential scanning calorimetry (DSC), X-ray diffractometry (XRD), and scanning electron microscopy (SEM).

5.3 Theoretical Background

5.3.1 Particle suspension

In the proposed SAS-DEM method excipient particles are suspended and mixed forming drug particles with continuous agitation. The particles can be easily suspended in supercritical CO_2 due to a high density of the fluid and agitation. Equation can be used for calculation of minimum impeller speed required to keep particles just suspended in the vessel [21, 22].

$$N_{js} = Sv^{0.1} \left[\frac{g_c (\rho_s - \rho_l)}{\rho_l} \right]^{0.45} X^{0.13} d_p^{0.2} D^{-0.85} \quad (1)$$

where, N_{js} is just suspended impeller speed (rps), g_c is gravitational acceleration (9.8 m/s^2), d_p is mass mean particle diameter, v is kinematic viscosity of fluid (for supercritical CO_2 at mentioned experimental condition, $8.09 \times 10^{-8} \text{ m}^2/\text{s}$), ρ_s is density of solid particle, ρ_l is density of fluid (709 kg/m^3 [23]), X is mass fraction (mass of

solids/mass of fluid), D is impeller diameter (1 inch, 4 pitched blade), and S is dimensionless number function of impeller type (for impeller clearance above base vessel /vessel diameter =1/5, diameter of impeller =vessel diameter/2.5, width of impeller=diameter of impeller/3, S value can be approximated to 3.4). Therefore N_{js} required for various compounds of different particle sizes is given in Table 5.1. In actual practice, there will be mixture of solids (drug and excipient) present in the vessel. Therefore for mentioned experimental condition in this paper, we have used impeller speed of 400 rpm. Use of multiple impellers does not have any significant effect on N_{js} . It is related to particle pick up from bottom of the vessel and not to the distribution of particles. Upward fluid (CO_2) velocity in pressure vessel is 0.01 cm/s. The combined effect (upward fluid velocity and agitation due to impeller) will keep particles suspended in supercritical CO_2 media.

5.3.2 Mixture definitions

Figure 5.1 shows cartoon representing different types of terms used in defining various mixtures and their homogeneity (0 corresponds to non homogenous mixture while 1 to highly homogenous mixture) which are influenced by gravitational and surface forces. There are two main types of mixing: (a) ordered and (b) random [24]. Ordered mixing is considered interactive where finer particles adhere to the coarse particles of other constituent materials [25]. Ordered mixing does not require equal size particles but does require particle interactions of any forms of adhesion. Ordered mixing is further divided into perfect, imperfect, and pseudo- random. Figure 5.1 shows the arrangement of particles. Random mixing as defined by Staniforth, 1982 [26] is a statistical process in which a bed of particles is repeatedly split and recombined until there is an equal chance

of any individual particle being at any given point in mix at any one time. Random mixing is also further divided into ideal, random, and non random (as of shown in Figure 5.1).

5.4 Materials and methods

5.4.1 Materials

Nevirapine (Aurobindo Pharma, Hyderabad, India), spray dried lactose NF (Fast Flo 316, Average size - ~100 μm , Foremost, Inc. Baraboo, WI), microcrystalline cellulose (Avicel PH-101, Nominal particle size – 50 μm , FMC Corp. Newark, DE), dichloromethane (HPLC grade, EMD Chemicals, Inc. Gibbstown, NJ), and CO₂ (bone dry, Air Gas, Opelika, AL) were used as received.

5.4.2 Production and Co-mixing of Microparticles of Drug with Excipients

Figure 5.2 shows the schematic of SAS-DEM apparatus used in the production of microparticles and simultaneous co-processing with excipient(s). It consists of compressed carbon dioxide gas cylinder, chiller, piston pump for pumping CO₂, heater, high pressure stirred vessel, high pressure liquid pump, and back pressure regulator. A desired amount of the excipient (lactose or MCC) or mixture of excipients (1-3 grams) was placed inside the high pressure vessel. The vessel (450 ml) was subjected to a desired pressure (116 bar) using CO₂. A high pressure was preferred due to ease in suspension of excipient particles. Stirrer speed was maintained at 400 rpm during operation. Temperature of vessel was maintained at 40°C using heating tape. Nevirapine solution (8 mg/ml) was prepared by dissolving the drug in dichloromethane. Flow rate of the drug

solution was maintained at 1 ml/min while the antisolvent flow rate (supercritical CO₂) was kept at 15 gm/min. The capillary nozzle (PEEKsil, Upchurch Scientific, Oak Harbor, WA) of 75 µm in diameter and 15 cm in length was used for delivery of drug solution inside the pressure vessel. To prevent the loss of powder, a filter (Millipore Inc. Billerica, MA, Fluropore membrane filter, polytetrafluoroethylene bonded to high density polyethylene, 0.22 µm) was installed near the top exit of the vessel. After complete injection of the drug solution (quantity was based on required drug loading in the mixture), high pressure vessel was flushed with supercritical fluid for three times the volume of vessel. After flushing with supercritical CO₂, vessel was slowly depressurized to recover the final drug/excipient mixture.

5.4.3 *Preparation of Physical mixture*

Drug/excipient(s) physical mixtures were prepared in various ratios by spatula mixing for 2-5 minutes and stored in air tight glass vials.

5.4.4 *Drug Content Homogeneity*

Mixing of NEV with lactose, MCC, and lactose + MCC (50:50 wt %) at various drug loadings was carried out in the supercritical fluid vessel. For determination of NEV concentration in the final mixture, the mixture (50 mg) was dissolved into methanol. The concentration of drug in the solution was obtained using UV spectroscopy at 280 nm after filtering the solution through 0.45 µm inline syringe filter (Nylon, 13 mm in size, Fisher Scientific, Fisher Scientific, Suwanee, GA). Also any absorbance at 280 nm due to lactose was checked for lactose in methanol solution. Relative standard deviation

(RSD) of drug for 10 samples was calculated using following equations:

$$RSD = \frac{\sigma}{\bar{C}} \quad (2)$$

$$\sigma^2 = \frac{\sum_{i=1}^n (\bar{C} - C_i)^2}{n-1} \quad (3)$$

where n is the total number of samples, σ^2 is the variance, σ is the standard deviation, \bar{C} is the mean concentration determined experimentally, and C_i is the sample concentration. Concentration or content variation (σ^2) is sum of variances due to (a) variation in weight of sample, (b) analytical errors, and (c) mixing. According to food and drug administration, up to 6% relative standard deviation (RSD) of drug content is acceptable [27].

5.4.5 Particle Size analysis

Particle size analysis was performed using Mastersizer 2000 (Malvern Instruments Inc. Worcestershire, UK). The size of drug particles in the NEV – lactose mixture was determined by dissolving lactose by suspending the mixture in 0.2 wt% sodium dodecyl sulfate in deionized water. A saturated solution of drug was prepared so that majority of drug particles are suspended in the liquid, while lactose was solubilized completely. For analysis, obscuration was kept in the range of 20-30%. Sample was added to approx. 200 ml of dispersion media in dispersion cell with stirring speed of 1250 rpm. In case of drug/lactose mixture, care has been taken to insure that lactose was completely dissolved before performing analysis.

5.4.6 *Dissolution Studies*

Drug dissolution tests were performed by placing the sample (equivalent to 10 mg of NEV) in 900 ml water containing 0.2 wt% containing sodium dodecyl sulfate (SDS) in a USP II dissolution apparatus at 37 °C and 50 rpm. To determine the amount of drug dissolved, 5 ml of the samples were drawn through a 10 micron filter (Sun Sri, Rosewood, TN) at time interval of 5, 10, 15, 20, 30, 45, 60, 75, 90, 120, 150, and 180 minutes. Fresh solution was added after each sample withdrawal. Solutions were filtered using 0.45µm inline syringe filter (Nylon, 13 mm in size, Fisher Scientific, USA), to remove any suspended particles. Drug concentrations were measured using an UV spectrophotometer (Jasco, V680 spectrophotometer, Tokyo, Japan) at $\lambda = 280$ nm. The tests were performed in triplicate and the dissolution data was presented as mean \pm standard deviation. The desired sink condition was maintained for the studies. Complete dissolution of drug was observed within 24-48 hours for the drug samples which were not dissolved in 180 minutes.

In this work, we did not analyze the concentration of residual solvent in the final drug powder. It has been already demonstrated in the literature [34-36] that with sufficient CO₂ flow rate (in this study, 15 gm/min), and with further flushing (three times the volume of vessel), drug powder should contain residual solvent less than maximum allowed (600 ppm for dichloromethane).

5.4.7 *Scanning Electron Microscopy*

Surface morphologies of the various mixtures were studied using environmental scanning electron microscope (Zeiss EVO 50, UK). The sample was spread using a

spatula onto a surface of two sided adhesive carbon tape on aluminum stub, and a thin coating (~15 nm) of gold is applied onto the sample using sputter coater (Electron Microscopy Services, EMS 550X) before microscopy.

5.4.8 *Powder X-ray diffractometry*

Crystallinity of the formulation was analyzed using the Rigaku X-ray diffractometer which is equipped with a Cu K α_1 radiation source at 40 kV, 40 mA and a miniflex goniometer. Diffraction patterns were obtained in 2 θ range of 5-50° using 0.05° step size and 5°/minute scan speed.

5.4.9 *Differential scanning calorimetry*

DSC analysis (thermograph) of samples was done using TA Instruments, model DSC Q2000. 5-10 mg samples were weighed in hermetic aluminum pans, sealed and thermographs were recorded with heating rate of 10° C/min over the temperature range of 25-300°C.

5.4.10 *Fourier Transform Infrared Spectroscopy (FT-IR spectroscopy)*

Infrared spectra of the samples were obtained using FT-IR (Nicolet IR 100, Thermo Scientific, USA). The formulation sample was mixed with 100 fold KBr for preparing the pellets. The final spectra are composed of 64 scans performed in range of 400-4000 cm⁻¹ with 2 cm⁻¹ resolution.

5.5 Result and Discussion

This study demonstrates a method of production of micro particles of NEV and simultaneous mixing with excipients at various drugs loadings. Fast flo lactose and MCC PH -101 were selected because of their wide use as pharmaceutical diluents. Excipient grades with appropriate particle range were selected to achieve suspension of particles in the product container so that the micronized drug particles can be evenly deposited on the surface of excipient particles. We also used mixture of lactose and MCC (50:50 wt. %) because it can offer good flowability and compressibility and drug dissolution [28].

5.5.1 *Simultaneous particle formation and mixing*

5.5.1.1 *Characterization by SEM and particle size analysis*

Figure 5.3 (a) shows the SEM image of NEV particles, which are the rectangular or flaky in shape. It also shows wide particle size distribution which is confirmed by particle size analysis as shown in Table 5.2 and Figure 5.4. Nevirapine microparticles produced by SAS method without the presence of excipient(s), were cubic to circular shape with few porous aggregates (fused particles), as compared to rectangular shaped particles from the supplier. As shown in Table 5.2, drug particles obtained by SAS method in the particle size distribution pattern ($D_{v(0.5)} = 45.7$ and $69.6 \mu\text{m}$ for SAS and control, respectively). Even though the specific surface area was similar for SAS drug and control (supplier drug), the SAS drug demonstrated a narrow particle size distribution as compared to control. Various studies involving precipitation of drug particles through SAS obtained narrower particle size distribution [29-31]. SAS produced drug should show more surface area due to presence of porous aggregates as well as rough surface

than shown in Table 5.2. To determine whether fine drug particles formed loose agglomerates, the samples were suspended in water and sonicated for 10 minutes and examined the particles by SEM imaging. This process would have resulted in the drug at its saturation levels in the solution and the excess drug particles were undergone sonication process to break the aggregates. We found that the SAS process produced finer drug particles but they formed aggregates as observed in SEM. Various general studies on re-crystallization of drug by SAS method also indicated a change in particle morphology [29, 32]. The other process parameters like solution flow rate, type of solvent, drug concentration, pressure, temperature, and antisolvent (CO₂) flow rate can affect primary particle size [29-33]. We have obtained somewhat large and irregular drug particles from SAS process. The size of drug particle obtained from SAS process depends on physico-chemical properties drug (e.g., melting point, logP). We have used process parameters close to optimized conditions which we have known through our experience and literature study. Even with variation of process parameters, drug particle size should not be significantly different what we have obtained here. If significantly smaller particles are required then one can use SAS-EM process [32].

We presumed that self agglomeration of drug particles can be overcome by depositing the particles on the surface of inert filler like lactose or MCC so that we can achieve few advantages such as improving the solubility and dissolution rate of NEV, uniformity of the drug/carrier blend, and enhancement of flow of the drug particles, etc. Figure 5.5 shows SEM images of SAS-DEM mixture of drug and lactose at various drug loadings. Figure 5.5(a) shows image for lactose particles which are mostly spherical in morphology. From Figure 5.5(b), it is clear that drug and lactose mixture formed highly

ordered mixture at 10 wt. % drug loading. Figure 5.5 c&d show deposition of drug particles on the surface of larger lactose particles. Formation of ordered mixture is preferred due to better flow properties and less tendency of drug to segregate from excipient. As the drug loading increases, drug particles formed ordered random mixture which is shown in 5.5(d). The ordered random mixture is obtained at high drug loading because most of the surface of excipient particle is occupied by drug particles and excess drug particles contribute to randomness. As excess free drug particles increase at high drug loading in the mixture, drug particle has tendency to form large agglomerates.

Figure 5.5(e) shows the presence of drug agglomerates at higher drug loading in the mixture. These agglomerates can be made from fusion of several drug particles or formed due to van der Waals attraction. To determine whether free drug particles which are not associated with lactose formed loose agglomerates, the samples were suspended in saturated drug solution and sonicated for 10 minutes and examined the particles by SEM imaging, as described earlier. The SEM images indicate that, there is still presence of few smaller aggregates (fused 2-3 particles) in the sample. Table 5.2 and Figure 5.4 show particle size distribution of drug in SAS-DEM drug/lactose mixture. Particle size analysis using laser diffraction was used only for drug/lactose mixture because lactose can be easily dissolved in particle suspension media. Therefore there will be no interference of excipient particles in particle size analysis. Drug particle are much smaller in SAS-DEM drug/lactose mixture as compared to only SAS drug. This is due to presence of excipient(s) particles which reduces the further growth and/or aggregation of drug particles. But as drug loading increases in the mixture, drug particle size also increases but it is still smaller as compared to SAS drug. Similar type of observations

(decrease in drug particle size) have been found by Thakur et.al 2009 [37] for griseofulvin particles in presence of silica particles. At lower drug loading (10 wt. %) for SAS-DEM mixture, span of drug particle size distribution is larger than SAS drug only which could not be explained completely. One of the possible reasons for broader particle size distribution is non-uniform temperature and composition within high pressure vessel during initial start of the operation. For small drug loading, process was carried out for less than 30 minutes. Non uniformity of temperature and composition can affect two concurring phenomenon of nucleation and growth which can lead to broader particle size distribution [29, 31]. One way to avoid this is by injecting only solvent initially. Once temperature is stabilized inside the vessel, then drug solution can be injected. At higher drug loading for SAS-DEM mixture, span of drug particle size distribution is lower or same as compared to SAS drug only.

Similar type of particle formation and mixing phenomenon has been observed in the cases of SAS-DEM drug/MCC and SAS-DEM drug/MCC + lactose mixture. Figure 5.6(a) shows image for MCC particles which are mostly flaky or needle-like in morphology. Figure 5.6b shows SEM images for SAS-DEM mixture of drug/MCC. Figure 5.6c and 6d shows very ordered mixture of drug and MCC particles at 8 wt. % drug loading. As drug loading increases, the drug and MCC particles form an ordered random mixture (Figure 5.6d). With increased drug loading, free drug particles form larger agglomerates (Figure 5.6e). These larger drug agglomerates can cause poor flowability and lower dissolution rate. From visual observations of flow, at lower drug loading, drug/excipient mixture shows characteristics of high flowability while at higher drug loading mixture is somewhat cohesive and less flowable. For comparison, Figure

5.6f shows SEM image for physical mixture of SAS drug and MCC particles at 10 wt. % drug loading. For physical mixture, drug and MCC particles form mostly random mixture which can be prone to segregation during further pharmaceutical processing.

Any changes in the surface morphology of excipient particles due to stirring in the SAS-DEM vessel as well as organic solvent were examined. Figure 5.7 shows surface of lactose as received from supplier and drug/lactose mixture by SAS-DEM. Presence of scaled rough lactose surface can be easily seen in both images. Hence, there was no significant morphological change observed on lactose surface.

It will be worthwhile to investigate applicability of SAS-DEM with more drug compounds which are differing in particle size and shape. For flaky/rectangular shape drug particles, which are difficult to mix due to their shape, will find more usefulness of SAS-DEM method. Our future work will address this aspect in more detail.

5.5.1.2 Characterization by XRD

Figure 5.8 shows the XRD patterns for unprocessed drug from the supplier (control) and SAS processed drug. Figure 5.9 shows the physical mixture of SAS drug/lactose, and SAS-DEM mixture of drug/lactose. Nevirapine crystals show various diffraction peaks due to its crystalline structure. From Figure 5.8, it is clear that SAS processed drug has similar crystallinity as that of supplier drug (control). Drug has maintained its crystallinity during SAS-DEM process with lactose (Figure 5.9). Drug also maintained its crystallinity during SAS-DEM process with MCC and mixture of lactose/MCC (data not shown here).

5.5.1.3 Characterization by FT-IR

Figure 5.10 shows IR spectra of supplier drug (control), SAS drug, physical mixture of SAS drug/lactose and SAS drug/MCC, and SAS-DEM mixture of drug/lactose and drug/MCC. FT-IR spectra of physical mixture and mixture obtained by SAS-DEM method were similar, and there is no shift of peaks due to SAS process with or without the excipients; indicating that there is no significant changes in physicochemical properties of NEV and there is no chemical interaction between drug and excipient with this process. Specific NEV peaks are observed at 3190, 3060, 1930, 1520, and 1181 cm^{-1} both in physical mixture of drug/excipient(s) and SAS-DEM mixture of drug/excipient(s).

5.5.1.4 Characterization by DSC

Figure 5.11 show DSC thermographs for supplier drug (control), SAS drug, and SAS-DEM mixture (drug/MCC)-21 wt. % drugs loading. Nevirapine showed a typical behavior of anhydrous crystalline drug with a well defined melting peak at 246° C ($\Delta H = 1404 \text{ J/g}$). The SAS treated drug also showed distinct endothermic peak with no change in heat flow (at 246° C, $\Delta H = 1404 \text{ J/g}$) indicating there is no change in crystallinity. The thermograph of SAS-DEM mixture shows distinct endothermic peaks for drug and MCC indicating that this process did not induce any detectable amorphous content and decrease in heat flow ($\Delta H = 380.5 \text{ J/g}$) is due to less amount of the drug in the mixture (21 wt % drug). We were not able to perform DSC on the samples containing lactose because lactose was decomposing at lower temperatures.

5.5.1.5 Drug content homogeneity

The drug content uniformity data of SAS-DEM processed drug/lactose and

drug/lactose+MCC samples containing various drug loadings is shown in Table 5.3. Results indicate that the drug is uniformly dispersed in the mixture(s) produced by this process at various drug loadings and the RSDs for all the mixtures are less than 6%. The formation of ordered mixture was also confirmed from SEM studies, which provided high drug content uniformity for drug/excipient(s) mixture at various drug loadings. Due to formation of highly ordered mixture in case of lower drug loading, mixture shows low RSD.

5.5.1.6 Dissolution Studies

A test for drug-drug de-agglomeration, most useful for drug delivery, is the dissolution profile; the deagglomerated particles will exhibit a fast dissolution. Figure 5.12, 13 and 14 show the dissolution curves for SAS-DEM processed drug/excipient(s) at various drug loading, physical mixture of drug/excipient obtained by spatula mixing (20 wt. % drug), SAS, and supplier drug (control). Similarity in dissolution profiles for SAS drug and supplier drug was due to agglomeration of particles even though different particle size distribution (Figure 5.4). Due to the presence of drug particle agglomerates, the dissolution of the drug was not improved. In the case of SAS-DEM processed drug/excipient(s), a rapid dispersion or deagglomeration of drug particles has been visually observed in the dissolution media. The improvement in the dissolution rate in case of SAS-DEM drug /excipient (s) mixture is due to deagglomeration of the drug particles and also because of improved wetting of the drug particles in the presence of the excipient. An efficient dispersion of drug particles (for SAS-DEM processed drug/excipient(s) mixture with various drug loadings) resulted in complete drug

dissolution in less than 15-30 minutes as compared to ~60-70% (of total drug) in the case of physical mixture and ~20-30% (of total drug) for SAS processed drug and control (unprocessed drug from the supplier). From SEM images of physical mixture Figure 5.6f, it is clear that drug and excipient particles form random mixture predominantly as compared to ordered mixing by SAS-DEM method. SAS drug particles are partially deagglomerated in physical mixing therefore show a lower dissolution rate as compared to respective drug mixture by SAS-DEM but show at least 2 fold increase in dissolution rate as compared to unprocessed drug (control). The substantial increases in the dissolution by SAS-DEM treated drug/excipient products in comparison to their physical mixtures indicate the formation of highly ordered drug/excipient mixture by SAS-DEM method and deagglomeration of the drug particles. Rapid dissolution (complete dissolution within 10-15 minutes!) of drug/excipient(s) mixture at lower drug loading is due to smaller drug particle size (Table 5.2) and absence of agglomerated drug particles. Smaller particle size in case of low drug loading lead to significant increase in the surface area and which resulted into higher dissolution rate according to Noyes-Whitney equation. Initial decrease in dissolution rate for SAS-DEM drug/excipient(s) mixture in case of higher drug loading can be attributed to agglomeration several non-coated (on excipient) drug particles as well as due to increase in particle size. During the initial 10 minutes, drug/lactose mixture has shown a faster dissolution as compared to drug/MCC mixture, due to rapid dissolution of lactose particle leading to instantaneous dispersion of drug particles. In case of drug/MCC mixture, drug particles need to get dislodged from surface of swelled MCC particles, which is a slower process as compared to instantaneous dispersion in drug/lactose mixture. For drug/lactose+MCC mixture, initial drug

dissolution rate was in between that of drug/MCC and drug/lactose mixtures.

Efficient deagglomeration or mixing is required in order to see the benefits of nano/micro sizing for poorly-water-soluble drugs [38]. The rate of drug dissolution (bulk effect) can be used along with SEM characterization (microscopic observation) and drug homogeneity (drug quantification) as a tool to determine the extent of mixing of fine drug particles with excipients.

5.6 Conclusions

The drug dissolution profiles, RSD analysis, and physico-chemical characterization of drug/excipient(s) mixture indicate formation of highly ordered mixture by SAS-DEM method. Particle formation in the presence of excipient particles in SAS-DEM environment prevents drug-drug particle agglomeration, depending on the extent of loading. Due to the formation of homogenous micro-mixture (ordered to ordered-random depending on drug loading in the mixture), a 3-4 fold faster dissolution was obtained. The high drug dissolution rate is attributed to efficient deagglomeration and mixing as well as sufficient wetting of drug particles due to surrounding excipient particles.

5.7 Acknowledgment

Financial supports from National Science Foundation (NIRT grant DMI-0506722) and from Harrison School of Pharmacy, Auburn University are appreciated.

5.8 References

- [1]. G.L. Amidon, H. Lennernas, V.P. Shah, and J.R. Crison. A theoretical basis for a

- biopharmaceutical drug classification: the correlation of in vitro drug product dissolution and in vivo bioavailability. *Pharm Res (N Y)*. 12:413-420 (1995).
- [2]. N. Rasenack and B.W. Muller. Dissolution rate enhancement by in situ micronization of poorly water-soluble drugs. *Pharm Res (N Y)*. 19:1894-1900 (2002).
- [3]. A. Jounela, P. Pentikainen, and A. Sothmann. Effect of particle size on the bioavailability of digoxin. *Eur J Clin Pharmacol*. 8:365-370 (1975).
- [4]. G.G. Liversidge and K.C. Cundy. Particle size reduction for improvement of oral bioavailability of hydrophobic drugs: absolute oral bioavailability of nanocrystalline danazol in beagle dogs. *Int J Pharm (Kidlington)*. 125:91-97 (1995).
- [5]. A.J. Aguiar, A.W. Zelmer, and A.W. Kinkel. Deaggregation behavior of a relatively insoluble substituted benzoic acid and its sodium salt. *J Pharm Sci*. 56:1243-1252 (1967).
- [6]. P. Finholt and S. Slovang. Dissolution kinetics of drugs in human gastric juice the role of surface tension. *J Pharm Sci*. 57:1322-1326 (1968).
- [7]. E. Swanepoel, W. Liebenberg, and M.M.D. Villiers. Dissolution properties of proxicam powders and capsules as a function of particle size and the agglomeration of powders. *Drug Dev Ind Pharm*. 26:1067-1076 (2000).
- [8]. M.M. DeVilliers. Influence of agglomeration of cohesive particles on the dissolution behaviour of furosemide powder. *Int J Pharm (Kidlington)*. 136:175-179 (1996).
- [9]. G.P. Sanganwar and R.B. Gupta. Enhancement of shelf-life and handling properties of drug nanoparticles: mixing of itraconazole with silica at nanoscale.

- Ind Eng Chem Res. 47:4717-4725 (2008).
- [10]. K. Kale, K. Hapgood, and P. Stewart. Drug agglomeration and dissolution-What is the influence of powder mixing. *Eur J Pharm Sci.* 72:156-164 (2009).
- [11]. T.P. Garcia, A. Carella, and V. Pansa. Identification of factors decreasing the homogeneity of blend and tablet uniformity. *Pharmaceutical Technology* (2004).
- [12]. M.M. DeVilliers and J.G. VanderWatt. The measurement of mixture homogeneity and dissolution to predict the degree of drug agglomerate breakdown achieved through powder mixing. *Pharm Res (N Y).* 11:1557-1561 (1994).
- [13]. J.K. Prescott and R.A. Barnum. On the powder flowability. *Pharmaceutical Technology.* 10:60-84 (2000).
- [14]. K. Thalberg, D. Lindholm, and A. Axelsson. A comparison of different flowability tests for powders for inhalation. *Powder Technol.* 146:206-213 (2004).
- [15]. N. Harnby, M.F. Edwards, and A.W. Nienow. *Mixing in process industries*, Butterworth, London, 1990.
- [16]. I. Krycer and J.A. Hersey. A comparative study of comminution in rotary and vibratory ball mill. *Powder Technol.* 27:137-141 (1980).
- [17]. I. Krycer and J.A. Hersey. Fine powder mixing in vibratory ball mill. *Int J Pharm (Kidlington).* 6:119-129 (1980).
- [18]. N. Harnby. An engineering view of pharmaceutical powder mixing. *Pharmaceutical Science Technology Today.* 3:303-309 (2000).
- [19]. D.S. Wishart, C. Konx, A.C. Guo, S. Shrivastava, M. Hassanali, P. Stothard, Z. Chang, and J. Woolsey. Drugbank: a comprehensive resource for in silico drug discovery and exploration. *Nucleic Acids Res.* 34:D668-D672 (2006).

- [20]. B.G. Pereira, F.D. Fonte-Boa, J.A.L.C. Resende, C.B. Pinheiro, N.G. Fernandes, M.I. Yoshida, and C.D. Vianna-Soares. Pseudopolymorphs and intrinsic dissolution of nevirapine. *Cryst Growth Des.* 7:2016-2023 (2007).
- [21]. N.T. Zwietering. Suspending of solid particles in liquid by agitators. *Chem Eng Sci.* 8:244-253 (1958).
- [22]. E.L. Paul, V. Atiemo-Obeng, and S.M. Kresta. *Handbook of Industrial Mixing: Science and Practice* Wiley-Interscience 2003.
- [23]. NIST Chemistry WebBook. <http://webbook.nist.gov/chemistry>. Accessed August 2009.
- [24]. L.T. Fan and Y.-M. Chen. Recent development in solids mixing. *Powder Technol.* 61:255-287 (1990).
- [25]. M. Poux, P. Fayolle, and J. Bertrand. Powder mixing: Some practical rules applied to agitated systems. *Powder Technol.* 68:213-234 (1991).
- [26]. J.N. Staniforth. Advances in powder mixing and segregation in relation to pharmaceutical processing. *International Journal of Pharmaceutical Technology and Product Manufacture* 3:1-12 (1982).
- [27]. B.R. Rohrs, G.E. Amidon, R.H. Meury, P.J. Secreast, H.M. King, and C.J. Skoug. Particle size limits to meet USP content uniformity criteria for tablets and capsules. *J Pharm Sci.* 95:1049-1059 (2006).
- [28]. N.K. Patel, A.H. Upadhyay, J.S. Bergum, and G.E. Reier. An evaluation of microcrystalline cellulose and lactose excipients using an instrumented single station tablet press. *Int J Pharm (Kidlington).* 110:203-210 (1994).
- [29]. M.-S. Kim, S. Lee, J.-S. Park, J.-S. Woo, and S.-J. Hwang. Micronization of

- cilostazol using supercritical antisolvent process: effect of process parameters. Powder Technol. 177:64-70 (2007).
- [30]. G.A. Sacha, W.J. Schmitt, and S.L. Nail. Identification of critical process variables affecting particle size following precipitation using a supercritical fluid. Pharm Dev Technol. 11:187-194 (2006).
- [31]. G.A. Sacha, W.J. Schmitt, and S.L. Nail. Identification of physical-chemical variables affecting particle size following precipitation using supercritical fluid. Pharm Dev Technol. 11:195-205 (2006).
- [32]. P. Chattopadhyay and R.B. Gupta. Protein nanoparticles formation by supercritical antisolvent with enhanced mass transfer. AIChE J. 48:235-244 (2002).
- [33]. I.D. Marco and E. Reverchon. Supercritical antisolvent micronization of cyclodextrins. Powder Technol. 183:239-246 (2008).
- [34]. O. Boutin, T. Petit-Gas, and E. Badens. Powder micronization using a CO₂ supercritical antisolvent type process: comparison of different introduction devices. Ind Eng Chem Res. 48:5671-5678 (2009).
- [35]. F. Ruchatz, P. Kleinebudde, and B.W. Muller. Residual solvents in biodegradable microparticles. Influence of process parameters on the residual solvent in microparticles produced by the aerosol solvent extraction system (ASES) process. Journal of Pharmaceutical Science. 86:101-105 (1997).
- [36]. V. Majerik, G. Charbit, E. Badens, G. Horvath, L. Szokonya, N. Bosc, and E. Teillaud. Bioavailability enhancement of an active substance by supercritical antisolvent precipitation. J Supercrit Fluids. 40:101-110 (2007).

- [37]. R. Thakur, A.E. Hudgins, E. Goncalves, and G. Muhrer. Particle size and bulk powder flow control by supercritical antisolvent precipitation. *Ind Eng Chem Res.* 48:5302-5309 (2009).
- [38]. G.P. Sanganwar and R.B. Gupta. Nano-mixing of dipyridamole drug and excipient nanoparticles by sonication in liquid CO₂. *Powder Technol.* 196:36-49 (2009).
- [39]. S.J. Kothari, V. Kumar, and G.S. Banker. Comparative evaluations of powder and mechanical properties of low crystallinity cellulose, microcrystalline cellulose, and powdered celluloses. *Int J Pharm (Kidlington).* 232:69-80 (2002).

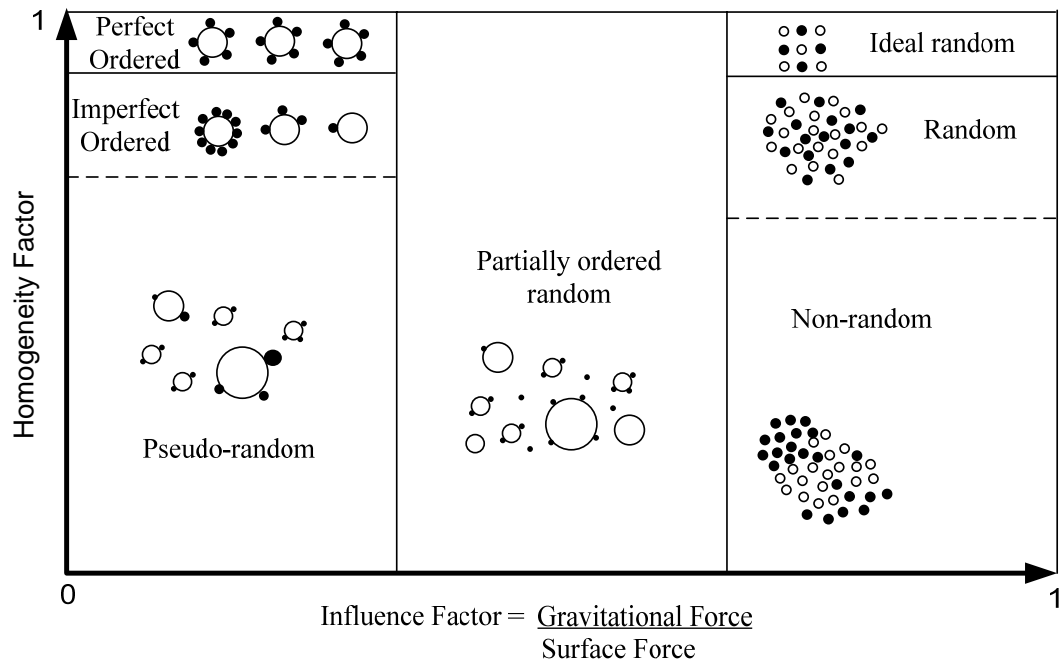


Figure 5.1 Different type of mixing with their homogeneity factor dependent on influence of gravitational and surface forces [24].

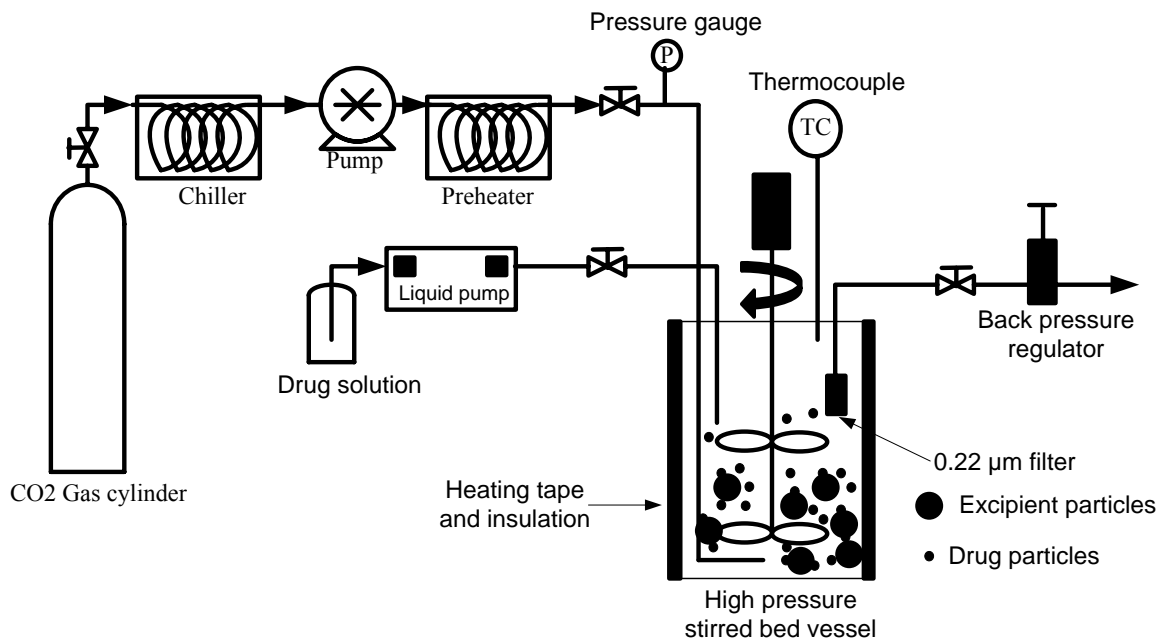


Figure 5.2 Schematic of apparatus for simultaneous particle formation and mixing using supercritical antisolvent (SAS-DEM).

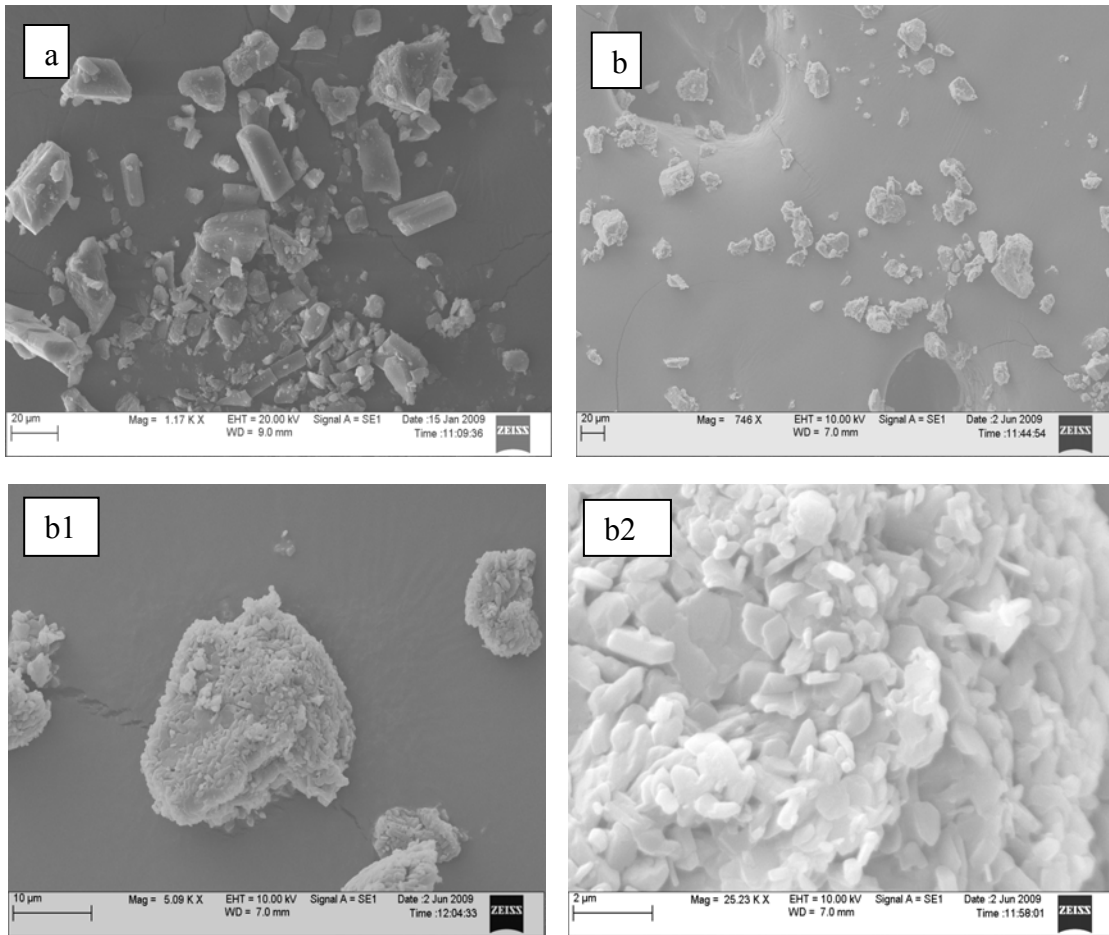


Figure 5.3 SEM images of (a) supplier drug, (b) drug produced by SAS, (b1) higher magnification of (b) showing individual particle, and (b2) close-up of (b1) showing particle made up of aggregates of several micron size particles.

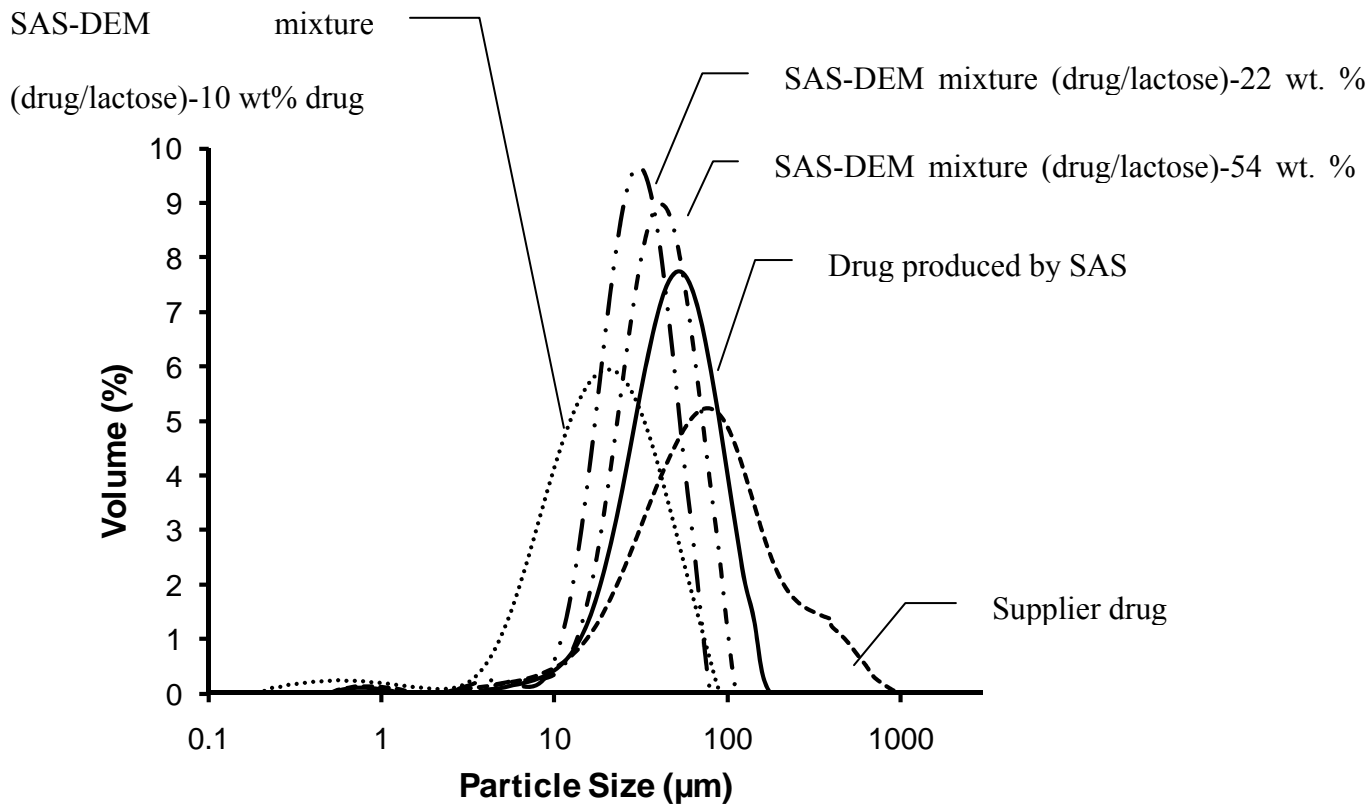


Figure 5.4 Particle size distribution on volume basis of (---) supplier drug, (—) drug produced by SAS, (.....) SAS-DEM mixture (drug/lactose) – 10 wt. % drug, (– · –) SAS-DEM mixture (drug/lactose) – 22 wt. % drug, and (– – –) SAS-DEM mixture (drug/lactose) – 54 wt. % drug.

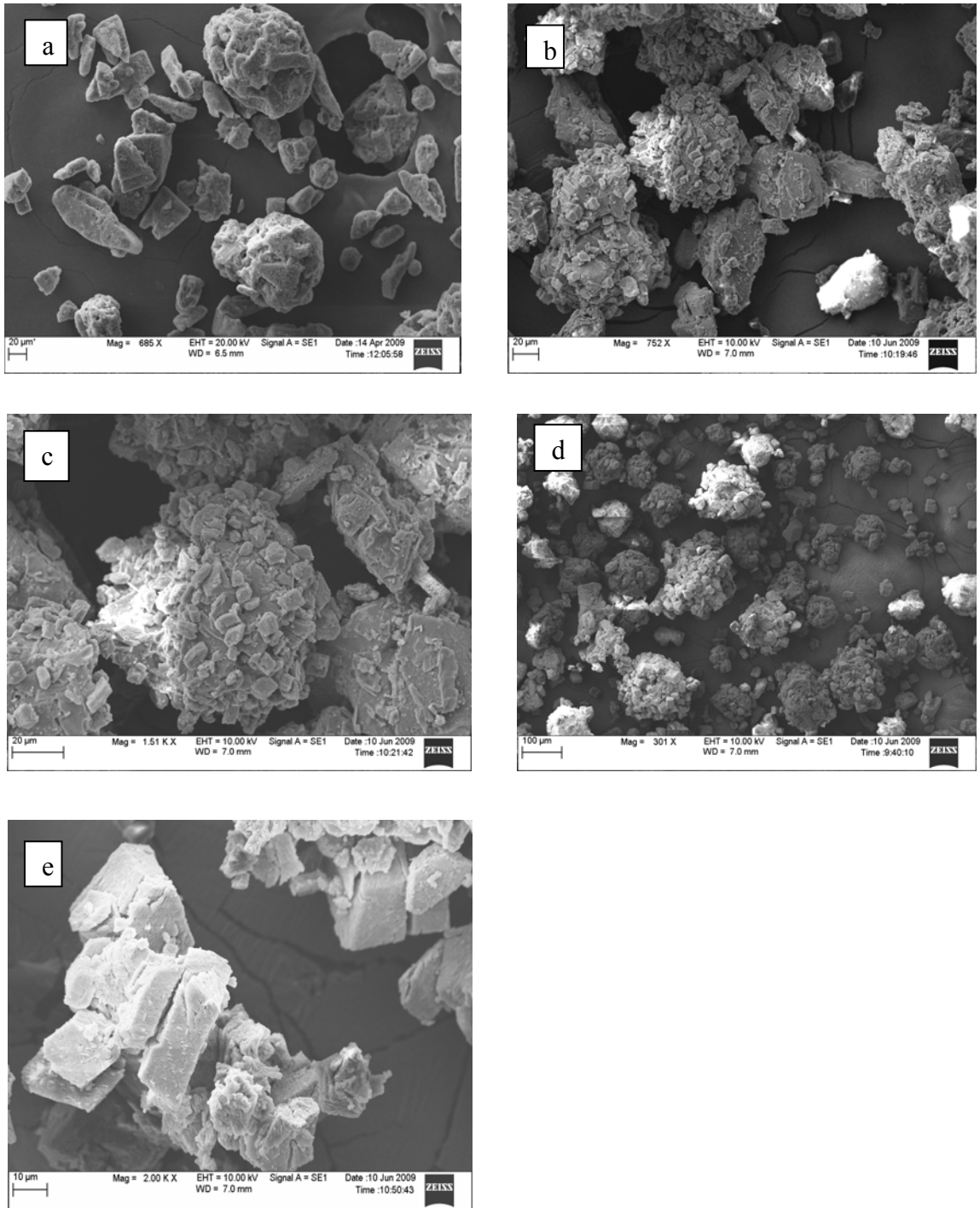


Figure 5.5 SEM images of drug and lactose mixture prepared by SAS-DEM method: (a) lactose particles (b) formation of interactive (ordered) mixture in which drug particles coated onto larger lactose particles for drug loading of 8 wt. % in the mixture, (c) higher magnification of (b) showing individual lactose particle and drug particles on the surface on lactose, (d) formation of ordered random mixture for drug loading of 22, 31, and 54 wt. %, and (e) presence of drug agglomerates at drug loading of 31 and 54 wt. %

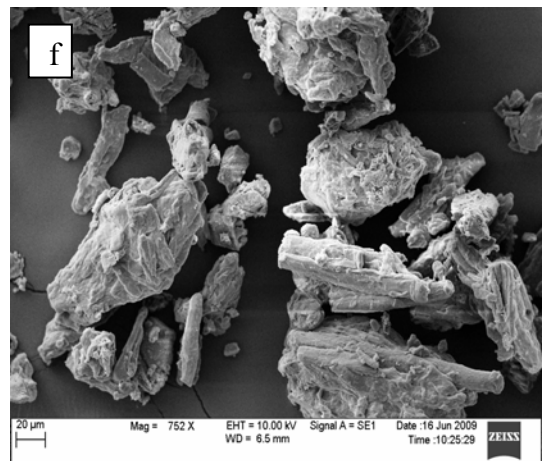
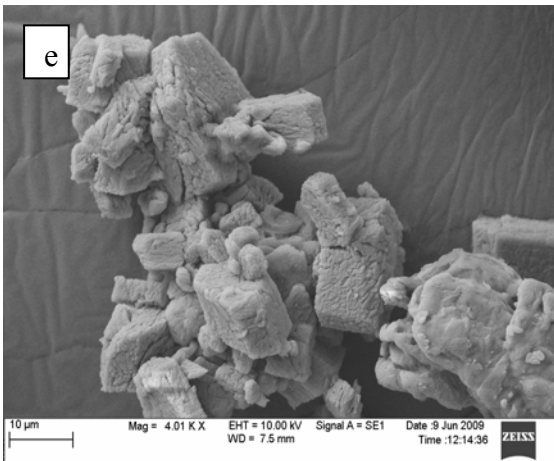
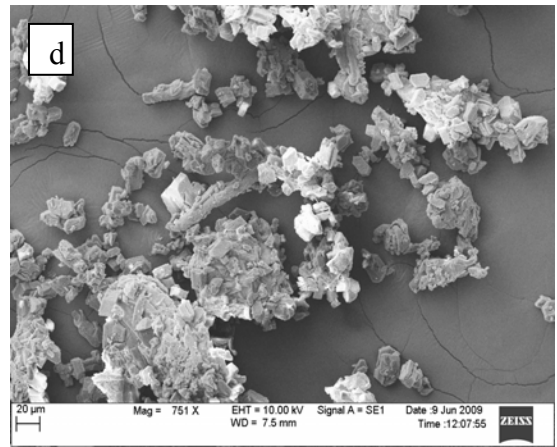
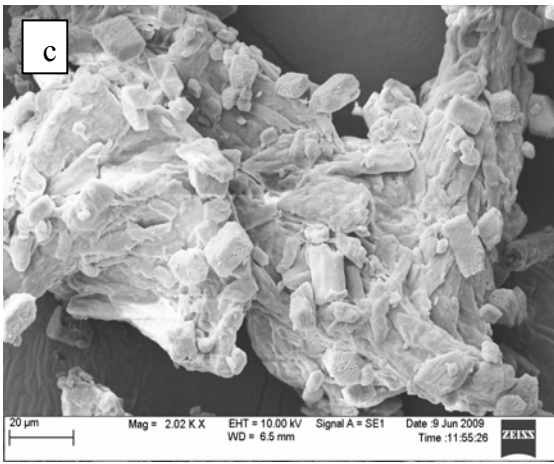
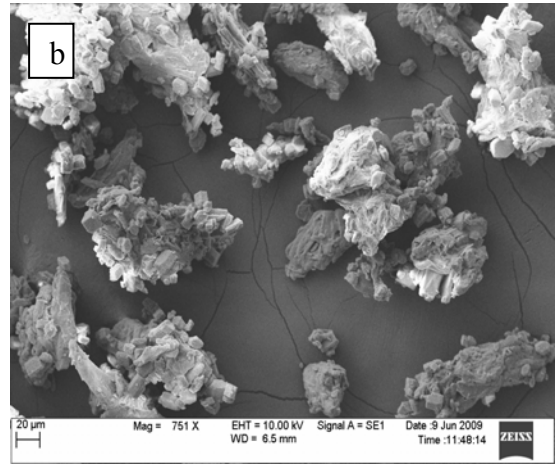
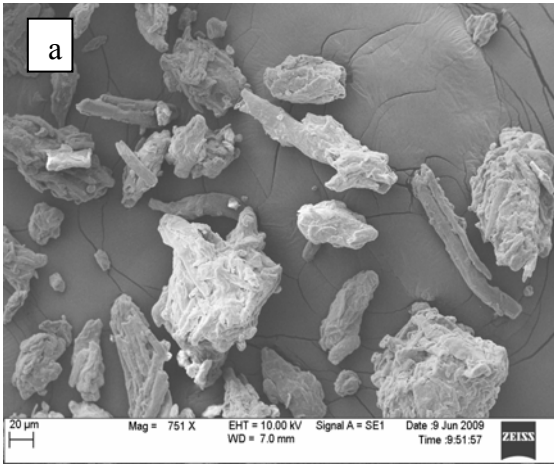


Figure 5.6 SEM images of drug and MCC mixture prepared by SAS-DEM method: (a) MCC particles (b) formation of interactive (ordered) mixture in which drug particles coated onto larger MCC particles for drug loading of 8 wt. % in the mixture, (c) higher magnification of (b) showing individual MCC particle and drug particles on the surface on MCC, (d) formation of ordered random mixture for drug loading of 21, 37, and 51 wt. %, (e) presence of drug agglomerates at drug loading of 37 and 51 wt. %, and (f) random mixture (spatula mixing) of drug (by SAS) and MCC at 10 wt. % drug loading

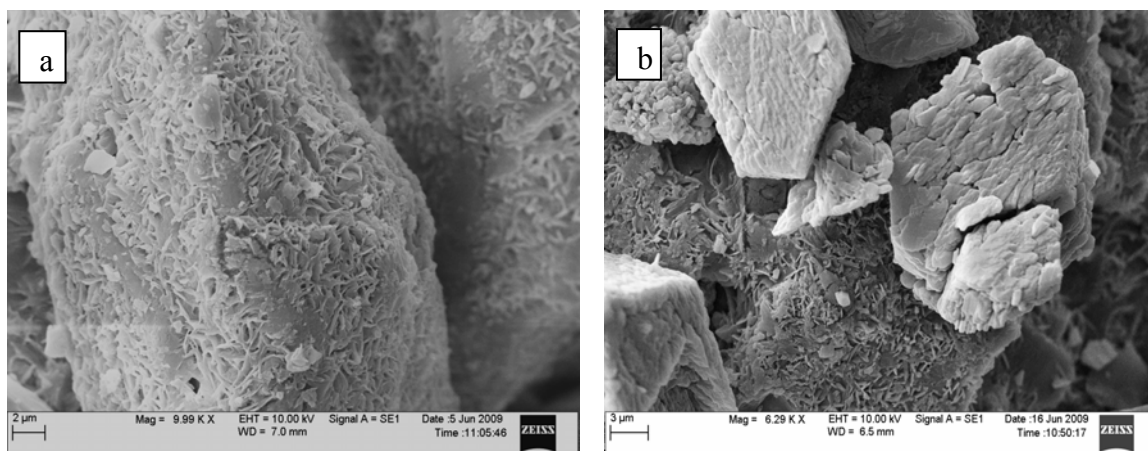


Figure 5.7 SEM images of (a) lactose surface and (b) lactose surface in drug and lactose mixture by SAS-DEM

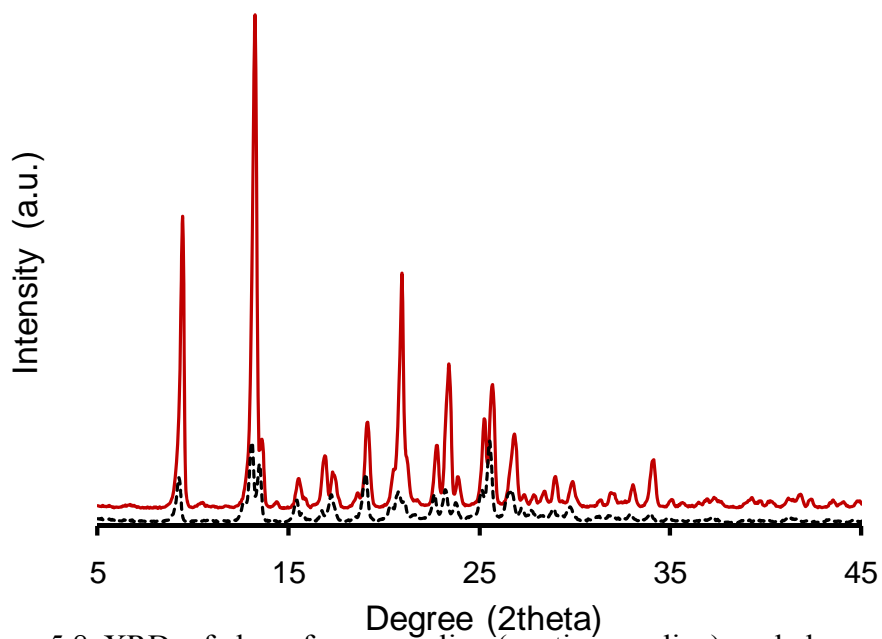


Figure 5.8 XRD of drug from supplier (continuous line) and drug obtained by SAS method (dotted line)

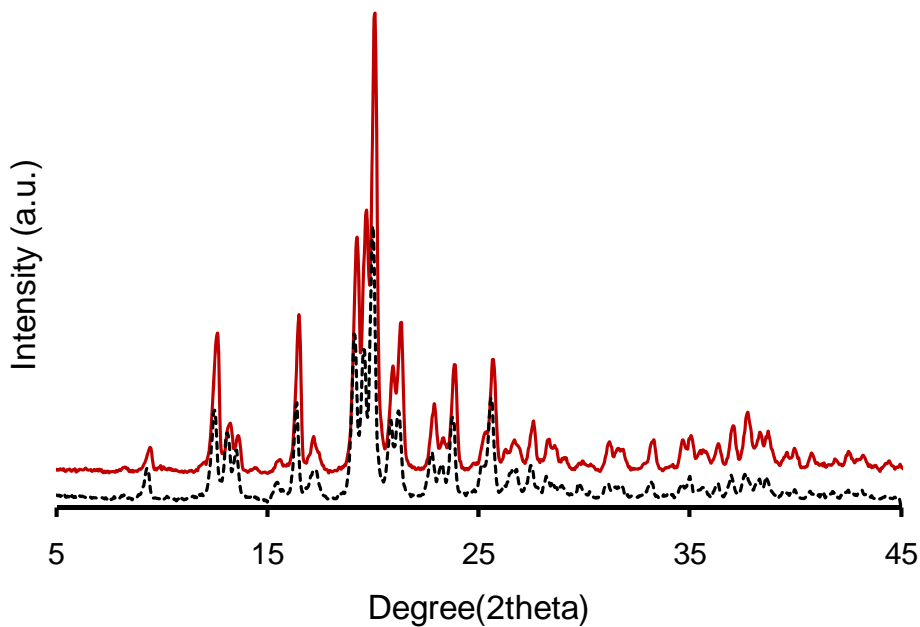


Figure 5.9 XRD of physical mixture (obtained by spatula mixing) of lactose and SAS drug (continuous line) and mixture of lactose and drug obtained by SAS-DEM method (dotted line).

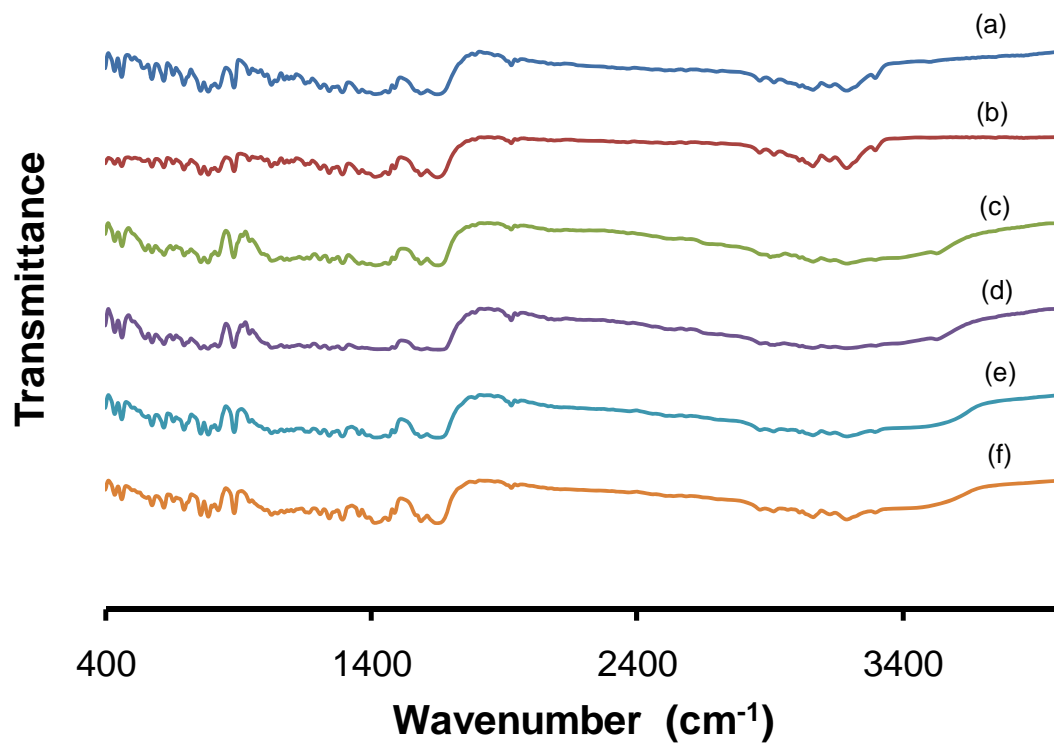


Figure 5.10 FT-IR spectra of (a) supplier drug, (b) SAS drug, (c) physical mixture (spatula mixing) of SAS-DEM drug/lactose, (d) SAS-DEM mixture of drug/lactose, (e) physical mixture of SAS drug/MCC, and (f) SAS-DEM mixture of drug/MCC.

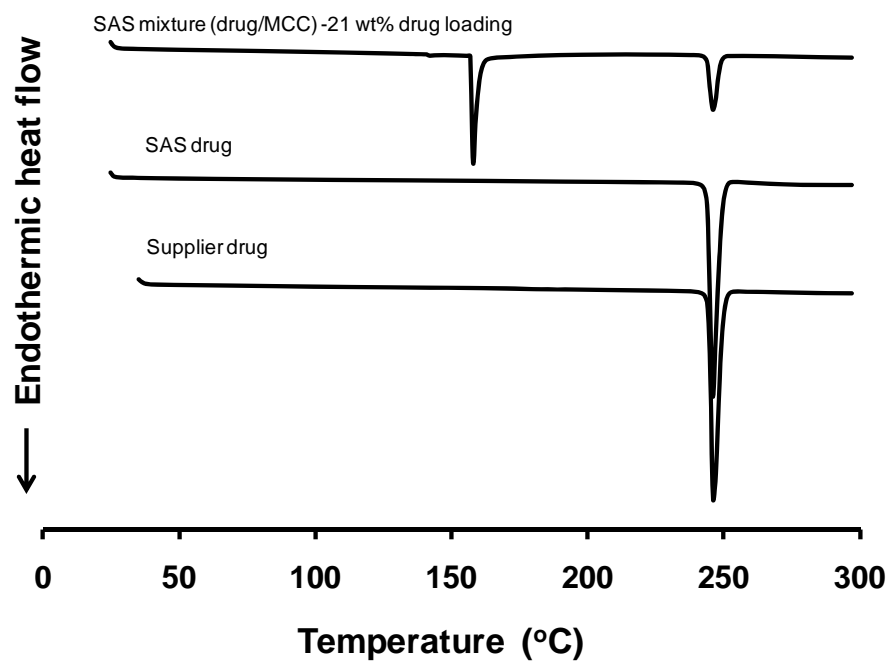


Figure 5.11 DSC thermographs of (a) supplier drug, (b) SAS drug, and (c) SAS-DEM mixture of drug/MCC- 21 wt. % drug loading.

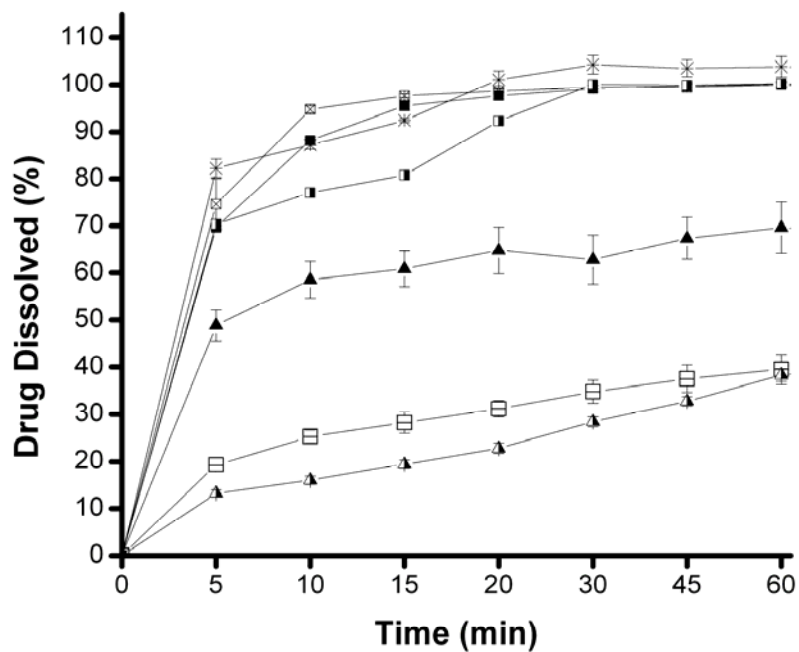


Figure 5.12 Dissolution profiles (from top to bottom) of (a) \square SAS-DEM mixture (drug/lactose) – 10 wt. % drug, (b) \blacksquare SAS-DEM mixture (drug/lactose) – 21 wt. % drug, (c) \ast SAS-DEM mixture (drug/lactose) – 31 wt. % drug, (d) \blacksquare SAS-DEM mixture (drug/lactose) – 54 wt. % drug, (e) \blacktriangle physical mixture of SAS drug/lactose – 20 wt. % drug, (f) \square supplier drug, and (g) \blacktriangle SAS drug.

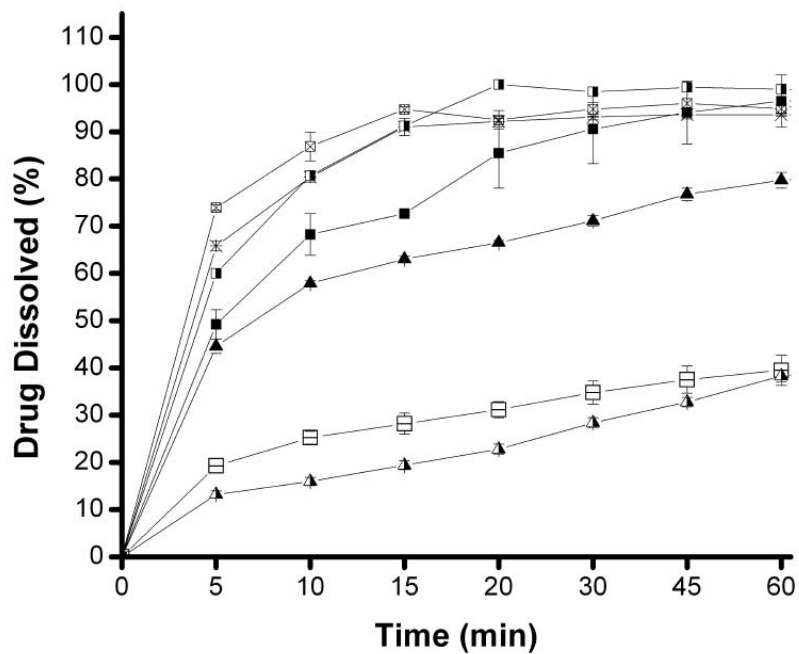


Figure 5.13 Dissolution profiles (from top to bottom) of (a) \square SAS-DEM mixture (drug/MCC) – 13 wt. % drug, (b) \blacksquare SAS-DEM mixture (drug/MCC) – 21 wt. % drug, (c) \ast SAS-DEM mixture (drug/MCC) – 37 wt. % drug, (d) \blacksquare SAS-DEM mixture (drug/ MCC) – 51 wt. % drug, (e) \blacktriangle physical mixture of SAS drug/ MCC – 20 wt. % drug, (f) \square supplier drug, and (g) \blacktriangle SAS drug.

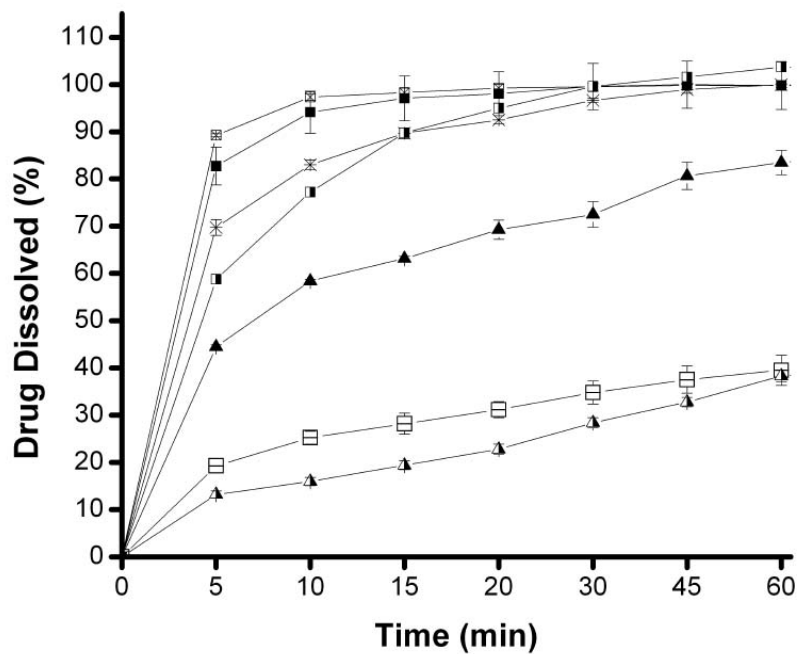


Figure 5.14 Dissolution profiles (from top to bottom) of (a) \square SAS-DEM mixture (drug/lactose & MCC) – 13 wt. % drug, (b) \blacksquare SAS-DEM mixture (drug/ lactose & MCC) – 21 wt. % drug, (c) \ast SAS-DEM mixture (drug/ lactose & MCC) – 37 wt. % drug, (d) \blacksquare SAS-DEM mixture (drug/ lactose & MCC) – 51 wt. % drug, (e) \blacktriangle physical mixture of SAS drug/ lactose & MCC – 20 wt. % drug, (f) \square supplier drug, and (g) \blacktriangle SAS drug.

Table 5.1 Minimum stirrer speed (N_{js}) required to keep particles just suspended for various compounds.

Compound	Particle size (μm)	N_{js} (rpm)
Lactose (assumed particle density =1500 kg/m ³)	100	395
MCC PH101 (particle density =1557 kg/m ³ , [39])	50	355
Drug (assumed particle density =1500 kg/m ³)	5	217
	10	249
	20	286
	50	344

Note: Percentage mass fraction of solids is used as 0.63 for the calculation of N_{js} .

Table 5.2 Particle size (on volume basis) range for compound/mixture.

Compound/Mixture	D _v (0.1) (μm)	D _v (0.5) (μm)	D _v (0.9) (μm)	Specific Surface area* (m ² /g)	Span [D _v (0.9)- D _v (0.1)]/[D _v (0.5)]
Supplier drug	20.4	69.6	264.1	0.21	3.5
SAS drug	19.6	45.7	91.2	0.22	1.6
SAS-DEM mixture (drug/lactose)- 10 wt. % drug	6.3	17.7	43.2	0.81	2.1
SAS-DEM mixture (drug/lactose)- 22 wt. % drug	14.8	27.8	48.5	0.26	1.2
SAS-DEM mixture (drug/lactose)- 31 wt. % drug	17.4	39.4	78.7	0.25	1.6
SAS-DEM mixture (drug/lactose)- 54 wt. % drug	18.4	36.9	67.1	0.20	1.3

*derived parameter from particle size analysis

Table 5.3 Relative standard deviation at various drug loadings with excipient(s)

Mean Drug Loading (wt. %)	Relative Standard Deviation (%)
<i>Mixing with spray dried lactose by SAS-DEM</i>	
10	1.9
22	3.4
31	2.9
47	3.1
<i>Mixing with spray dried lactose and microcrystalline cellulose (50:50 wt. %) by SAS-DEM</i>	
10	2.9
20	3.7
30	1.9
47	3.1

6 DISSOLUTION-RATE ENHANCEMENT BY ADSORPTION ONTO SILICA

6.1 Abstract

Dissolution rate of a poorly water-soluble drug, fenofibrate, is increased by adsorbing the drug onto silica. The adsorption is achieved by first dissolving the drug in supercritical carbon dioxide and then depressurizing the solution onto silica. Loadings of up to 27.5 wt.% drug onto silica are obtained. Since solvents are not used in the loading process, the fenofibrate/silica formulation is free of any residual solvent, and carbon dioxide is freely removed upon depressurization. The formulation is characterized using infrared spectroscopy, ultraviolet spectroscopy, X-ray diffraction, differential scanning calorimetry and scanning electron microscopy. Based on *in vitro* dissolution study, a significant increase in the dissolution rate (~80% drug release in 20 min) of drug-silica formulation is observed as compared to micronized fenofibrate (~20% drug release in 20 minutes), which can be attributed to increase in the surface area and decrease in the crystallinity of drug after adsorption onto silica. Two different formulations are compared: (A) amorphous fenofibrate/silica and (B) slightly crystalline fenofibrate/silica. The second formulation is found to be more stable on storage.

6.2 Introduction

Bioavailability of poorly water-soluble hydrophobic drugs [Class II in Biopharmaceutics Classification System] is limited by their solubility and dissolution rate [1]. The dissolution rate of these drugs can be improved by decreasing particle size, decreasing crystallinity, and/or increasing the surface area. Several studies have been carried out to increase the dissolution rate of drugs by decreasing the particle size, by creating nano- and micro-particles [2-4]. However, the fine drug particles have high tendency to agglomerate due to van der Waals attraction or hydrophobicity, which both result in a decrease in surface area over time [5,6]. Another way of increasing the dissolution rate is adsorption of the drug onto a high-surface-area carrier. In this technique, the drug is dissolved in an organic solvent (e.g., methanol, acetone, methylene chloride) followed by soaking of the solution by a high-surface-area carrier such as silica [7-11]. Here, agglomeration of the drug particles is prevented due to the binding of drug to the carrier. However, due to the presence of the residual solvent in the drug formulation, it is disadvantageous to use toxic solvents. To overcome the problem, supercritical carbon dioxide, which is non-toxic and non-flammable, is used as a solvent to adsorb drug onto high surface area carriers [12].

Supercritical fluids have liquid-like densities and gas-like diffusivities. Out of various supercritical fluids, carbon dioxide is suitable for processing of pharmaceutical compounds due to its mild critical point (73.7 bar and 31.1°C). Also, small non-polar or hydrophobic molecules can be easily solubilized in CO₂ which is in relatively non-polar, and the solubility can be adjusted with the CO₂ density [13]. Also, due to the high molecular diffusivity, the drug can be easily transported to the carrier nanopores. Upon

depressurization, CO₂ leaves the solid matrix without any residues.

In this study, adsorption of fenofibrate through supercritical CO₂ onto silica was carried out for dissolution enhancement. Till now, there have been several studies to increase dissolution of fenofibrate, for example, (a) complexing with cyclodextrin [14,15], (b) solid dispersion in PEG and PVP [16], and (c) micronization [17,18]. However, no attempt was made to adsorb fenofibrate onto a high-surface-area carrier. Also, it is interesting to study the adsorption of fenofibrate onto high-surface-area carrier due to the low glass transition temperature (-20 °C) of the drug.

Fenofibrate (2-(4-[4-chlorobenzoyl] phenoxy)-2-methyl-propanoic acid, 1-methylsethyl ester) is hydrophobic/lipophilic (MW = 360.831 gm/mol, logP =5.575; [19]) drug with negligible solubility in water [17]. Bioavailability of fenofibrate solely depends on dissolution rate in the gastrointestinal tract. This drug is used in lipid regulation as it decreases low-density lipoprotein (LDL) and very-low-density lipoprotein (VLDL) levels, and increases high-density lipoprotein (HDL) level.

Non-porous fumed silica has been used in oral formulation as glidant, and as a carrier [20]. We have utilized pharmaceutical grade fumed silica consisting of 200-300 nm long aggregates of 9-30 nm size primary nanoparticles. This silica also forms 30-44 µm size macro-agglomerates with a very high (>98%) void volume [21-23]. The hydrophilic silica adsorbs moisture therefore can be used in moisture sensitive drug formulations. Also, hydroxyl groups located on siloxane surface can hydrogen bond with drug molecule providing additional interaction [24].

6.3 Materials and Method

6.3.1 *Materials*

Fenofibrate (>99% pure, Sigma-Aldrich), CAB-O-SIL M-5P fumed silica (200 ± 15 m²/g surface area, 40 g/l tapped density, Cabot, Inc.), dichloromethane (99.9% pure, Sigma-Aldrich), sodium chloride (ACS grade, Fisher Scientific), sodium dodecyl sulfate (>99% pure, Sigma Aldrich), hydrochloric acid (ACS grade, Fisher Scientific), methanol (>99.9% pure, Fisher Scientific), and CO₂ (bone dry, Air Gas) were used as received.

6.3.2 *Adsorption of drug onto silica*

Figure 6.1 shows a schematic of the experimental setup used for adsorption of a drug onto silica. Silica is sealed in a porous Whatmann filter paper (11 μm pore size) pouch and kept inside the pressure vessel (V, 100 ml) containing an excess amount of fenofibrate. CO₂ is pumped inside the pressure vessel to the desired pressure (2550 ± 50 psig) and temperature is maintained (40 or 50 ± 0.1 °C) using a heating tape. The content is allowed to equilibrate for 150 minutes at a constant pressure and temperature. Afterwards, the vessel is slowly depressurized over 4 hours to remove CO₂, after which the silica-fenofibrate formulation is collected from the filter paper pouch. Experiments are repeated to obtain sufficient amount of the formulation needed for analyses; the formulations are mixed before further analyses. Drug loading (g drug/g silica-drug formulation) was measured by dissolving a known amount of the formulation into methanol, followed by concentration analysis using UV spectroscopy at 287 nm. Weight measurements are done at 50% relative humidity (air conditioned laboratory), to avoid

moisture uptake by hydrophilic silica which usually occurs at >70% relative humidity.

6.3.3 *Fourier Transform Infrared Spectroscopy (FT-IR spectroscopy)*

Infrared spectra of the samples were obtained using Avatar 360 FT-IR (Nicolet). The formulation sample was mixed with 100 fold KBr for preparing the tablets. The final spectra are composed of 64 scans performed in range of 400-4000 cm^{-1} with 2 cm^{-1} resolution.

6.3.4 *Powder X-ray diffraction*

Crystallinity of the formulation was analyzed using the Rigaku X-ray diffractometer which is equipped with a $\text{Cu K}\alpha_1$ radiation source at 40 kV voltage, 40 mA current and a miniflex goniometer. Diffraction patterns were obtained in 2θ range of 10-80° using 0.05° step size and 5°/minute scan speed.

6.3.5 *Differential scanning calorimetry (DSC)*

DSC analysis (thermograph) of samples was done using TA Instruments, model DSC Q2000. 1-4 mg samples were weighed in aluminum pans and analyzed with heating rate of 5° C/min over the temperature range of 20-100°C. Degree of crystallinity (X) was determined from calorimetric data as follows [25].

$$X = \frac{(\Delta H_s - \Delta H_a)}{(\Delta H_c - \Delta H_a)} \times 100(\%) \quad (1)$$

where ΔH_s , ΔH_a , and ΔH_c are the heats of fusion for actual, completely amorphous, and completely crystalline formulations, respectively.

6.3.6 *Scanning electron microscopy (SEM)*

Surface morphologies of the drug and drug-silica formulation were studied using field emission scanning electron microscope (JEOL 7000 F). The sample is blown onto adhesive carbon tape on aluminum stub followed by sputter coating of gold.

6.3.7 *Saturation Solubility*

Saturation solubility of fenofibrate was obtained by intense stirring (using wrist action shaker) excess amount of drug in 10 ml of 0.1 N HCl containing 0.3 % (w/v) sodium dodecyl sulfate and 0.2% (w/v) NaCl at 23 °C for 8 hours. Sample was filtered using 200 nm inline syringe filter (PTFE, 17 mm, Alltech) to remove any suspended particles. UV absorbance of sample was measured at 287 nm after appropriate dilution.

6.3.8 *Drug dissolution*

Drug dissolution was carried out by placing sample (equivalent to 7 mg of drug) in 400 ml freshly prepared 0.1 N HCl solution (pH 1.2 ± 0.1) containing 0.3 % (w/v) sodium dodecyl sulfate and 0.2% (w/v) NaCl at 37 °C [26] in a horizontal shaker (Environ Shaker, Lab-line Instruments) at 100 rpm. Although dissolution data obtained using a USP dissolution apparatus (or method) can be easily compared with the data for other formulations in the literature, but the fundamental conclusion on the efficacy of the supercritical fluid technique is still valid with the dissolution method used here. Similar kind of horizontal shaker has been used by Friedrich et al. [7] to study drug dissolution. The ratio of drug saturation concentration to actual drug concentration in dissolution media was 4 (at 23°C) which is more than 3-fold required for maintaining desired sink

condition while conducting dissolution experiments [27]. 2 ml samples were drawn at time interval of 10, 20, 30, 45, 60, 75, and 90 min. Change in volume of solution due to sample withdrawal was considered during concentration determinations. Samples were filtered using 200 nm inline syringe filter (PTFE, 17 mm, Alltech) to remove any suspended particles. Drug concentrations were measured using UV spectroscopy (Spectronic Genesys 2) at 287 nm. The measurements were done in duplicate and averages are reported here.

6.3.9 *Physical Stability*

For stability analysis, a known amount of fenofibrate-silica formulation was kept in a capped glass vial at 40 °C and 75% relative humidity [28]. Desired humidity was maintained using saturated NaCl solution. After 1 month, the samples were tested for drug release and crystallinity.

6.4 Result and Discussion

6.4.1 *Loading of drug onto silica*

Loading of fenofibrate onto silica was carried out at two temperatures: 40 and 50 °C. The loading of 27.5 wt.% drugs onto silica (formulation *A*) was obtained at 2550 psig and 40°C (CO₂ density, 0.82 g/ml) while drug loading of 25 wt.% (formulation *B*) was obtained at 2550 psig and 50 °C (CO₂ density, 0.75 g/ml). The variation in the drug loading was achieved from the phenomenon that the drug solubility in supercritical density depends upon the CO₂ density.

6.4.2 *Infrared spectroscopy*

State of drug molecule onto surface of silica was determined using FT-IR. Figure 6.2 shows IR spectra of physical mixture of fenofibrate and silica and fenofibrate adsorbed onto silica. Characteristic intensity peaks for fenofibrate and silica have been reported by Lin-Vein et al. [29]. IR-spectra of physical and loaded mixtures are exactly the same, and there is no shift of peaks after adsorption of drug onto silica surface; indicating that there is no change in chemical structure of drug after loading onto silica. Specific fenofibrate peaks are observed at 2990, 1740, 1660, and 1600 cm^{-1} both in physical mixture of silica and fenofibrate and silica-fenofibrate formulation.

6.4.3 *Crystallinity*

Figure 6.3 shows the XRD patterns for silica, fenofibrate and silica-fenofibrate formulation. Fenofibrate crystals show various diffraction peaks due to its crystalline structure. However, silica does not show any peak due to its amorphous nature. Figure 6.3b shows a loss of drug crystallinity for formulation *A* due to drug loading onto silica surface. In formulation *B*, a few less intense and wide diffraction peaks of fenofibrate are observed, which can be attributed to the adsorption process in which some of amorphous drug may have crystallized due to higher temperature (50 °C). In fact, Zhou et al., [30] reported that at temperature higher than 40 °C [i.e., above $(T_c - T_g)/(T_m - T_g)$ value of 0.6, where, T_c is crystallization temperature (40 °C), T_g is glass transition temperature (-20 °C), and T_m is melting point (80.5°C)], the molecular mobility of fenofibrate becomes exponentially high, resulting in a high probability of spontaneous crystallization.

6.4.4 DSC study

DSC thermographs for fenofibrate, physical mixture (0.72:0.28 (w/w)) of silica and fenofibrate, and fenofibrate-silica formulation were obtained. The corresponding melting point depressions, enthalpy of fusion, and degree of crystallinity are shown in Table 6.1. A depression in melting point of fenofibrate was found for physical mixture with silica, which indicates an interaction of silica with similar to observations by Wang et al. [31] and Medieh et al. [24]. Decrease in melting point depression for formulations *A* and *B* upon storage is due to increase in crystallinity of formulation. The DSC thermograph for fenofibrate-silica formulation *A* shows only endothermic peak; the absence of exothermic recrystallization peak may be attributed to interaction between silica and drug, similar to observations of Vogt et al. [18]. Based on XRD data, formulation *A* was assumed to be completely amorphous and its enthalpy data was used for calculation of degree of crystallinity.

For formulation *B*, the degree of crystallinity was found to increase from 4% to 21% upon storage. While in the case of formulation *A*, decrease in enthalpy of fusion upon storage could not be explained. For physical mixture, crystallinity cannot be accurately determined as it is difficult to have a homogenous sample of 4 mg which was used for DSC analysis. Though, Wang et al. [31] have observed that the crystallinity decreases after physically mixing with silica.

6.4.5 Morphology

Figure 6.4 a&b shows the spongy structure of silica-fenofibrate formulation without any crystals of fenofibrate due to the agglomeration of silica nanoparticles. Since

fenofibrate is adsorbed on to surface of silica, there is no change in morphological structure of silica.

6.4.6 *Saturation solubility*

In this study, solubility of fenofibrate was found to be ~ 70 $\mu\text{g/ml}$ as compared to literature value of ~ 92 $\mu\text{g/ml}$ [32].

6.4.7 *Dissolution*

Figure 6.5 shows the dissolution profile for fenofibrate (crystalline, micronized) and for both the fenofibrate-silica formulations. Dissolution of fenofibrate adsorbed onto silica (fenofibrate-silica formulation) was substantially higher ($\sim 80\%$ drug release in 20 minutes) than that of micronized fenofibrate ($\sim 18\%$ drug release in 20 minutes). Drug dissolution of 90% was obtained in 30 min for drug-silica formulation, whereas complete (100%) dissolution of fenofibrate was observed within 24 h. The high dissolution rate of fenofibrate-silica formulation can be attributed to an increase in the surface area of fenofibrate after adsorption onto silica, and a good wetting due to the hydrophilic nature of silica. In general, the amorphous structure of hydrophobic compound has higher dissolution rate than the crystalline compound, in aqueous media [33,34]. Dissolution profiles for formulation *A* and formulation *B* are almost similar even though fenofibrate-silica formulation obtained at 50 °C (formulation *B*) shows some degree of crystallinity as shown in Figure 6.3c due to the formation of nanocrystals from amorphous drug at loading conditions of 50°C. Fraction drug release (F) versus time (t) data was fitted to three different dissolution models: (1) Higuchi [$F = k_h t^{0.5}$], (2) Korsmeyer-Peppas [$F =$

$k_p t^n$], and (3) Hixson-Crowell cube root [$F = 1 - (1 - k_b t)^3$] [35]. The model constants obtained from release profiles data are given in Table 6.2. The Korsmeyer-Peppas and Hixson-Crowell models accurately correlate the dissolution of fenofibrate. A value of $n=0.765$ for the Korsmeyer-Peppas model indicates anomalous transport of drug (i.e., non-fickian mass transfer) in pure drug dissolution. Korsmeyer-Peppas model is applicable to initial 60% release of drug; therefore, dissolution constants for silica-fenofibrate formulation were not obtained due to absence of more readings for drug release between 0 to 60%. Good fit for dissolution rate of fenofibrate-silica formulation could not be obtained with aforementioned dissolution models, indicating the deviation from the models.

6.4.8 *Physical stability*

High-energy, amorphous form of drugs may be unstable during storage due to a high tendency to transform into a more stable crystalline form having lower energy [36,37]. Fenofibrate has a low glass transition temperature of $-20\text{ }^\circ\text{C}$; therefore, it will have a high tendency (due to a high molecular mobility) to crystallize at ambient storage conditions, which can reduce the dissolution rate. However, specific fenofibrate-silica H-bonding interaction can prevent the crystallization of drug during storage conditions. Figure 6.5 shows the dissolution profiles for the fenofibrate-silica formulations stored for 1 month at $40\text{ }^\circ\text{C}$ and 75% relative humidity. During the storage, a significant decrease in the dissolution rate of formulation A (Figure 6.5, only ~50% drug release in 20 minutes) is observed due to crystallization of amorphous fenofibrate (Figure 6.3d; sharp crystalline fenofibrate peaks are observed.). Melting point data from DSC thermograph (Table 6.1)

also shows increase in melting temperature for formulation *A* after 1 month storage as compared to initial amorphous formulation. Upon crystallization during storage, drug particles may have grown in size due to multilayer adsorption of drug onto surface of silica, which results in a decrease in surface area. According to Noyes-Whitney equation, dissolution rate is proportional to surface area (with rest of parameters being constant). Using density of fenofibrate as ~ 0.9 g/ml, the thickness of drug molecule layer can be calculated from wt. % drug loading, surface area of silica, and an approximate width of a single fenofibrate molecule as 5 \AA [38,19]. The thickness of drug layer was calculated as 12.5 \AA for formulation *A* and 11.3 \AA for formulation *B*, indicating that formulation *B* has less number of drug molecules available for growth during storage than for formulation *A*. Growth of drug molecules can be confirmed by comparing DSC thermograph (melting temperature, Table 6.1) for both the formulations after 1 month storage. For formulation *B*, dissolution rate was only slightly changed due to increase in crystallinity upon storage ($\sim 68\%$ drug release in 20 min, and $\sim 95\%$ drug release in 90 min), which is consistent with no substantial differences between the X-ray diffraction patterns (Figure 6.3c and 3e). Hence, fenofibrate-silica formulation *B* is more stable than formulation *A*, which may be due to the fact that formulation *B* already has some crystallinity upon production.

6.5 Conclusions

Adsorption of fenofibrate on high-surface-area silica significantly increases the drug dissolution rate. In addition, the adsorption of fenofibrate from supercritical carbon dioxide does not leave any residual solvent in the final formulation. Amorphous drug-silica formulation obtained using CO_2 at 2550 psig and $40 \text{ }^\circ\text{C}$ is found to be unstable

during storage due to crystallization. On the other hand, slightly crystalline drug-silica formulation obtained using CO₂ at 2550 psig and 50 °C is found to be stable during storage.

6.6 Acknowledgments

Financial support from National Science Foundation through NIRT grant DMI-0506722 and experimental assistance from Andrew Scott (a NSF REU student for site 0552557) are highly appreciated.

6.7 References

- [1] G. L. Amidon, H. Lennernas, V. P. Shah, J. R. Crison. A theoretical basis for a biopharmaceutical drug classification: the correlation of in vitro drug product dissolution and in vivo bioavailability. *Pharm Res.* 12 (1995) 413-20.
- [2] G. G. Liversidge, K. C. Cundy. Particle size reduction for improvement of oral bioavailability of hydrophobic drugs: absolute oral bioavailability of nanocrystalline danazol in beagle dogs. *Int J Pharm.* 125 (1995) 91-7.
- [3] A. Jounela, P. Pentikainen, A. Sothmann. Effect of particle size on the bioavailability of digoxin. *Eur J Clin Pharmacol.* 8 (1975) 365-70.
- [4] N. Rasenack, B. W. Muller. Dissolution rate enhancement by in situ micronization of poorly water-soluble drugs. *Pharm Res.* 19 (2002) 1894-900.
- [5] P. Finholt, S. Slovang. Dissolution kinetics of drugs in human gastric juice the role of surface tension. *J Pharm Sci.* 57 (1968) 1322-6.
- [6] A. J. Aguiar, A. W. Zelmer, A. W. Kinkel. Deaggregation behavior of a relatively insoluble substituted benzoic acid and its sodium salt. *J Pharm Sci.* 56 (1967) 1243-52.
- [7] H. Friedrich, B. Fussnegger, K. Kolter, R. Bodmeier. Dissolution rate improvement of poorly water soluble drugs obtained by adsorbing solutions of drugs in solvents onto high surface area carriers. *Eur J Pharm Biopharm.* 62 (2006) 171-7.
- [8] C. Charnay, S. Begu, C. Tourne-Peteilh, L. Nicole, D. A. Lerner, J. M. Devoisselle. Inclusion of ibuprofen in mesoporous templated silica: drug loading and release property. *Eur J Pharm Biopharm.* 57 (2004) 533-40.
- [9] T. Heikkila, J. Salonen, J. Tuura, M. S. Hamdy, G. Mul, N. Kumar, et al.

Mesoporous silica material TUD-1 as drug delivery system. *Int J Pharm* (Kidlington). 331 (2007) 133-8.

[10] D. C. Monkhouse, J. L. Lach. Use of adsorbents in enhancement of drug dissolution I. *J Pharm Sci.* 6 (1972) 1430-5.

[11] J. W. McGinity, C.-T. Ku, R. Bodmeier, M. R. Harris. Dissolution and uniformity of ordered mixes of micronized griseofulvin and a perfectly compressible excipient. *Drug Dev Ind Pharm.* 11 (1985) 891-900.

[12] I. Smirnova, S. Suttiruengwong, M. Seiler, W. Arlt. Dissolution rate enhancement by adsorption of poorly soluble drugs on silica aerogels. *Pharm Dev Technol.* 94 (2004) 443-52.

[13] R. B. Gupta, J. J. Shim. *Solubility in supercritical carbon dioxide.* New York: Taylor and Francis Group 2007.

[14] Z. Aigner, I. Bencz, M. Kata. Increasing the solubility characteristics of fenofibrate with cyclodextrin. *J Inclusion Phenom.* 20 (1995) 241-52.

[15] A. R. Patel, P. R. Vavia. Effect of polymer on solubilization of fenofibrate by cyclodextrin complexation. *J Inclusion Phenom Macrocyclic Chem.* 56 (2006) 247-51.

[16] M. T. Sheu, C. M. Yeh, T. D. Sokoloski. Characterization and dissolution of fenofibrate solid dispersion systems. *Int J Pharm.* 103 (1994) 137-46.

[17] A. Munoz, J. P. Guichard, P. Reginault. Micronized fenofibrate. *Atherosclerosis.* 110 (Suppl.) (1994) S45-S8.

[18] M. Vogt, K. Kunath, J. B. Dressman. Dissolution enhancement of fenofibrate by micronization, cogrinding and spray-drying: comparison with commercial preparations. *Eur J Pharm Biopharm.* 68 (2008) 283-8.

- [19] D. S. Wishart, C. Konx, A. C. Guo, S. Shrivastava, M. Hassanali, P. Stothard, et al. Drugbank: a comprehensive resource for in silico drug discovery and exploration. *Nucleic Acids Res.* 34 (2006) D668-D72.
- [20] D. C. Monkhouse, J. L. Lach. Use of adsorbents in enhancement of drug dissolution II. *J Pharm Sci.* 6 (1972) 1435-41.
- [21] Cabot Corp. Applications of CAB-O-SIL M-5P fumed silica in formulation and design of solid dosage forms. Available via www.cabot-corp.com (accessed on june 20, 2007)
- [22] Cabot Corp. Functions of CAB-O-SIL fumed silica in pharmaceutical applications. Available via www.cabot-corp.com (accessed on june 20, 2007)
- [23] Cabot Corp. Properties of CAB-O-SIL fumed silica. Available via www.cabot-corp.com (accessed on june 20, 2007).
- [24] S. Madieh, M. Simone, W. Wilson, D. Mehra, L. Augsburger. Investigation of drug-porous adsorbent interactions in drug mixtures with selected porous adsorbents. *J Pharm Sci.* 96 (2007) 851-63.
- [25] M. J. Pikal, A. L. Lukes, J. E. Lang, K. Gaines. Quantative crystallinity determinations for β -lactam antibiotics by solution calorimetry: correlation with stability. *J Pharm Sci.* 67 (1978) 767-73.
- [26] U.S. Department of Health and Human Services Food and Drug administration. administration. Guidance for industry Q1A stability testing of new drug substances and products. Available via <http://www.fda.gov/cder/guidance/index.htm> (accessed on June 20, 2007).

- [27] United States Pharmacopeial Convention, 2005. In Vitro and in Vivo Evaluation of Dosage forms. United States Pharmacopeial Convention Inc., USP 28, Rockville, MD, p.1088.
- [28] U.S. Department of Health and Human Services Food and Drug administration. Guidance for industry. Dissolution testing of immediate release solid oral dosage forms. Available via <http://www.fda.gov/cder/Guidance/1713bp1.pdf> (accessed on June 20, 2007).
- [29] D. Lin-Vien, N. B. Colthup, W. G. Fateley, J. G. Grasselli. The Handbook of Infrared and Raman Characteristic Frequencies of Organic Molecule. San Diego: Academic Press Inc 1991.
- [30] A. Zhou, G. Z. Z. Geoff, D. Law, J. W. G. David, E. A. Schmitt. Physical stability of amorphous pharmaceuticals: importance of configurational thermodynamic quantities and molecular mobility. *J Pharm Sci.* 1 (2002) 1863-72.
- [31] L. Wang, F. D. Cui, H. Sunada. Preparation and evaluation of solid dispersions of nitrendipine prepared with fine silica particles using melt mixing method. *Chem Pharm Bull.* 54 (2006) 37-43.
- [32] S. Jamzad, R. Fassihi. Role of surfactant and pH on dissolution properties of fenofibrate and glipizide-technical note. *AAPS Pharm Sci Tech.* 7 (2006) E1-E6.
- [33] O. I. Corrigan, E. M. Holohan. Amorphous spray-dried hydroflumethiazide-polyvinylpyrrolidone systems: physicochemical properties. *J Pharm Pharmacol.* 36 (1984) 217-21.
- [34] A. Froster, J. Hempenstall, T. Rades. Characterization of glass solutions of poorly water-soluble drugs produced by melt extrusion with amorphous polymers. *J*

Pharm Pharmacol. 53 (2001) 303-15.

[35] P. Costa, J. M. S. Lobo. Modeling and comparison of dissolution profiles. Eur J Pharm Sci. 13 (2001) 123-33.

[36] A. M. Kaushal, P. Gupta, A. K. Bansal. Amorphous drug delivery systems: molecular aspects, design, and performance. Crit Rev Ther Drug Carrier Syst. 21 (2004) 133-93.

[37] B. C. Hancock, G. Zorafi. Characteristics and significance of the amorphous state in pharmaceutical systems. J Pharm Sci. 86 (1997) 1-12.

[38] Jmol: An open-source java viewer for chemical structures in 3D. Available via <http://jmol.sourceforge.net/> (accessed on August 15, 2007).

Table 6.1 Melting point depression, heat of fusion, and degree of crystallinity for fenofibrate and fenofibrate-silica formulations.

Formulation	Melting point depression (°C)	Heat of fusion (J/g)	Degree of crystallinity (%)
Fenofibrate (Micronized, from supplier)	0 ($T_m = 81.27\text{ °C}$)	94.78	100
Fenofibrate-silica (Physical mixture)	0.73	33.70	-----
Formulation <i>A</i>	2.48	10.11	0 (completely amorphous)
Formulation <i>B</i>	2.26	9.83	4.4
Formulation <i>A</i> after 1 month storage	1.83	5.21	-----
Formulation <i>B</i> after 1 month storage	2.19	12.24	21.0

Table 6.2. Dissolution-rate constants from three dissolution models.

Compound	Higuchi		Korsmeyer-Peppas			Hixson-Crowell	
	K_h	R^2	K_{kp}	R^2	N	K_{hc}	R^2
Fenofibrate	0.057	0.934	0.019	0.994	0.765	0.003	0.994
Formulation <i>A</i>	0.13	0.59	----	----	----	0.016	0.79
Formulation <i>B</i>	0.128	0.76	----	----	----	0.016	0.91

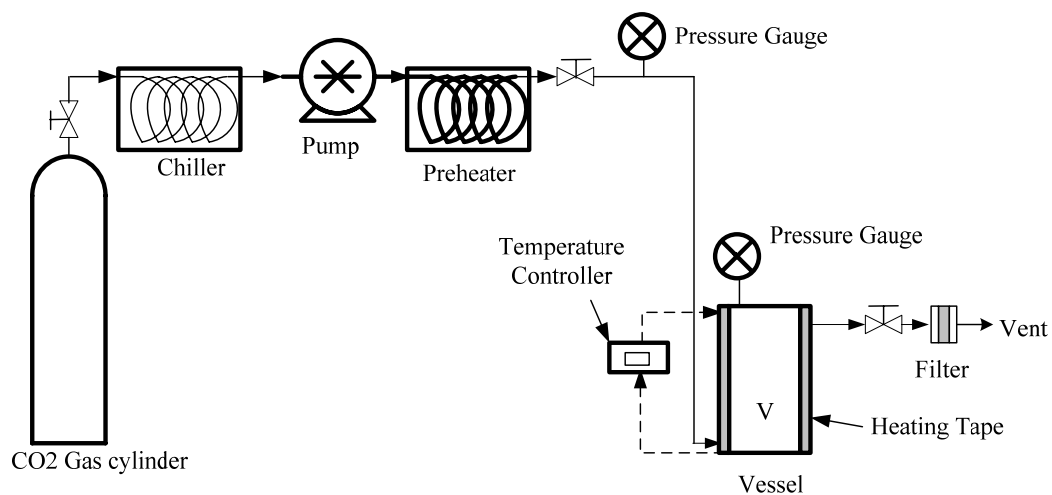


Figure 6.1 Schematic of supercritical CO₂ apparatus for drug adsorption onto silica

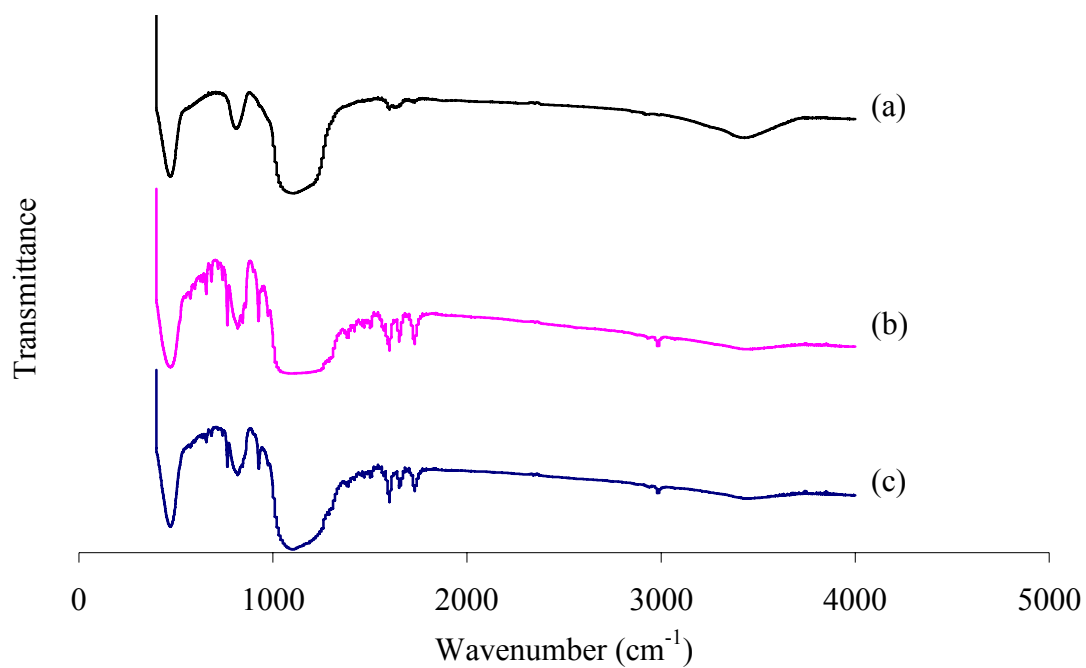


Figure 6.2 FTIR spectra of (a) silica, (b) physical mixture of fenofibrate and silica, and (c) fenofibrate adsorbed onto silica formulation.

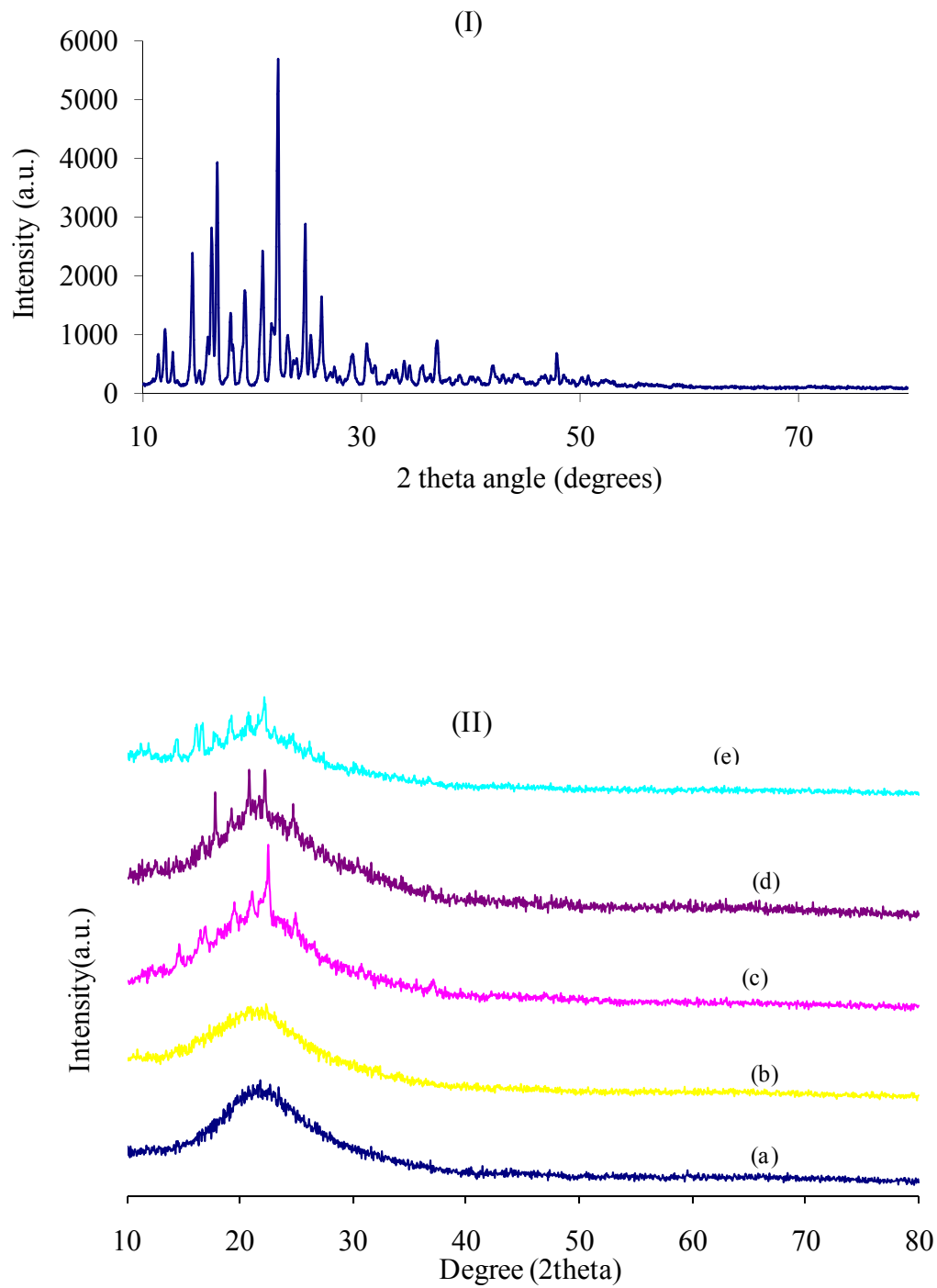
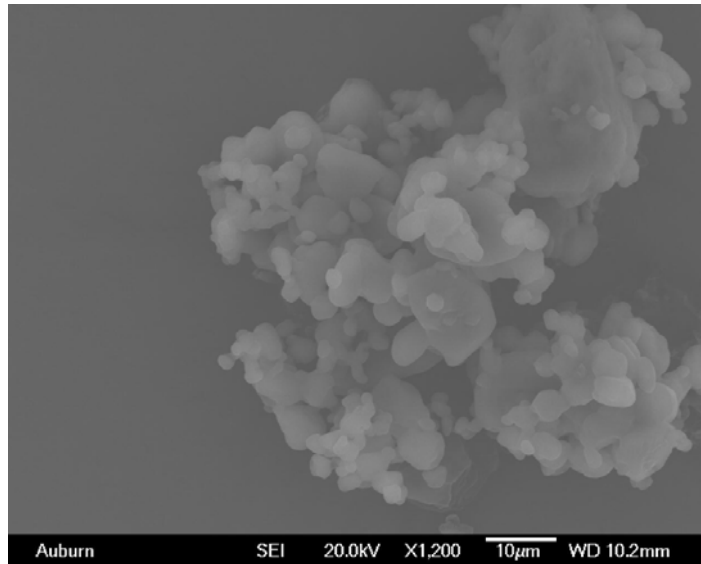
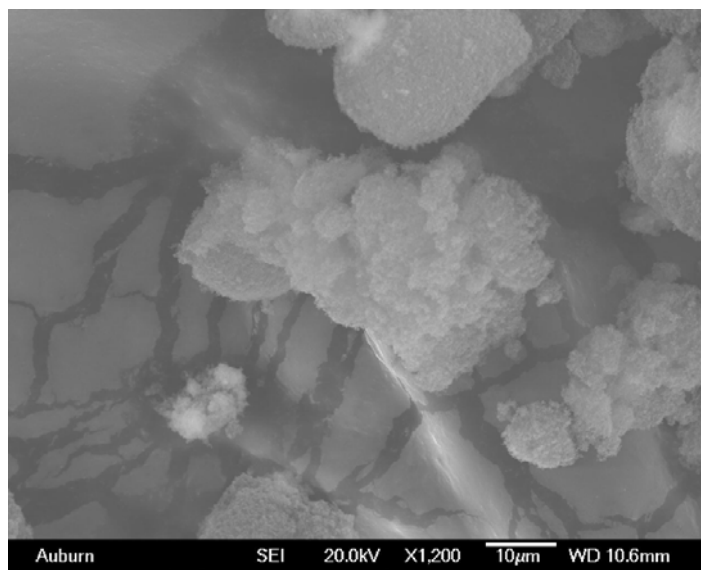


Figure 6.3 XRD of (I) crystalline fenofibrate, and (II) (a) silica, (b) formulation A, (c) formulation B, (d) formulation A after 1 month storage, and (e) formulation B after 1 month storage.



(a)



(b)

Figure 6.4 SEM micrographs of (a) microcrystalline fenofibrate, and (b) fenofibrate adsorbed onto silica.

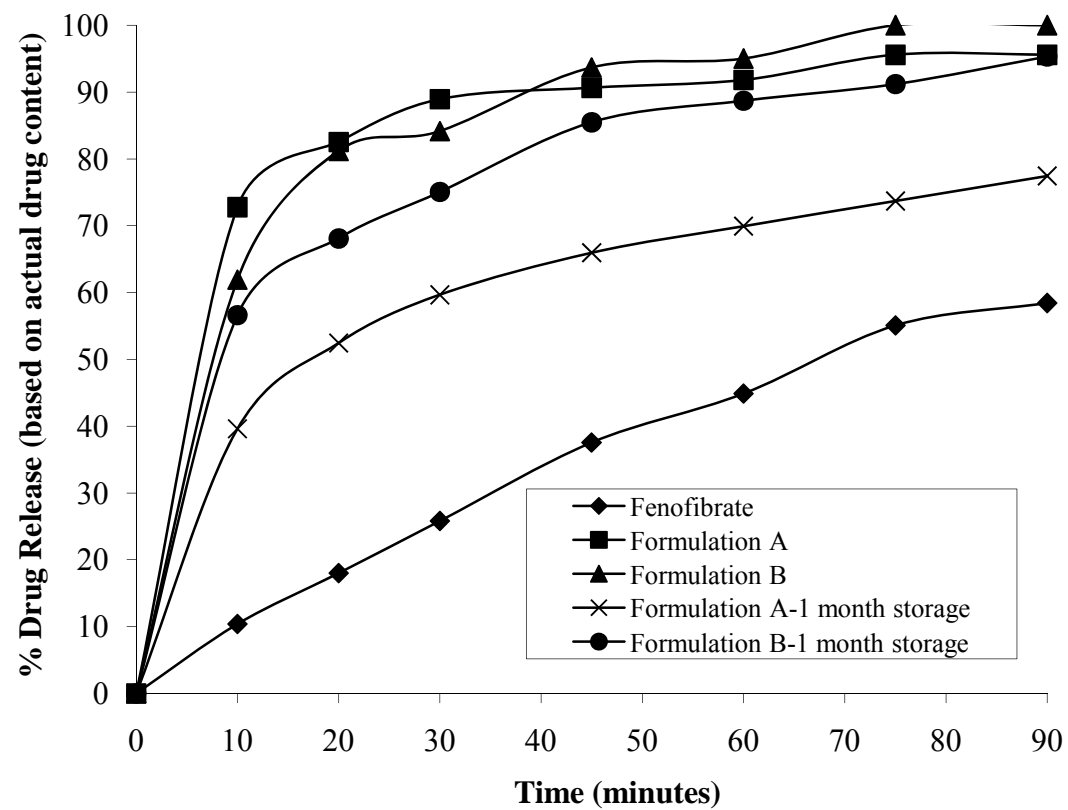


Figure 6.5 Dissolution profiles of fenofibrate and fenofibrate-silica formulations.

7 CONCLUSIONS AND FUTURE WORK

The study has successfully demonstrated the use of carbon dioxide as media for effective deagglomeration and mixing of various nanoparticles. Various types of forces (shear, cavitation, and impact) have been created in high pressure CO₂ media for deagglomeration and mixing of inorganic as well as pharmaceutical active ingredient nano/micro particles. High pressure CO₂ (gaseous, liquid, and supercritical) can be a replacement to liquid solvents which are used in wet mixing methods. Final mixture obtained contains no residual solvent as well as no steps of filtration and drying as compared to conventional wet mixing method. Quality of mixing using high pressure CO₂ found to be as good as or better than wet mixing method. Methods developed in this work can be used for heat sensitive ingredients due to lower operating temperatures. There is less amount of work input required for deagglomeration of particles due to decrease in Vander Waals attraction between particles because of presence of CO₂ media. The developed simultaneous particle formation and mixing method called as supercritical antisolvent with drug excipient mixing (SAS-DEM) combines two steps thus saving on processing cost. The applicability of SAS-DEM method has been successfully confirmed by obtaining highly homogenous mixture with significant increase in the drug dissolution rate. The whole dissertation work has proved the importance of nanomixing by showing enhancement of properties of nanomixed mixture.

Following are the suggestions for further demonstration of importance of nanomixing concept:

1. *Simultaneous particle formation and mixing using supercritical antisolvent method*

The above method's applicability has been shown successfully for the preparation of fast release nevirapine drug formulation. There is need for more study on how different shape and size of drug particles affects mixing as well homogeneity of the final mixture. It is difficult to deagglomerate and mix rectangular to flaky particles due to high cohesion and mechanical interlocking in particle agglomerates. SAS-DEM method can handle such particle shapes easily as particles get mixed with excipient particles as soon as they get formed. Another interesting parameter that needs to be studied is the effect of excipient size particles on the formation of drug particles. There is a possibility of decreasing drug particle size with presence of smaller excipient particle size.

2. *Stirred mixing in liquid CO₂*

Preliminary calculation (Hamaker Constant) has shown that there is significant decrease (up to 60 times in case of lactose particles) in Vander Waals attractive force between particles due to presence of liquid CO₂ media as compared to in the air (Table 7.1). Liquid CO₂ (depending on temperature and pressure) has density and Hamaker constant comparable to n-hexane. Therefore it is required to have less input of work in order to deagglomerate and mix the particles. Preliminary work involving stirred mixing in liquid CO₂ for various size and shape of drug and excipient has shown effectiveness of the proposed method. Therefore it will

be interesting to investigate this method in more detail.

Table 7.1 Hamaker constants for solids, fluids and solid-fluid interactions.

Solid	Hamaker Constant (J)	Air (approx. to nitrogen)	Liquid Nitrogen (at -196 °C)	Liquid CO ₂ (at 100 bar and 10 °C)	n-hexane	Water
		$\sim 10^{-25}$	$\sim 10^{-20}$	1.9×10^{-20}	2.4×10^{-20}	$\sim 10^{-19}$
Lactose	7.2×10^{-20}	7.18×10^{-20}	2.83×10^{-20}	1.08×10^{-21}	1.29×10^{-20}	2.29×10^{-21}
Silica	5×10^{-19}	4.99×10^{-19}	3.69×10^{-19}	2.22×10^{-19}	3.05×10^{-19}	1.53×10^{-20}

APPENDIX A: AGGLOMERATES AND AGGREGATES

A.1 Introduction and Definitions

Agglomerates and aggregates are the term commonly used in powder and particle characterization. There is confusion among various authors in the literature regarding the definition of agglomerates and aggregates. However, here in this dissertation, we are using the definitions suggested by Nichols et al. [1] for characterization of nanopowders. A group of particles that is loosely bound with particles, which are loosely attached by contact at their corners and edges, are called soft agglomerate (also referred as agglomerate unless otherwise specified in this dissertation work). A group of particles that is rigidly bound with particles, which are firmly attached at their faces by fusion, sintering or growth, are called hard agglomerate (also referred as aggregate in this dissertation work). Soft agglomerates are easily dispersible as opposed to hard agglomerates. Formation of soft agglomerates is preferred in the nanoparticles synthesis because of ease of dispersion. Hard agglomerates cannot be dispersed to individual primary particle size level, but only be milled for smaller size requirement [1].

Nanopowders are made up of agglomerates. These agglomerates are in the typical size range of 100-500 microns having high porosity ($\epsilon=0.99$). These agglomerates are made up of further sub agglomerates in size range of 10-50 microns. Furthermore, these sub agglomerates are made up of primary agglomerates of 1-4 microns. Primary agglomerates are made up of chains of nanoparticles (hard agglomerates of primary

nanoparticles with an average size of 0.2-0.4 microns) or nets of individual nanoparticles. Figure A.1 shows a cartoon representing agglomerates, sub agglomerates, and primary agglomerates [2]. Figure A.2 shows sub agglomerates and a chain of silica nanoparticles.

A.2 References

- [1] G. Nichols, S. Byard, M. J. Bloxham, J. Botterill, N. J. Dawson, A. Dennis, et al. A review of the terms agglomerate and aggregate with a recommendation for nomenclature used in powder and particle characterization. *J Pharm Sci.* 91 (2002) 2103-9.
- [2] R. Dave, R. Pfeffer, S. Sundaresan, R. Gupta. NIRT: Environmentally benign mixing of nanoparticles. Project Description. (2005).

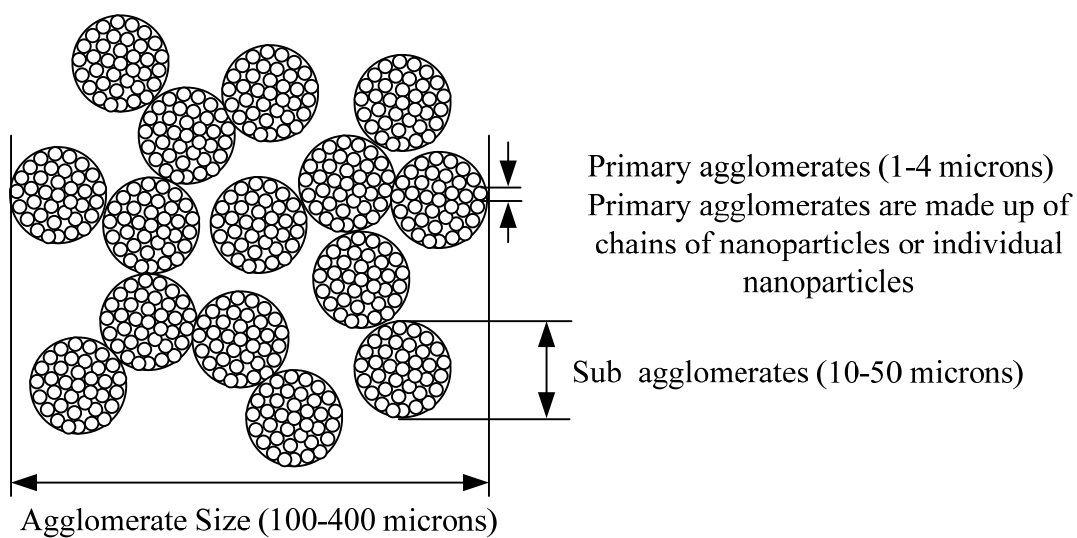


Figure A.1 Cartoon showing agglomerate, sub agglomerates, and primary agglomerates [2].

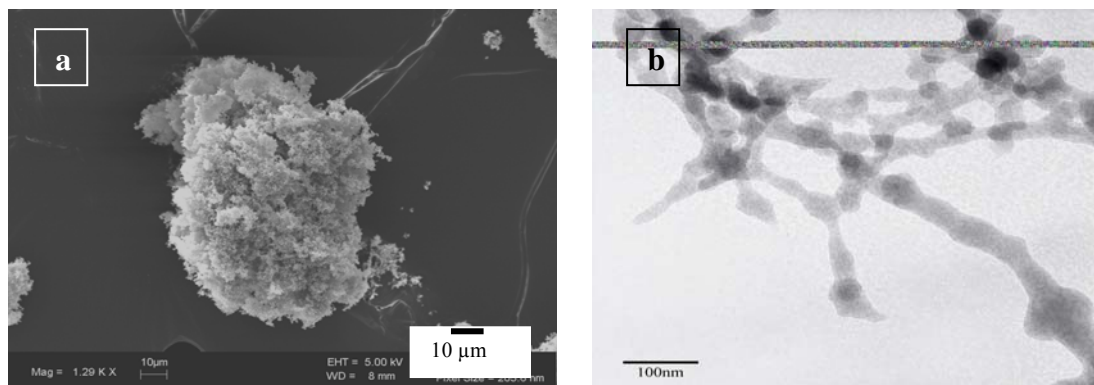


Figure A.2 Images of silica (a) sub agglomerates and (b) chain of nanoparticles.

APPENDIX B: FORCES AMONG NANOPARTICLES

B.1 Van der Waals Forces

When the particle size gets smaller, attractive forces like capillary, electrostatic, and van der Waals forces (proportional to particle diameter) become dominant as compared to gravitational forces (proportional to cube of particle diameter). If we assume the absence of charge on particles as well as the absence of capillary forces which is mostly true for hydrophobic organic compounds (poorly water soluble drugs), then van der Waals forces will be solely responsible for cohesiveness of the powder having particle size less than 30 μm [1].

Figure B.1a shows a cartoon representation of particles (host) with diameter d separated by distance h (usually 4 nm) whose van der Waals attractive force is given by [2]

$$F_{vdW} = \frac{A}{12} \times \frac{d_{host}}{2h^2} \quad (1)$$

where, A is the Hamaker constant. With the presence of another material particle called guest or spacer particle, the effect of guest particle on attractive force between host particles (Figure B.1b) is given by [2]

$$F_{vdW} = \underbrace{\frac{A}{12} \times \frac{d_{host} d_{guest}}{(d_{host} + d_{guest}) h^2}}_X + \underbrace{\frac{A}{12} \times \frac{d_{host}}{2(2h + d_{guest})^2}}_Y \quad (2)$$

where, d_{host} is the diameter of host particle, d_{guest} is the diameter of guest particle, A is the

Hamaker constant, and h is separation distance between particles. The overall attractive force between the system consisting of host and guest particle as seen in Figure B.1b is the summation of an attractive force between the host-guest (term X in the equation) and host-host (term Y in equation). The ratio of attractive force with spacer (guest particle) to attractive force without spacer reaches a minimum for a guest particle size around 0.01 micron on a host particle size of 1-10 micron [2]. Therefore silica particles of size 10-30 nm are used to coat 1-100 micron size particles for reduction in attractive force which results into better flowability of micron size particles. Increasing in guest particle size increases the ratio of attractive force (with spacer to without spacer) and leads to the agglomeration of host and guest particles (Figure B.2).

B.1 References

- [1] I. Zimmermann, K. Meyer. Effects of glidant in binary powder mixtures. Powder Technol. 139 (2004) 40-54.
- [2] M. Linsenbuhler, K.-E. Wirth. An innovative dry powder coating process in non-polar liquids producing tailor-made micro-particles. Powder Technol. 158 (2005) 3-20.

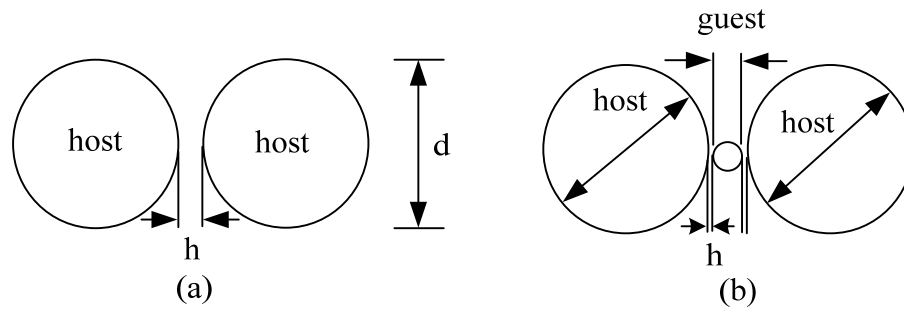


Figure B.1 Cartoon representing (a) host particle of diameter “d” separated by distance “h” and (b) host particles separated by guest particle.

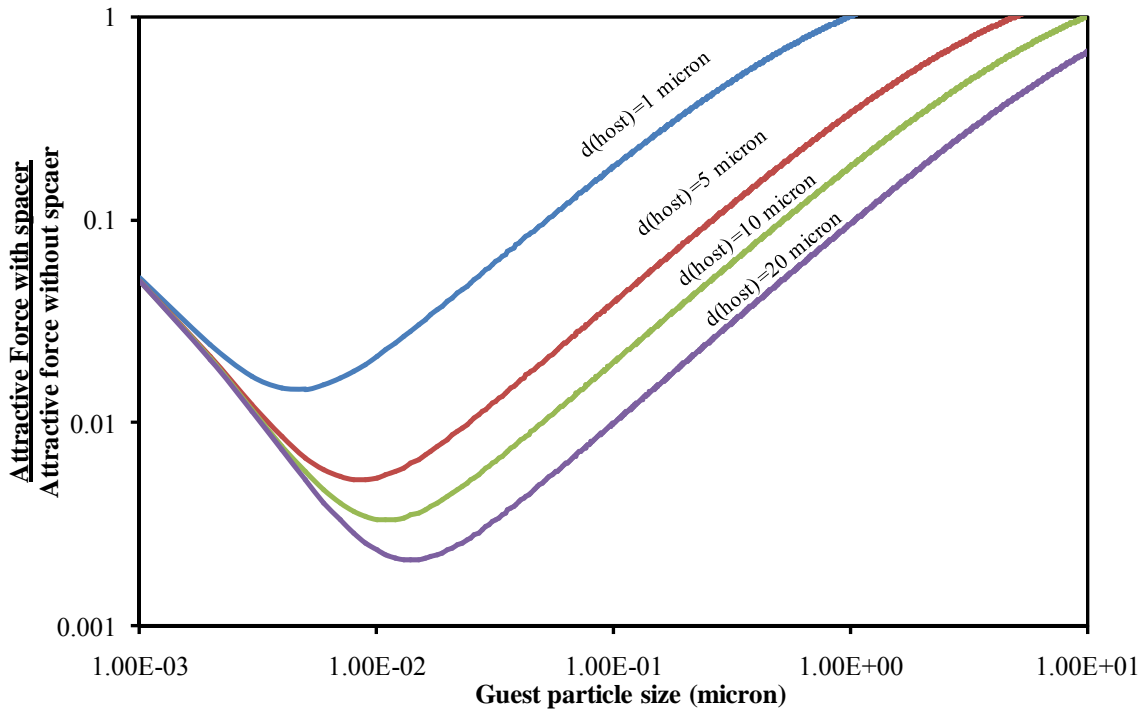


Figure B.2 Effect of guest particle on ratio of attractive force with spacer and without spacer for various host particle size.

APPENDIX C: POWDER MIXING

C.1 Introduction

In this section, the conventional type of dry mixing has been discussed using discussion on the following topics: definitions of mixture types, characterization of mixtures, mixing mechanisms, and various types of mixers used in the industry.

C.2 Definitions

Figure C.1 shows cartoon representing different types of terms used in defining various mixtures and their homogeneity (is discussed in “mixing characterization”) which are influenced by gravitational and surface forces. There are two main types of mixing: (a) ordered and (b) random [1]. Ordered mixing is considered interactive where finer particles adhere to the coarse particles of other constituent materials [2]. Ordered mixing does not require equal size particles but does require particle interactions of any forms of adhesion. Ordered mixing is further divided into perfect, imperfect, and pseudo- random. Figure C.1 shows the arrangement of particles. Random mixing as defined by Staniforth [3] is a statistical process in which a bed of particles is repeatedly split and recombined until there is an equal chance of any individual particle being at any given point in mix at any one time. Random mixing is also further divided into ideal, random, and non random as of shown in Figure C.1.

C.3 Mixing mechanisms

Powder mixing is obtained by three various mechanisms of mixing: (a) mixing by convection, (b) mixing by diffusion, and (c) shear mixing [2]. Convection mixing involves the movement of groups of particles to another which results in contact between different components or circulation pattern developed in powder mix. Diffusion mixing is due to movement of each individual particle to each other or particles roll over each other on sloping surface. Shear mixing is slipping of particle planes in the mixture volume. During the process of mixing, opposing phenomenon called segregation also takes place. Mixing of powders is affected by segregation, which is dependent on the particle density (e.g. bulk or aerated density, tapped density), shape (e.g. needle shaped (acicular), roughly polyhedral (angular), irregular thread like (fibrous), equidimensional irregular shape (granular), global shape (spherical)), size/ratio, surface properties, intensity of cohesion, flowability, and angle of repose. Segregation of pharmaceutical powder is result of three mechanisms: (a) fluidization where fine particles remain fluidized near the top surface, (b) sifting (also called as percolation) where fine particles move through a matrix of coarse ones, and (c) dusting (trajectory segregation) where fine airborne particles settle in regions within the bin [2,4].

C.4 Characterization of mixture

Homogeneity of pharmaceutical mixtures is important due to the requirement of drug content in a mixture to lie within 90 % and 110 % of stated amount by the United States Pharmacopeia. A mixture considered being homogenous, if samples taken from mixture have similar composition and properties as each other. The homogeneity of

samples depends on the size of sample; a large enough sample will be homogenous. Size (or volume) of the sample depends on particle size. In the case of pharmaceutical drug mixtures, the sample size is equal to the unit dose containing desired drug content. There are various mixing indices for determining the quality of mix that have suggested by various authors for free flowing powder [2]. Relative standard deviation has been mostly used for determining the homogeneity of a pharmaceutical mix. The definition of relative standard deviation is given as

$$RSD = \frac{\sigma}{\bar{X}} \quad (1)$$

$$\sigma = \sqrt{\frac{\sum_{i=1}^n (\bar{X} - X_i)^2}{n-1}} \quad (2)$$

where n is the total number of samples, σ is the concentration variance, \bar{X} is the mean concentration determined experimentally, and X_i is the sample concentration. Concentration or content variation (σ) is the sum of variance due to variation in weight of sample, variance due to analytical errors, and variance due to mixing. The total number of samples required is given [5].

$$n = 1 + \left[\frac{ts}{\Delta d} \right] \quad (3)$$

where n is total number of samples, t is confidence level ($t=2$ for 95 % confidence, $t=3$ for 99.9% confidence), s is the sample standard deviation (e.g. $s= 0.5 \mu\text{m}$), and Δd is maximum allowable difference between estimate and actual value of particle diameter (e.g. $\Delta d = 0.5 \mu\text{m}$). The minimum sample size (mass of sample) depended on the particle size distribution of coarse particles. The limiting weight of sample required is given by

[6].

$$m_s = 5 \times 10^{-7} d^3 \left[\frac{\rho}{\sigma^2} \right] \left[\frac{1}{w_c} - 2 \right] \quad (4)$$

where m_s (mg) is the limiting weight of the sample, d (μm) is the mean diameter of coarsest particles in the sample, ρ (g/cm^3) is powder density, σ is the total accepted sampling error, and w_c is the fractional mass of the coarsest class being sampled.

Danckwerts [7] has proposed two concepts for determining the quality of mixture. He has proposed the scale of segregation and intensity of segregation. The scale of segregation can be explained as [8].

$$SS \text{ (Scale of Segregation)} = \int_0^{\varepsilon} R(r) dr \quad (5)$$

$$R(r) = \frac{(x' - \bar{x})(x'' - \bar{x})}{(x - \bar{x})^2}(r) = \frac{1}{Ns^2} \sum_{i=1}^N (x' - \bar{x})(x'' - \bar{x})(r) \quad (6)$$

$$s^2 = \frac{1}{n-1} \sum_{i=1}^n (x_i - \bar{x})^2 \quad (7)$$

$$\bar{x} = \frac{1}{n} \sum_{i=1}^n x_i \quad (8)$$

Where SS is the scale of segregation (Figure C.2), $R(r)$ is coefficient of correlation, ε is the distance at which $R(r)$ becomes zero, x' and x'' are the concentration at two points (samples) in the mixture separated by distance r . \bar{x} is the mean concentration of whole mixture, N is number of sample pair in the eq.6, while n is the number of samples taken in eq.8, and s^2 is the variance. The value of $R(r)$ lies between 0 and 1. The values ($R(r)$) close to 1 are found for small values of r in an imperfect mixture. For values of $R(r) = 0$,

there is a random relation between concentrations at points distant r apart. Convective type of mixing reduces the scale of segregation.

As a measure of degree of mixing, the intensity of segregation parameter, is given as [7]

$$I = \frac{\sigma^2}{ab} \quad (9)$$

$$\sigma^2 = \frac{\sum_{i=1}^N (a_i - \bar{a})^2}{N-1} = \frac{\sum_{i=1}^N (b_i - \bar{b})^2}{N-1} \quad (10)$$

$$a + b = 1 \quad (11)$$

where a and b is the weight concentrations components, N is number of samples in the mixture, \bar{a} and \bar{b} are the average concentrations, and σ^2 is the variance. Intensity of segregation is a variance of concentrations in a mixture normalized by the variance in completely segregated, unmixed powders. Thus, in the case of complete segregation of two components, the index of segregation is 1. The index of segregation for a perfect random mixture would be close, and at the current level of scrutiny for all practical purposes can be taken as equal, to 0. Therefore, the index of segregation shows how good the mixture is, and can vary in the range from 0 (complete uniform mixture) to 1 (completely unmixed components).

C.5 Mixers ^[9]

Powder mixers are generally categorized based on the type of mixing mechanism taking place. Mixers that reply on diffusive or shear action are called segregating mixers. Tumbler, V- and Y- cone mixers are the most common mixers in the pharmaceutical

industry are based on diffusive or shear mixing in which mixers rotate along the horizontal axis. Segregating mixers are not effective if breakage of fine particle agglomerates is required and they cannot be used for segregating powders (difference in size and density of particles). Mixers that rely on convective action are called non-segregating mixers. The Ribbon blender and Nauta mixer are common examples of non-segregating mixers. These mixers are good for segregating mixtures and can rapidly produce a better random mix. Mixing of cohesive powders requires mixers with baffles or intensifier bar for breakage of agglomerates as well as high shearing action. Mixing of cohesive powders in conventional blenders depends on several parameters such as initial loading pattern, percentage fill level, component concentration, mixing time, blender geometry, use of preblending, and presence of baffles or intensifier bar. Continuous and fluidized bed mixers are also available. The selection of mixers is mostly based on the type of powders to be mixed, the mixture homogeneity requirement, the ease of cleaning and removing the mixture after mixing operation, the operation and maintenance, the power requirement, and the capital cost.

C.1 References

- [1] L. T. Fan, Y.-m. Chen. Recent development in solids mixing. Powder Technol. 61 (1990) 255-87.
- [2] M. Poux, P. Fayolle, J. Bertrand. Powder mixing: Some practical rules applied to agitated systems. Powder Technol. 68 (1991) 213-34.
- [3] J. N. Staniforth. Advances in powder mixing and segregation in relation to pharmaceutical processing. Int J Pharm Technol and Product Manufacture 3(1982) 1-12.

- [4] E. Maynard. Blender selection and avoidance of post-blender segregation. *Chemical Engineering*. May (2008) 67-72.
- [5] R. Davis. In: Grayson IM, ed. *Kirk-Othmer Encyclopedia of Chemical Technology*. 3 rd ed: John Wiley 1982:528.
- [6] B. Y. Shekunov, P. Chattopadhyay, H. H. Y. Tong, A. H. L. Chow. Particle size analysis in pharmaceuticals: principles, methods and applications. *Pharm Res*. 24 (2007) 203-27.
- [7] P. W. Danckwerts. The definition and measurement of some characteristics of mixtures. *Appl Sci Res*. A3 (1952) 279-96.
- [8] K. Ridgway. Mixing mechanisms in particulate systems (quarterly reviews: aspects of pharmaceutical engineering). *Pharmaceutical Journal*. (1972) 271-4.
- [9] H. J. Venables, J. I. Wells. Powder Mixing. *Drug Dev Ind Pharm*. 27 (2001) 599-612.

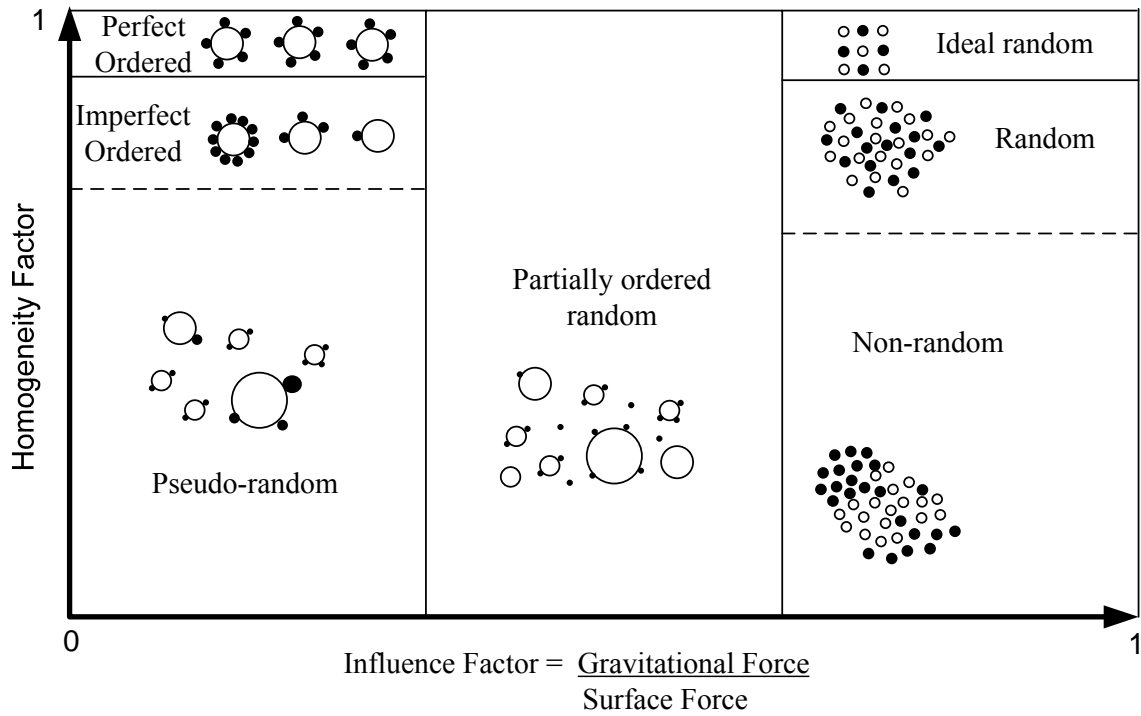


Figure C.1 Different type of mixing with their homogeneity factor dependent on influence of gravitational and surface forces [1].

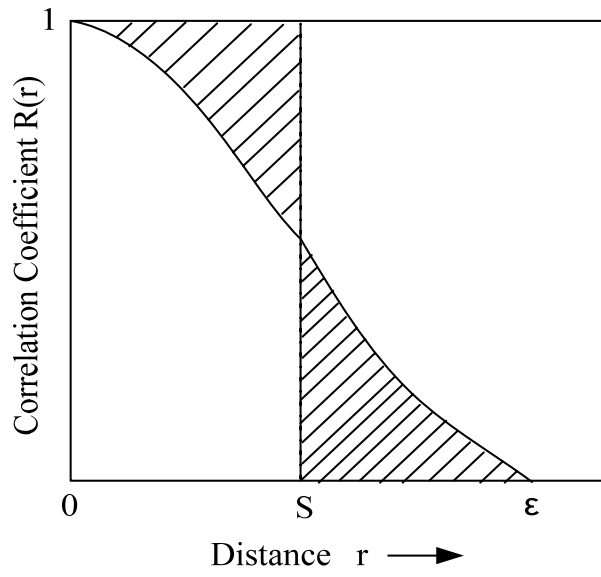


Figure C.2 Scale of Segregation [8].

Table C.1 Various types of blenders and their properties [4].

Blender Type	Range of materials	Handle cohesive materials	Handle segregating materials	Blending time	Easy to clean	Lump Breaking	Jacket Vessel	Ability to add liquid	Potential dead spots	Power Required
Ribbon, plow	Wide	Yes	Yes	Moderate	Moderate	Good	Yes	Yes	Likely	High
Tumble	Moderate	Moderately	Moderately	Long	Yes	Poor	Difficult	Difficult	Possible	Moderate
In-bin tumbler	Moderate	Moderately	Yes	Long	Yes	Poor	Difficult	Difficult	Possible	Moderate
Fluidized	Narrow	No	No	Fast	Yes	Poor	Yes	Yes	Possible	Low
High shear	Moderate	Yes	Moderately	Fast	Moderate	Excellent	Yes	Yes	Unlikely	High

APPENDIX D: EXCIPIENTS

D.1 Introduction

Various types of excipients are used in formulations of solid dosage forms. Table D.1 shows detailed information on various excipients with their use and typical amount in solid dosage unit [1].

D.1 References

[1] K. Y. Fung, K. M. Ng. Product-centered processing: pharmaceutical tablets and capsules. *AIChE J.* 49 (2003) 1193-215.

Table D.1 Type of excipients used in tablets, capsules and powders [1].

Excipient	Desired Function	Typical Examples	Typical Amount (%)
Diluent/Filler (Tablet, Hard gelatin capsule, Powder)	Make up tablet size, capsule size or the required dosage	Microcrystalline Cellulose	20-90
		Calcium sulfate dehydrate	----
		Sucrose	----
		Lactose	65-85
Binder (Tablet, Hard gelatin capsule, Powder)	Increase cohesiveness of powder and hold them together to form granules	Starch	5-75
		Sucrose (Solvent:Water)	2-25
		Microcrystalline Cellulose	5-20
		Pregelatinized starch (Solvent:Water)	2-5
		(Dry addition)	5-10
		Povidone (Solvent:Water or Water-alcohol solution)	2-5
Alginic acid (Solvent:Water)	5-10 (water insoluble)		
Filler-Binder (Tablet)	Used in direct compression	Spray dried lactose	>80
		Starch 1500	----
		Microcrystalline Cellulose	10-25
Disintegrant (Tablet, Hard gelatin capsule,	To facilitate the breakup of tablet or granule	Starch	5-20
		Microcrystalline cellulose	5-15
		Cross-linked povidone	0.5-5

Powder)		Alginic acid	5-10
Lubricant (Tablet, Hard gelatin capsule, Powder)	Reduce friction during tablet ejection or facilitate drug transport to filling machine	Magnesium stearate (water insoluble) Talc (water insoluble) Starch (water insoluble) Magnesium lauryl sulfate (water soluble) Polyethylene glycol (water soluble)	0.25-2 5-10 5-10 1-3 5-10
Anti-Adherent (Tablet)	Reduce sticking of tablets to the punches or die wall	Talc Magnesium stearate Microcrystalline Cellulose	1-5 0.25-1 5-10
Glidant (Tablet, Hard gelatin capsule, Powder)	Promote flow of granules or powders by reducing friction between them	Calcium silicate Silicon dioxide Magnesium stearate Starch	0.5-2 0.1-0.5 0.2-2 1-10
Pigment (Tablet, powder)	Add color to tablet or powder	Titanium dioxide	----
Flavoring (Tablet, Powder)	Add taste to tablet or powder	Flavor oils Sweetners Salt	----
Surfactant (Tablet, Hard	Wetting agent	Sodium lauryl sulfate	----

gelatin capsule, Powder)			
Plasticizer (Tablet, Hard gelatin capsule, Powder)	Add to binder solution to increase binder efficiency	Glycerol Propylene glycol	----
Salt (Tablet, Hard gelatin capsule, Powder)	Modify aqueous solubility of API	Hydrochloride Citrate Tartrate	----
Cosolvent (Soft gelatin capsule)	To aid in the preparation of solutions incorporated in soft gelatin capsules	Water and alcohol Glycerin and polyethylene glycol	Up to 5 Up to 10
Suspending agent (Soft gelatin capsule)	To prevent the settling of solids and to maintain homogeneity	Paraffin wax Polyethylene glycol Acetylated monoglycerides	5 1-15 5

APPENDIX E: DRUG NANOPARTICLES SYNTHESIS

E.1 Introduction ^[1-4]

Drug nanoparticles are produced by two approaches: (a) top-down (smaller particles from larger particles by mechanism of breaking) and (b) bottom-up (growth of nanoparticles from molecules). Drug nanoparticles produced by top-down (grinding) method involve the application of force that breaks the particles depending on brittleness of particles. Sometimes there is a limit of smallest particle size that can be produced by the top-down or grinding method. The most common top-down methods employed in the industry are wet milling and high pressure homogenization. In the case of bottom-up approach, there are several methods that have been used in industry and published in the literature. The prominent bottom-up methods are emulsification technology, supercritical fluid technology, spray freezing into liquid and evaporative precipitation into aqueous solution. Nanoparticles technologies should be simple, continuous, efficient, scalable, able to meet regulations, and flexible to handle various quantities of drug. Table E.1 shows various methods of drug nanoparticles synthesis and their commercial application [4,5]. Table E.2 shows various methods of nanoparticle synthesis and their percentage usage [6].

E.1.1 Wet Milling

Wet milling is based on grinding/attrition/disintegration of particles to produce nanoparticles. In this method, the drug is dispersed in the water with surfactant and is

subjected to milling using pearls. Typically pearls are made of glass, zircon oxide, or polystyrene resin (approx. of 0.4-3.0 mm in diameter). Due to impaction of drug particles with milling media, larger drug particles get converted into nanoparticles. A lower temperature is used during milling operation to increase friability of drug particles as well as stability. Milling can last hours to several days depending on the requirement of drug particle size and physical property of the drug. Wet milling has some concerns regarding contamination of the drug sample due to abrasion of milling media and microbiological pollution due to long hours of milling operation.

E.1.2 High-pressure homogenization

This technique involves passing a suspension consisting of drug, surfactant and water through a narrow gap ($\sim 25 \mu\text{m}$) with high velocity (Figure E.1). During its passage through the narrow gap, water reaches below vapor pressure and forms the bubbles. Upon exit of gap, as pressure increases, bubble implodes leading to cavitation phenomena. Due to cavitation, drug particles in the suspension disintegrate into smaller particles. Liquid pressure as high as 100-1500 bar is used during homogenization. As pressure increases, the velocity of liquid through gap increases, leads into more formation of bubbles. A high number of bubbles lead to more comminuting of particles. The number of homogenization cycles required, which can be 5, 10 or more, depends on the hardness of the drug particles. This technique is simple and suitable for the laboratory as well as large scale purposes.

E.1.3 Emulsification Technology

This technology is used to prepare nanoparticle suspensions. In this method, first the drug is dissolved in an organic solvent and then is dispersed into an aqueous solution containing surfactant. After dispersion of drug solution into aqueous solution, evaporation of organic solvent is carried out at reduced pressure. Evaporation of the solvent leads to precipitation of drug nanoparticles, which are stabilized by surfactants in the aqueous solution. This technique is not useful when drugs are not soluble enough in organic solvents or when a lower limit of residue solvent is required.

E.1.4 Spray Freezing into Liquid

In this process, which was developed at the University of Texas, Austin, involves atomizing an aqueous, aqueous-organic co-solvent solution, aqueous-organic emulsion, or suspension containing a drug and pharmaceutical excipients into compressed gases like CO₂, helium, propane, ethane or cryogenic liquids like nitrogen, argon, and hydrofluoroethers. Frozen particles are lyophilized to obtain free flowing nanopowders. Due to rapid freezing, amorphous drug nanoparticles are formed in this process.

E.1.5 Evaporative precipitation into aqueous solution

This technique is also developed at University of Texas, Austin. In this method drug is dissolved into low boiling organic solvent. Then heated drug solution above boiling point of organic solvent is sprayed into heated aqueous solution containing surfactants which leads into rapid phase separation. Surfactants in the aqueous solution prevent the growth of particles leading into formation of nanoparticles.

E.1.6 Supercritical Fluid Technology^[5-9]

A fluid above its critical temperature and pressure is called a supercritical fluid. Supercritical fluids (SCF) possess unique properties which are tunable with pressure and temperature. SCF have liquid-like density and gas-like transport properties. Carbon dioxide is an environmentally benign, inert, non toxic, non flammable, inexpensive, low viscosity fluid with comparatively higher molar density. Supercritical carbon dioxide is used in processing of pharmaceutical compounds, due to its mild critical point (73.7 bar and 31.1°C). There are various supercritical carbon dioxide based technologies like rapid expansion of supercritical solutions (RESS), rapid expansion of supercritical solution with solid co-solvent (RESS-SC), rapid expansion of supercritical solution into liquid solvent (RESOLV), rapid expansion from supercritical to aqueous solutions (RESAS), particles from gas saturated solutions (PGSS), gas antisolvent (GAS), aerosol solvent extraction system (ASES), supercritical antisolvent (SAS), supercritical antisolvent with enhanced mass transfer (SAS-EM), solution enhanced dispersion by supercritical fluids (SEDS), supercritical fluid extraction emulsions (SFEE), etc.

E.1.7 RESS/RESS-SC/RESOLV/RESAS

These processes are based on nucleation of drug after rapid expansion of supercritical solution (containing dissolved drug) due to decrease in solubility with rapid pressure change (supercritical to atmospheric). Figure E.2-4 shows schematics for the above processes. In RESS, first supercritical fluid (especially carbon dioxide) is passed through a bed of active ingredient or drug. After supercritical fluid gets saturated with

drug, it is then rapidly expanded through nozzle to the atmospheric pressure resulting in the formation of fine particles. This process is limited by relatively low solubility of compounds in supercritical fluids for industrial use. Solubility data of various compounds has been presented in a book by Gupta and Shim [10]. The problem of limited solubility has been tried to circumvent by addition of co-solvent which can be solid (or liquid) then process is called RESS-SC. A co-solvent should have good solubility in supercritical fluid and should have high affinity for active ingredient. A process involving solid co-solvent like menthol has been developed at Auburn University, Auburn, Alabama. Due presence of solid co-solvent, it was found that the solubility of various drug compounds in supercritical CO₂ increased several hundred folds [11] as well as produced smaller particles as compared to samples without solid co-solvent. In the process of RESOLV and RESAS, a supercritical solution is sprayed into a liquid solvent or aqueous solution containing stabilizers for prevention of growth and stabilization of particles. More details of the process can be found elsewhere [12]. Efficient recovery of fine particle during all above processes is major problem for its commercialization to industrial scale. Various parameters like pre-expansion temperature and pressure, nozzle diameter, and nozzle temperature affects the size of particles produced during the process.

E.1.8 PGSS

In this process, the active compound does not need to be soluble in compressed fluid. Compressed fluid is passed through a melted active compound, and then a solution becomes gas saturated and then expanded through a nozzle to form fine solid particles. Figure E.5 shows schematics of the PGSS process. This process takes advantage of

solubilities of compressed gases in liquids and solids like polymers which are higher than in solubilities of liquids and solids in compressed gases. This process can be used to form composite materials, including active ingredients.

E.1.9 GAS/SAS/ASES/SAS-EM/SEDS

These processes are developed for the hydrophobic materials which are not able to be process by RESS methods due to solubility limits. In this process, the drug or desired substance is not soluble in compressed gases. In these processes, first the active ingredient is dissolved in organic solvents, like methanol, acetone, dichloromethane, ethanol, dimethylsulfoxide, which have good solubility in compressed gases like CO₂. When the process is operated in batch manner, it is called gas antisolvent. In the gas antisolvent process, organic solution containing drug is compressed to desired pressure and temperature with CO₂. Due to the addition of compressed gases to the organic solvent, the whole solution is expanded and dissolution strength of organic solvent decreases leading to the formation of fine particles. Other processes are operated in semi-continuous way in which the organic solution containing drug is sprayed though a nozzle counter-currently (ASES and SAS) or co-currently (SEDS) with supercritical fluid (CO₂). Figure E.6-7 shows schematics of the above processes. A process using ultrasound (SAS-EM) for droplet atomization of drug solution and enhanced mass transfer in precipitation chamber lead to formation of nanoparticles of narrow distribution. This process was developed at Auburn University, Auburn, Alabama [13] and commercialized by Thar Technologies Inc. Figure E.8 shows schematics of the SAS-EM process which is used here in this dissertation work. Various parameters like pressure, temperature, nozzle

diameter, antisolvent (supercritical CO₂) flow rate, drug solution flow rate, and ultrasound amplitude (in case of SAS-EM) have an effect on the size of particles produced.

E.1 References

- [1] V. Kharb, M. Bhatia, H. Dureja, D. Kaushik. Nanoparticle technology for the delivery of poorly water soluble drugs. *Pharm Technol.* 30 (2006) 82,4, 6,8, 90-2.
- [2] J. E. Kipp. The role of solid nanoparticle technology in the parenteral delivery of poorly water-soluble drugs. *Int J Pharm.* 284 (2004) 109-22.
- [3] L. Gao, D. Zhang, M. Chen. Drug nanocrystals for the formulation of poorly soluble drugs and its application as a potential drug delivery system. *J Nanopart Res.* 10 (2008) 845-62.
- [4] E. M. Merisko-Liversidge, G. G. Liversidge. Drug nanoparticles: formulating poorly water-soluble compounds. *Toxicol Pathol.* 36 (2008) 43-8.
- [5] C. Vemavarapu, M. J. Mollan, M. Lodaya, T. E. Needham. Design and process aspects of laboratory scale SCF particle formation systems. *Int J Pharm.* 292 (2005) 1-16.
- [6] K. Byrappa, S. Ohara, T. Adschiri. Nanoparticles synthesis using supercritical fluid technology-towards biomedical applications. *Adv Drug Delivery Rev.* 60 (2008) 299-327.
- [7] J. Jung, M. Perrut. Particle design using supercritical fluids: literature and patent survey. *J Supercrit Fluids.* 20 (2001) 179-219.
- [8] H. Okamoto, K. Danjo. Application of supercritical fluid to preparation of powders of high-molecular weight drugs for inhalation. *Adv Drug Delivery Rev.* 60

(2008) 433-46.

[9] T. Yasuji, H. Takeuchi, Y. Kawashima. Particle design of poorly water-soluble drug substances using supercritical fluid technologies. *Adv Drug Delivery Rev.* 60 (2008) 388-98.

[10]. R.B. Gupta and J.J. Shim. *Solubility in supercritical carbon dioxide*, Taylor and Francis Group, New York, 2007.

[11] R. Thakur, R. B. Gupta. Formation of phenytoin nanoparticles using rapid expansion of supercritical solution with solid cosolvent (RESS-SC) process. *Int J Pharm* .308 (2006) 190-9.

[12] M. J. Meziaia, P. Pathaka, F. Beachama, L. F. Allardb, Y.-P. Sun. Nanoparticle formation in rapid expansion of water-in-supercritical carbon dioxide microemulsion into liquid solution *J Supercrit Fluids*. 34 (2005) 91-7.

[13] R. B. Gupta, P. Chattopadhyay, inventors; Method of forming nanoparticles and microparticles of controllable size using supercritical fluids with enhanced mass transfer. US Patent 6620351. 2003.

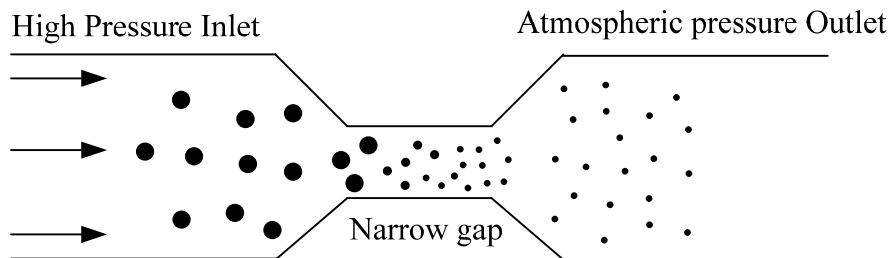


Figure E.1 Schematic of high-pressure homogenization technique [1].

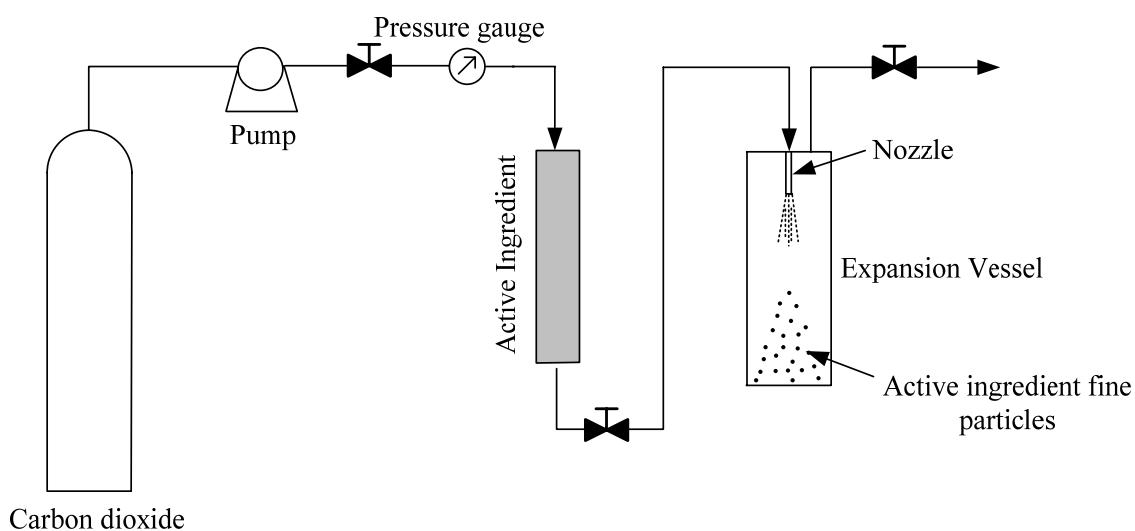


Figure E.2 Schematic of rapid expansion of supercritical suspension (RESS).

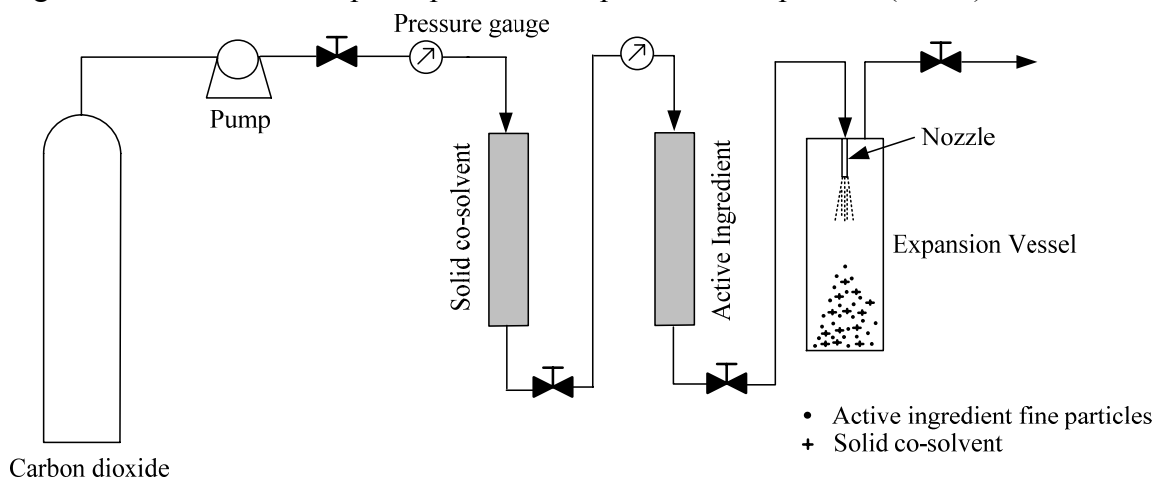


Figure E.3 Schematic of rapid expansion of supercritical solution with solid co-solvent.

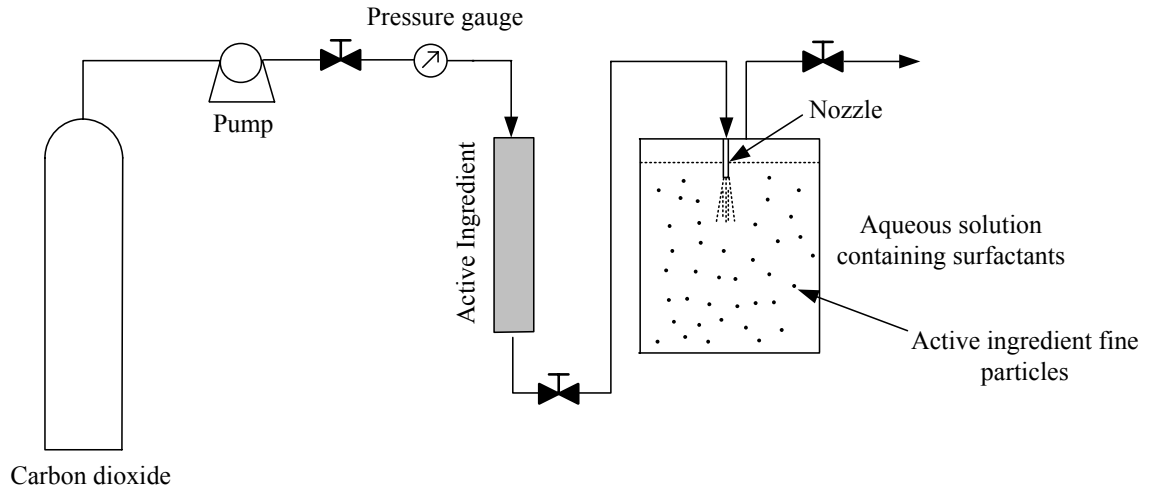


Figure E.4 Schematics of rapid expansion of supercritical solution in liquid solvent.

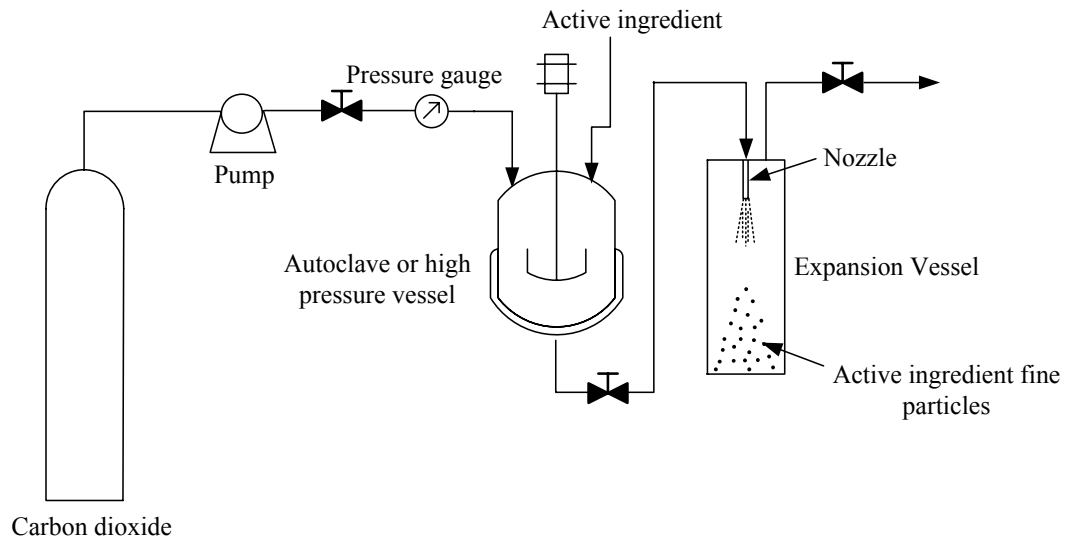


Figure E.5 Schematic for particles from gas saturated solution (PGSS).

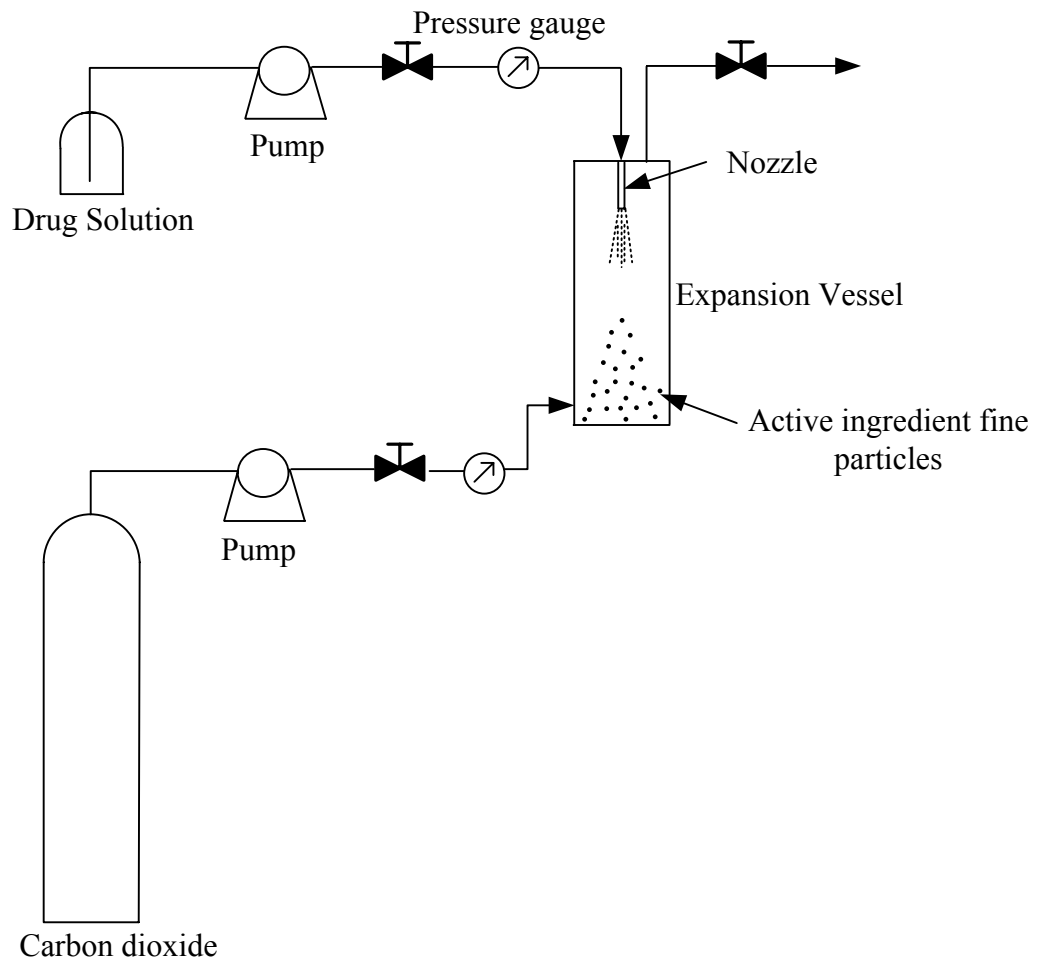


Figure E.6 Schematics of supercritical antisolvent (SAS)/ gas antisolvent (GAS)/aerosol solvent extraction (ASES).

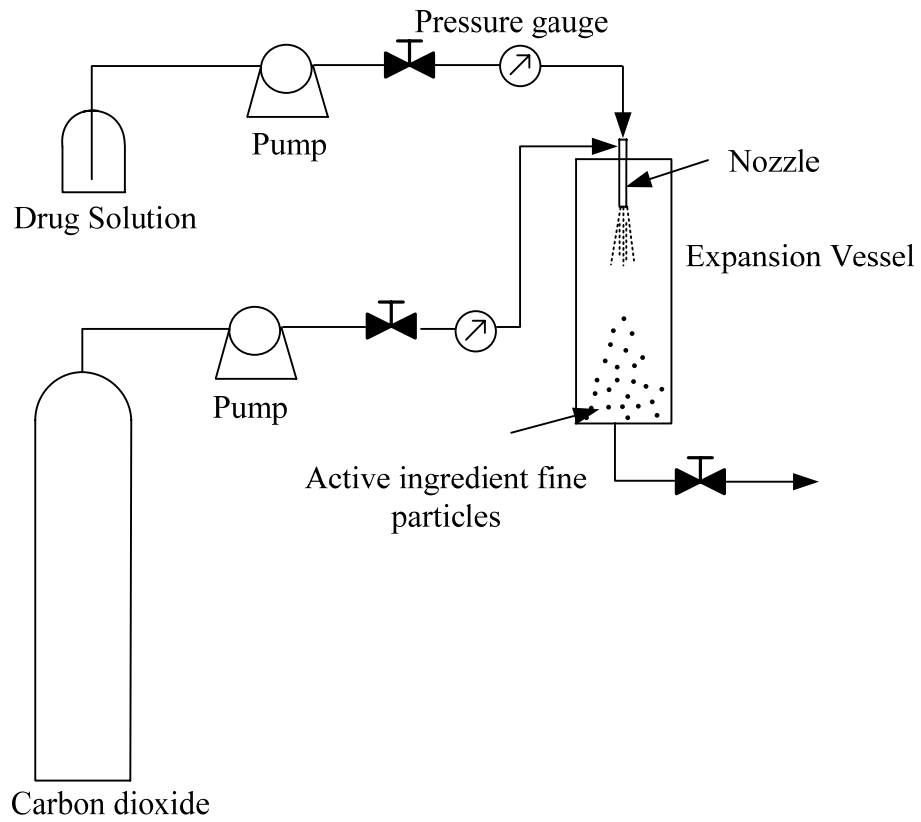


Figure E.7 Schematics of solution enhanced dispersion by supercritical fluids (SEDS).

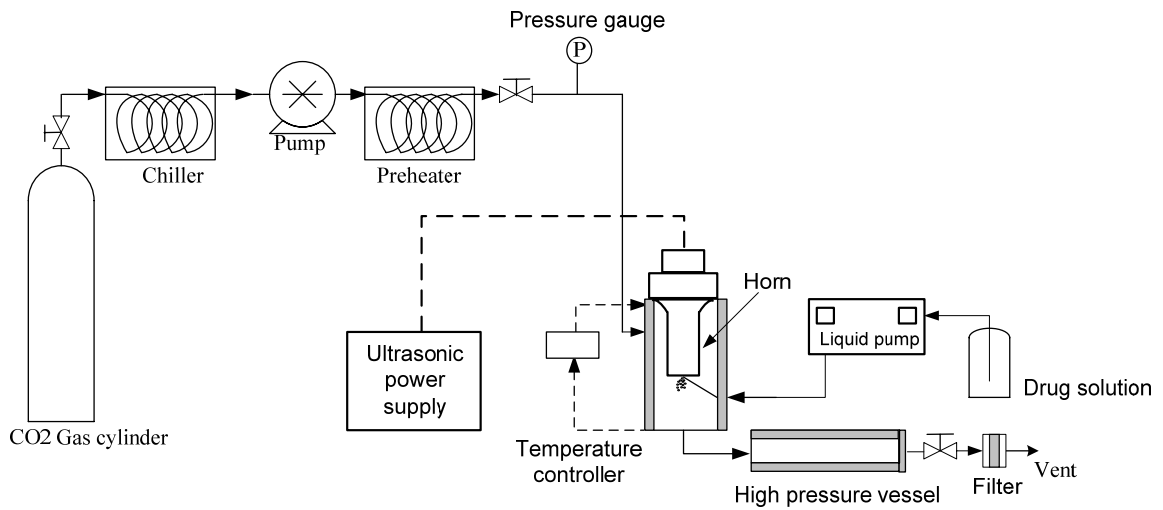


Figure E.8 Schematics of supercritical antisolvent with enhanced mass transfer (SAS-EM).

Table E.1 Various methods of drug nanoparticles synthesis and their commercial applications [4,5].

Category	Descriptions	Owners/Company
Top-Down	Media Milling	Elan Drug Technologies
	SCF(supercritical fluid) milling	DuPont
	Homogenization	Skye Pharma
		PharmaSol
		Baxter
Bottom-up	SCF Technology	Ferro Corp., Thar Tech., Nektar, Lavipharm, RxKinetics, Eurand, Skye Pharma, Nektar, Bristol Myer Squibb, Glaxo Smithkline, Astra, Alcon, Crititech, BASF, Ethypharm, Schwarz Pharma, Rohm and Hass, Hoffman-La Roche
	Spray Freezing into liquid	Dow

	Evaporative precipitation into aqueous solution	Dow
--	--	-----

Table E.2 Various methods for nanoparticle synthesis and their % usage [6].

Processing Method	% of usage
Physical vapor deposition	10
Colloidal chemistry approach	25
Mechanical alloying techniques	10
Mechanical milling	22
Chemical vapor deposition	>20
Sol-gel technique	35
Mechanical grinding	20
Hydrothermal/solvothermal method	>6
Supercritical fluid precipitation process	9
Biological/biomimetic techniques	9
Flame pyrolysis	6

Laser ablation	12
Ultrasound Techniques	<3
Electrodeposition Process	>9
Electro-explosion	<3
Plasma synthesis techniques	3
Microwave techniques	<3
Other precipitation processes	<3

APPENDIX F: ULTRASOUND

F.1 Introduction

The process of nanoparticle dispersions has been carried out effectively by sonication in liquids like water, and n-hexane. Propagation of ultrasound through fluid media creates high pressure and low pressure cycles. During a low pressure cycle in liquid media, it creates small vacuum bubbles and void in it. The bubble attains a particular size when it stops absorbing more energy. During a high pressure cycle, the bubble collapses violently, creating shock waves and liquid jet streams. This phenomenon is called cavitation. Figure F.1 shows the bubble formation and collapse cycle. Cavitation produces a high local pressure (~1000 atm), and high temperature (~5000k) [1]. It was observed that it is possible to break micro agglomerates of nanoparticles due to cavitation [2]. Agglomerate fragmentation is function of power output, pressure amplitude, suspension volume, and agglomerate size. Therefore, liquid jet streams created during cavitations are effective in overcoming cohesive forces among particles when wetted in the liquid. Ultrasound has been used for various purposes like surface cleaning, emulsification, particle size reduction depending on various ultrasound amplitude used in the process. Table F.1 shows the amplitudes of ultrasound used in various applications [3].

F.2 Ultrasound processor and design of probe

The ultrasonic processor consists of three major components: an ultrasonic power

supply, a transducer (converter), a booster (optional) and a horn typically $\frac{1}{2}$, $\frac{3}{4}$, and 1 inch in diameter. Figure F.2 shows the cartoon representing various components in the ultrasonic processor and their functions. The ultrasonic processor is designed to deliver constant amplitude (horn is 0.75 inch in diameter, 61 μm at 100% amplitude settings for a horn used in this dissertation work), i.e. it automatically adjusts power to maintain constant amplitude during the operation. Therefore, power delivered from the processor depends on the resistance to the movement of the horn which is affected by setup and process parameters, such as volume of a mixing vessel, horn size, mixture viscosity, and pressurized environment.

Figure F.3 shows the detailed arrangement of the horn inside the pressure vessel that is used in this dissertation work. Arrangement of the horn (or probe) is such that nothing can come in contact with probe except at the nodal point (point of no activity). During the operation, the upper and bottom part of horn expands and contracts longitudinally about the nodal point, which results in contraction and expansion of probe around flange radically.

The intensity of ultrasound (ratio of power delivered to surface area of probe) delivered depends on the diameter of probe. The smaller the probe, the larger the intensity of ultrasound delivered in a smaller area. Depending on the type of application, probe diameter can be selected. Probes are typically made from high grade titanium alloy (TI-6AL-4V) due to high tensile strength, good acoustical properties at selected ultrasonic frequencies, high resistance to corrosion, low toxicity, and excellent resistance to cavitation erosion. The design of probe is typically carried out in following steps: (a) selection of frequency (20 kHz is the minimum frequency used in various applications

which gives larger component size with maximum available power), (b) selection of suitable material (based on properties as discussed previously), (c) calculation of wavelength, and (d) calculation of theoretical dimensions (half the wavelength). For 20 kHz frequency and material of high grade titanium alloy, the calculations of the theoretical dimensions of the horn are presented in Table F.2. Formulae used in the calculations are also presented here (www.powerultrasonics.com)

$$C_a = \sqrt{\frac{E}{\rho}} \quad (1)$$

$$\lambda = \frac{C_a}{f} \quad (2)$$

$$L = \frac{\lambda}{2} \quad (3)$$

$$a_{out} = a_{in} \left(\frac{d_{in}}{d_{out}} \right)^2 \quad (4)$$

where, C_a is axial mode sound velocity, E is the young's modulus, ρ is the material density, f is the sound frequency, λ is the wavelength, L is the length of probe, a_{in} is the input amplitude, and a_{out} is the output amplitude. Table F.2 shows typical values used for calculation of probe length. Figure F.4 shows design values of ultrasound probe.

F.1 References

- [1] K. S. Suslick. Sonochemistry. *Kirk Othemer Encyclopedia of Chemical Technology*: 1-21.
- [2] K. K. Kusters, S. E. Pratsinis, S. G. Thoma, D. M. Smith. Ultrasonic fragmentation of agglomerate powders. *Chem Eng Sci.* 48 (1993) 4119-27.

- [3] T. Hielscher. Ultrasonic production of nano-size dispersions and emulsions.
Dans European Nano Systems Workshop-ENS. Paris, France 2005.

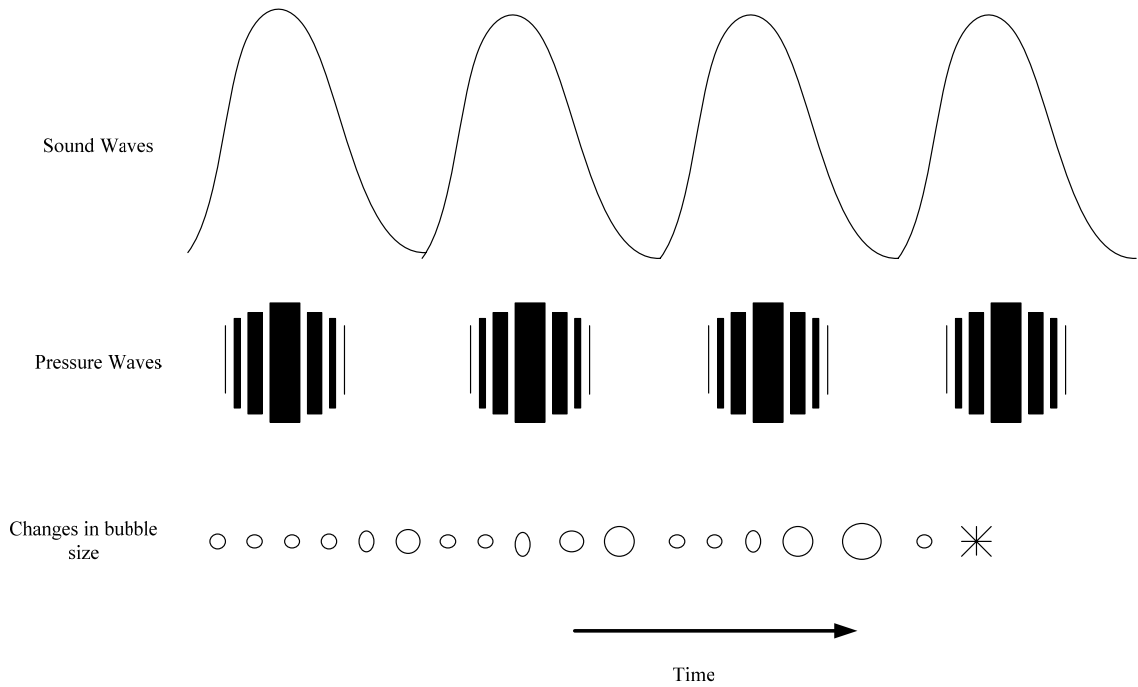


Figure F.1 Cartoon representing the cavitation cycle [www.sonics.biz]

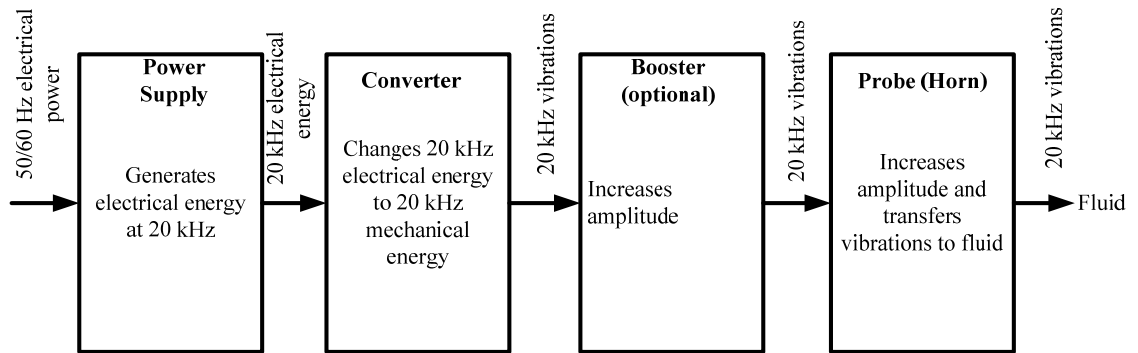


Figure F.2 Cartoon representing the various components of ultrasonic processor and their functions [www.sonics.biz].

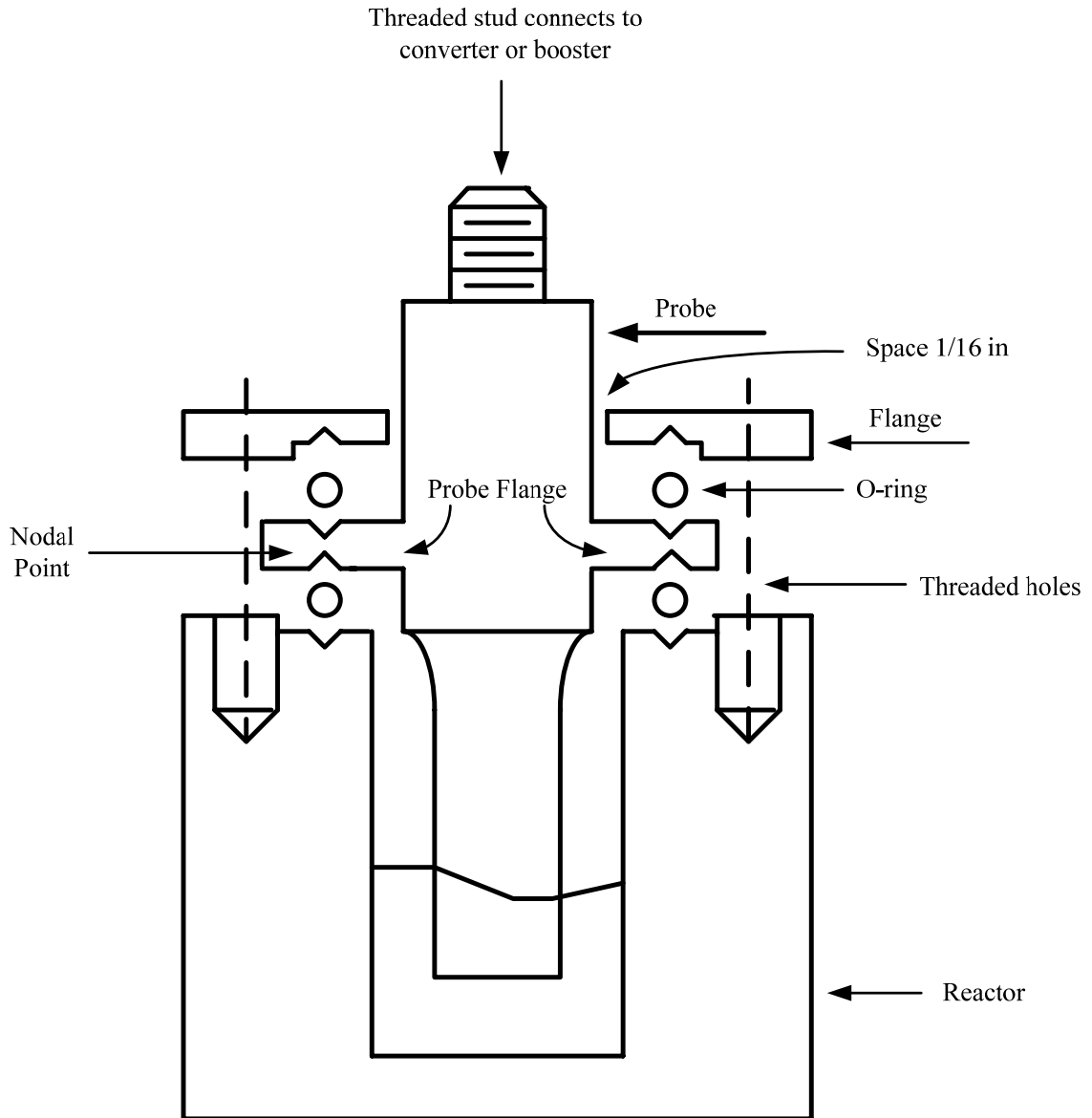


Figure F.3 Arrangement of ultrasound horn (probe) inside the pressure vessel
 [www.sonics.biz]

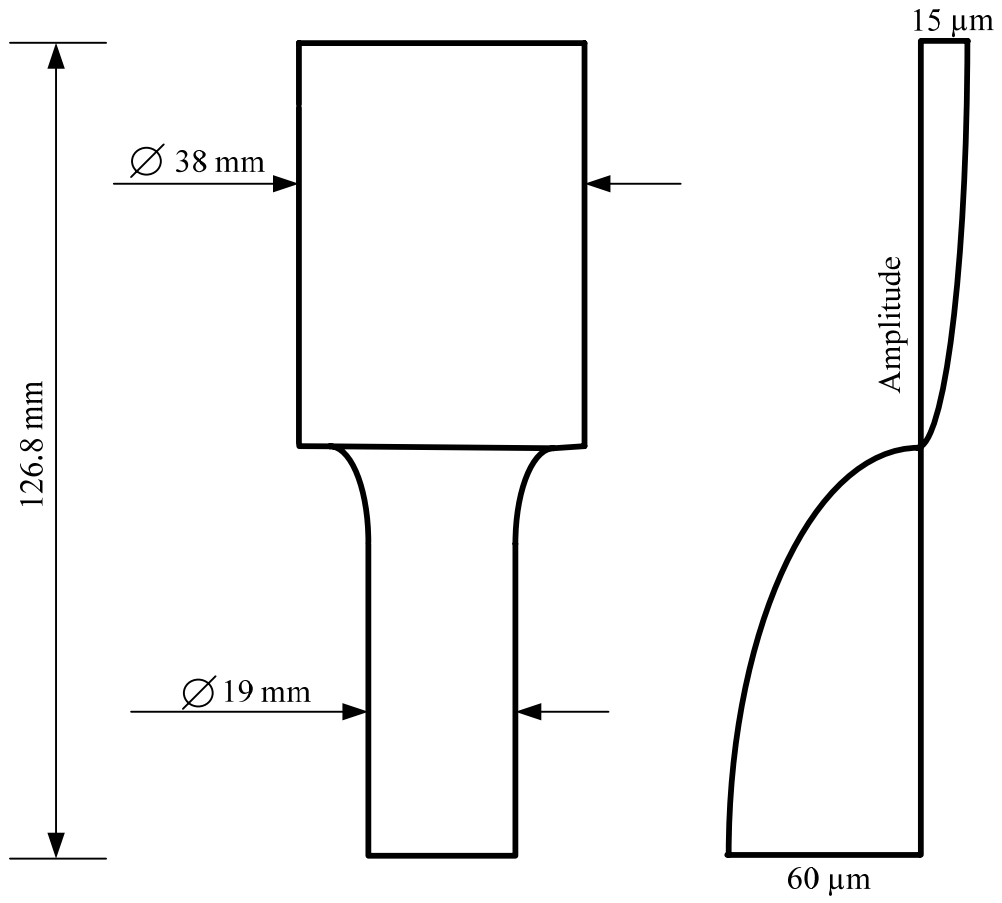


Figure F.4 Cartoon showing design parameters of horn (probe).

Table F.1 Application of variable ultrasound amplitude for different processes [3].

Process	Amplitude (μm)
Cleaning	0.5-2
Intensive cleaning	10-20
Dispersing/deagglomeration	10-30
Emulsifying	20-60
Primary particle reduction	40-120

Table F.2 Values of various parameters used in calculations of ultrasound horn (probe) length.

Parameters	Value
Ultrasound Frequency	20 kHz
Input diameter	38 mm
Output diameter	19.0 mm
Materials	Ti-6Al-4V
Density	4430 kg/m ³
Young's modulus	114 MPa
Sound velocity (axial)	5073 m/s

Wavelength	253.6 mm
Length of probe	126.8 mm
Input amplitude (for example)	15 μm
Output amplitude	60 μm

APPENDIX G: PUBLICATIONS AND PRESENTATIONS

G.1 Patent Application

Ganesh P. Sanganwar, Ram B. Gupta, Sateesh Sathigari, and Jayachandra Ramapuram. Simultaneous Particle Formation and Mixing Using Supercritical Antisolvent. US 61/215,891.

G.2 Journal Publications

Ganesh P. Sanganwar, Ram B. Gupta, Alexandre Ermoline, James V. Scicolone, and Rajesh N. Dave, 2008. Environmentally Benign Nano-mixing by sonication in High Pressure Carbon Dioxide. *J. Nanopart. Res.* 11(2009) 405-419.

Ganesh P. Sanganwar, Ram B. Gupta, 2008. Dissolution-rate enhancement of fenofibrate by adsorption onto silica using supercritical carbon dioxide. *Int. J. Pharm.* 360(2008)213-18.

Ganesh P. Sanganwar, and Ram B. Gupta, 2008. Enhancement of Physical stability and Handling Properties of Drug Nanoparticles: Nanoscale Mixing of Itraconazole with Silica. *Ind. Eng. Chem. Res.* 47(2008) 4717-25.

Ganesh P. Sanganwar, and Ram B. Gupta, 2009. Nano-mixing of Dipyridamole Drug and Excipient Nanoparticles by Sonication in Liquid CO₂. *Powder Technolog.* 196(2009)36-49.

Ganesh P. Sanganwar, Sateesh Sathigari, Jayachandra Ramapuram, and Ram B. Gupta, 2009. Simultaneous Production and Co-mixing of Microparticles of Nevirapine with Excipients by Supercritical Antisolvent Method for Dissolution Enhancement. *Accepted in Eur. J. Pharm. Sci.*

G.3 Conferences

Ganesh P. Sanganwar, Ram B. Gupta, Alexandre Ermoline, James V. Scicolone, and Rajesh N. Dave, 2007. Environmentally Benign Nano-mixing by Sonication in High Pressure Carbon Dioxide. AIChE Conference, Salt lake city, Utah, USA.

Ganesh P. Sanganwar, and Ram B. Gupta, 2008. Enhancement of Physical stability and Handling Properties of Drug Nanoparticles: Nanoscale Mixing of Itraconazole with Silica. AIChE Conference, Philadelphia, PA, USA.

Ganesh P. Sanganwar, and Ram B. Gupta, 2008. Dissolution-rate enhancement of fenofibrate by adsorption onto silica using supercritical carbon dioxide. AIChE Conference, Philadelphia, PA, USA.

Ganesh P. Sanganwar, and Ram B. Gupta, 2008. Nano-mixing of Dipyridamole Drug and Excipient Nanoparticles by Sonication in Liquid CO₂. AIChE Conference, Philadelphia, PA, USA.

Ganesh P. Sanganwar, Sateesh K. Sathigari, Jayachandra Ramapuram, and Ram B. Gupta. 2009. Simultaneous particle formation and mixing by supercritical antisolvent method. Fast release nevirapine formulation, AIChE Conference, Nashville, TN, USA.